Few- to many-body physics in ultracold gases

An exact diagonalization approach

Bjerlin, Johannes

2017

Few- to many-body physics in ultracold gases

Few- to many-body physics in ultracold gases

An exact diagonalization approach

by Johannes Bjerlin

LUND
UNIVERSITY

Thesis for the degree of Doctor of Philosophy in Engineering
Thesis advisor: Stephanie M. Reimann
Faculty opponent: Wilhelm Zwerger

To be presented, with the permission of the Faculty of Physics of Lund University, for public criticism in the lecture hall Rydbergsalen at the Department of Mathematical Physics on Friday, the 22th of September 2017

Organization
LUND UNIVERSITY

Department of Mathematical Physics
Box 118
SE–221 00 LUND
Sweden

Document name
DOCTORAL DISSERTATION

Date of disputation
2017-09-22

Sponsoring organization

Author(s)
Johannes Bjerlin

Title and subtitle
Few- to many-body physics in ultracold gases: An exact diagonalization approach

Abstract
This dissertation concerns studies of few-particle quantum systems, with a particular focus on few- to many-body behavior of interacting particles. The thesis is based on five included papers in which exact diagonalization is employed to solve the Schrödinger equation for microscopic Hamiltonians of ultracold atoms. The introductory chapters contain a brief background on ultracold systems, an overview of the related experimental research, as well as a summary of a few concepts in the methodology of exact diagonalization. Also included is an introduction to 1D-systems with effective interaction, introducing concepts such as Wigner localization, Tonks-Girardeau states, and super-Tonks-Girardeau states. The main part of the text is a summary of the papers, including background, methodology and main results. These sections are organized into three parts:

Chapter 5 involves papers II-IV and demonstrates the few-body realization of a Heisenberg spin-chain without optical lattices. Here, contact-interacting atoms in a 1D harmonic confinement are shown to constitute a model for quantum magnetism, which is confirmed by exact diagonalization of the microscopic Hamiltonian. Through collaboration with experimentalists, the results are also confirmed in a few-body experimental setup with ultracold atoms.

Chapter 6 concerns paper I and investigates a few-body precursor of a Higgs-mode, a concept known from condensed matter physics. A 2D harmonic oscillator with up to twelve spin-1/2 fermions is studied, revealing a few-body precursor of a normal-to-superfluid transition which gives rise to Higgs-like excitations.

Chapter 7 involves paper V and concerns a few-body setup of two parallel quasi-1D quantum wires with dipolar bosons or fermions. Here, both static and dynamic properties of the dipole-dipole interaction are studied. We see that changing the alignment of dipole moments relative to the longer semiaxis of the traps can bring particles in-and-out of a few-body localized state, where the speed of this change strongly effects the transition.

Key words
few- to many-body physics, exact diagonalization, quantum magnetism, Heisenberg spin-chain, Tonks-Girardeau gas, ultracold gases, Higgs mode, pairing-vibration mode, dipolar gases

Classification system and/or index terms (if any)

Supplementary bibliographical information

Language
English

ISSN and key title

ISBN
978-91-7753-401-3 (print)
978-91-7753-402-0 (pdf)

Recipient's notes

Number of pages
141

Price

Security classification

Signature _____ Date 2017-9-18

Few- to many-body physics in ultracold gases

An exact diagonalization approach

by Johannes Bjerlin

LUND
UNIVERSITY

This thesis consists of two parts. An introductory text puts the research work into context and summarizes the results of the papers. Then, the research publications themselves are reproduced, together with a description of my individual contribution. The research papers I-IV are published, and the last paper V is a manuscript in preparation.

Cover illustration front:

Cover illustration back: Picture showing my research (Paper I).

Funding information: The thesis work was financially supported by the Swedish Research Council and NanoLund

Faculty of Physics, Department of Mathematical Physics

ISBN: 978-91-7753-401-3 (print)
ISBN: 978-91-7753-402-0 (pdf)

Printed in Sweden by Media-Tryck, Lund University, Lund 2017

Once in a while you get shown the light
in the strangest of places if you look at it right.
The Grateful Dead

Contents

List of publications ii
Acknowledgments iv
Popular summary v
Populärvetenskaplig sammanfattning på svenska viii

Introduction **1**
1 Ultracold atoms and few-body systems 1
2 Exact diagonalization - an overview of methods 4
3 Short-range interacting gases in one dimension – an introduction to Tonks-Girardeau states 9
4 Short-range interacting ultracold gases in two dimensions 12

Results **13**
5 Quantum magnetism in a one-dimensional harmonic oscillator . 13
6 Higgs modes of a two-dimensional harmonically trapped Fermi gas 26
7 Few-body localization and short-range behavior in parallel quasi one-dimensional traps with dipoles 43

Appendix **55**
1 Short-range interaction potentials between particles in harmonic traps. 57

Bibliography **65**

Scientific publications **77**
Author contributions 77
Papers 79

List of publications

This thesis is based on the following publications, referred to by their Roman numerals:

I **Few-body precursor of the Higgs mode in a fermi gas**

J. Bjerlin, S.M. Reimann, G.M. Bruun
Phys. Rev. Lett. **116**, 155302 (2016)

II **Quantum magnetism without lattices in strongly interacting one-dimensional spinor gases**

F. Deuretzbacher, D. Becker, **J. Bjerlin**, S. M. Reimann, and L. Santos
Phys. Rev. A **90**, 013611 (2014)

III **Antiferromagnetic Heisenberg spin chain of a few cold atoms in a one-dimensional trap**

S. Murmann, F. Deuretzbacher, G. Zürn, **J. Bjerlin**, S. M. Reimann, L. Santos, T. Lompe, and S. Jochim
Phys. Rev. Lett. **115**, 215301 (2015)

IV **Spin-chain model for strongly interacting one-dimensional Bose-Fermi mixtures**

F. Deuretzbacher, D. Becker, **J. Bjerlin**, S. M. Reimann, and L. Santos
Phys. Rev. A **95.4**, 043630 (2017)

V **Dipolar particles in a double-trap confinement: Response to tilting the dipolar orientation**

J. Bjerlin, J. Bengtsson, F. Deuretzbacher, and S. M. Reimann
manuscript in preparation; to be submitted

Publications not included in this thesis:

Total current blockade in an ultracold dipolar quantum wire

L. H. Kristinsdóttir, O. Karlström, **J. Bjerlin**, J. C. Cremon, P. Schlagheck, A. Wacker, and S. M. Reimann
Phys. Rev. Lett. **110**, 085303 (2013)

Density-functional theory for strongly correlated bosonic and fermionic ultracold dipolar and ionic gases

F. Malet, A. Mirtschink, C. B. Mendl, **J. Bjerlin**, E. Ö. Karabulut, S. M. Reimann, and Paola Gori-Giorgi
Phys. Rev. Lett. **115**, 033006 (2015)

Acknowledgments

First, I would like to thank my supervisor Stephanie Reimann. I could not have wished for a better person to guide me through my PhD studies. I have felt inspired, trusted, challenged, I have learned a great deal about physics and research, and I have, most importantly, felt happy. I would also like to give extra thanks to some of my collaborators - Frank Deuretzbacher, Georg Bruun, Líney Halla Kristinsdóttir, Gillis Carlsson, Jakob Bengtsson, and Jonas Cremon, and also the members (past and present) of my group. I have learned so much from all of you.

Also, I wish to thank all the great people at mathematical physics for providing an inspiring and uplifting atmosphere. Extra thanks goes to Gunnar for organizing fun social events for the PhD students (and for *still* inviting me to join for lunch), and to Katarina and Peter, for making the department such a friendly and accommodating place.

I would like to thank my family for supporting me and always being there when I need them, and to my friends for making everything worthwhile. I would especially like to thank my closest friends here in Skåne: Jon, David (You'll get back soon, right?), Fredrik, and Lena – everything is more fun when you guys are around. And thank you Sanna, for being the best in the world.

Popular summary

Playing is fundamental for the development of a child into a, hopefully, functioning adult. Social skills may be acquired by arguing over the swings, and hand-eye coordination can be developed by throwing snowballs. Similarly, ultracold atoms and few-body physics can provide a simple environment where physicists can play with ideas and theories in a controlled fashion.

To describe physics in an efficient way, mathematics is almost exclusively the preferred language. Mathematics allows us to generalize a problem or a question so that for example $7+7=14$ both can describe how many apples "Mark" gets, and how many days there are in two weeks. Of course, there are countless examples of this.

The fact that we can use a similar set of mathematical tools to describe lots of different areas in physics has created many examples where two seemingly distinct theories turn out to be connected. This thesis concerns studies where well-known physical effects and concepts can be linked to models that describe only a few atoms.

Most of the particles around us are small parts of large ensembles that together make up stuff like metals, gases, or ice cubes. Such things can be broken down into smaller components, but it is in general hopeless to try to predict the motion of a single atom in, for example, a gas. We can compare this to making a survey of some general political opinions in a country; using a statistical treatment of the citizens can give us insight into the overall mood of the country, but not the personal views of one person on the street. In a statistical model for, let us say a metal, particles are parts of statistical ensembles with collective properties such as temperature or pressure. The large-scale (macroscopic) effects in a material with millions of atoms will, in general, require some statistical model, whereas the short-scale (microscopic) behavior of individual systems with only a few particles can be investigated more directly, and with more details.

Quantum mechanics and ultracold systems

To perform experiments and measurements on microscopic systems with a high level of detail, it is often crucial that one can cool down the surroundings to extremely low temperatures, close to zero Kelvin. For such (ultracold) temperatures it is much easier to understand the behavior of a system on the microscopic scale. We can imagine a box with a number of atoms in it. When the temperature is high, the particles bounce around and travel at different speed

in all directions, and it is, therefore, hard to predict the motion of single atoms. If the temperature is extremely low, however, one can say that the atoms move more slowly and more predictably, and it is, in general, easier to exercise control over the system. In ultracold, or cold-atom, systems it is often possible to directly control certain properties of the atoms, like for example how they interact. By modifying the interactions and other parameters, we can build artificial systems that resemble naturally occurring materials, like for example magnets. In this way, ultracold systems are easy to work with and are perhaps the ultimate "physicist's playground."

To accurately describe happenings in the microscopic world, which is inhabited by things like atoms and electrons, we generally use the language of *quantum mechanics*. It is rare to observe any direct examples of quantum mechanical behavior with our own eyes, even though we know it is a fundamental tool in describing the fabric of the universe. From the perspective of our daily life, this is probably a good thing, since it would be confusing if things behaved according to quantum mechanics. In the microscopic quantum world, objects can, for example, be at different places at the same time and go through walls and barriers - things that do not happen to us macroscopic beings.

Quantum mechanics provides an excellent tool for physicists to describe physics on the microscopic scale. It allows us to formulate detailed equations for particles and their interactions, and to successfully predict the outcomes of experiments based on the solutions of these equations.

From a few atoms to millions of atoms

In theoretical physics, going from a microscopic quantum model of a small interacting system, like a molecule, to a larger interacting system, like a gas of atoms, is not a trivial task. We may have a deep understanding of a small ultracold system in terms of highly detailed quantum equations, and in principle, one could often use similar equations for much larger systems, with millions of atoms. For a small system with only a few interacting atoms the equations can actually be solved, and we can then extract measurable quantities from the solutions. The same can not be said for a detailed quantum description of a large interacting system. In fact, a detailed quantum equation for a handful of interacting particles could take today's fastest computers several weeks to solve. Compare this to the task of sorting a phone book, containing all people in Sweden, in order of increasing number, which would take a standard laptop less than a second.

Here lies one of the core challenges in modern physics - how can we understand physical behavior for an ultracold system with large numbers of interacting particles in terms of quantum models at the microscopic level? In general, the solution is to greatly simplify the quantum-mechanical model of particles so that the equations become solvable. Another way to go is to keep the highly detailed description of particles in a system but to actually only consider very few particles. That is, of course, an enormous simplification if the end goal is to, for example, simulate and study magnetic behavior in a lump of metal that contains trillions and trillions of atoms. The situation is however not hopeless since clever minds over history have managed to characterize what a magnet is and how it works in terms of relatively simple models. Many of these models can be applied more or less directly to describe some behavior of an ultracold system. Armed with the predictions of a simpler, large-scale model, one can search for some reminiscent behavior in a few-body system, which then can be identified as a *precursor* of some physical effect that is present in the larger system.

In this thesis, a number of different few-particle quantum systems are investigated. We set up equations to determine the microscopic nature of the particles and develop methods for solving them using computers, here with a special focus on details that are important for systems with larger numbers of particles.

A specific example - Higgs particles in few-body systems

Thanks to the relatively recent experiments at CERN, we now believe that Higgs particles are everywhere present in the universe and that they constitute the proof of the Higgs mechanism, which gives all particles their mass. Higgs particles themselves are bi-products of this mechanism. One of the fascinating aspects of the Higgs mechanism is that the building-blocks of the theory come from a different branch of physics: the field of condensed matter. Years before the Higgs mechanism was invented, people found rather similar theories to explain the behavior of, for example, superconductors. It turns out that one particular theory for ultracold gases actually has the same building blocks as the theory for the Higgs particle. Here, we study this particular case of an ultracold gas, but for very few particles. By selecting and using a set of known properties of the Higgs particle in the macroscopic gas, we can show that the few-particle system indeed exhibits some of the distinct properties associated with Higgs particle. Our work highlights a theoretical connection between a few-particle ultracold system and the Higgs particle. Furthermore, we suggest an experimental setup in which to measure the properties of this system.

Populärvetenskaplig sammanfattning på svenska

Många människor är av den klara uppfattningen att lek är enormt viktigt för ett barns utveckling. Under ett bråk om vem som ska ha den bästa gungan tränar barn sin sociala förmåga, och genom att kasta snöboll förbättrar barnet sin motorik. På ett liknande sätt kan ultrakalla atomer fungera som en lekplats för fysiker, där komplicerade teorier och fysikaliska kuriositeter kan undersökas i en enkel och kontrollerad miljö.

För att beskriva fysik används matematik. Matematik tillåter oss att generalisera problem och frågor på ett tydligt sätt. Till exempel kan $7 + 7 = 14$ kan användas för att beskriva hur många äpplen "Åke" har fått, men också för att beskriva hur många dagar som går på två veckor. På liknande sätt kan vi använda samma matematiska verktyg för att beskriva många olika områden inom fysiken. Sådana likheter har gång på gång genom historien visat på hur skilda koncept inom fysiken kan vara besläktade. I denna avhandlingen kommer vi att se exempel på hur kända fysikaliska koncept kan undersökas genom att titta på små, enkla system. Vi studerar dessa (fåpartikel) system för att avgöra om de uppvisar beteende som är nära besläktat med större och mer komplicerade system.

De partiklar som bygger universum, och som vi alla omges av, är i regel delar av större sammanhang. Partiklar utgör ofta mindre delar av stora *statistiska* "ensemblar" av partilkar, såsom metaller, gaser, eller isblock. I viss mån går det att studera enskilda partiklar inom fysiken, men det är ofta mycket svårt att förutsäga exakt hur en enskild atom rör sig i en metall. Man kan jämföra med politiska opinionsundersökningar, vilka effektivt kan beskriva det allmänna politiska klimatet i ett land, men inte kan förutsäga exakt hur Åke Gustavsson (53 år) i Falköping ska rösta. I en statistisk modell av, till exemplel, en metall är partiklarna på samma sätt delar av ett större sammanhang, och deras kollektiva egenskaper beskrivs enklast med koncept såsom temperatur eller elektrisk resistans. Man kan enkelt säga att storskaliga (makroskopiska) effekter hos material med miljontals atomer ofta kräver en förenklad, statistisk modell, medan småskaliga (mikroskopiska) effekter hos ett fåtal atomer kan beskrivas på ett mer direkt sätt. Det är kanske möjligt att författa en uttömmande bokserie om Åke och hans familj för att förklara hans politiska ställningstaganden, men svårt att göra detsamma för alla personer i Sverige och samtidigt presentera en allmän bild om det politiska läget.

Kvantmekanik och ultrakalla system

Många av de mest intressanta experimenten inom ämnet fysik sker idag vid så kallade *ultrakalla* temperaturer. Ultrakalla temperaturer innebär att ett system är nedkylt till endast några få nanokelvin (10^{-9}) över absoluta nollpunkten $T_0 \approx -273.15°$ Celsius. Vid dessa temperaturer är det ofta enklare att förstå och renodla fysikaliska processer. Man kan föreställa sig en låda innehållande en gas av atomer. Vid höga temperaturer far atomerna runt och studsar i ett enda virrvarr, och det är därför mycket svårt att förutsäga hur en enskild atom rör sig. Vid låga temperaturer rör sig däremot atomerna långsammare och på ett mer förutsägbart sätt, vilket kan göra det lättare att studera, eller till och med att styra dem, på detaljnivå. Vid ultrakalla temperaturer är det ofta möjligt att kontrollera viktiga egenskaper hos en gas, som till exempel interaktionen mellan dess atomer. Det är därför möjligt att bygga artificiella system som liknar naturliga material, (som till exempel magneter eller molekyler), och därigenom studera dem.

För att korrekt beskriva vad som händer i den mikroskopiska världen, som befolkas av atomer och elektroner, används i regel *kvantmekanik*. Kort sagt är kvantmekanik ett språk som förklarar hur den mikroskopiska världen beter sig. Ett sådant språk är helt nödvändigt eftersom det i denna värld sker saker som annars är svåra att formulera och beskriva. I kvantmekanikens värld kan partiklar till exempel ”vara på olika platser samtidigt”, eller färdas rakt igenom väggar”; saker som är omöjliga i vår vanliga värld. Vi kan genom kvantmekanikens språk formulera frågeställningar och svar för hur mikroskopiska system beter sig. På samma sätt som vi kan förutsäga solförmörkelser genom att ställa upp formler och ekvationer för himlakroppars rörelse, kan vi förutsäga partiklars beteende genom att formulera ekvationer och sedan lösa dem. Ett exempel på en ekvation inom kvantmekaniken är den berömda Schrödingerekvationen.

Från en handfull till miljoner atomer

Att beskriva ett litet system med ett fåtal atomer som interagerar, exempelvis genom att krocka med varandra, är relativt enkelt. Till exempel är det mycket väl möjligt att i detalj förutsäga mycket om hur en vätemolekyl, bestående av två atomer, kommer att bete sig. Att däremot beskriva en miljon krockande atomer är en stor utmaning. Det är ofta möjligt att formulera en ekvation som indirekt beskriver alla atomers rörelse, även om det rör sig om miljoner atomer. Problemet är dock att lösa ekvationen. För ett fåtal atomer är detta ofta möjligt, till exempel med hjälp av datorer, även om det kräver mycket arbe-

te. En detaljerad ekvation som beskriver en handfull atomer kan till exempel ta dagens snabbaste datorer flera veckor att lösa. Jämför detta med uppgiften att sortera en vanlig telefonkatalog i nummerordning istället för namnordning. Även om telefonkatalogen innehåller *alla* personer i hela Sverige skulle detta ta mindre än en sekund för en vanlig bärbar dator.

Detta visar på en av de stora utmaningarna inom modern fysik. Hur kan vi beskriva ultrakalla system med miljontals atomer utifrån detaljerade beskrivningar av de enskilda atomerna? Ofta ligger lösningen i att förenkla ekvationerna genom att slänga bort oviktiga delar av de detaljerade beskrivningarna. En annan lösning är att istället behålla alla detaljer, men att faktiskt bara studera ett fåtal atomer. Detta är såklart en stor förenkling om målet i slutändan är att, till exempel, beskriva magnetism för en miljon ultrakalla atomer. Situationen är dock inte hopplös, eftersom det faktiskt finns flera mer eller mindre enkla teorier om hur magnetism fungerar. Ofta kan teorierna direkt användas till att beskriva de ultrakalla systemen, och därigenom göra enklare förutsägelser för hur de beter sig. Vi kan då luta oss mot dessa förutsägelser och leta efter tecken på samma beteende i de detaljerade, små, systemen. Vi kan därigenom skapa en bryggamellan de detaljerade modellerna (som fungerar för få partiklar) och de enklare modellerna (som fungerar för många partiklar).

I denna avhandling undersöker vi en rad olika fysikaliska effekter genom att simulera dem med små fåpartikel system". Vi formulerar detaljerade ekvationer för en rad olika system, och utvecklar parallellt metoder för att lösa dessa med hjälp av datorer. Vi fokuserar främst på att utveckla ekvationer och lösningsmetoder som kan användas för att studera fysikaliska processer som uppkommer i system med ett större antal partiklar.

Ett exempel. Higgspartikel i system med ett fåtal atomer

Tack vare de uppmärksammade experimenten på partikelacceleratorn CERN är det nu mycket troligt att Higgspartiklar faktiskt existerar. Dessa partiklar bekräftar teorin om Higgsmekanismen, vilken förklarar hur alla partiklar i universum får sin massa. Higgspartiklarna själva kan sägas vara en biprodukt av Higgsmekanismen.

En av de mest intressanta aspekterna av partikelfysikens Higgsmekanism är att dess teoretiska byggstenar faktiskt kommer från ett helt annat fält inom fysiken, nämligen *kondenserad materia*. Flera år innan teorin för Higgsmekanismen formulerades arbetade folk på liknande teorier för att förklara hur, till exempel, supraledare fungerade. Det visar sig att särskilt en modell, vilken används

för att beskriva vissa typer av ultrakalla atomgaser, har många likheter med Higgspartikeln själv. Vi nudersöker här en modell för denna speciella typ av gas, fast med endast ett fåtal atomer, för att se om den uppvisar några tecken på de egenskaper som vi associerar med Higgspartikeln. Genom att lösa Schrödingerekvationen för detta artificiella system kan vi påvisa en rad likheter mellan Higgspartikeln och vår modell. Därför tror vi oss ha identifierat ett förstadium till en Higgspartikel i ett system med få atomer. Vi visar även hur det med dagens tillgängliga experiment är möjligt att direkt mäta egenskaperna hos detta förstadium till Higgspartikeln.

Introduction

1 Ultracold atoms and few-body systems

The research field of ultracold atoms is today very active both within experimental and theoretical physics. In principle, the cooling of atomic gases is a way to exercise control over happenings in the microscopic world. Much like when taming a wild animal, we need control to understand and harness the complex nature of the beast, or in this case the atoms.

A dilute gas of atoms or molecules can be cooled down to extremely low (ultracold) temperatures, typically lower than a few microkelvins (μK) where particles essentially have no thermal motion [1–5]. Such systems allow for the study of coherent macroscopic many-body states, in which a large number of particles share the same quantum-mechanical state, and might, therefore, exhibit quantum interference effects. The perhaps most well known example of such a state is the atomic Bose-Einstein condensate [6, 7], which was first realized in 1995 [1, 8, 9].

Coherent many-body states of macroscopic matter are typically associated with concepts such as superconductivity, known from the field of condensed matter which dates back to Ginzburg and Landau [10]. These types of systems may exhibit exotic many-body behavior, such as, for example, superfluidity and quantized vortices, see e.g. [11–14], arising from statistics of the constituent particles and the interactions amongst them.

In particular, ultracold systems with short-range interactions between particles is a well-studied topic. For ultracold systems, the van der Waals forces between two atoms can be approximated by considering only the lowest order of angular momentum l in their relative motion, see for example [15]. For $l = 0$ (s-wave scattering), the low-energy scattering is spherically symmetric and can be approximated with Fermi's contact pseudopotential [16, 17]. Short-range in-

teractions can dramatically influence the properties of an ultracold system and have given rise to a plethora of intriguing many-body effects. For a review see e.g. [15, 18].

However, different types of interactions can be considered. In an ultracold gas of dipolar atoms or molecules, dipole-dipole interactions may have striking effects on the physical properties of the system. This type of interaction is, in contrast to s-wave scattering, long-range and anisotropic, and can give rise to complex correlations between particles and additional experimental parameters, such as the dipole's alignment relative to a trapping potential [19, 20].

An ultracold system can be made very pure and free from imperfections, and it can also be kept trapped and isolated from the surrounding environment until measured upon. This isolation allows for a high degree of control where, for example, the scattering properties of atoms may be tuned via so-called Feshbach resonances, see e.g. [21, 22] for a general background and [23, 24] for cold-atom implementations. In cold-atom experiments the effective dimensionality of the system can also be designed experimentally, see for example [15, 18, 25].

When building a model for an ultracold system, it is in many cases possible to write down highly accurate, but relatively straightforward, microscopic equations in terms of only a few parameters which correctly describe the particles and their interactions. This high degree of control manifests a strong connection between experiments and theory, where simple quantum mechanical models are employed to make predictions of the physical features in a system, and where experiments often can directly test predictions. Furthermore, if we can solve the equations for a range of values for the fundamental parameters, we may also predict new phenomena in a larger set of systems, simply by tuning the parameters. It is possible to compare distinct but closely related systems - for example, two different atomic ultracold gases with similar scattering properties, but with different atomic masses. We may also answer hypothetical questions like; "What would happen if the atoms in this gas were subject to interactions that are not spherically symmetric?". For a review on ultracold many-body systems, see for example [15, 19, 20].

Cold-atom *few-particle* systems with tunable interactions are especially valuable since they allow for a highly detailed description of the microscopic physics, but yield equations that are possible to solve. For a trapped ultracold system of fermions, it is now possible to deterministically prepare and measure on states with only one to ten interacting particles [26, 27]. This possibility has opened up a new area of research in which solvable interacting few-body systems can be directly investigated in experiments. By directly accessing the observables

of a few-body system in this way, it is possible to gain deeper insight into the microscopic physics and hopefully understand how macroscopic interaction effects develop with increasing particle number, both in theory and experiments.

At ultracold temperatures, particles go into the lowest energy state, or ground state, of the system and consequently many of the measurable features of the gas crucially depend on the nature of this ground state. However, many properties of a quantum-mechanical system are also determined by the nature of its excited states especially in cases where the system responds to external perturbations. This thesis concerns quantum-mechanical simulations of ultracold few-body systems with interactions, both in their ground state and in excited states.

The starting point for all the studies here is the formulation of a few-particle Hamiltonian and the time-independent Schrödinger equation for the eigenvalues and eigenstates

$$\hat{H}|\psi\rangle = E|\psi\rangle.$$

To begin with, the Hamiltonian $\hat{H}$ should include all relevant physics and characteristics of some basic model, such that interesting emergent phenomena are reproduced in the correct limits. Secondly, it should represent a microscopic few-body system that is numerically solvable to high precision, at least in the limit of very few particles. Finally, it should be a microscopic representation of an experimentally realizable system, so that the predictions can be tested.

In short, we deal with physics that in different ways manifest itself in simple few-particle model Hamiltonians. Some examples of the few-body systems in question are sketched in Fig. 1. The focus here lies on cases where the solutions of microscopic few-particle systems can be found using exact diagonalization. The results are used in predictions for experiments, and also to investigate and scrutinize phenomenological or less detailed models. In this way, the few-body systems offer table-top tools for simulation of larger systems and more general physical effects, which all the projects in this thesis are examples of.

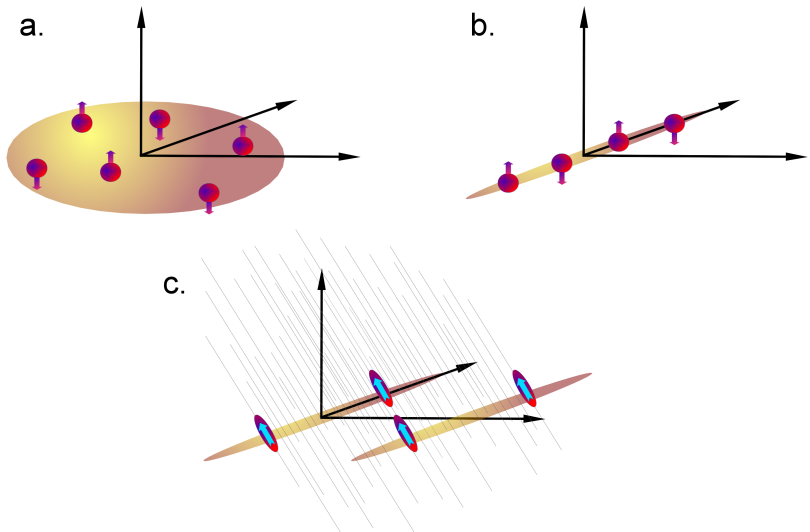

Figure 1: Sketch of a few different setups used throughout the thesis. The round balls with arrows indicate particles with either up $(+1/2)$, or down $(-1/2)$ spin. The ovals with cyan arrows indicate dipolar particles with dipole-moment along the arrows. Upper left: 2D harmonic trap with spin-$1/2$ particles. Upper right: Quasi-1D Harmonic trap with spin-$1/2$ particles. Lower: Two 1D harmonic traps filled with particles with dipole-moments aligned by an external field, with field-lines indicated by thin, gray lines.

2 Exact diagonalization - an overview of methods

A starting point for investigations of a model Hamiltonian $\hat{H}$ is to ask if the resulting equations can be solved directly or if they are subject to approximations. We want to solve the Schrödinger equation, which means that we look for eigenvalues of the Hamiltonian. An exact solution can sometimes be found analytically, but in general numerical methods are required. One of the most common methods for numerically solving the Schrödinger equation is exact diagonalization. Depending on the particular branch of physics, different names may be used for this method, like for example *configuration interaction* in quantum chemistry and theoretical atomic physics. For a detailed overview of these methods, see e.g. [28, 29].

In this method, which we from now on call exact diagonalization, a series expansion over some set of basis states $|v_i\rangle$ is used to approximate the equations. An a priori unknown state $|\psi_j\rangle$ is expanded in terms of the basis states and a set of expansion coefficients c_i as

$$|\psi_j\rangle = \sum_{i=1}^{M} c_i |v_i\rangle. \tag{1}$$

Here M denotes the number of basis states that are used in the expansion. The exactness of the series expansion approximation crucially depends on the choice of basis states $|v_i\rangle$. If the basis states correspond directly to exact solutions of the original equation, $|\psi_j\rangle$ will naturally be exact. On the other hand, the basis states might be chosen so that $|\psi_j\rangle$ merely represents an approximation of the exact solution $|\tilde{\psi}_j\rangle$.

In many cases, it is possible to construct an infinite complete set of basis states for the Schrödinger equation, such that any exact solution may be expanded in that basis. In theory, the solutions and the corresponding physical observables can then be calculated to arbitrary precision. In practice, however, depending on the choice of basis, a finite (truncated) expansion is often sufficient if all relevant observables converge with respect to the number of terms in the series. The projection of the Schrödinger equation onto a finite space leads to a representation of the Hamiltonian as a finite-size matrix and the solutions as finite-size vectors. The goal is to diagonalize the matrix to reveal the eigenvalues and eigenvectors, which correspond to approximate solutions of the original equation. We generally look for high precision in the approximations, but for time-purposes, we naturally want to keep the matrix small and easy to diagonalize. Here, the selection of basis states again plays a role. By properly selecting and ordering the basis states, for example by exploiting symmetries in the Hamiltonian, the form and size of the matrix may be designed to make the task of diagonalization easier. In many cases a proper exploitation of symmetries allows us to construct block-diagonal matrices, which significantly reduces the time required for diagonalization. For an overview of numerical diagonalization see for example [30].

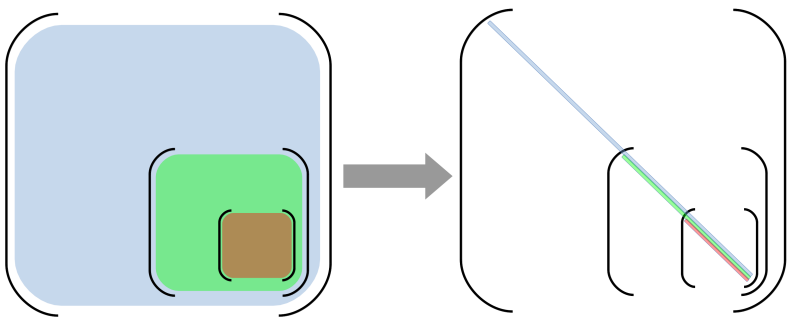

Figure 2: Sketch of a set of successively larger matrices corresponding to successively larger basis-sizes. Increasing the size of the basis corresponds to a more accurate representations of the system and a larger set of eigenvalues.

Within this thesis, I present results that are retrieved via many different methods and techniques to solve this one basic task. For any given project a lot of different

methods and tricks were tried and tested, and some of them did not turn out to be successful. It is, however, relevant to briefly summarize some of these methods, even if all of them are not used for the final results. In fact, the success or failure of a method often gives deep insight into the system which it is applied to.

2.1 Cut-off parameters

In most cases, a basis set can be labeled according to one or more relevant parameters. For example, we can choose to label a basis of 1D plane-wave functions $e^{ip\cdot x}$ in terms of the maximum value of momentum p in the set. (Here x is the spatial coordinate). The right choice of parameters is therefore often crucial to achieving convergence in calculations; since the parameters directly represent the level of detail in which we describe a physical process. Let us consider a Hamiltonian comprised of two terms

$$\hat{H} = \hat{H}_A + \gamma \hat{H}_B$$

where γ is a small number. If one has access to a complete set of eigenstates and eigenvalues for the operator $\hat{H}_A$ it is often beneficial to choose a basis comprised of these states to solve for the complete Hamiltonian $\hat{H}$. A typical choice for a parameter which defines a set of basis states $|v_i^B\rangle$ is an upper bound on the corresponding eigenvalues ϵ_i^B, such that the basis-set ζ is defined by

$$|v_i^B\rangle \in \zeta \quad \text{if and only if} \quad \epsilon_i^B < \epsilon_{\text{cut}}.$$

In general, multiple combined cut-off parameters are used in a single simulation, forming a "cut-off scheme." Choosing the correct cut-off scheme requires an understanding of the basis and the system, but can often significantly improve convergence in numerical simulations.

2.2 Iterative selection of basis states

Iterative methods of basis selection are used in different areas of physics and can often help to improve convergence in complex simulations - especially when a system does not have a known structure, or it changes over time. For implementations and a more comprehensive overview of the iterative basis selection, see e.g. [31].

Here, the method consists of an iterative scheme (outlined in Fig. 3) which uses some operator $\hat{H}$ and a complete set $\mathcal{F}$ of analytical functions as a reference.

One starts with some initial guess for a small truncated basis $\mathcal{G}_1$ and proceeds to diagonalize the Hamiltonian within this subspace, retrieving the ground state $|0\rangle_1$. Stepping through the elements of $\mathcal{G}_1$, all parts in $\mathcal{F}$ that couple to $\mathcal{G}_1$ via $\hat{H}$ are added to an intermediate set. For each element in the intermediate set, the overlap with the ground state is calculated. An element is then added to the basis $\mathcal{G}_1$ if the overlap exceeds some cut-off parameter c, which may vary over the iterations. After adding all new states to $\mathcal{G}_1$ we rename it $\mathcal{G}_2$ and the process is repeated until convergence of the relevant observables.

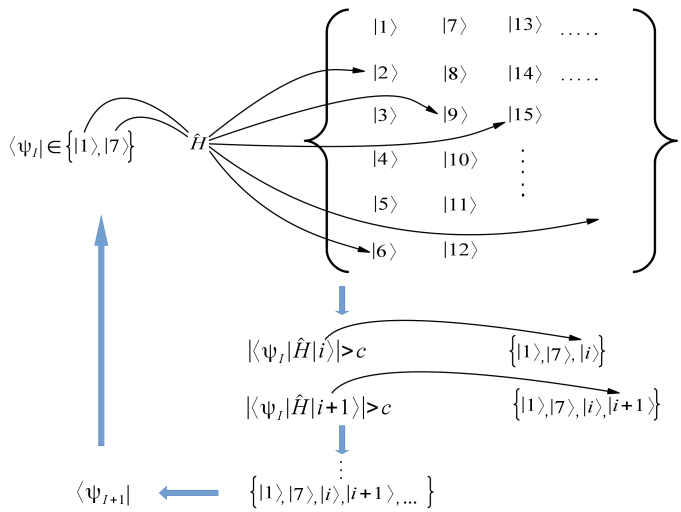

Figure 3: Sketch of the iterative basis selection method. The basis grows successively by including states with sufficient overlap with the ground state.

2.3 Tailored basis

An alternative to optimizing the selection of basis states from some set of analytical functions is to optimize the basis states themselves. This may be done in different ways, for example by diagonalizing the single-particle part of the Hamiltonian (if it is not already diagonal) and building a new basis from the eigenstates. Another common method is to define single-particle functions on a spatial grid and optimize them using the Hartree-Fock method, see e.g. [32] for applications in atomic physics. Recently, a multi configuration Hartree-Fock approach has been successfully applied for ultracold atoms [33].

One of the most commonly used methods for exact diagonalization is to employ the B-spline basis, also discussed in section 7. B–splines are piece-wise polyno-

mials which may be defined through recursive relations [34]. In principle, the single-particle basis can then be adapted to a given problem by defining spatial regions which are described with a high level of detail. Therefore, an intuitive understanding of a system in terms of spatial properties can be transferred directly into the B-spline basis, which in most cases proves to be a very effective choice, for a review see e.g. [35].

Other choices of tailored basis functions include for example correlated Gaussian functions, for a review see e.g. [36, 37], and Jastrow-type wavefunctions [38, 39], for a review see e.g. [40].

2.4 Approximated and modified operators

In many cases, the form of the Hamiltonian proves to be a problem that cannot be solved by optimizing the basis. In these cases, the only remedy is often to eliminate parts of the Hamiltonian that are known to cause problems. The hope is to capture the necessary features in the initial model but to remove or regularize parts in the Hamiltonian representation in a way that can be justified. The numerical limitations may enter already in the setup of a problem so that the choice of, for example, a pseudopotential is motivated both by physical accuracy and by numerical stability.

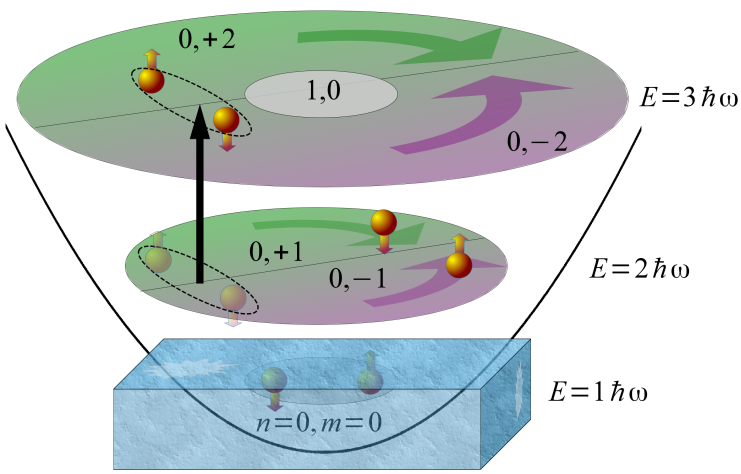

Figure 4: Sketch of a frozen-core 2D harmonic oscillator with two-component fermion system. The pseudopotential allows for excitations from the highest occupied shell, but not from the "frozen" core shells.

One example is the frozen-core model, well known in nuclear physics (see e.g. [41]), for a filled-shell 2D harmonic oscillator with interacting fermions,

which is discussed in relation to Higgs modes in section 6.6. Here we choose a delta function $\delta(\mathbf{x_1} - \mathbf{x_2})$, where $\mathbf{x_i}$ denotes spatial position of particle i, to represent the interaction in 2D. The pseudopotential is however also subject to the approximation that excitations from shells below the Fermi level are forbidden (the core-shells are frozen). In effect, this gives a more sparse Hamiltonian matrix that is easier to diagonalize. The approximation can be implemented by imposing conditions on the second-quantized form of the Hamiltonian, and it can be shown to give a good approximation of the exact system in the limit of weak interaction.

3 Short-range interacting gases in one dimension – an introduction to Tonks-Girardeau states

This section gives a brief introduction to 1D systems with short-range interactions, and in particular to Tonks-Girardeau states and super Tonks-Girardeau states, which are central in papers II-IV. For a more detailed overview of Tonks-Girardeau states and 1D systems with short-range interaction, see for example [42].

Let us first focus on an effective 1D system with short-range s-wave scattering. Cold atoms with strong short-range interaction confined in 1D quantum wire geometries have been achieved using deep optical lattices [43–45]. Let us consider atoms with mass m trapped in a 1D harmonic wire with oscillator length $l_\perp = \sqrt{\hbar/m\omega_\perp}$, where $\omega_\perp$ is the radial frequency of the trap. Here, the low-energy s-wave scattering between atoms, with spatial coordinates z_1 and z_2, can be represented by an effective 1D delta pseudopotential as

$$V(z) = g_{1D}\delta(z_1 - z_2). \tag{2}$$

This potential is obtained from Fermi's 3D contact pseudopotential for s-wave scattering [16, 17], where the scattering amplitude is specified by the 3D scattering length a_{3D}. In the effective 1D model the interaction strength g_{1D} can be given in terms of the 3D scattering length a_{3D} as $g_{1D} = 2\hbar\omega_\perp a_{3D}/(1 - C \cdot a_{3D}/l_\perp)$, with the numerical constant $C = 1.034$ [46]. By changing a_{3D}, for example with Feshbach resonances, g_{1D} can thus be changed to both positive and negative values with a so-called confined-induced resonance (CIR) at $l_\perp = C \cdot a_{3D}$ [15, 46]. In the following, we can, therefore, treat the interaction strength as a tunable parameter in effective 1D models.

3.1 Tonks-Girardeau states

The concept of Tonks-Girardeau (TG) states was first described by Girardeau in 1960 [47], who showed that in 1D, the wavefunction for a set of bosons with impenetrable cores could be one-to-one mapped to that of spinless fermions. An impenetrable core means that two particles cannot be found at the same position, a boundary condition that can be said to mimic the Pauli exclusion principle between spinless fermions [47]. The impenetrable core boundary condition can be realized by an infinitely strong, $1/g_{1D} \to 0$, effective 1D contact pseudopotential, see for example [48–51]. By using Feshbach resonances and CIRs, TG states have in this way been realized experimentally, see e.g. [43, 44]. The significance of TG states has been highlighted in papers on effective models applied to trapped few-body 1D ultracold atoms (see paper II and [52]). One important aspect of TG states, which is exploited in these models, is that in the unitary limit, $1/g_{1D} \to 0$, the configuration space of a few-particle state splits into several distinct sectors [53].

In a TG state, the absolute value of the many-body wave function is reduced to that of non-interacting spinless fermions. This is known as *fermionization* of particles, a word that comes from the fact the many of the properties and observables of the bosonic 1D gas are similar to that of a fermionic gas. There are however some significant differences between a fermionized gas and a true fermionic gas, like for example the momentum distribution which is rather different in the two cases, see e.g. [47, 48, 50]. For the momentum distributions to also become identical, the particles must enter the localized regime where there is no overlap between the wave packets of the individual particles in the system. The localization cannot be achieved by a zero-range potential such as the delta function but requires a long-range interaction like, for example, the dipole-dipole interaction which has been seen to give rise to a few-body precursor of a Wigner localized state [54].

Fermionization has been studied for a number of different 1D systems with strong short-range interactions, where the wavefunction of the interacting particles can be mapped onto that of spinless fermions. It occurs for both bosons, different-spin fermions, and for distinguishable particles, see for example [47, 49, 55–58] and paper IV.

A TG many-body state has a spatial separation between the constituent particles, which avoid each other due to repulsion, and is sometimes referred to as a "gaseous" state. When the repulsive interaction in a 1D system is infinitely strong, the probability of finding two particles at the same position is zero in states with finite energy. For a contact-interacting set of particles, this means

that the states become insensitive to changes in the interaction strength in this limit and appear as horizontal lines in spectra plotted for varying interactions. In a homogeneous system, this means that the energy per particle is purely kinetic [15, 43]. The formation of a TG gas has also been investigated for two-body bound complexes, known as *dimers*. A system with attractive spin-1/2 fermions can evolve into a superfluid of bound complexes which behave as bosonic particles, which in turn can form a TG gas [56].

A number of numerical studies on few-body systems have specifically addressed the development of TG states in the intermediate regime of finite interaction strength g_{1D} in terms of eigenenergies, as well as 1D single-particle densities

$$\rho^1(z) = \langle \hat{\Psi}^\dagger(z)\hat{\Psi}(z)\rangle \tag{3}$$

and two-body correlations

$$\rho^2(z_1, z_2) = \langle \hat{\Psi}^\dagger(z_1)\hat{\Psi}^\dagger(z_2)\hat{\Psi}(z_1)\hat{\Psi}(z_2)\rangle. \tag{4}$$

Here $\hat{\Psi}(z) = \sum_i v(z)_i \hat{a}_i$ denotes a field operator with respect to a basis of single-particle wavefunctions $\{v(z)_i\}$ and annihilation operator $\hat{a}_i$. It was seen that these properties evolve continuously towards the TG-limit [50, 58, 59].

A TG state can also be realized for dipolar particles in a quasi 1D trap, where the dipoles can be aligned perpendicular to the trapping direction. In 1D, the $1/x^3$-behavior of the dipolar interaction can serve to completely fermionize particles at finite interaction strengths [54, 60].

3.2 Super-Tonks-Girardeau states

An extension of the concept of a TG state can be made by studying the regime of attractive interaction, $g_{1D} < 0$ in Eq. (2). We can imagine an experiment where a system is prepared into a TG state via an infinitely repulsive interaction. If the interaction is adiabatically changed from g_{1D} to $-g_{1D}$ the state develops into a bound few-body complex, i.e., a cluster state, which is the true ground state for the strongly attractive interaction [61]. For a sudden shift in the interaction strength, which for example can be achieved by a slowly tuning of a_{3D} across a CIR, the outcome is however different. In fact, after a sudden switch in g_{1D}, the resulting state is metastable in the attractive region, as confirmed both by theory [61–63] and experiments, see e.g. [64] and paper III of this thesis. This type of metastable state is commonly known as a *super-Tonks-Girardeau* (STG) state, and it retains the fermionized nature of the TG state, which prevents it from collapsing into the cluster ground state [62]. The evolution of few-body

STG states from weak to strong attractive contact interactions has also been investigated by numerical solutions of few-body systems. When the contact interaction was tuned from $g_{1D} = 0$ towards $g_{1D} \to -\infty$, the eigenenergies, single-particle densities and two-body correlations evolved continuously towards those of spin-polarized fermions [51].

To showcase the formation of TG and STG states in a few-body system, a simple example with two harmonically trapped contact-interacting particles is presented in the appendix.

In general, the realization of an STG state depends on the possibility to tune the interaction strength from positive to negative values. This tunability is a well-known feature of dipolar systems [65], and a theoretical study predicts that dipolar version of an STG can be realized by sudden rotations of the dipolar orientation relative to the confinement in a 1D harmonic trap [66].

4 Short-range interacting ultracold gases in two dimensions

Like in the case of ultracold atoms confined in 1D, Fermi's pseudopotential for low-energy scattering in a 2D confined geometry can be reduced to an effective 2D form, see for example [67–69]. For a detailed overview of short-range interactions in 2D ultracold gases, see e.g. [15, 18].

We consider a trapped ultracold gas of atoms with mass m in the Gaussian ground state of a confining potential $V(z) = m\omega_z z^2/2$ with trapping frequency ω_z along the spatial direction z. In the regime where the trapping length $l_z = \sqrt{\hbar/m\omega_z}$ is much larger than the 3D scattering length $l_z \gg a_{3D}$ an effective 2D pseudopotential can be obtained by integrating the 3D pseudopotential over the lowest hamonic ground state. This gives an effective 2D coupling strength

$$g_{2D} = 2\sqrt{2\pi}a_{3D}/l_z.$$

We also note that, like in the case of 1D confinement, confinement induced resonances may be employed to reach the strongly interacting regime, see for example [18, 68].

Results

This chapter gives an overview of the papers in this thesis. The text is divided into three different sections, each representing a specific subject in the dissertation.

5 Quantum magnetism in a one-dimensional harmonic oscillator

In papers II-IV, a spin-chain model for quantum magnetism is investigated in terms of a few-particle 1D harmonic system with particle-particle contact interactions (upper left in Fig. 1). In the strongly interacting limit, the few-body Hamiltonian reduces to an interacting Heisenberg spin chain, which is used to predict several magnetic phases. These results are verified both numerically, by exact diagonalization in the few-body limit, and experimentally, via measurements of out-tunnelled particles. Through a collaboration involving numerical, analytical and experimental work, the magnetic properties of an ultracold, 1D Fermi gas are mapped out and investigated in the few-particle limit. This work lays the foundation for a cold-atom implementation of one of the fundamental tools in simulations of quantum magnetism.

5.1 Background

Over the recent years, ultracold atoms have been successfully applied in simulations of quantum magnetism in condensed matter systems, see e.g. [25, 70, 71]. As discussed in the introduction, the high degree of control offered by cold-atom experiments has made it possible to investigate models over large parameter-spaces, allowing experimentalists also to address, for example, the study of phase transitions in complex systems, see e.g. [15, 25, 72, 73].

In particular, ultracold gases in optical lattices have been used to simulate many simple models describing magnetism, for a review see for example [25, 73]. Optical lattices were used to realize the super-exchange of particles [74], here in a double-well potential, which is a crucial component of many models that describe magnetism. A quantum Ising model was realized for a 1D lattice and was used to simulate anti-ferromagnetic order for a spin chain [75, 76]. Another example of a model for magnetism is the Heisenberg spin chain [77].

5.2 The Heisenberg spin-chain Hamiltonian

A Heisenberg spin chain is a model for spin-1/2 particles on a 1D lattice interacting with spin-spin interactions and is commonly used in studies of quantum magnetism. Like the Ising model it describes phase transitions and magnetic behavior in the 1D system, but also it uses a quantum-mechanical treatment of the spins [77]. For an introduction to spin chains see e.g. [77, 78].

For a lattice with N sites and N spins, with either spin up or down, the total Hilbert space can be constructed as follows: Each site has a two-dimensional subspace $\mathcal{C}^2 = \{\uparrow, \downarrow\}$ spanned by the spin eigenstates in the spatial x-direction. For N sites, the Hilbert space then has 2^N dimensions. A spin-operator $\hat{S}_i^x$ along the spatial direction x acts only on one site i, and obeys the usual spin-commutations on that site. With nearest-neighbor spin-spin interaction and couplings $J = J_x = J_y = J_z$, the spin-space representation of the Heisenberg Hamiltonian (or so-called XXX-model, where the name hints at the isotropy of the couplings) reads

$$H_{XXX} = -J\frac{1}{2}\sum_{i}^{N-1}\left(\sigma_i^x\sigma_{i+1}^x + \sigma_i^y\sigma_{i+1}^y + \sigma_i^z\sigma_{i+1}^z\right) \tag{5}$$

where σ_i^x is the Pauli spin-matrix for direction x operating on site i. One example of a physical system modeled by a spin chain is a set of localized spin-1/2 particles on a line, with the spatial orbitals subject to exchange interaction. Here, the spin-chain model successfully accounts for (anti)ferromagnetic order amongst the spins. Since the Hamiltonian conserves total spin in x, an instructive example is to consider a subspace of $N_\uparrow$ spin-up particles and $N_\downarrow$ spin-down particles. This subspace is spanned by all different spin-functions $|\kappa\rangle$ constructed from the $N_\uparrow + N_\downarrow$ spins,

$$|\kappa\rangle = P\{|\uparrow,\uparrow,..,\downarrow,\downarrow,..\rangle\},$$

where P denotes all distinct permutations of the spin-order. The Hamiltonian in Eq. (5) can also be reformulated in terms of the permutation of two neighboring

spins

$$H_{XXX} = -\frac{NJ}{4} - \frac{J}{2}\sum_{i}^{N} P_{i,i+1}$$

with

$$P_{i,j}|... \uparrow_i, .. \downarrow_j, ..\rangle = |... \downarrow_i, .. \uparrow_j, ..\rangle,$$

The eigenstates to the Hamiltonian can be found numerically or via, for example, the Bethe ansatz, see e.g. [79].

5.3 Model for realization of the Heisenberg spin chain

The spin-spin interaction and ordering in the Heisenberg spin-chain model may be realized without the aid of an optical lattice, as is shown in paper II. This is done by employing an infinitely strong repulsive contact interaction between particles confined in a 1D harmonic trap, also discussed section 3, with oscillator frequency ω,

$$\hat{H} = \sum_{i=1}^{N}\left(-\frac{\hbar^2}{2m}\frac{\partial^2}{\partial z_i^2} + \frac{1}{2}m\omega z_i^2\right) + g_{1D}\sum_{i,j}\delta\left(z_i - z_j\right). \tag{6}$$

Here g_{1D} is the effective 1D interaction strength, as described in section 3. Throughout this chapter we use dimensionless units $\hbar = m = 1$. Energies are given in units of $\hbar\omega$, lengths in units of oscillator-length $l = \sqrt{\hbar/m\omega}$ and interaction strength g_{1D} in units of $\hbar\omega l$.

In the limit of $1/g_{1D} \to \pm 0$ the eigenvalues to this operator can be found by a generalization of Girardeau's Bose-Fermi mapping, as referenced in relation to Tonks-Girardeau states in sections 3. The spatial part of the eigenfunctions can then be defined in terms of ψ_F, the wavefunction of N non-interacting spinless fermions, and an additional factor that describes the spatial ordering of the particles. The so-called spatial *sector* wavefunctions are formally constructed according to

$$\langle z_1, ..., z_N|P\rangle = \sqrt{N!}\theta\left(z_{P(1)}, ..., z_{P(N)}\right) A\psi_F \tag{7}$$

where the *unit antisymmetric* function $A = \prod_{i<j}\mathrm{sgn}(z_i - z_j)$ ensures that the wavefunction is correctly symmetrized. Also, $\theta\left(z_{P(1)}, ..., z_{P(N)}\right) = 1$ if $z_1 \leq ... \leq z_N$ and otherwise zero, which defines the order.

An orthonormal subset of sector functions can be spanned by considering all possible permutations of the spin-order. Now, the full eigenstates of the non-

interacting systems should also include spin-functions,

$$|\chi\rangle = \sum_{m_1,...,m_N} c_{m_1,...,m_N} |m_1, ..., m_N\rangle$$

where $c_{m_1,...,m_N}$ is an expansion coefficient and m_i are spin quantum numbers. Since the asymmetry of the total wavefunction has to be conserved, the spin-functions must be paired with specific spatial functions. In fact, the eigenfunctions can be obtained directly via the map

$$W_\pm|\chi\rangle = \sqrt{N!} S_\pm \left(|\mathrm{id}\rangle|\chi\rangle\right), \tag{8}$$

where $|\mathrm{id}\rangle$ is the identical permutation of the spatial function, and $S_\pm$ is the (anti)symmetrization operator which includes the (anti)symmetric sum over all permutations P of the spin and order. The map in Eq. (8) gives a one-to-one correspondence between spin-functions and the eigenfunctions of the multicomponent system, and the Hamiltonian matrix can, therefore, be written purely in terms of the spin-functions. At infinite interaction, $1/g_{1D} \to \pm 0$, the two-component Hamiltonian is diagonal in the spin-functions, since the ground state becomes a degenerate manifold. For finite interactions, the degeneracy is broken, but for sufficiently strong interactions it is possible to describe the energy-splitting within degenerate perturbation theory. The coupling, arising from $1/g_{1D} \neq 0$, is then represented in terms of matrix-elements between the spin-functions. The spin density of component m can be fully determined by the N-tuple $\left(\rho_m^1, ..., \rho_m^N\right)$ which directly relates to the spin-function.

For lowest order in $1/g_{1D}$ the Hamiltonian of the multicomponent system can be represented as (see paper II)

$$H_S = \left(E_F - \sum_{i=1}^{N-1} J_i\right) \mathbb{I} \pm \sum_{i=1}^{N-1} J_i P_{i,i+1}, \tag{9}$$

which has the form of a spin-chain Hamiltonian with site-dependent couplings J_i, which are calculated via N-dimensional integrals involving the spatial sector-functions. Approximations of the couplings, with the accuracy growing with N, are also available.

5.4 Methods

The Hamiltonian in Eq. (6) is solved for different interaction strengths g_{1D} using exact diagonalization in the Fock-space built from single-particle harmonic basis functions with cut-off energy E_{cut}. The interaction is given in terms of an

exact delta function with matrix elements given by a recursive relation [42]. We treat the problem in the few-body limit with different configurations of spin-up and spin-down particles like, for example, a system with two spin-up and one spin-down fermion which we denote by (2+1). The convergence with respect to E_{cut} strongly depends on the interaction strength g_{1D}. As g_{1D} increases, particles in states of the low-lying spectrum acquire successively higher components of momentum, indicating that E_{cut} has to grow to represent the system correctly [50]. The calculations for the eigenstates are hence very tricky and time-consuming. Different approaches can also be used to solve this problem, such as the *coupled-cluster* method (see e.g. [80]). The spin-chain model for the microscopic Hamiltonian in Eq. (6) is therefore not only a goal in itself, but a tool for numerical simulations of strongly interacting 1D systems, since the low-energy properties in this regime can be calculated from the computationally cheaper spin-chain model.

5.5 Summary of the main results

This section is divided into two subsections, giving a summary on the theoretical basis for the spin-chain system. First, we test the spin-chain model against the results of exact diagonalization of the Hamiltonian in Eq. (6), establishing the validity of the model as compared to the microscopic system. Finally, a few important properties of the implemented spin-1/2 system are discussed.

5.5.1 A test of the spin-chain model

The spin-chain model with interacting spin-1/2 fermions is solved for two spin-up and one spin-down fermion (abbreviated throughout as "2+1"), as well as for 2+2 and 3+1. The structure of the resulting spectrum is compared to the lowest energy multiplet of the microscopic Hamiltonian in Eq. (6). For example, the energy levels in the lowest multiplet of the 2+1 system are denoted, in order of increasing energy, as E_0, E_1, E_F (the subscript F will be explained in the next section). The multiplet structure is recorded in terms of the fraction $(E_F - E_0)/(E_F - E_1)$, which accounts for the relative splitting between energy levels, and serves as a test for the validity of the spin-chain model (which is based on degenerate perturbation theory). These results are shown in Figs. 5 and 6. For other configurations, with larger multiplets, additional fractions are used to record multiplet structure.

In the limit of strong interaction, the spectra of the two models compare quant-

itatively for 2+1 and 3+1, and qualitatively for 2+2. The results improve with increasing interaction strength, owing to the fact that the spin-chain model is based on the STG/TG limit wave functions at $1/g_{1D} \to 0$. There is also a good agreement between the single-particle densities of the two models, as indicated in Fig. 5, which shows that the spin-chain model accounts for the antiferromagnetic behavior seen in the ground state of the 1D harmonic system.

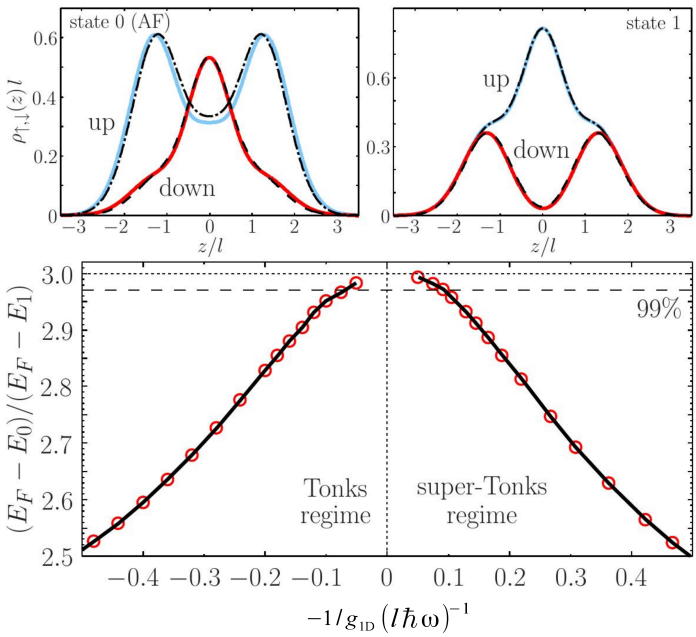

Figure 5: Comparison of the full microscopic model with exact diagonalization and a spin-chain model with $(N_\uparrow = 2, N_\downarrow = 1)$ Upper panel: Single-particle densities of spin-up and spin-down fermions. The solid lines show the densities obtained from the spin-chain model, while the dashed and dash-dotted lines represent exact diagonalization results. Lower panel: Relative splitting of energy-levels in the lowest multiplet as functions of the inverse interaction strength. For the spin-chain model, the ratio $(E_F - E_0)/(E_F - E_1) = 3$, as indicated by the dotted line. The red rings indicate the ratios obtained with exact diagonalization at different g_{1D}. Values above the dashed line indicate results within 99% of that predicted by the spin-chain model. This figure is taken from paper II.

5.5.2 Features of the cold-atom implementation of a spin chain without an optical lattice

Spin-chain models which employ optical lattices typically requires extremely low entropies and temperatures to exhibit antiferromagnetic spin-order, (for a review, see for example [25]). Only very recently, true long-range antiferromagnetic order was measured in a setup with optical lattices [81].

Although there are remedies to overcome these challenges, see e.g. [82] where

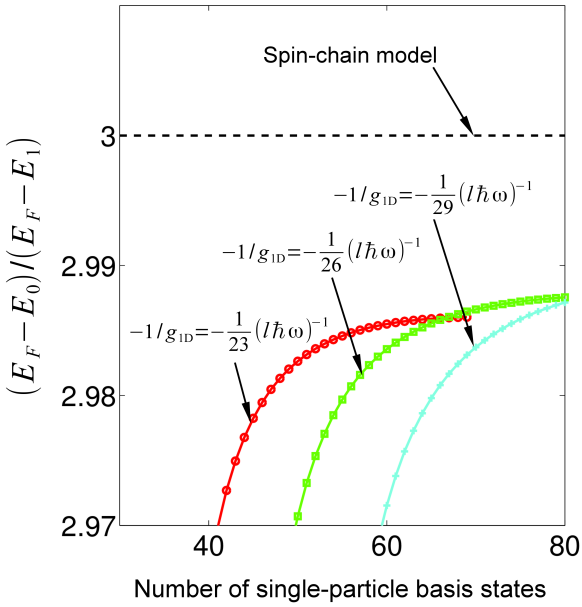

Figure 6: Structure of energy spectrum of 2+1 contact-interacting fermions calculated via exact diagonalization. The spin-chain model predicts the fraction $(E_F - E_0)/(E_F - E_1) = 3$, and when going toward higher repulsive interactions the numerical results converge towards this value.

two particles were prepared in an antiferromagnetic state, a simpler alternative is in demand.

Using the ultracold implementation of the spin-chain model presented in paper II it is possible to deterministically prepare an anti-ferromagnetic (AF), or a ferromagnetic (F) state. By preparing an imbalanced system into the non-interacting ground state, the AF state is reached by adiabatically ramping up the effective interaction strength towards the infinitely strong limit, see paper II. Preparation of the F state requires a more complex scheme, which involves population transfer into a metastable STG state (STG states were discussed in section 3.2).

Another implementation of the Heisenberg spin chain with strongly interacting two-component gases was presented in [52, 83], where Girardeau's Bose-Fermi mapping also was employed. More examples of spin-chain systems in strongly interacting 1D gases have since emerged, see for example [84, 85]

Before any further discussion of the experimental realization of the spin chain, it is important to note a distinction between the solutions of the microscopic Hamiltonian in Eq. (6) and the solutions of the spin-chain model. While Girardeau's Bose-Fermi mapping is exact regarding the expectation values such as

energies and single-particle densities [48, 50], the single-particle mean occupation numbers $\langle n_i \rangle$ and the momentum distribution of single particles represent properties that are hard to calculate directly for the spin-chain eigenstates. Therefore, solutions of the microscopic model are not only important to determine the validity of the spin chain regime, but were also crucial for comparisons to experiments which specifically measured those observables, as we shall see in section 5.6. We note that a method for calculation of momentum distributions and occupation numbers directly from the spin-chain model has become available since the publication of papers II and III [86].

5.5.3 Realizations of spin chains in ultracold mixtures

In paper IV, a spin chain was shown to be applicable also for a 1D system with a mixture of bosons and fermions, i.e. a Bose-Fermi mixture. Here, the spin-chain model is somewhat different from the case of multicomponent fermions, which realized an XXX spin chain with isotropic couplings. The Bose-Fermi mixture instead realizes an XXZ spin chain with non-isotropic couplings ($J = J_x = J_y \neq J_z$). This type of spin chain can also be realized in, for example, mixtures of two bosonic species, see e.g. [84].

The multiplet structure of the Bose-Fermi spin chain was checked with the full microscopic model and showed good agreement. The Bose-Fermi mixture further showed a rich phase diagram for variations in the relative couplings J_{BB} and J_{BF}, which stand for boson-boson coupling and boson-fermion coupling, respectively. Other ultracold realizations of XXZ spin chains without optical lattices have been discussed in, for example, Refs. [84, 87, 88].

5.6 Tunneling experiment

Paper III concerns the experimental realization of the model Hamiltonian described in the previous section. The experiments were performed by Selim Jochim's group in Heidelberg[1], who tested the predictions of the spin-chain system by measuring out-tunneled particles. Here, results from exact diagonalization of the Hamiltonian in Eq. (6) and the spin-chain model were both used for comparison. For completeness, the experimental procedure is here summarized.

The spin chain is realized experimentally in a setup with ultracold ^{6}Li atoms

[1] `http://ultracold.physi.uni-heidelberg.de/`

trapped in an optical dipole trap. The spin chain is prepared deterministically into the antiferromagnetic state by tuning g_{1D} using Feshbach resonances and confinement-induced resonances. The state is then probed by letting particles tunnel out of the trap. The tunneling is prompted by tilting one side of the 1D trap in the elongated direction, as shown in Fig. 7. Two different types measurements, **A** and **B**, can now be performed:

1. Experiment **A** is performed by letting precisely one particle escape. The spin of the out-tunneled particle is then measured, and the experiment is repeated for a range of interaction strengths to reveal the state in the spin chain.

2. In experiment **B** the occupation numbers can also be probed experimentally by using tunneling measurements on individual particles, and the results are in essence fingerprints for the microscopic states inside the trap. Here, the occupation numbers of a single spin-down fermion can be probed by removing all spin-up atoms from an interacting state and measuring the mean occupation numbers of the remaining particle. This measurement of the state is directly compared to the exact diagonalization results of the microscopic Hamiltonian in Eq. (6).

5.6.1 Model for simulation of the tunneling experiment

Experiment **A** constitutes a direct measurement of the spin-chain structure in a two-component 1D system. A theoretical description for the tunneling was therefore required, and a phenomenological spin-chain model, abbreviated as PSC-model, was introduced within the framework of the spin-chain model. This model is here briefly summarized.

The principle behind the PSC-model is that the spin-chain basis functions, with definite spin-order, are sufficient to describe the tunneling experiment **A**. The spin-order functions have a one-to-one correspondence to the sector functions (see section 7), which define a strict spatial ordering of particles. In other words, there is a strict spatial ordering of the spins in the trap basis functions. Now, a moderate perturbation in the rightmost region of the trap should only affect the rightmost particle, since the other particles are spatially separated from this region. We then assume that for short times, only that particular particle may escape the trap. For a given trap state $|\psi_{\text{trap}}\rangle$, the tunneling rates of spin-up versus spin-down particles, therefore, depend on the superposition of basis states, which each have a specific ordering of particles and spins. Other factors that influence the tunneling rates in the PSC-model are:

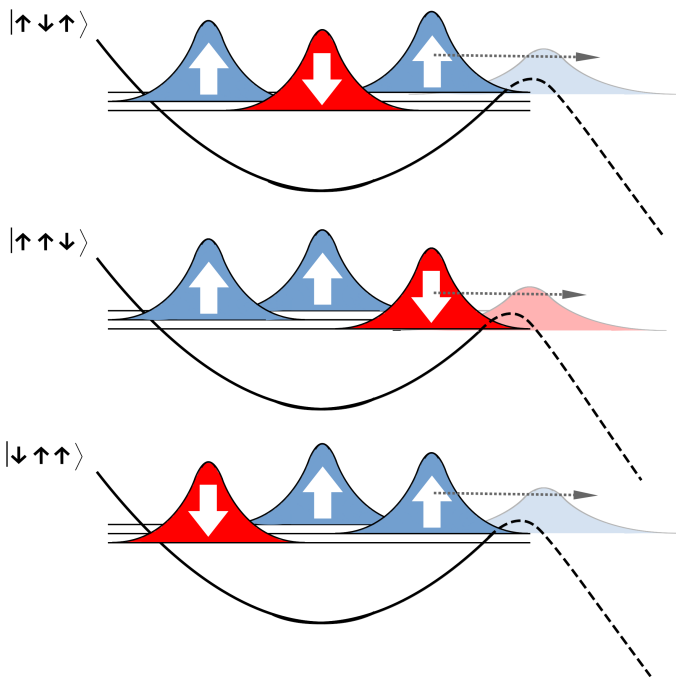

Figure 7: Sketch of the tunneling scheme where a single particle escapes from a trap with two spin-up and one spin-down fermion. The spin-order basis functions for this system $\{|\uparrow\uparrow\downarrow\rangle, |\uparrow\downarrow\uparrow\rangle, |\downarrow\uparrow\uparrow\rangle\}$ have a one-to-one correspondence to the spatial sector wavefunctions in Eq. (7), and the tunneling measurements can be linked directly to the state of the spin chain.

1. The energy of the "out-coupled" particle that breaks away from the spin-chain state. This particle travels towards an energy-barrier where the chance of tunneling is directly determined from its kinetic energy. Hence, the energy difference between the N-particle spin-chain state and the $(N-1)$-particle spin-chain state is a crucial factor that can block certain tunneling channels.

2. The direct overlap between the N-particle state and the $(N-1)$-particle state, which also can lead to blocked tunneling channels.

The PSC-model was investigated by numerical simulations of the microscopic Hamiltonian in Eq. (6). As discussed in the above, an important factor for determining tunneling rates was the probability of measuring spin-up or spin-down in the rightmost region of the trap. The simplest approximate measure of tunneling rates from the microscopic Hamiltonian is, therefore, for a given state $|\psi_{\text{trap}}\rangle$, the fraction of spin-down particles relative to the total density at some point far right of the center of the trap. Figure 8 shows the spin-down fractions,

$\rho_\downarrow(z)/(\rho_\uparrow(z)+\rho_\downarrow(z))$, for the AF state, calculated via exact diagonalization of the microscopic Hamiltonian in Eq. (6). The numbers do not account for possible blocked channels, but the data the show that there is qualitative agreement with the PSC-model, see Fig. 9, for positions in the far-right region of the trap. This is not unexpected since the single-particles densities agreed well for the spin-chain model and the exact diagonalization results.

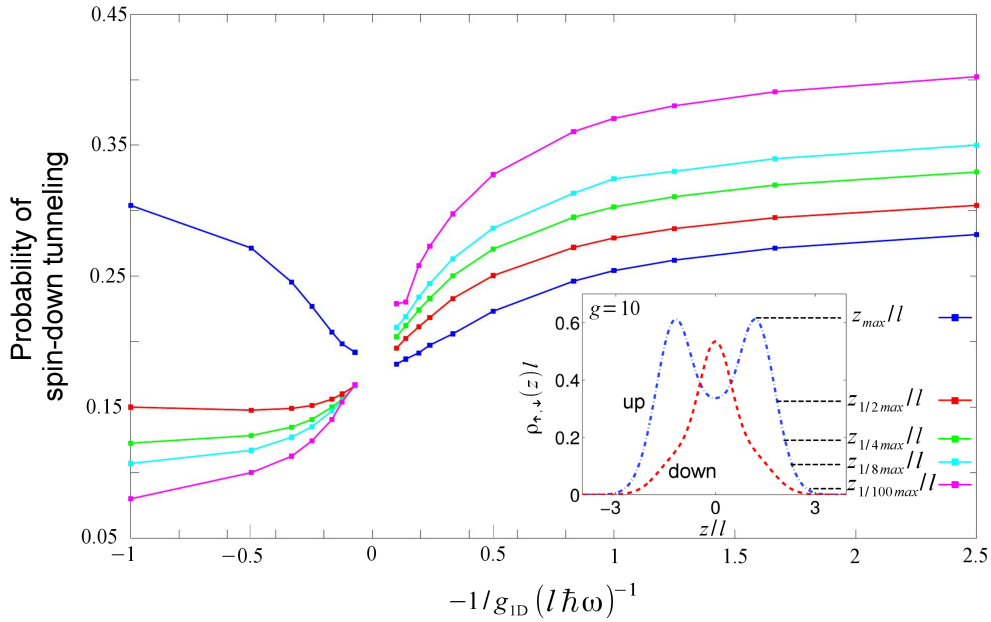

Figure 8: Numerically calculated spin-down fractions, $\rho_\downarrow(z)/(\rho_\uparrow(z)+\rho_\downarrow(z))$ (i.e, the fraction between the single-particle spin-down density and the total single-particle density), for the 2+1 AF state at different interaction strengths g_{1D}. Inset: Single-particle densities of spin-up and spin-down particles with indications of the positions in z at which the spin-down fraction is calculated. The overall curve matches well with experiments only for positions far right of the trap center.

5.6.2 Comparisons between experiment and theory

Figure 9 shows comparisons between tunneling experiment **A** and the phenomenological spin-chain tunneling (PSC) model. The spin-fractions for the tunneled particle are measured, and the model agrees very well with the prediction for the spin-chain AF state, which is distinct from predictions for tunneling from an intermediate (IM) state or an F state. For three different configurations, $(2+1)$, $(3+1)$ and $(2+2)$, the tunneling data indicate that an AF state was deterministically prepared and detected via tunneling measurements,

constituting a direct observation of quantum magnetism in an ultracold system without an optical lattice.

We now proceed to compare the outcomes of the independent experiment **B** to the solutions for the microscopic Hamiltonian in Eq. (6). The single-particle occupation-numbers for the AF and F states were measured by Selim Jochim's group and were then compared to the mean occupations $n_i = \langle \hat{a}_i^\dagger \hat{a}_i \rangle$ obtained from numerically diagonalizing the full Hamiltonian. Figure 10 shows the occupation numbers for a state in the STG regime, which was reached by starting in the AF state in the Tonks-regime and quickly tuning the interaction towards attractive values. The results show that the system indeed is in the metastable AF state, which manifests that a spin-chain AF state can be deterministically prepared and measured upon across the resonance at $1/g_{1D} = 0$. This confirms that the spin measurements in Fig. 9 were indeed performed for spin-chain AF states and that the experimental results match well with the predictions of the spin-chain model.

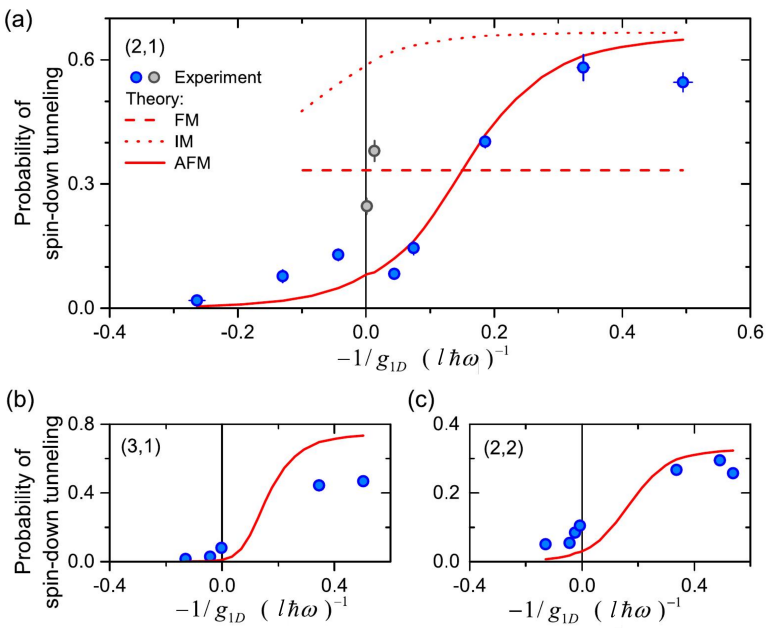

Figure 9: Tunneling probabilities for a spin-down atom at different interaction strengths g_{1D}. The blue dots are the experimental values, and the red lines represent theoretical calculations of the AF(solid line), F(dashed line) and an IM(dotted line) state. Lower left: $(3+1)$ fermions. Lower right: $(2+2)$ fermions. Upper: $(2+1)$ fermions. Note that blue dots fall closely to the theoretical prediction for an AF state in the trap. The gray dots at the resonance come from an emergent coupling, due to small irregularities in the trap, between the AF and the IM state, which influences the probability of spin-down tunneling. This figure is taken from paper III.

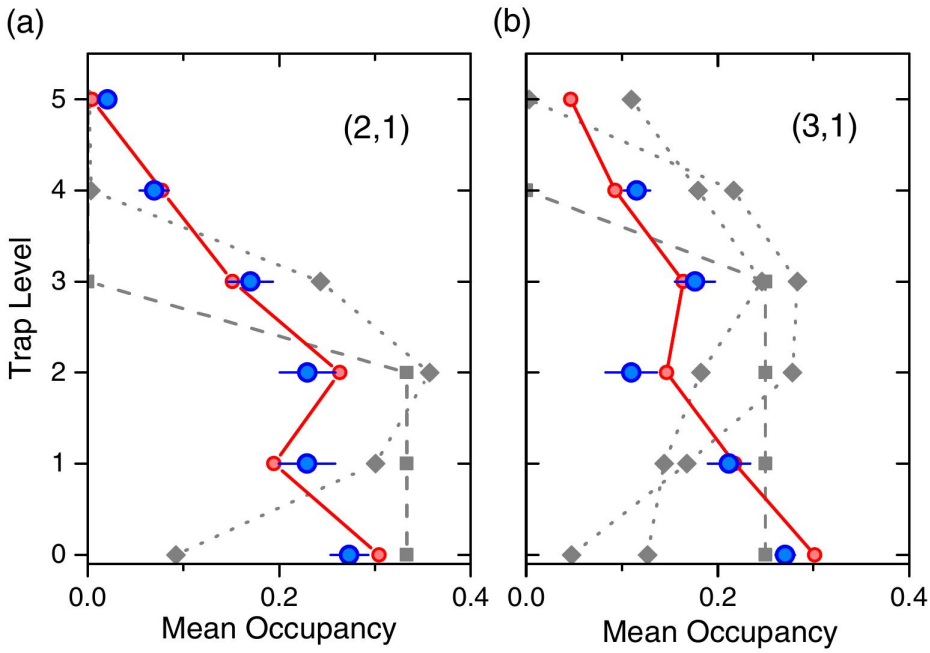

Figure 10: Occupation numbers for the single spin-down fermion in a $(2+1)$-system (a), and a $(3+1)$-system (b). The blue dots show experimental values while the red and gray markers show theoretical values from numerically solving the Hamiltonian in Eq. (6). The measurement was performed for $-1/g_{1D} = 0.586 \pm 0.014$ and $-1/g_{1D} = 0.536 \pm 0.013$ for the $(2+1)$ and $(3+1)$-system, respectively. The red dots show the occupations calculated for the AF state, and the gray markers show occupations for F and IM states. For both configurations, the experimental values match well with the theoretical prediction for an AF state. This figure is taken from paper III.

6 Higgs modes of a two-dimensional harmonically trapped Fermi gas

The Higgs-Anderson mode [89, 90] is an important many-body phenomenon that is recognized as a quasiparticle in Ginzburg-Landau theory [10]. In paper I of this thesis, we study an emerging Higgs mode few-body precursor for harmonically confined fermions in a 2D setup. By extensive numerical efforts, few-to-many body effects and the response of the Higgs-mode precursor to external probes are simulated. This paves the way for a table-top setup where the few-body fate of a Higgs mode can be studied systematically.

In this section, we first give a brief introduction to the concept of Higgs modes and then continue to showcase a setup for which they can be studied in both the many-body and the few-particle limit. Finite-size precursors of Higgs modes are not yet fully understood, and this thesis aims at filling the gap between the few- and many-body limit.

6.1 Background

A Higgs-Anderson mode [89, 90], or simply Higgs mode, is a fundamental concept within both elementary particle physics and, as mentioned in the above; condensed matter physics, see for example [91, 92]. It is one of the key components that link the theoretical description of a condensate to the standard model of elementary particles. The Higgs mode does play a major role in mathematical descriptions of physics in different areas - versions of the Higgs-mode also appear in nuclear physics. It turns out that the underlying mechanics for Higgs modes in nature is the concept of *broken symmetries*, which has different manifestations in distinct areas of physics. Over history, many different terms have therefore been associated with what is essentially very similar physics at the core. Concepts such as Higgs fields, Bogoliubov modes, amplitude modes, Goldstone modes, Higgs bosons, pairing vibrations and phase fluctuations are all strongly connected. Most of the original papers on the subject date back to the 50's and 60's and include contributions from Nambu [93], Bogoliubov [94], Higgs [90], Goldstone [95] and Anderson [89, 96, 97] (for reviews on this history see [98, 99]. For a detailed theoretical background see e.g. [92, 98, 100, 101] and references therein.) The manifestations of the Higgs mode is also a relevant topic in ultracold systems. For example, Higgs and Goldstone modes were found in connection with the realization of a supersolid a Bose-Einstein condensate in Refs. [103] and [104, 105]: In the latter references, the mode excitation energies,

along with other properties of the supersolid, pointed to the existence of Higgs and Goldstone modes that could be monitored and manipulated. In Ref. [106] spontaneously broken symmetries in a rotating gas of bosons, trapped in a 2D harmonic oscillator, were shown to give rise to Nambu-Goldstone modes which were identified via clear signals in the excitation spectra.

In Ginzburg-Landau theory the long-range order of superfluids and superconductors is described in terms of a complex scalar order parameter $\Phi(\mathbf{r})$ [10]. The physical behavior of this spatially varying object is described in terms of a functional for the free energy $F[\Phi]$. Many different physical systems turn out to be well-described by the particular Landau-Ginzburg form of the free energy density functional

$$F\left[\Phi\right] = \int d^3\mathbf{r} \ \left(\alpha \left|\Phi\left(\mathbf{r}\right)\right|^2 + \beta \left|\Phi\left(\mathbf{r}\right)\right|^4 + \gamma \left|\nabla\Phi\left(\mathbf{r}\right)\right|^2\right) \tag{10}$$

where α, β and γ are constant specific to the system (In the following $\beta = \gamma = 1$). The minimum of the free energy is sometimes referred to as the ground state energy of the system, with a corresponding ground state order parameter Φ_0. In a simplistic manner, one can refer to fluctuations in the order parameter around this ground state as excitation modes, or shorter; modes. Considering only slowly-varying order parameters in the long-range limit the order parameter can be written as

$$\Phi = \left|\Phi\right| e^{i\theta}.$$

Here, Φ is divided into an amplitude- and a phase-factor. In Fig. 11, the free energy density in Eq. (10) is plotted as a function of the order parameter. For $\alpha > 0$ there is a single minimum at $\Phi = 0$, but for $\alpha < 0$ the minimum energy becomes degenerate. Here, the order-parameter takes on finite values for the ground state solution, increasing continuously as α becomes increasingly negative. This is an example of a *spontaneously broken symmetry* and a continuous phase-transition where the order parameter is assigned to one of the degenerate points and therefore breaks the phase-translation symmetry of Φ_0. The low-energy modes of the theory are found by considering small fluctuations around the ground state, such that $\Phi = \Phi_0 + \Lambda$, and expanding the free energy up to second order in these fluctuations. In the *normal* phase, $\alpha > 0$, all fluctuations around the ground state are associated with an increased energy since they take the system away from the energy-minimum - one, therefore, speaks of massive - or gapped - modes. In the broken-symmetry phase, $\alpha < 0$, the ground state can be defined as $\Phi_0 = \left|\Phi_0\right| e^{i\cdot 0}$ where the phase is chosen to be zero and the minimum solution gives $\Phi_0 = \sqrt{-\alpha}$. The fluctuations are defined as

$$\Phi = \left(\Phi_0 + \Lambda\right) e^{i\theta}.$$

Inserting into the Landau-Ginzburg functional gives, to second order,

$$F[\Lambda, \theta] \approx \int d^3\mathbf{r} \ \left[-5\alpha \left|\Lambda\right|^2 + 0 \cdot \theta^2\right]$$

where terms linear in θ and Λ disappear since Φ_0 is a minimum. The first term is positive since $\alpha < 0$ and shows that amplitude fluctuations, or amplitude modes, of Φ are associated with a cost in free energy, interpreted as a mass of the mode. The factor in front of the phase-fluctuations is zero, which manifests that such modes cost zero energy. This amounts to fluctuations around the degenerate minimum in Fig. 11 c, and are the so-called massless *Goldstone* modes, which are associated with a spontaneously broken symmetry [95]. The massive modes are correspondingly known as *Higgs* modes [98, 99].

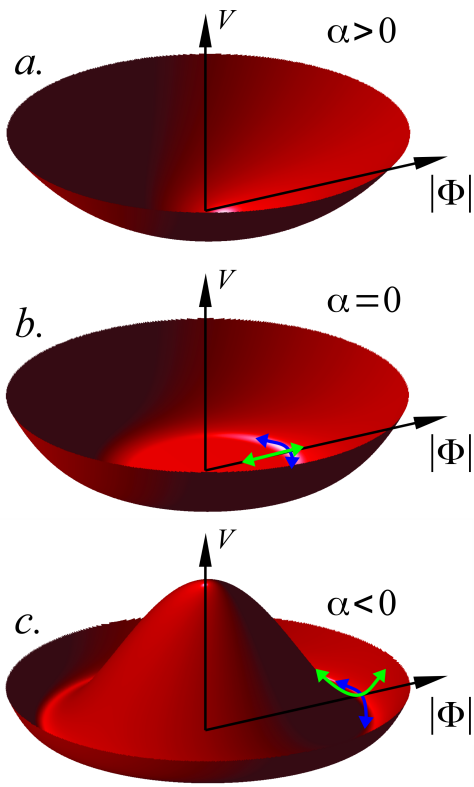

Figure 11: Potential part V (first two terms) of the Landau functional F in Eq. (10) , as a function of the order-parameter Φ. For a more detailed description of this type of figure, see e.g. [92] The green and blue arrows represent amplitude and phase-fluctuations of Φ, respectively. This Upper figure: $\alpha > 0$. Potential minimum for $\Phi = 0$. Middle figure: $\alpha = 0$. Potential minimum for $\Phi \approx 0$. (The extension of the flat bottom of the potential is exaggerated). Lower figure: $\alpha < 0$. Potential minimum for $\Phi = \sqrt{-\alpha/\beta} \cdot e^{i\theta}$. The minimum potential energy occurs at the bottom of this so-called *Mexican-hat potential*.

Now, as alluded to earlier, the starting point for the discussion on Higgs modes should be the form of the Landau-Ginzburg free energy F. This particular form of the free energy is the basis for many different models in physics and has also been seen to arise directly from microscopic theories [107]. There have been many publications on table-top systems where Higgs modes can be identified and studied to some degree, but in general, the short lifetime of the Higgs mode has been a complicating factor [108–110]. For a review on manifestations of the Higgs mode, see for example [98]. However, a system for which a Fermi gas is trapped in a 2D harmonic oscillator has been shown to exhibit long-lived Higgs modes that may be good candidates for experimental detection [111]. Importantly, this system is also simple to scale down to small numbers of particles, and the fate of the Higgs mode in the few-particle limit can, therefore, be studied in a controlled way.

6.2 Model

An ultracold Fermi-gas trapped in a 2D harmonic micro trap with attractive contact interaction is a simple system in which to study signatures of Higgs modes in finite-size systems [111]. Here particles are confined in a deep, narrow trap in the z-direction and a circular symmetric potential in the (x, y)-plane. The trapping frequency is much larger in the z-direction than in the other directions, $\omega_z \gg \omega_\perp$, so the system is effectively 2D. The microscopic Hamiltonian, similar to than in Eq. (6) in section 5.3, for particles with mass m and contact interactions $\delta(\mathbf{r_1} - \mathbf{r_2})$ reads

$$\hat{H} = \sum_{i=1}^{N} \left(-\frac{\hbar^2 \nabla_i^2}{2m} + \frac{1}{2} m\omega {\mathbf{r_i}}^2 \right) + g \sum_{i,j} \delta\left(\mathbf{r_i} - \mathbf{r_j}\right) \tag{11}$$

where $\mathbf{r_i}$ is the spatial coordinate of particle i. Like in the previous chapter, we consider dimensionless units ($\hbar = m = 1$) so that energies are given in terms of $\hbar\omega$, and interaction strength g in terms of $(\hbar\omega)\eta^2$, with $\eta = \sqrt{\hbar/m\omega}$.

The single-particle energy spectrum of the Hamiltonian in Eq. (11) is given in terms of the principal quantum number $n = 0, 1, 2, ...$ and the angular momentum quantum number $m = 0, \pm 1, \pm 2, ...$

$$E = \hbar\omega(2n + |m| + 1).$$

For $E > 1\hbar\omega$ the single-particle spectrum has degeneracies for the spatial states, giving rise to so-called *energy shells* in which two or more states have the same energy. The structure of the energy shells (shell structure) of the 2D harmonic

oscillator is presented in Fig. 12. The concept of shells is important since it is fundamental for our discussion of basis selection and convergence, as well as for the analysis of the many-body physics associated with the Higgs mode.

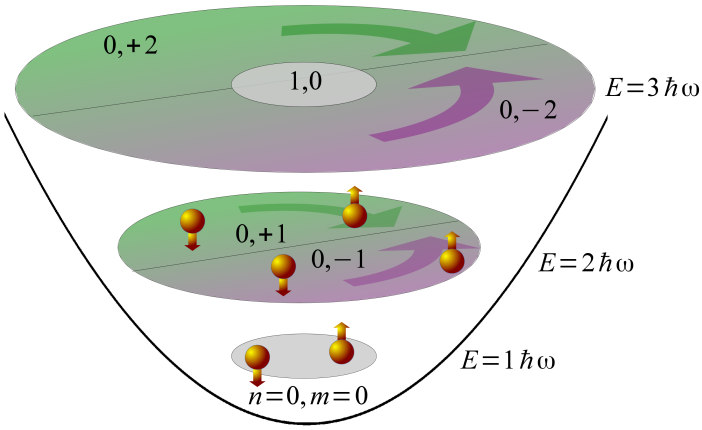

Figure 12: Sketch of a 2D harmonic oscillator with three spin-up and three spin-down fermions. The quantum numbers n and m denote the principal and angular momentum quantum number, respectively. For successively higher single-particle energies E the number of degeneracies, i.e., the size of the energy shell, increases. This figure is taken from paper I

Here we consider a system with N spin-1/2 fermions in a subspace with zero total angular momentum ($L = \sum_i^N m_i = 0$). This restricts the Fock-space for which we solve our Hamiltonian, but does not constitute an approximation since the Hamiltonian in Eq. (11) is block-diagonal in different L-subsets, see section 2.

The delta pseudopotential in Eq. (11) is a representation of the effective 2D contact interaction, see section 4. Cold-atom experiments allow for the contact interaction to be controlled experimentally via Feshbach resonances, as also briefly discussed in section 4. In particular, g can be modulated over time, see for example [112], which we will see is very useful when we want to excite the Higgs mode.

For an exact representation of the microscopic system, an expansion of the wave functions should in principle include the possibility for a particle to occupy *any* shell, or at least sufficiently many as to get convergent results when solving the Schrödinger equation. Unfortunately, in 2D the attractive delta pseudopotential does not converge with the number of shells allowed in the single-particle basis, so a regularization procedure which provides a well-defined theory for $E_i \to \infty$ is needed [113–115]. Here, the regularization procedure consists of first performing

a cut in the number of allowed shells in the Hamiltonian and then plotting all results in terms of the two-body binding energy ϵ, calculated within that same restricted space. This can be shown to act similarly as to a regularization in terms of a finite-width effective contact interaction [113], and hence the simulations are essentially performed for a finite-width effective interaction. This choice is motivated by the efficient calculation of the delta interaction matrix-elements which reduces the setup-time for the numerical simulation [42].

We aim to solve the Hamiltonian exactly for configurations with up to three spin-up and three spin-down fermions (abbreviated as 3+3) for a range of attractive interaction strengths $g < 0$, recording observables which we associate with Higgs modes. We then aim towards higher numbers of fermions with an approximate model, to study the few-to-many body aspects of the system.

6.3 Higgs modes of a 2D harmonic oscillator - the many-body limit

For attractive interactions the effective Hamiltonian in Eq. (11) is unstable towards pairing, that may result in a superfluid phase for sufficiently strong contact attraction in the many-body limit. The crossover into such a superfluid phase has already been observed for an ultracold system of a strongly interacting quasi-2D Fermi gas [112]. For a similar 2D system, the occurrence of Higgs modes close to a phase transition was investigated by Bruun [111]. There, a functional formulation, outlined in Fig. 13, was used to investigate the low-energy modes of a 2D harmonic system, with a particular focus on fluctuations in the pairing order parameter around the normal-to-superfluid phase-transition. The emergence of correlated fermion pairs was shown to be connected with the occurrence of a phase transition when the strength of the attractive contact interaction was increased beyond a critical value.

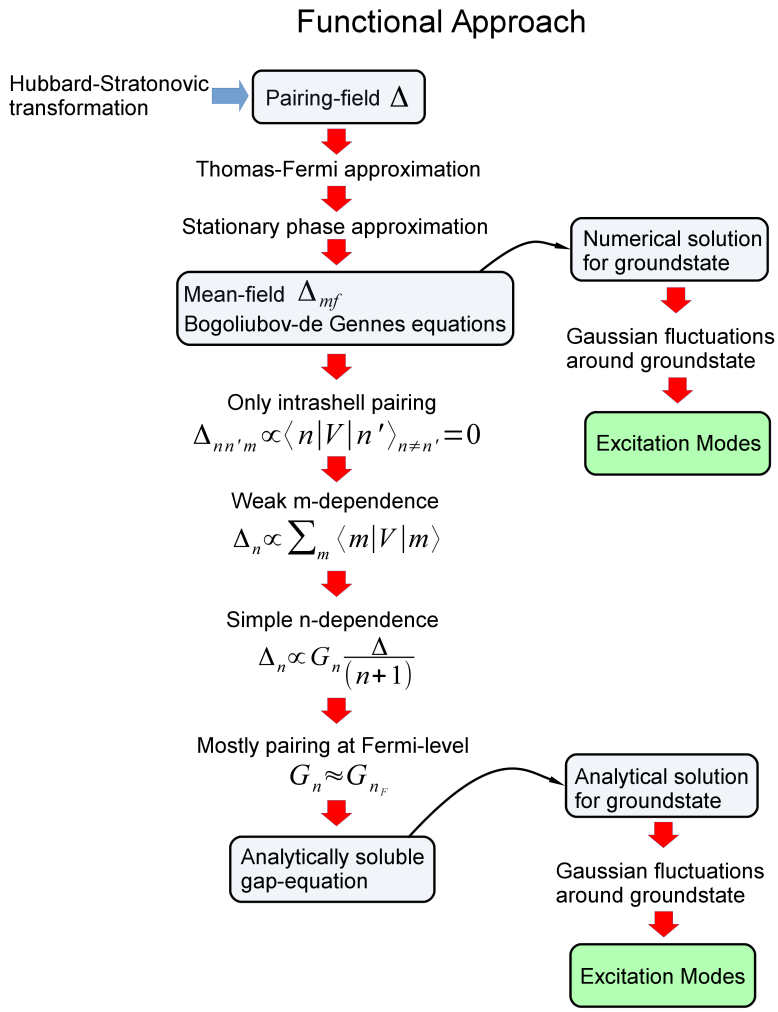

Figure 13: A map of the methods and approximations leading up to the identification of a long-lived Higgs-mode as in Ref. [111]. The calculations involve a mean-field treatment of a pairing-field Δ leading to the Bogoliubov-de Gennes equations which can be solved numerically or analytically. For a mean-field treatment of the filled-shell 2D harmonic oscillator, a clear minimum in excitation-energy is identified for oscillations in the pairing-field amplitude.

More specifically, in Ref. [111] a system of $N \sim 100$ particles was studied at zero temperature and within the Thomas-Fermi approximation. The system was then investigated for a mean pairing-field Δ, introduced via a Hubbard-Stratonovich transformation, within the stationary-phase approximation. The ground state solution was found via numerical simulations in parallel with an approximation scheme (see Fig. 13), giving analytical solutions in the appropriate limits.

The results of Bruun [111] revealed the normal-to-superfluid phase transition at

a critical binding energy ϵ_c resulting in a ground state with a broken symmetry. The origin of this broken symmetry is once again exemplified in the plot of the free energy in Fig. 14 b, where $\epsilon > \epsilon_c$ gives a Mexican-hat shaped potential like in Fig. 11. For systems close to the transition point, fluctuations of the pairing-field around the ground state were then considered in the $L = 0$ subspace. The mode-frequencies were found via a Gaussian approximation which yielded pairing correlation-functions with poles at the low-lying excitation-modes.

Both the numerical and analytical solutions of the system give rise to excitation modes that can be decomposed into two distinct classes Λ_G and Λ_H. In the superfluid phase ($\epsilon > \epsilon_c$) these modes correspond exactly to Higgs and Goldstone modes that become completely decoupled from each other in the limit of perfect particle-hole symmetry in the system (hence the subscripts G and H). For a closed-shell configuration the mode-frequency of Λ_H has an interesting non-monotonic behavior across the phase transition, as shown in Fig. 14. The Higgs mode frequency is zero at the point of the phase transition, associated with amplitude fluctuations confined to the flat-bottom potential surface of Fig. 11 b. An analogous behavior of amplitude modes was seen both in nuclear physics, see e.g. [116], and for superconductors, see for example [98], and it provides a smoking gun for the existence of the broken symmetry and the associated Higgs mode. In the open-shell configuration, the non-monotonic behavior of the Higgs-mode is lost, because there is always pairing. There is, therefore, no quantum phase transition between a superfluid and a normal state. This limits the number of setups for which this particular signal of the Higgs mode can be found.

As mentioned at the beginning of the chapter, the lifetime of the Higgs mode is generally short in the realized table-top system, mainly due to decay into a continuum of low-energy modes. This means that the spectral signal of the Higgs mode is broad, which complicates experimental detection with, for example, Raman spectroscopy [98]. A large obstacle is that any presence of particle-hole asymmetry in a system couples Higgs and Goldstone modes and consequently opens strong decay channels. However, in the cold-atom 2D harmonic system of Ref. [111], the mode frequencies depend only weakly on the asymmetry, as seen by comparing the numerical and analytical results. Importantly, the decay is further inhibited by the trapping potential. The Goldstone modes in the system correspond largely to fluctuations in the total density of particles and have a discrete spectrum with energies typically associated with the trapping frequencies. Hence, there is no continuum of low-energy Goldstone modes to decay into, and the system supports stable Higgs modes. The ultracold system furthermore allows for a high degree of control over the interaction parameter,

and the Higgs mode may be selectively excited by a time-dependent modulation of the interaction strength, which directly causes fluctuations in the pairing field.

6.4 Higgs modes of a 2D harmonic oscillator - the few-body limit

A few-body study of the harmonically trapped Fermi gas is valuable for three main reasons. Firstly, it provides an unbiased microscopical treatment which uses very few approximations and therefore gives a solid basis for comparison with the mean-field treatment of pairing in [111]. Secondly, it provides a framework for which to study the few-to-many body development of a concept that is, essentially, of many-body origin. This may give us a microscopic glimpse into the inner workings of a phase-transition and the collective modes of a system. Lastly, the few-body system offers a considerable chance to realize a highly controlled experiment. As shown in paper II of this thesis, tunneling measurements on a 1D multicomponent cold-atom system were able to resolve internal details in a set of microscopic few-body states. In principle, there is a strong possibility that a similar procedure could be applied to a 2D system, like the one in [112], where the Higgs mode could be selectively excited and then studied. For two recent examples of experimental studies on the pairing mechanisms in a 2D Fermi gas at the normal-to superfluid transition, see [117, 118].

6.5 Methods for solving the few-body Hamiltonian

In the few-body limit, a two-parameter cut-off scheme was used to solve the Hamiltonian in Eq. (11) exactly. Here, the highest allowed single-particle shell energy E_i and highest allowed many-body energy E_{MB} were increased in a systematic manner as to reach convergence. For $3 + 3$ particles the results are fully converged with respect to both parameters, whereas the results for $6 + 6$ particles are not fully converged with respect to E_i. However, for $6 + 6$ particles all plotted quantities are lower bounds in the sense that the features which emphasize the Higgs mode behavior are expected to improve with E_i. Extensive efforts were made to go towards higher numbers of particles. Iterative basis selection (see section 2) was tested but was found to be ineffective due to the dense nature of the coupling matrices.

6.6 Discussion on indentification of few-body precursors

The starting point for identifying a few-body Higgs mode precursor is to establish which properties we are looking for in the few-body limit.

In the many-body study of the filled-shell 2D harmonic oscillator [111], a minimum in excitation energy for $N \sim 100$ was unequivocally identified with a Higgs mode in terms of its origin in vibrations of the pairing-field. The approximations were here systematic, and an exact treatment is expected to reproduce similar results for the low-energy excitations. Solving the full microscopic Hamiltonian for $N \sim 100$ particles is not possible within the highly correlated regime of the normal-to-superfluid transition. However, by successively increasing the number of particles in the few-body limit, we should be able to identify precursors to the Higgs mode, since we know that a band of closely-spaced levels, which make up the Higgs mode, is formed when N is large. Each of these levels should have properties that are associated with the Higgs mode, and we expect that these properties will become more pronounced when N is increased. Based on the many-body study of the Higgs modes in a Fermi-gas, we attribute two main properties to the Higgs excitation mode:

1. A minimum in energy around a transition in the ground state. The minimum energy should decrease with larger N, as should the smoothness in the transition. We believe this to be the case since in the limit $N \gtrsim 100$, the transition is sharp and the minimum in excitation energy approaches zero [111].

2. The coupling between the ground state and the excitation should be weak for modulations of the trapping frequency, and strong for modulations in the interaction strength. This is an inherent property of the many-body Higgs mode in [111], which is shown to be comprised entirely out of paired excitations out of the ground state. Therefore, the Higgs mode cannot be excited utilizing single-particle operators such as the single-particle density, as they are unable to couple the ground state to the Higgs mode [111]. Since the Higgs mode is completely decoupled from density fluctuations in the limit of $N \to \infty$ [98, 111], we believe that this behavior should become more pronounced for successively larger N.

We will study the lowest few eigenstates $|E_n\rangle$ in terms of energy and transition matrix elements Γ^E with respect to the ground state. To represent modulations in the trapping frequency, we consider matrix elements for a single-particle density operator

$$\Gamma_{\text{trap}}^{E_n} = |\langle G| \sum_i \hat{\mathbf{r}}_i^2 |E_n\rangle|^2. \tag{12}$$

For a few test-cases, other forms of density-operators were used to capture a more general trapping modulation

$$\hat{d} = \sum_i \frac{1}{C} \left(c_1 \cdot \hat{\mathbf{r}}_i^2 + c_2 \cdot (\hat{\mathbf{r}}_i^2)^2 + c_3 \cdot (\hat{\mathbf{r}}_i^2)^3 + ... \right)$$

where the set of expansion coefficients $\{c_i\}$ defines a specific operator. Here C is a normalization constant, and the series continues to some arbitrary cut-off point. These operators were however seen to give the same qualitative trends as the simpler $\hat{r}^2$-operator in Eq. (12).

Interaction modulations were represented in terms of the delta function $g \sum_{i,j} \delta(\mathbf{r}_i - \mathbf{r}_j)$, as it appears for the two-body interaction of the Hamiltonian in Eq. (11). This operator can excite pairs of particles, and can, therefore, create the type of pair-vibrations that were identified as Higgs modes in Ref. [111]. The matrix elements of the interaction modulation are given as

$$\Gamma_{\text{int}}^{E_n} = |\langle G| g \sum_{i,j} \delta(\mathbf{r}_i - \mathbf{r}_j) |E_n\rangle|^2. \tag{13}$$

6.7 Few-body results

The few-body spectrum in Fig. 14 shows the minima in excitation energy which we associated with a Higgs-mode precursor. Furthermore, the minimum becomes deeper for larger particle numbers N which indicates a development towards the many-body limit, as previously discussed. Analysis of the ground state wavefunctions for 3+3 respective 6+6 particles shows a soft transition close to the point of the minimum. The transition comes from the onset of pairing in the ground state, and therefore represents the few-body limit of the normal-to-superfluid transition. The observation of a few-body Higgs mode precursor is further emphasized by the transition matrix elements in Fig. 15, which show that the Higgs mode precursors mainly couple to the ground state in terms of interaction modulations. The modes are also insensitive to fluctuations in the trapping frequency, which is consistent with fluctuations that do not change the pairing. These two characteristics, which only occur at a filled-shell configuration, lead to the interpretation that the few-body systems with contact

interaction[2] show behavior that is consistent with a precursor of the many-body Higgs mode.

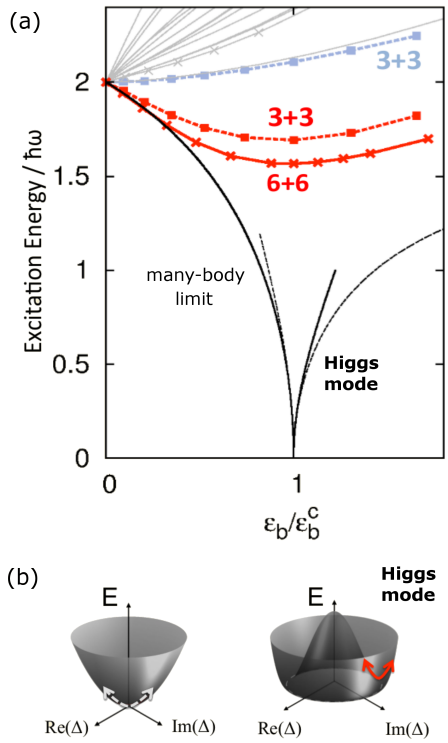

Figure 14: Numerical excitation energies for $3+3$ fermions (dashed red line) and for $6+6$ fermions (red solid line) obtained in the $L = 0$ subspace (the energy for $6 + 6$ fermions is an upper bound). The blue dashed line is the second excited state. The solid gray lines are higher excitations for the $3 + 3$ system. The black solid (dotted) lines show the results of the numerical (analytic) many-body calculations of a sharp Higgs mode in [111]. This figure is taken from paper I.

Comparing with the results in Ref. [111] we note that the few-body simulations take into account effects far beyond the mean field-calculations, most importantly in the sense that all two-body correlations are considered. In the approximation scheme in Fig. 13, the Hubbard-Stratonovich transformation was applied to introduce a pairing field, which was then approximated by a saddle-point. Therefore the many-body calculations only involved a single Slater-determinant, which constitutes a clear simplification compared to our few-body calculations. Another difference is that there is no phase transition in the few-body system, but instead a smooth change in the ground state properties. The effects of

[2] A few simple test-cases with a narrow Gaussian two-body interaction function gave qualitatively the same results as for the delta pseudopotential otherwise applied here.

increasing N, i.e., the lowering of energy minima and an increase in the pairing coupling matrix elements, however, shows how the few-body precursor approaches the many-body sharp quantum phase transition. This behavior can be partly understood by the trend that the critical binding energy decreases with particle number, which is confirmed in the few-body limit and within the analytical model of [111]. Therefore, the interaction strength for the phase transition decreases with N, which indicates that when going towards larger particle numbers, higher-order correlations are expected to become less important to describe the low-energy physics around ϵ_c. The accuracy of the mean-field results should, therefore, increase with N, so that the gap in the excitation energy reduces as $N \to \infty$.

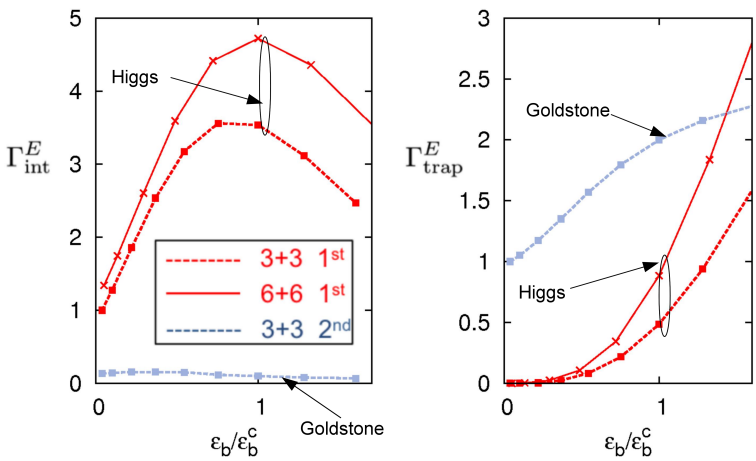

Figure 15: Left: Transition matrix elements $\Gamma^E_{\rm int}$ corresponding to the interaction-modulation operator in Eq. (13) for a $3+3$ and a $6+6$ system. The quantities are plotted as functions of the two-body binding energy ϵ_b, normalized with respect to the critical binding energy ϵ_b^c which occurs at the minimum in excitation energy. The matrix elements are normalized by $\Gamma^E_{\rm int}$, calculated for the Higgs mode at near-zero coupling strength for the $3+3$ system. (The result for $6+6$ fermions is a lower bound) Right: Transition matrix elements $\Gamma^E_{\rm trap}$ corresponding to the density-modulation operator in Eq. (12). The matrix elements are normalized by $\Gamma^E_{\rm trap}$ calculated for the second excited state at near-zero coupling strength (the result for $6+6$ fermions is an upper bound). This figure is taken from paper I.

We finally note an important property of the Higgs mode precursors in Fig. 14: The Higgs modes are isolated in the spectrum around the transition where the transition matrix elements reach a maximum. This again establishes the idea that the modes can be selectively excited using modulations in the interaction strength. Since there are no other states close to the Higgs mode precursor at the transition point, we believe that a time-dependent modulation, where the frequency directly relates to the gap in the spectrum, could be used to access the Higgs mode directly. We, therefore, conclude that the Higgs mode precursors not only show strong similarities to the pairing fluctuations but are also accessible

via cold-atom experiments.

6.8 Higgs modes in a core-less 2D harmonic oscillator

An adapted model of a core-less 2D harmonic oscillator, pictured in Fig. 16 and discussed in section 2.4, was seen to capture the essential physics of the Higgs-modes, while at the same time allowing for larger particle numbers than the full microscopic system. Most of the excitations which are responsible for the Higgs modes are expected to occur around the highest occupied shells. Therefore this type of artificial Hamiltonian, with shells only around the Fermi-level, can be used to represent the development of Higgs-modes with increasing particle number.

The spectrum in Fig. 17 shows that the trend of decreasing minima in excitation energy persisted, further exemplifying the few-to-many body fate of the Higgs mode.

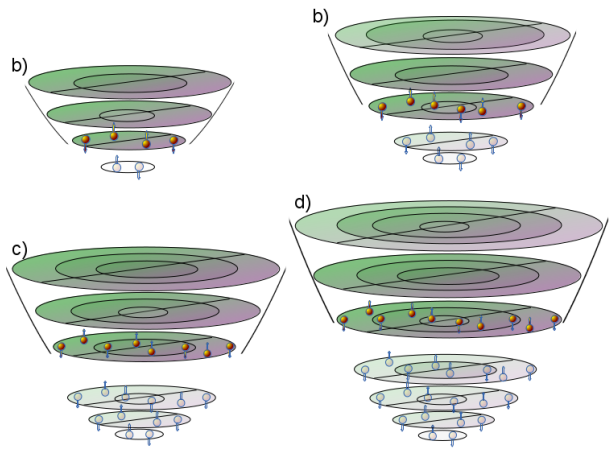

Figure 16: Sketch of a core-less 2D harmonic oscillator where the lowest shells (here shown as transparent shells) are cut from the regular harmonic oscillator, so that the four lowest configurations of filled shells occurs for 4,6,8 and 10 particles, respectively. This figure is taken from the supplementary material of paper I.

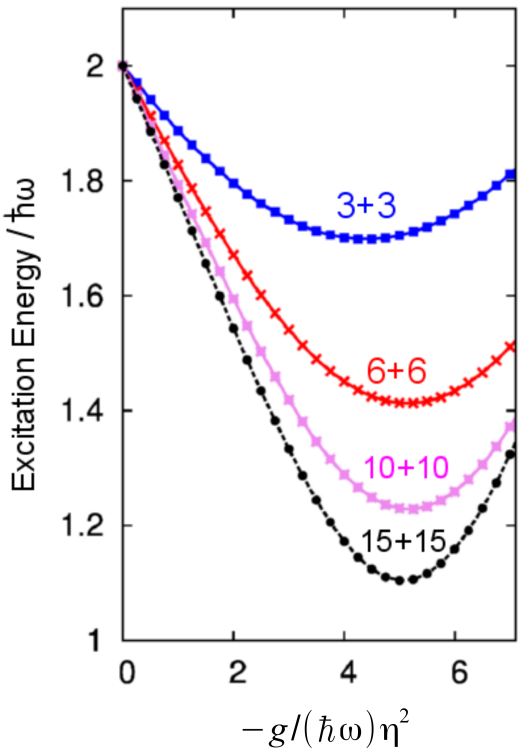

Figure 17: Numerical excitation energies for a sequence of particle numbers each corresponding to a filled-shell configuration in the core-less harmonic system of Fig. 16. Each line corresponds to the lowest monopole excitation of the respective systems, showing a decrease in the excitation gap with increasing particle number. Here, the regularization-procedure is not applied since it becomes ambiguous for the core-less Hamiltonian. The results are hence not fully converged, but rather represent upper limits of the true excitation-energies. This figure is taken from the supplementary material of paper I.

6.9 Outlook - Hartree-Fock Bogoliubov calculations

The normal-to-superfluid transition has also been studied for the Hartree-Fock Bogoliubov (HFB) method [119], which is a self-consistent field method that, contrary to the regular Hartree-Fock (HF) method, accounts for some degree of pair correlation between particles. For a recent example relating to few-body Higgs modes, see [120]. The HFB method can be extended to a multiconfiguration-type scheme where a set of HFB solutions form a non-orthogonal basis for solving the Hamiltonian in Eq. (11). Such a method is a promising candidate for calculations involving larger particle numbers, and also offers another perspective on Higgs modes around the normal-to-superfluid transition in the few-body 2D harmonic oscillator.

The basic HFB method is based on the Bogoliubov transformation which introduces quasi-particle operators that are used in a minimization procedure of the ground state energy. The ground state $|HFB\rangle$, retrieved from the self-consistent minimization, is partly defined in terms of the so-called abnormal density matrix,

$$\kappa_{ij} = \langle HFB|\hat{a}_i\hat{a}_j|HFB\rangle$$

where $\hat{a}_i$ is the annihilation operator associated with single-particle state i [119]. The strength of pairing in an HFB solution is represented by the matrix,

$$\Delta_{ij} = \frac{1}{2}\sum_{kl} V^{\delta}_{ijkl}\kappa_{kl} \tag{14}$$

where V^{δ}_{ijkl} is the many-body matrix element for the delta function in Eq. (11). A suitably chosen and normalized matrix norm $\Delta_{pairing} \equiv |\Delta_{ij}|$, represents a scalar measure of the amount of pairing in an HFB-state.

To showcase the applicability of the basic HFB method for our system, the HFB equations [119] were solved over a range of values for the interaction strength g for a model-space of six single-particle harmonic shells. The same configurations of particles, $3+3$ and $6+6$, as in the previous section were used here.

In Fig. 18 the ground state energies from the HFB-solutions are compared to the regular HF-method and the exact CI-calculations within the same single-particle basis. At the point of the phase transition, $g \sim 3.5(\hbar\omega)\eta^2$, the HFB energies become considerably lower than the HF energies, indicating that the pairing energy gives a large contribution to the ground state that is not accounted for in HF. This indicates that the HFB method captures some of the pair-correlations that are responsible for the transition in the ground state, and for the appearance of Higgs modes.

This fact is further established in Fig. 19, where the energies of some HFB-states are plotted against $\Delta_{pairing}$. By introducing a scaling parameter, the pairing strength was forced towards higher or lower values with respect to the actual value Δ_{min} found for the HFB-solution. The energy reaches a minimum for $\Delta_{pairing} = \Delta_{min}$. Each curve represents the energy associated with a modulation in pairing strength, with respect to the actual pairing in the ground state. We can see how the energy cost of a pairing modulation here reaches a minimum around the phase transition, consistent with the results in the previous section.

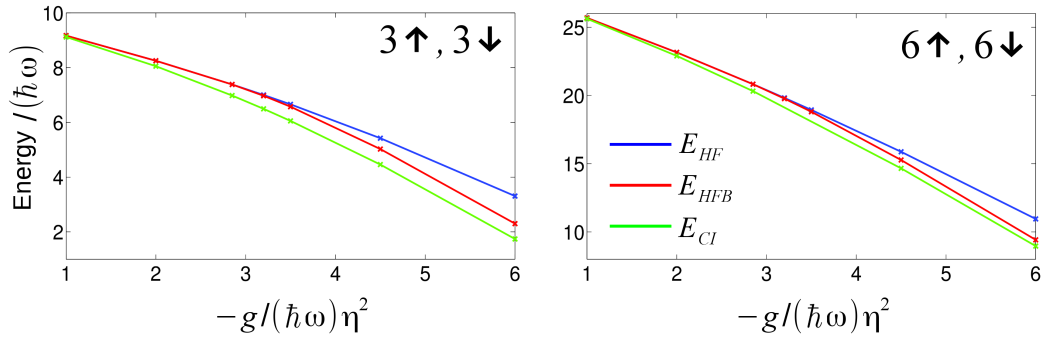

Figure 18: Ground state energy for a 2D harmonic oscillator with $3+3$ (left), and $6+6$ (right) particles. The energies are calculated using HF (blue lines), HFB (red lines) and CI (green lines) for a model-space with six harmonic shells. For $6+6$ the CI-energies represent an upper bound. After the point of the transition into a paired ground state , $g \sim -3$, the HFB calculations give considerably better results than the HF-calculations.

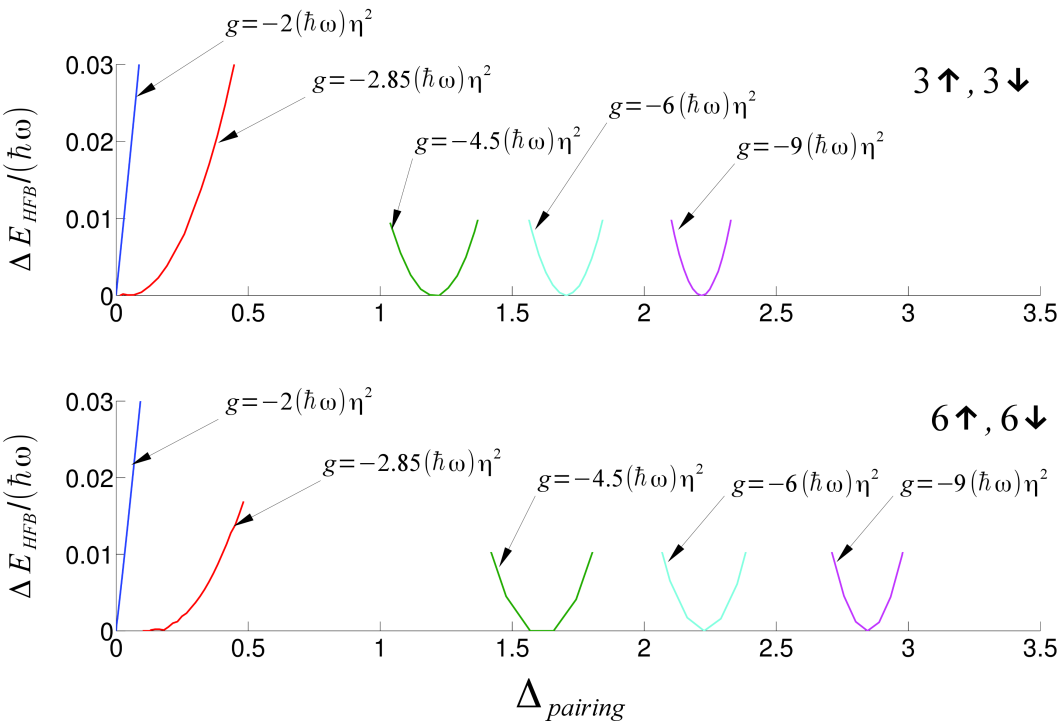

Figure 19: HFB ground state energies for a few different interaction strengths g. The parameter $\Delta_{pairing}$ represents a scalar measure on the amount of pair-correlation in the ground state. Each curve is sampled by "forcing" the pairing towards higher or lower values than that of the true value, Δ_{min}, for the ground state. Note that the sensitivity of the HFB energy with respect to pairing-modulations is smallest around the transition at $g \sim -3$.

7 Few-body localization and short-range behavior in parallel quasi one-dimensional traps with dipoles

As mentioned in the introduction, ultracold systems with dipoles have shown to give rise to a lot of different many-body and few-body effects, for a review see for example [19, 20]. In particular, the long range of the dipole-dipole interaction (DDI) is relevant for studies of systems comprised of two or more spatially separated traps. For example, in so-called bi-layer systems with two separated quasi-2D traps, the DDI between the layers may realize a superfluid state of dimer pairs, see e.g. [121–123].

Setups with two parallel quasi-1D traps have also been studied extensively, both in the many- and few-body limit, see e.g. [124–129]. In particular the (intertrap) interaction between different traps is responsible for the formation of bound dimers between the separate traps [130]. Interestingly, the low-energy limit of the inter-trap DDI can be approximated by a delta function with suitably rescaled interaction strength, see for example [129, 131, 132].

In paper V we study the dynamical properties of a system with two parallel quasi-1D harmonic traps with a few dipolar bosons or fermions. We consider an exact form of the interaction potential, showing that by tuning the alignment of the dipoles relative to the confinement, few-body localization within the traps can be enhanced by the formation of dimers between particles in different traps [126]. We investigate the crossover region between a localized dimer state and a separated, non-bound state by analyzing some of the dynamical properties of the system. It is seen that the short-range part of the DDI gives rise to a particular kind of excited state, which has some analogies to the super-Tonks-Girardeau states in mixtures of particles with short-range interaction.

7.1 Model

We consider two parallel quasi-1D harmonic traps, T_n and $T_{n'}$, with fermionic or bosonic dipoles. The trapping potential reads

$$V_n^{\text{trap}}(\mathbf{r}) = \frac{m}{2}\omega_x^2 x^2 + \frac{m}{2}\omega_\perp^2 \left[y^2 + (z - nz_w)^2\right] \ . \tag{15}$$

where n denotes the trap index, m is the mass, and ω_x and $\omega_\perp$ are the trapping frequencies in the x-direction and yz-plane, respectively. The setup is sketched in Fig. 20.

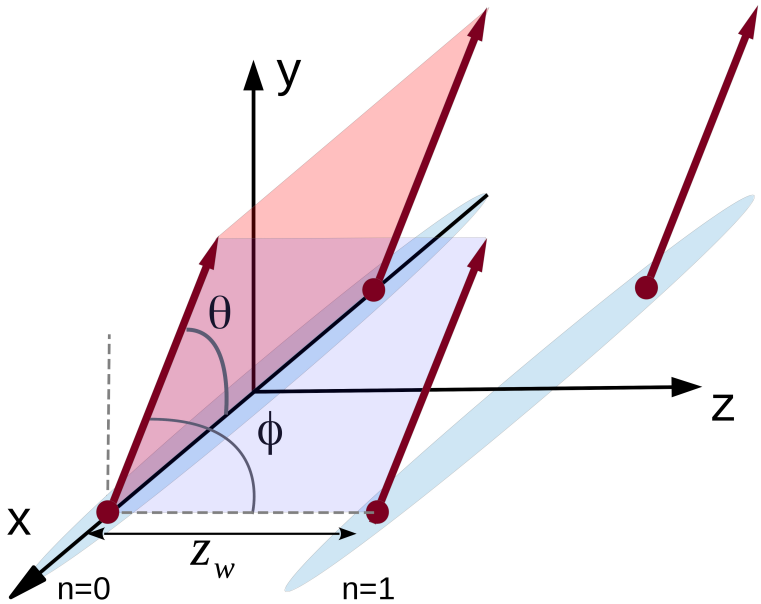

Figure 20: Sketch of two quasi 1D harmonic traps with four dipolar particles. The direction of the dipole moments are indicated by the red arrows, with directions defined by the two angles θ and ϕ. The distance between the traps is denoted by z_w. This figure is taken from paper V.

The effective DDI is calculated by assuming that the traps always are in the lowest transversal energy state of the harmonic confinement so that particles only move along the x-direction. We can separate the DDI into two parts: *inter-trap* interaction $V^{\text{eff}}_{n,n'}(x)$, meaning DDI between traps, and *intratrap* interaction $V^{\text{eff}}_{n,n}(x)$, meaning DDI within one trap. We use dimensionless units $\hbar = m = 1$, and energies are given in units of oscillator frequency $\hbar\omega_x$ and lengths in terms of oscillator length $l_x = \sqrt{\hbar/m\omega_x}$.

We only consider the case $\theta = 90°$, where the dipoles are aligned perpendicular to the x-axis, giving an effectively repulsive $V^{\text{eff}}_{n,n'}$. The interaction strength is given in terms of the dimensionless parameter $d^2 m/\left(\hbar^2 l_x \gamma\right) = 8\pi$, where $\gamma = \epsilon_0$ for electric dipoles and ϵ_0 is the permittivity of free space. The interaction strength is chosen so that the single-trap states are always in the fermionized regime, which means that for more than one particle in each trap, the particles cannot be found at the same position (see section 3). Since particles are fermionized within each trap, we can also neglect the delta-function term sometimes included in the effective 1D DDI of a single trap [124, 133, 134]. The inter-trap distance is given in terms of the parameter $z_w = 25 l_x/l_\perp$, which is sufficiency large for the tunneling between traps to be strongly suppressed.

With these restrictions, it is convenient to express a general state in terms of a tensor product of the different traps

$$|\psi\rangle = |\psi_n\rangle \bigotimes |\psi_{n'}\rangle$$

where n and n' denotes the pseudo spin associated with trap T_n and trap $T_{n'}$, respectively. The intertrap interaction may then expressed as an operator which couples different pseudo spin states. An approximate form of the intertrap interaction potential can be found by taking $\sqrt{\hbar/m\omega_\perp} \to 0$.

$$V_{n,n'}^{\text{eff},\theta=90}(\tilde{x}) = d^2 \left[\frac{1}{(z_\omega^2 + \tilde{x}^2)^{3/2}} - \frac{3z_\omega^2}{(z_\omega^2 + \tilde{x}^2)^{5/2}} \cos^2\phi \right] \tag{16}$$

where $\tilde{x}$ is the relative distance between two particles, along the x-axis. This form is exact for our choice of parameters, so we use it hereafter. $V_{n,n'}^{\text{eff}}$ specifically depends on the alignment of the dipoles relative to the trap, given by the angle ϕ, on the distance between traps z_w, and on the distance $\tilde{x}$ between particles along x.

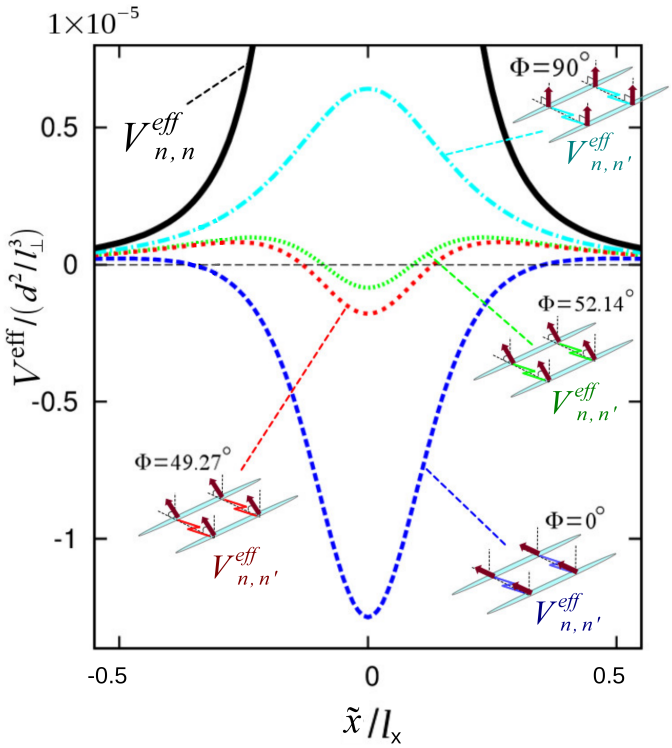

Figure 21: Effective DDI, approximated by Eq. (16) for different angular configurations of the double trap system, as a function of the relative The short-range part of $V^{\text{eff}}_{n,n'}$ can be changed toward positive or negative values by tuning ϕ, as sketched in the insets. This figure is taken from paper V.

7.2 Methods

The Hamilton matrix of the double trap system is diagonalized with the B-spline piece-wise polynomial basis [34], see section 2. For details on the numerical calculations, see paper V. The dipolar angle ϕ is tuned over a region of values, giving a crossover from repulsive to attractive short-range $V^{\text{eff}}_{n,n'}(x)$, as shown in Fig. 21. Two different configurations of particles are investigated; one with a single particle in each trap, and one with two particles in each trap.

7.3 One particle in each trap

For a simple system with one particle in each trap (1+1), we study the ground state transitions from a non-bound state at angle $\phi = 90°$ into a bound dimer state at angle $\phi \lesssim 49°$. In Fig. 21 we see how an attractive core of $V^{\text{eff}}_{n,n'}$ appears for $\phi \sim 54°$, and becomes deeper and wider for successively smaller angles. A bound state is formed when the depth and width of the attractive core are sufficiently large for the binding energy to overcome the cost in kinetic energy associated with confining the particles within the attractive range.

In Fig. 22 the superimposed single particle densities, $\rho_{T_n} + \rho_{T_{n'}}$, see Eq. (3), of the two parallel traps are shown for two ground states - one on each side of the transition at $\phi \sim 51°$. The particular choices of angles are motivated by the numerical treatment of the Hamiltonian. For angles $\lesssim 49°$, the convergence with respect to increasing size of the single-particle basis is so slow that exact diagonalization becomes impractical.

We see that the non-bound ground state, here at $\phi = 52°$, has two distinct peaks of higher density, similar to the density of two spin-polarized fermions in a single trap, hinting at the separation between particles along x. The pair-correlated density further emphasizes this separation; for a reference particle at $x = 0$ in trap T_n, there is a diminished probability of also finding the particle in trap $T_{n'}$ at $x = 0$.

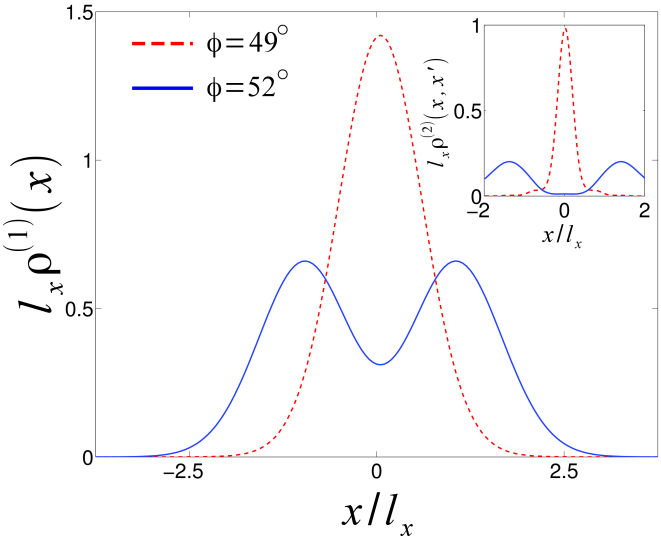

Figure 22: Single-particle density $\rho_{T_n} + \rho_{T_{n'}}$ for the ground state of a doubletrap system with one particle in each trap. The densities are plotted for two different dipolar angles, $\phi = 49°$ and $\phi = 52°$. Inset: Pair-correlated densities for a reference particle at $x = 0$. For $\phi = 49°$ the attractive part of $V^{\text{eff}}_{n,n'}$ produces a bound dimer with high probability of finding two particles at the same position. For $\phi = 52°$ the repulsive parts of $V^{\text{eff}}_{n,n'}$ produces a separated state with very small probability of finding two particles at the same position.

The curves for the dimer ground state at $\phi = 49°$ show an entirely different behavior, where the single-particle density does not have the characteristic "wiggles" of a fermionic state [50], but rather suggests a single compound of two particles that are bound together. This is again manifested in the pair-correlated density for a reference particle at $x = 0$ in trap T_n, which shows a significant probability of finding the particle in $T_{n'}$ at the same position in x. The existence of few-body bound states has been discussed for setups with multiple parallel quasi-1D traps, see for example [130].

7.3.1 Transition into a dimer

Now, we imagine a situation where the ground state is prepared in a non-bound state at $\phi_0 \gtrsim 51°$, and ϕ is adiabatically tuned towards angles which give a bound state $\phi \lesssim 51°$. This procedure will slowly transform the state into a bound (dimer) state [130].

However, we find that a sudden change in the angle, $\phi_0 \to \phi = 49°$, does not necessarily bring the system into a dimer state, but might instead populate a particular excited state at $\phi = 49°$. This state was shown to have an overlap

close to unity with the ground state at $\phi = 90°$. Since the excited state is very similar to the separated ground state, it only has a weak dependence on the dipolar angle ϕ, which means that the state is weakly affected by the attractive short-range part of the effective DDI.

To further investigate the outcome of a sudden change $\phi_0 \to \phi = 49°$ we calculate the uncertainty in energy,

$$\sigma_E = \sqrt{\langle\psi_0(\phi_0)|H^2(\phi)|\psi_0(\phi_0)\rangle - \langle\psi_0(\phi_0)|H(\phi)|\psi_0(\phi_0)\rangle^2}, \tag{17}$$

which represents the shortest time scale that characterize a significant change in the system, where the time scale decreases with increasing σ_E. For $\sigma_E = 0$, $\psi_0(\phi_0)$ is an eigenstate of the Hamiltonian $H(\phi)$. A non-zero σ_E means non-stationary states. The uncertainty shows that for $\phi_0 = 90°$ we have reached a state which is close to stationary compared to the state reached for $\phi_0 = 52°$. Furthermore, the uncertainty depends only weakly on ϕ for $\phi_0 = 90°$, confirming that the state is largely separated.

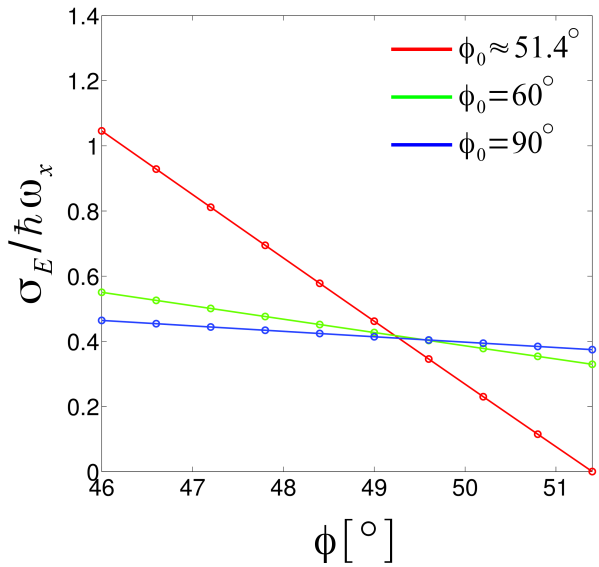

Figure 23: Energy uncertainty σ_E for a state ψ_0 after a sudden change in the dipolar angle to $\phi \lesssim 49°$, which corresponds to the attractive regime where the true ground state is a bound dimer. When ψ_0 prepared in the non-bound ground state at $\phi = 90°$, the energy uncertainty is weakly dependent on ϕ, compared to a state prepared at $\phi \sim 52°$.

Since the particles remain separated in the excited state, the formation of a dimer is suppressed. The existence of such a state was predicted in [130], where it was noted that the short-range nature of the inter-trap DDI should give rise

to physics that was analogous to that of particles interacting via a delta pseudo-potential. The analogy here is the super-Tonks-Girardeau state, discussed in section 3, which can be populated by a sudden quench in the interaction. We expand on this analogy in the appendix.

7.4 Two particles in each trap - Enhanced localization by formation of dimers

For a configuration with more than one particle in each trap (N_n+$N_{n'}$), the formation of bound states between particles in different traps is especially interesting. The binding between wires is known to greatly affect the single trap states, for example by enhancing localization [126]. Dipole-dipole coupling between separated traps is responsible for many interesting quantum phases, such as dimer- and trimer-liquids [127, 128].

Figure 25 shows the single-particle densities of trap T_n for a non-bound state at $\phi = 52°$, either with fermions or bosons. We note four distinct region of high density, which indicates that a particle in trap T_n avoids the remaining particle in the same trap, and also the two particles in trap $T_{n'}$. The particles in T_n feels the repulsive part of $V^{\text{eff}}_{n,n'}$ from each of the two particles in $T_{n'}$. Therefore, particles repel each other, both within the same trap and across the different traps.

Looking at the projected single-trap states at $\phi = 52°$, $|\psi_{n_0}\rangle$ and $|\psi_{n_1}\rangle$, we see that they each are in the fermionized regime, since the single-particle densities are identical for bosons and fermions. However, there is non-zero overlap in the probability distributions of particles in the same trap. This overlap is subtle and can not be seen directly in the pair-correlated plots in Fig. 25, but can be inferred from the fact that the momentum distributions of fermions and bosons differ, which means that the state is not localized [42, 54]. From the pair-correlation between two particles in different traps, one can again see that the repulsive part of $V^{\text{eff}}_{n,n'}(x)$ causes particles to line up in a checkerboard-pattern, with a small but non-zero probability of finding particles at the same position in x.

By tuning ϕ towards smaller values, we can dramatically alter the ground state of the double-trap system. Figure 24 shows the ground state of a 2+2 system at $\phi \sim 49°$, where two bound complexes have formed between particles in different traps. Compared to a system with no interaction between the traps, the localization in the single trap is enhanced by the formation of dimers. As a measure of this, we again compare the momentum distribution of the fermionic

and the bosonic system. As noted before, when localization sets in, the bosonic and fermionic momentum distributions converge onto the same curve. This is understood by the simple fact that there is zero overlap between the different wave functions of each particle so that the statistics no longer matter. The existence of bound dimers is also recognized from the pair-correlated densities in Fig. 24. For a reference particle in trap T_n, there is a large probability of finding a second particle in the opposite trap at the same position in x. The pair-correlation plots also confirm that the overlap of particles in the same trap is diminished by the binding since the pair-correlation between two particles at the same position is close to zero.

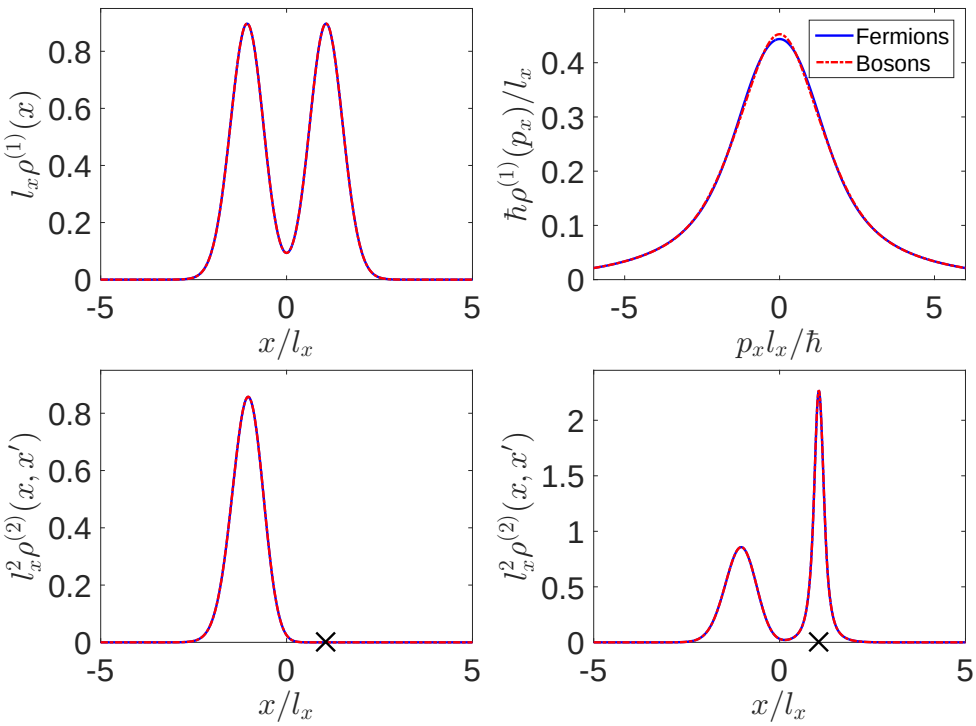

Figure 24: Ground state density distributions for a $2+2$ system ($N_n = N_{n'} = 2$) with $\phi \sim 49°$, for which the attractive part of $V^{\text{eff}}_{n,n'}$ is sufficiently strong to form a bound ground state (see Fig. 21). The solid blue lines correspond to a system of fermions, and the dashed red lines to a system of bosons. **Top left:** Single particle density in trap T_n. The fermionic and bosonic densities are next to identical, so the state is fermionized. **Top right:** Density distribution in momentum space. The fermionic and bosonic densities are identical, which indicates that the state is localized. **Bottom left:** Pair-correlated density for particles in the same trap. A reference particle is placed at the position of the second peak in the top left figure, as indicated by an X. **Bottom left:** Pair-correlated density for particles in opposite traps, with the reference particle again placed at the position of the second peak. This figure is taken from paper V.

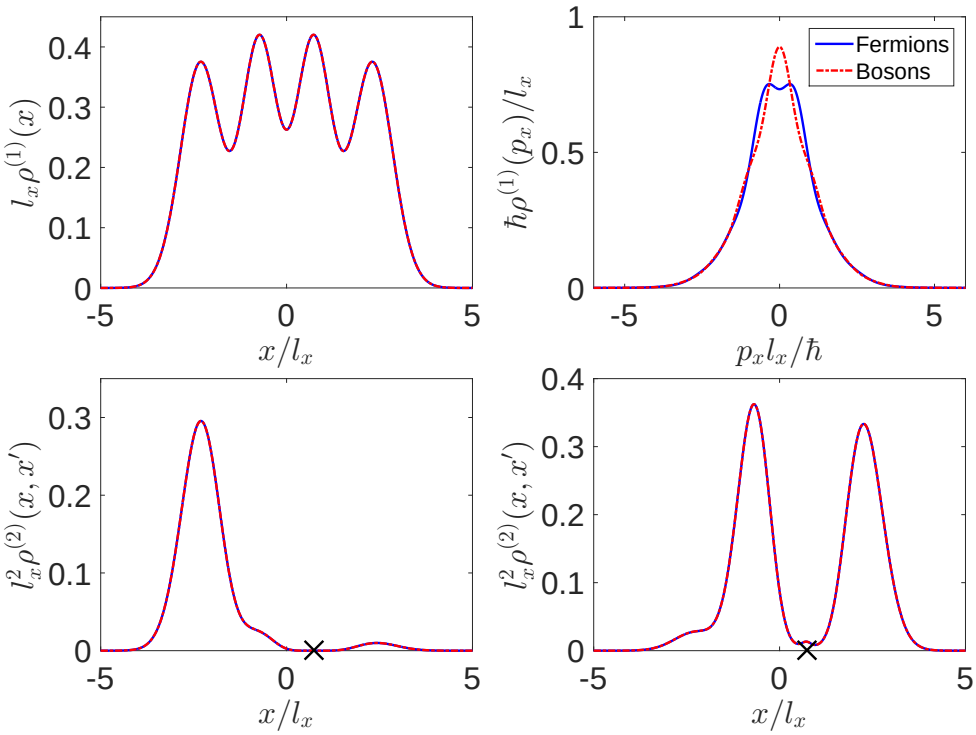

Figure 25: Similar to Fig. 24 but for $\phi \sim 52°$. Here, the ground state does not have bound dimers between traps. This figure is taken from paper V.

7.4.1 Transition into a localized state with two dimers

We saw that it was possible to bring the double trap system in and out of localization by tuning ϕ. By preparing the state in the non-localized and non-bound state at some angle between $\phi \sim 52°$ and $\phi = 90°$ and adiabatically tuning ϕ towards smaller values one can continuously change the few-body state towards stronger localization. However, like in the case of one particle in each wire, a quick change in ϕ gives a very different outcome.

In the energy-spectrum above the bound ground state at $\phi \sim 49°$, one finds, like in the 1+1 system, highly excited states that that have significant overlaps with the non-bound ground state at $\phi \gtrsim 52°$. The outcome of a quick change in ϕ strongly depends on the nature of these highly excited states. Since the non-bound ground state at $\phi \gtrsim 52°$ may be close to a stationary state of the Hamiltonian at $\phi \sim 49°$, sudden changes in ϕ may transfer a significant part of the population into such excited states, rather than into a bound and localized

state. Simulations showed that after a fast sweep of ϕ from $\phi_0 = 90°$ to $\phi = 49°$, mainly two excited states were occupied. Both states had a weak dependency on ϕ compared to other states and showed the very similar densities as those for the repulsive ground state at ϕ. The energy uncertainty in the initial state was hence only weekly dependent on ϕ and was furthermore restricted to comparatively small values also in the strongly attractive regime, as shown in Fig. 26. We can hence conclude that the formation of dimers and the resulting onset of localization was prohibited.

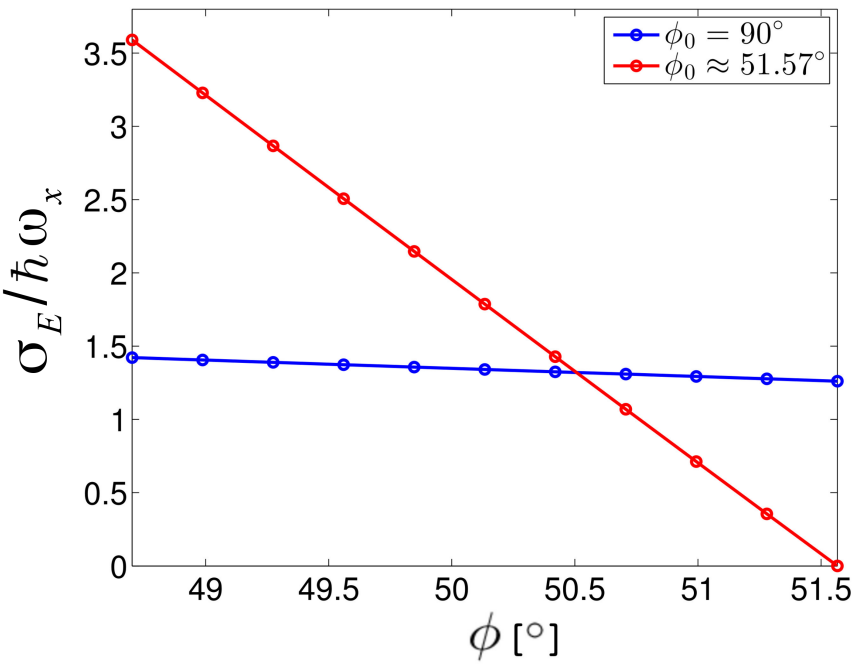

Figure 26: Energy uncertainty σ_E for a state Ψ_0 after a sudden change in the dipolar angle to $\phi = 49°$, which corresponds to the attractive regime where the true ground state has bound dimers. When ψ_0 prepared in the non-bound ground state at $\phi = 90°$, the energy uncertainty is weakly dependent on ϕ, compared to a state prepared at $\phi \sim 52°$.

When starting at $\phi_0 \sim 52°$ the initial state has less separation between particles than an initial state prepared at $\phi_0 \sim 90°$, and when tuning to $\phi = 49°$ the energy uncertainty σ_E depends strongly on ϕ, reaching comparatively large values in the strongly attractive regime. This indicates a larger overlap with dimer states in the trap, which means that in order to suppress dimer formation after a quench to $\phi = 49°$, the initial state should be prepared at $\phi = 90°$, rather than at $\phi_0 \sim 52°$.

Appendix

Appendix

1 Short-range interaction potentials between particles in harmonic traps.

As noted in section 7, the effective intertrap dipole-dipole interaction between two quasi-1D traps is sometimes approximated with a delta pseudopotential, see for example [129, 131, 132]. This has led to discussions on how short-range phenomena, such as Tonks-Girardeau (TG) and super-Tonks-Girardeau (STG) states (see section 3), may appear in double-trap few-body systems [130]. Here, we explicitly compare behavior for a few different types of pseudopotentials with short-range properties, including the dipole-dipole intertrap pseudopotential in Eq. (16).

For comparison, we first consider the Hamiltonian in Eq. (6). This Hamiltonian represents an effective 1D system with contact-interacting particles, which is the typical setting to observe TG and STG states, see for example [48–51]. Here we use the same system of units as in section 5.3.

We specifically consider a setup for a Bose-Fermi mixture, which offers a direct comparison to the setup in the double-trap system in section 7. This is the case since both setups can be described in terms of two pseudo-spin states, each representing a particle species that is distinguishable from the other. We note that Girardeau's mapping of strongly interacting bosons onto spinless non-interacting fermions, see section 3, is applicable also to Bose-Fermi mixtures [55]. For example, this mapping was employed to construct a spin chain from mixtures in paper IV.

For a setup with one boson and one fermion, the Hamiltonian in Eq. (6) is diagonalized for a range of values of interaction strength g_{1D}. We then analyze the spectrum and the corresponding energy eigenfunctions.

Figure 28 shows the spectrum of one boson and one fermion. The horizontal lines in the spectrum correspond to spatially antisymmetric wave functions, which are independent of the interaction. For a system of spinless fermions, only the spatially antisymmetric spatial functions would appear in the spectrum, and the system would be non-interacting. For $g_{1D} \gtrsim \pm 9\hbar\omega l$ the ground state, marked blue in the plot, approaches energy $E = 2\hbar\omega$, which is the energy of two non-interacting spinless fermions. The particular value of g_{1D} is chosen for numerical reasons; the identification of the relevant states in the spectra becomes increasingly complex with stronger attraction.

In the TG limit, $g \to \infty$, analytic results state that the energy completely saturates, see for example [48, 49]. This is the case since the hard-core boundary

condition $\Psi(x_1 = x_2) = 0$ there applies to the wavefunction, and the energy is therefore independent of the interaction strength g_{1D}. In the infinitely attractive limit, $g_{1D} \to -\infty$, the same boundary condition applies to a set of excited states, as briefly discussed in section 3.2. The lowest of these states, which saturates at $E = 2\hbar\omega$ for $g_{1D} \to -\infty$, is marked red in Fig. 28. This state was identified as a few-body, finite-interaction precursor of an STG in Ref. [51], in which a narrow Gaussian contact pseudopotential was employed.

Like the energy, other observables of the wave function also approach those of spinless non-interacting fermions for $g_{1D} \to -\infty$, see section 3 again. Figure 27 shows that the single-particle density distributions in the states marked in the spectrum each become similar to that of spinless fermions, and thus also to each other.

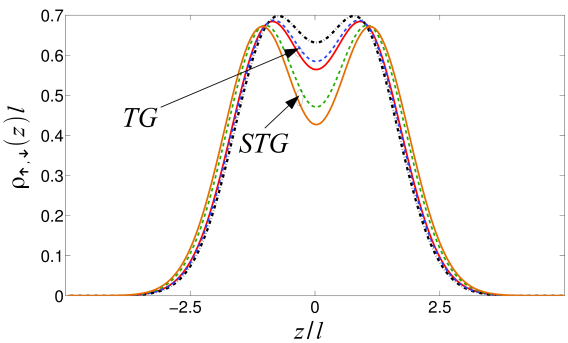

Figure 27: Single particle densities for one fermion and one bosons in a harmonic trap, corresponding to the spectrum in Fig. 28, of the Hamiltonian in Eq. (6). The solid lines correspond to $g_{1D} = \pm 9\hbar\omega$, the dashed lines to $g_{1D} = \pm 20l\hbar\omega$, and the dash-dotted line to the spatially antisymmetric state of two non-interacting spin-polarized fermions (included for comparison). The density profiles of the states marked TG and STG each converge onto the dash-dotted line for successively stronger interaction and in the unitary limit, $g_{1D} = \pm\infty$, their density profiles are identical to that of the spatially antisymmetric state.

As also mentioned in section 3, STG states are typically produced by preparing a system in the TG ground state at strong repulsion, and then make a sudden quench the interaction towards strong attraction. This works if the TG states are stationary in the regime of strong attraction. In Fig. 29 we plot the uncertainty in energy, (see Eq. (17) and the following discussion in section 7), for the ground state $|\psi(g_{1D}^0)\rangle$ prepared at different interaction strengths in the repulsive regime. The uncertainty shows that states prepared at strong repulsion have smaller uncertainty in the attractive regime $g_{1D} \sim -30l\hbar\omega$ than those prepared for weak repulsion. Also, the uncertainty of the strongly repulsive states only depends weakly on the interaction strength. (Note that the exact values in Fig. 17 are not fully converged, but represent lower bounds of the uncertainty. The overall trend is however correct.) This indicates that one particular excited state at $-g_{1D}^0$

becomes increasingly similar to the ground state at g_{1D}^0 for successively stronger repulsion and also suggests that it develops into a stationary state for $g_{1D}^0 \to \infty$ and $g_{1D}^0 \to -\infty$. This behavior is consistent with the findings in Ref. [51], in which it was shown that the few-body TG and STG precursors indeed develop towards completely fermionized states at strong contact repulsion/attraction.

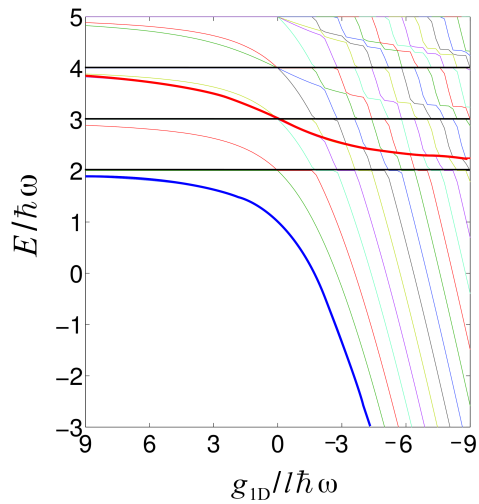

Figure 28: Energy spectra of the Hamiltonian in Eq. (6), for a system with one boson and one fermion in a harmonic trap at different interaction strengths g_{1D}. The thick blue and red lines indicate the TG and STG state precursors, respectively. In the limit $g_{1D} \to \pm\infty$, the lines fall onto the same energy, $E = 2\hbar\omega$, as the spatially antisymmetric state, which is independent of the interaction strength.

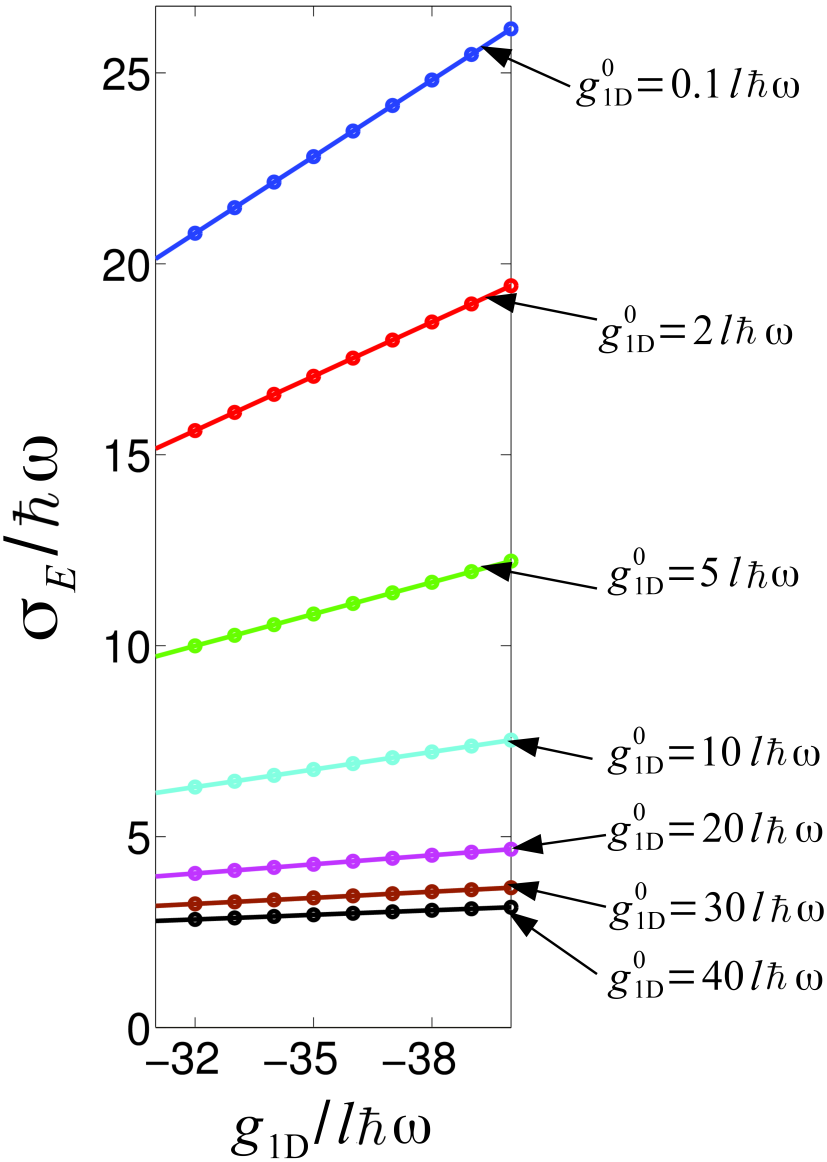

Figure 29: Energy uncertainties, defined in Eq. (17), as functions of the delta pseudopotential interaction strength g_{1D}. Each line represents an interaction strength g^0_{1D} at which the ground state is calculated. The values on the y-axis represents the spread in energy after a fast change in interaction strength $g^0_{1D} \to g_{1D}$ (Note that the exact values of uncertainty are not fully converged with respect to single-particle basis size, but represent lower bounds of the uncertainty. The overall trend is however correct.)

For two particles, in different pseudo-spin states, we calculate the spectrum for a few different choices of interaction potentials. We study an effective 1D harmonic system with trapping length $l_x = \sqrt{\hbar/m\omega_x}$, where ω_x is the trapping frequency along x. We study the effective 1D Gaussian contact potential,

$$V_{\text{Gauss}} = g \cdot e^{-z^2/2W^2}, \tag{18}$$

the effective dipole-dipole interaction between particles in different parallel traps (see Eq. (16)) (normalized so that g represents the peak value, i.e. $V(0) = g$), and the effective 1D dipole-dipole interaction between particles in the same quasi-1D trap,

$$V_{DDI} = g(\theta)\sqrt{\frac{1}{2\pi}}\left(2\frac{z}{W} + \sqrt{2\pi}(1 + \frac{z^2}{W^2})e^{z^2/W^2}\text{erfc}(\frac{z}{W\sqrt{2}})\right), \tag{19}$$

where erfc() is the complementary error function. Here, $g(\theta)$ points to the fact that the effective interaction strength for the dipole-dipole interaction in a 1D trap can be changed by the angle θ, which represents the alignment of the dipolar moments relative to the longest semiaxis in the trap.

For each of these potentials, we identify a parameter W which represents the width of the potential function. For the interaction between parallel traps in Eq. (16), we consider $W = z_w$. Figure. 30 is a schematic view of the spectra for different potentials. We see that the spectra are qualitatively similar to that of the delta pseudopotential in Fig. 28, with levels approaching the spatially antisymmetric state at $E \sim 2\hbar\omega_x$. The similarities are not surprising since all potentials have a short-range nature for $W \to 0$. For example, TG and STG states can be found for quasi-1D systems, either by considering a narrow Gaussian interaction pseudopotential or an effective 1D DDI [51, 66]. In contrast to the spectrum for the delta pseudopotential, we can, however, see that the spatially antisymmetric state feels the finite range of the other potentials, causing shifts in the energy.

For each of the systems, we also investigate the overlaps between the ground state at strong short-range repulsion and a particular excited state (marked red in Fig. 30) at strong short-range attraction. The results are summarized in table 1 and we see that for successively smaller W, meaning a more strongly peaked short-range potential, the overlaps increase. The excited state may hence be populated by preparing the ground state at strong repulsion, and then suddenly change the short-range interaction toward strong attraction. For the double trap system, this can be achieved by a quick shift in the dipolar angle ϕ. In section 7 the energy uncertainty after such a sudden shift in ϕ was calculated, see Fig. 23. We can compare this to the corresponding uncertainty calculated

for a system with a delta pseudopotential, see Fig. 29, after a sudden change in the interaction strength g. Both figures indicate that the ground state, prepared at successively stronger repulsion, develops towards a stationary state in the regime of strong attraction.

To summarize: the spectra, the overlaps and the uncertainties all points towards an analogy between the highly excited states discussed for the double trap in section 7, and the few-body STG precursor states discussed in Ref. [51].

Table 1: Overlap between the ground state at strong short-range repulsion g_0, and a highly excited states at strong short-range attraction $-g_0$. Here $g_0 \sim 20 l_x \hbar\omega_x$ represents the peak value of each potential i.e. $V(0) = g_0$. The results are obtained for three different interaction potentials; V_{Gauss} in Eq. (18), V_{DDI} in Eq. (19), and $V^{\text{eff}}_{n,n'}$ in Eq. (16). In the limit of small W, each potential is strongly peaked around $x_i = x_j$. Note that $V^{\text{eff},\theta=90}_{n,n'}$ reproduces a large overlap for a small inter-wire length, which was discussed in section 7. Also V_{DDI} produces large overlaps with the ground state, as predicted in [66].

Width-parameter W	0.1	0.25	0.5	0.8
$V(W)_{Gauss}$	0.99	0.99	0.92	0.8
$V(W)_{DDI}$	0.98	0.97	0.91	0.82
$V(W)^{\text{eff}}_{n,n'}$	0.99	0.98	0.98	0.8

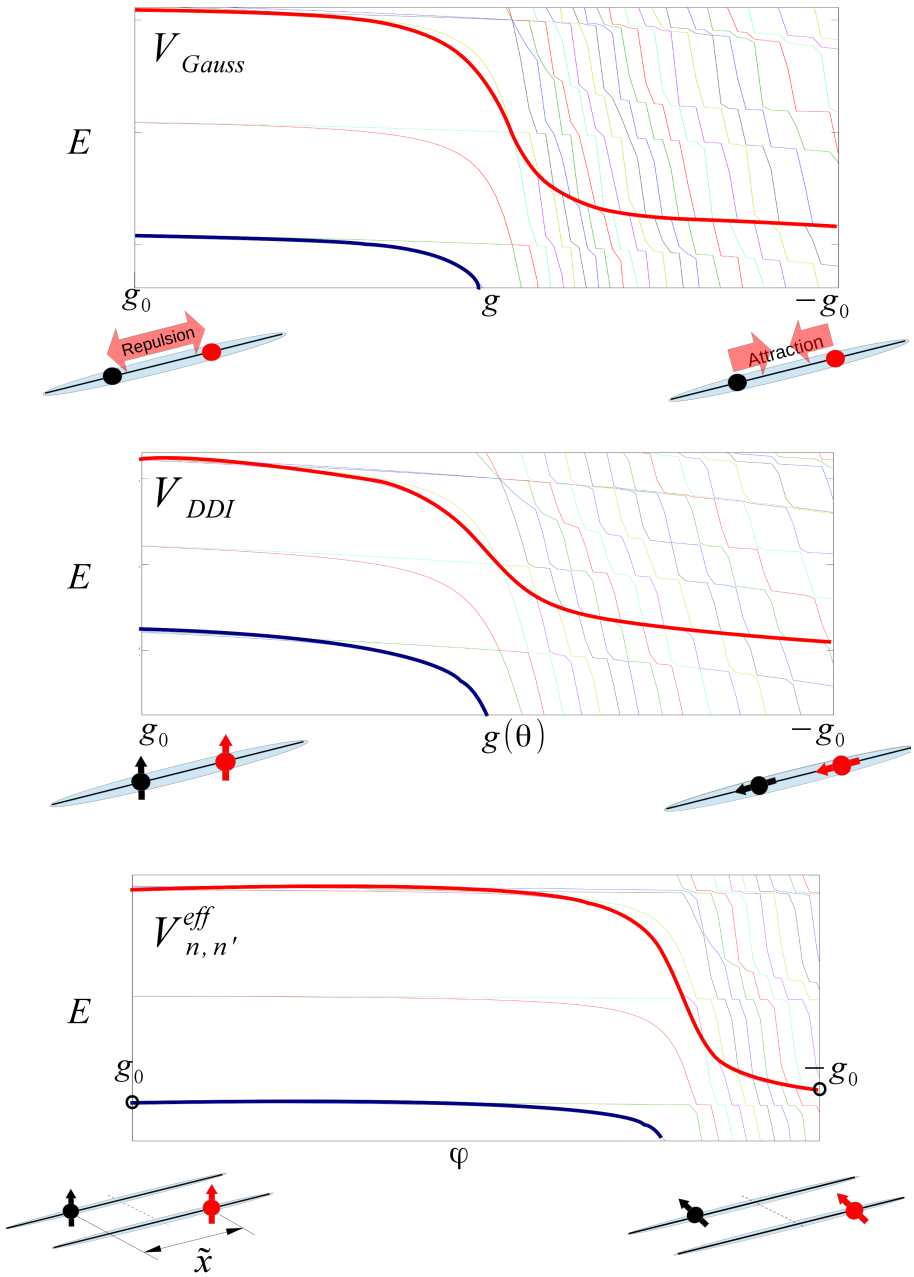

Figure 30: A schematic view of the different energy spectra for two particles in a quasi 1D harmonic trap. The spectra are sketched for three different interaction pseudopotentials; V_{Gauss} in Eq. (18), V_{DDI} in Eq. (19), and $V^{\text{eff}}_{n,n'}$ in Eq. (16). Here, g represents the peak value of each potential $V(0) = g$. The spectra all have a similar structure.

Bibliography

[1] M. H. Anderson, J. R. Ensher, M. R. Matthews, C. E. Wieman, E. A. Cornell, et al. Observation of Bose-Einstein condensation in a dilute atomic vapor. *Science*, 269(5221):198–201, 1995.

[2] B. DeMarco and D. S. Jin. Onset of Fermi degeneracy in a trapped atomic gas. *Science*, 285(5434):1703–1706, 1999.

[3] E. A. Cornell and C. E. Wieman. Nobel Lecture: Bose-Einstein condensation in a dilute gas, the first 70 years and some recent experiments. *Reviews of Modern Physics*, 74(3):875, 2002.

[4] C. A. Regal, M. Greiner, and D. S. Jin. Observation of resonance condensation of fermionic atom pairs. *Physical Review Letters*, 92(4):040403, 2004.

[5] M. W. Zwierlein, C. A. Stan, C. H. Schunck, S. M. F. Raupach, A. J. Kerman, and W. Ketterle. Condensation of pairs of fermionic atoms near a Feshbach resonance. *Physical Review Letters*, 92(12):120403, 2004.

[6] S. N. Bose. Planck's gesetz und lichtquantenhypothese. *Zeitschrift für Physik*, 26:178–181, 1924.

[7] A. Einstein. *Quantentheorie des einatomigen idealen Gases*. Akademie der Wissenshaften, in Kommission bei W. de Gruyter, 1924.

[8] C. C. Bradley, C. A. Sackett, J. J. Tollett, and R. G. Hulet. Evidence of Bose-Einstein condensation in an atomic gas with attractive interactions. *Physical Review Letters*, 75(9):1687, 1995.

[9] K. B. Davis, M.-O. Mewes, M. R. Andrews, N. J. Van Druten, D. S. Durfee, D. M. Kurn, and W. Ketterle. Bose-Einstein condensation in a gas of sodium atoms. *Physical Review Letters*, 75(22):3969, 1995.

[10] V. L. Ginzburg and L. D. Landau. On the theory of superconductivity. *Zhurnal Eksperimentalnoi i Teoreticheskoi Fiziki*, 20(1064-1082):35, 1950.

[11] M. R. Matthews, B. P. Anderson, P. C. Haljan, D. S. Hall, C. E. Wieman, and E. A. Cornell. Vortices in a Bose-Einstein condensate. *Physical Review Letters*, 83(13):2498–2501, 9 1999.

[12] M. Greiner, C. A. Regal, and D. S. Jin. Emergence of a molecular Bose-Einstein condensate from a Fermi gas. *Nature*, 426(6966):537–540, 2003.

[13] M. W. Zwierlein, J. R. Abo-Shaeer, A. Schirotzek, C. H. Schunck, and W. Ketterle. Vortices and superfluidity in a strongly interacting Fermi gas. *Nature*, 435(7045):1047–1051, 2005.

[14] A. L. Fetter. Rotating trapped Bose-Einstein condensates. *Reviews of Modern Physics*, 81(2):647, 2009.

[15] I. Bloch, J. Dalibard, and W. Zwerger. Many-body physics with ultracold gases. *Reviews of Modern Physics*, 80(3):885, 2008.

[16] E. Fermi et al. Motion of neutrons in hydrogenous substances. *Ricerca Sci*, 7:13–52, 1936.

[17] K. Huang and C. N. Yang. Quantum-mechanical many-body problem with hard-sphere interaction. *Physical Review*, 105(3):767, 1957.

[18] J. Levinsen, M. M. Parish, et al. Strongly interacting two-dimensional Fermi gases. *Annual Review of Cold Atoms and Molecules*, 3:1–75, 2015.

[19] M. A. Baranov. Theoretical progress in many-body physics with ultracold dipolar gases. *Physics Reports*, 464(3):71–111, 2008.

[20] T. Lahaye, C. Menotti, L. Santos, M. Lewenstein, and T. Pfau. The physics of dipolar bosonic quantum gases. *Reports on Progress in Physics*, 72(12):126401, 2009.

[21] H. Feshbach. Unified theory of nuclear reactions. *Annals of Physics*, 5(4):357–390, 1958.

[22] U. Fano. Effects of configuration interaction on intensities and phase shifts. *Physical Review*, 124(6):1866, 1961.

[23] P. Courteille, R. S. Freeland, D. J. Heinzen, F. A. Van Abeelen, and B. J. Verhaar. Observation of a Feshbach resonance in cold atom scattering. *Physical Review Letters*, 81(1):69, 1998.

[24] S. Inouye, M. R. Andrews, J. Stenger, H. J. Miesner, et al. Observation of Feshbach resonances in a Bose-Einstein condensate. *Nature*, 392(6672):151, 1998.

[25] M. Lewenstein, A. Sanpera, V. Ahufinger, B. Damski, A. Sen, and U. Sen. Ultracold atomic gases in optical lattices: mimicking condensed matter physics and beyond. *Advances in Physics*, 56(2):243–379, 2007.

[26] F. Serwane, G. Zürn, T. Lompe, T. B. Ottenstein, A. N. Wenz, and S. Jochim. Deterministic preparation of a tunable few-fermion system. *Science*, 332(6027):336–338, 2011.

[27] A. N. Wenz, G. Zürn, S. Murmann, I. Brouzos, T. Lompe, and S. Jochim. From few to many: Observing the formation of a Fermi sea one atom at a time. *Science*, 342(6157):457–460, 2013.

[28] C. J. Cramer. *Essentials of computational chemistry: theories and models*. John Wiley & Sons, Chichester, 2013.

[29] R. D. Cowan. *The theory of atomic structure and spectra*. Number 3. University of California Press, 1981.

[30] L. N. Trefethen and D. Bau III. *Numerical linear algebra*, volume 50. Siam, Philadelphia, 1997.

[31] R. Roth. Importance truncation for large-scale configuration interaction approaches. *Physical Review C*, 79(6):064324, 2009.

[32] C. F. Fischer. *Hartree–Fock method for atoms. A numerical approach*. John Wiley and Sons, Inc., New York, 1977.

[33] V. J. Bolsinger, S. Krönke, and P. Schmelcher. Beyond mean-field dynamics of ultra-cold bosonic atoms in higher dimensions: facing the challenges with a multi-configurational approach. *Journal of Physics B: Atomic, Molecular and Optical Physics*, 50(3):034003, 2017.

[34] C. De Boor. *A practical guide to splines*, volume 27. Springer, New York, 1978.

[35] H. Bachau, E. Cormier, P. Decleva, J. E. Hansen, and F. Martín. Applications of B-splines in atomic and molecular physics. *Reports on Progress in Physics*, 64(12):1815, 2001.

[36] J. Mitroy, S. Bubin, W. Horiuchi, Y. Suzuki, L. Adamowicz, W. Cencek, K. Szalewicz, J. Komasa, D. Blume, and K. Varga. Theory and application

of explicitly correlated Gaussians. *Reviews of Modern Physics*, 85(2):693, 2013.

[37] W. Cencek and J. Rychlewski. Many-electron explicitly correlated Gaussian functions. I. General theory and test results. *The Journal of Chemical Physics*, 98(2):1252–1261, 1993.

[38] R. Jastrow. Many-body problem with strong forces. *Physical Review*, 98(5):1479, 1955.

[39] R. B. Dingle. LI. The zero-point energy of a system of particles. *The London, Edinburgh, and Dublin Philosophical Magazine and Journal of Science*, 40(304):573–578, 1949.

[40] W. M. C. Foulkes, L. Mitas, R. J. Needs, and G. Rajagopal. Quantum Monte Carlo simulations of solids. *Reviews of Modern Physics*, 73(1):33, 2001.

[41] P. Navrátil, S. Quaglioni, I. Stetcu, and B. R. Barrett. Recent developments in no-core shell-model calculations. *Journal of Physics G: Nuclear and Particle Physics*, 36(8):083101, 2009.

[42] F. Deuretzbacher. *Spinor Tonks-Girardeau gases and ultracold molecules*. PhD thesis, Universität Hamburg, 2009.

[43] T. Kinoshita, T. Wenger, and D. S. Weiss. Observation of a one-dimensional Tonks-Girardeau gas. *Science*, 305(5687):1125–1128, 2004.

[44] B. Paredes, A. Widera, V. Murg, O. Mandel, et al. Tonks-girardeau gas of ultracold atoms in an optical lattice. *Nature*, 429(6989):277, 2004.

[45] M. H. G. De Miranda, A. Chotia, B. Neyenhuis, D. Wang, G. Quéméner, S. Ospelkaus, J. L. Bohn, J. Ye, and D. S. Jin. Controlling the quantum stereodynamics of ultracold bimolecular reactions. *Nature Physics*, 7(6):502–507, 2011.

[46] M. Olshanii. Atomic scattering in the presence of an external confinement and a gas of impenetrable bosons. *Physical Review Letters*, 81(5):938, 1998.

[47] M. Girardeau. Relationship between systems of impenetrable bosons and fermions in one dimension. *Journal of Mathematical Physics*, 1(6):516–523, 1960.

[48] M. D. Girardeau, E. M. Wright, and J. M. Triscari. Ground-state properties of a one-dimensional system of hard-core bosons in a harmonic trap. *Physical Review A*, 63(3):033601, 2001.

[49] G. E. Astrakharchik, D. Blume, S. Giorgini, and B. E. Granger. Quasi-one-dimensional Bose gases with a large scattering length. *Physical Review Letters*, 92(3):030402, 2004.

[50] F. Deuretzbacher, K. Bongs, K. Sengstock, and D. Pfannkuche. Evolution from a Bose-Einstein condensate to a Tonks-Girardeau gas: An exact diagonalization study. *Physical Review A*, 75(1):013614, 2007.

[51] E. Tempfli, S. Zöllner, and P. Schmelcher. Excitations of attractive 1D bosons: binding versus fermionization. *New Journal of Physics*, 10(10):103021, 2008.

[52] A. G. Volosniev, D. V. Fedorov, A. S. Jensen, M. Valiente, and N. T. . Strongly interacting confined quantum systems in one dimension. *Nature Communications*, 5:5300, 2014.

[53] N. L. Harshman. Spectroscopy for a few atoms harmonically trapped in one dimension. *Physical Review A*, 89(3):033633, 2014.

[54] F. Deuretzbacher, J. C. Cremon, and S. M. Reimann. Ground-state properties of few dipolar bosons in a quasi-one-dimensional harmonic trap. *Physical Review A*, 81(6):063616, 2010.

[55] M. D. Girardeau and A. Minguzzi. Soluble models of strongly interacting ultracold gas mixtures in tight waveguides. *Physical Review Letters*, 99(23):230402, 2007.

[56] J. N. Fuchs, A. Recati, and W. Zwerger. Exactly solvable model of the BCS-BEC crossover. *Physical Review Letters*, 93(9):090408, 2004.

[57] L. Guan, S. Chen, Y. Wang, and Z.-Q. Ma. Exact solution for infinitely strongly interacting Fermi gases in tight waveguides. *Physical Review Letters*, 102(16):160402, 2009.

[58] E. J. Lindgren, J. Rotureau, C. Forssén, A. G. Volosniev, and N. T. Zinner. Fermionization of two-component few-fermion systems in a one-dimensional harmonic trap. *New Journal of Physics*, 16(6):063003, 2014.

[59] F. Deuretzbacher, K. Fredenhagen, D. Becker, K. Bongs, K. Sengstock, and D. Pfannkuche. Exact solution of strongly interacting quasi-one-dimensional spinor Bose gases. *Physical Review Letters*, 100(16):160405, 2008.

[60] A. S. Arkhipov, G. E. Astrakharchik, A. V. Belikov, and Y. E. Lozovik. Ground-state properties of a one-dimensional system of dipoles. *Jounal of Experimental and Theoretical Physics*, 82(1):39–43, 2005.

[61] S. Chen, L. Guan, X. Yin, Y. Hao, and X.-W. Guan. Transition from a Tonks-Girardeau gas to a super-Tonks-Girardeau gas as an exact many-body dynamics problem. *Physical Review A*, 81(3):031609, 2010.

[62] G. E. Astrakharchik, J. Boronat, J. Casulleras, and S. Giorgini. Beyond the Tonks-Girardeau gas: Strongly correlated regime in quasi-one-dimensional Bose gases. *Physical Review Letters*, 95(19):190407, 2005.

[63] L. Guan and S. Chen. Super-Tonks-Girardeau gas of spin-1/2 interacting fermions. *Physical Review Letters*, 105(17):175301, 2010.

[64] E. Haller, M. Gustavsson, M. J. Mark, J. G. Danzl, R. Hart, G. Pupillo, and H.-C. Nägerl. Realization of an excited, strongly correlated quantum gas phase. *Science*, 325(5945):1224–1227, 2009.

[65] H. P. Büchler, E. Demler, M. Lukin, A. Micheli, N. Prokof'ev, G. Pupillo, and P. Zoller. Strongly correlated 2D quantum phases with cold polar molecules: controlling the shape of the interaction potential. *Physical Review Letters*, 98(6):060404, 2007.

[66] M. D. Girardeau and G. E. Astrakharchik. Super-Tonks-Girardeau State in an Attractive One-Dimensional Dipolar Gas. *Physical Review Letters*, 109(23):235305, 2012.

[67] D. S. Petrov, M. Holzmann, and G. V. Shlyapnikov. Bose-Einstein condensation in quasi-2D trapped gases. *Physical Review Letters*, 84(12):2551, 2000.

[68] D. S. Petrov and G. V. Shlyapnikov. Interatomic collisions in a tightly confined Bose gas. *Physical Review A*, 64(1):012706, 2001.

[69] Z. Idziaszek and T. Calarco. Two atoms in an anisotropic harmonic trap. *Physical Review A*, 71(5):050701, 2005.

[70] J. Struck, C. Ölschläger, R. Le Targat, P. Soltan-Panahi, A. Eckardt, M. Lewenstein, P. Windpassinger, and K. Sengstock. Quantum Simulation of Frustrated Classical Magnetism in Triangular Optical Lattices. *Science*, 333(6045):996–999, 2011.

[71] I. Bloch, J. Dalibard, and S. Nascimbene. Quantum simulations with ultracold quantum gases. *Nature Physics*, 8(4):267, 2012.

[72] M. Greiner, O. Mandel, T. Esslinger, T. W. Hänsch, and I. Bloch. Quantum phase transition from a superfluid to a Mott insulator in a gas of ultracold atoms. *Nature*, 415(6867):39–44, 2002.

[73] I. Bloch. Ultracold quantum gases in optical lattices. *Nature Physics*, 1(1):23–30, 2005.

[74] S. Trotzky, P. Cheinet, S. Fölling, M. Feld, U. Schnorrberger, A. M. Rey, A. Polkovnikov, E. A. Demler, M. D. Lukin, and I. Bloch. Time-resolved observation and control of superexchange interactions with ultracold atoms in optical lattices. *Science*, 319(5861):295–299, 2008.

[75] J. Simon, W. S. Bakr, R. Ma, M. E. Tai, P. M. Preiss, and M. Greiner. Quantum simulation of antiferromagnetic spin chains in an optical lattice. *Nature*, 472(7343):307–312, 2011.

[76] F. Meinert, M. J. Mark, E. Kirilov, K. Lauber, P. Weinmann, A. J. Daley, and H. C. Nägerl. Quantum Quench in an Atomic One-Dimensional Ising Chain. *Physical Review Letters*, 111:053003, 2013.

[77] A. Auerbach. *Interacting electrons and quantum magnetism*. Springer, New York, 1994.

[78] J. B. Parkinson and D. J. J. Farnell. *An Introduction to Quantum Spin Systems*. Springer,Berlin Heidelberg, 2010.

[79] L. D. Faddeev. Fifty Years of Mathematical Physics: Selected Works of Ludwig Faddeev. pages 370–439. World Scientific, Singapore, 2016.

[80] T. Grining, M. Tomza, M. Lesiuk, M. Przybytek, M. Musiał, R. Moszynski, M. Lewenstein, and P. Massignan. Crossover between few and many fermions in a harmonic trap. *Physical Review A*, 92(6):061601, 2015.

[81] A. Mazurenko, C. S. Chiu, G. Ji, M. F. Parsons, M. Kanász-Nagy, R. Schmidt, F. Grusdt, E. Demler, D. Greif, and M. Greiner. A cold-atom Fermi–Hubbard antiferromagnet. *Nature*, 545(7655):462–466, 2017.

[82] D. Greif, T. Uehlinger, G. Jotzu, L. Tarruell, and T. Esslinger. Short-range quantum magnetism of ultracold fermions in an optical lattice. *Science*, page 1236362, 2013.

[83] A. Dehkharghani, A. Volosniev, J. Lindgren, J. Rotureau, C. Forssén, D. Fedorov, A. Jensen, and N. Zinner. Quantum magnetism in strongly interacting one-dimensional spinor bose systems. *Scientific reports*, 5, 2015.

[84] P. Massignan, J. Levinsen, and M. M. Parish. Magnetism in strongly interacting one-dimensional quantum mixtures. *Physical Review Letters*, 115(24):247202, 2015.

[85] J. Levinsen, P. Massignan, G. M. Bruun, and M. M. Parish. Strong-coupling ansatz for the one-dimensional fermi gas in a harmonic potential. *Science Advances*, 1(6):e1500197, 2015.

[86] F. Deuretzbacher, D. Becker, and L. Santos. Momentum distributions and numerical methods for strongly interacting one-dimensional spinor gases. *Physical Review A*, 94(2):023606, 2016.

[87] A. G. Volosniev, D. Petrosyan, M. Valiente, D. V. Fedorov, A. S. Jensen, and N. T. Zinner. Engineering the dynamics of effective spin-chain models for strongly interacting atomic gases. *Physical Review A*, 91(2):023620, 2015.

[88] L. Yang and X. Cui. Effective spin-chain model for strongly interacting one-dimensional atomic gases with an arbitrary spin. *Physical Review A*, 93(1):013617, 2016.

[89] P. W. Anderson. Random-phase approximation in the theory of superconductivity. *Physical Review*, 112(6):1900, 1958.

[90] P. W. Higgs. Broken symmetries and the masses of gauge bosons. *Physical Review Letters*, 13(16):508, 1964.

[91] P. B. Littlewood and C. M. Varma. Amplitude collective modes in superconductors and their coupling to charge-density waves. *Physical Review B*, 26(9):4883, 1982.

[92] C. M. Varma. Higgs boson in superconductors. *Journal of low temperature physics*, 126(3-4):901–909, 2002.

[93] Y. Nambu. Quasi-particles and gauge invariance in the theory of superconductivity. *Physical Review*, 117(3):648, 1960.

[94] N. N. Bogoljubov, V. V. Tolmachov, and D. V. Širkov. A new method in the theory of superconductivity. *Fortschritte der physik*, 6(11-12):605–682, 1958.

[95] J. Goldstone. Field theories with Superconductor solutions. *Il Nuovo Cimento (1955-1965)*, 19(1):154–164, 1961.

[96] P. W. Anderson. Plasmons, gauge invariance, and mass. *Physical Review*, 130(1):439, 1963.

[97] P. W. Anderson. New method in the theory of superconductivity. *Physical Review*, 110(4):985, 1958.

[98] D. Pekker and C. M. Varma. Amplitude/Higgs modes in condensed matter physics. *Annual Review of Condensed Matter Physics*, 6(1):269–297, 2015.

[99] P. W. Anderson. Superconductivity: Higgs, Anderson and all that. *Nature Physics*, 11(2):93–93, 2015.

[100] H. T. C. Stoof, K. B. Gubbels, and D. B. M. Dickerscheid. *Ultracold quantum fields*, volume 1. Springer, Netherlands, 2009.

[101] M. E. Peskin, D. V. Schroeder, and E. Martinec. *An introduction to quantum field theory*. Westview Press, Boulder, 1995.

[102] G. L. Kane. *Modern elementary particle physics: the fundamental particles and forces*. Perseus publishing, Cambridge, Massachusetts, 1993.

[103] J. Lang, F. Piazza, and W. Zwerger. Collective excitations and supersolid behavior of bosonic atoms inside two crossed optical cavities. *arXiv preprint arXiv:1707.00017*, 2017.

[104] J. Léonard, A. Morales, P. Zupancic, T. Esslinger, and T. Donner. Supersolid formation in a quantum gas breaking a continuous translational symmetry. *Nature*, 543(7643):87–90, 2017.

[105] J. Léonard, A. Morales, P. Zupancic, T. Donner, and T. Esslinger. Monitoring and manipulating Higgs and Goldstone modes in a supersolid quantum gas. *arXiv preprint arXiv:1704.05803*, 2017.

[106] M. Ueda and T. Nakajima. Nambu-Goldstone mode in a rotating dilute Bose-Einstein condensate. *Physical Review A*, 73(4):043603, 2006.

[107] L. P. Gor'kov. Microscopic derivation of the Ginzburg-Landau equations in the theory of superconductivity. *Soviet physics JETP*, 9(6):1364–1367, 1959.

[108] T. Cea and L. Benfatto. Nature and Raman signatures of the Higgs amplitude mode in the coexisting superconducting and charge-density-wave state. *Physical Review B*, 90(22):224515, 2014.

[109] T. Cea, C. Castellani, G. Seibold, and L. Benfatto. Nonrelativistic dynamics of the amplitude (Higgs) mode in superconductors. *Physical Review Letters*, 115(15):157002, 2015.

[110] M. Endres, T. Fukuhara, D. Pekker, M. Cheneau, P. Schauβ, C. Gross, E. Demler, S. Kuhr, and I. Bloch. The/Higgs/'amplitude mode at the two-dimensional superfluid/Mott insulator transition. *Nature*, 487(7408):454–458, 2012.

[111] G. M. Bruun. Long-lived Higgs mode in a two-dimensional confined Fermi system. *Physical Review A*, 90(2):023621, 2014.

[112] M. G. Ries, A. N. Wenz, G. Zürn, L. Bayha, I. Boettcher, D. Kedar, P. A. Murthy, M. Neidig, T. Lompe, and S. Jochim. Observation of pair condensation in the quasi-2D BEC-BCS crossover. *Physical Review Letters*, 114(23):230401, 2015.

[113] M. Rontani, G. Eriksson, S. Åberg, and S. M. Reimann. On the renormalization of contact interactions for the configuration-interaction method in two-dimensions. *Journal of Physics B: Atomic, Molecular and Optical Physics*, 50(6):065301, 2017.

[114] M. Randeria, J.-M. Duan, and L.-Y. Shieh. Superconductivity in a two-dimensional Fermi gas: Evolution from Cooper pairing to Bose condensation. *Physical Review B*, 41(1):327, 1990.

[115] S. Zöllner, G. M. Bruun, and C. J. Pethick. Polarons and molecules in a two-dimensional Fermi gas. *Physical Review A*, 83(2):021603, 2011.

[116] A. Bohr and B. R. Mottelson. *Nuclear Structure:(In 2 Volumes) Volume I: Single-Particle MotionVolume II: Nuclear Deformations*. World Scientific, Singapore, 1998.

[117] P. A. Murthy, M. Neidig, R. Klemt, L. Bayha, I. Boettcher, T. Enss, M. Holten, G. Zürn, P. M. Preiss, and S. Jochim. High temperature pairing in a strongly interacting two-dimensional Fermi gas. *arXiv preprint arXiv:1705.10577*, 2017.

[118] I. Boettcher, L. Bayha, D. Kedar, P. A. Murthy, M. Neidig, M. G. Ries, A. N. Wenz, G. Zürn, S. Jochim, and T. Enss. Equation of state of ultracold fermions in the 2D BEC-BCS crossover region. *Physical Review Letters*, 116(4):045303, 2016.

[119] P. Ring and P. Schuck. *The nuclear many-body problem*. Springer, Berlin Heidelberg, 2004.

[120] M. Piibeleht. A mean-field approach to attractive few-body Fermi gas. MSc Thesis, Lund University, 2016.

[121] A. Pikovski, M. Klawunn, G. V. Shlyapnikov, and L. Santos. Interlayer superfluidity in bilayer systems of fermionic polar molecules. *Physical Review Letters*, 105(21):215302, 2010.

[122] A. Macia, G. E. Astrakharchik, F. Mazzanti, S. Giorgini, and J. Boronat. Single-particle versus pair superfluidity in a bilayer system of dipolar bosons. *Physical Review A*, 90(4):043623, 2014.

[123] N. T. Zinner, B. Wunsch, D. Pekker, and D.-W. Wang. BCS-BEC crossover in bilayers of cold fermionic polar molecules. *Physical Review A*, 85(1):013603, 2012.

[124] N. Bartolo, D. J. Papoular, L. Barbiero, C. Menotti, and A. Recati. Dipolar-induced resonance for ultracold bosons in a quasi-one-dimensional optical lattice. *Physical Review A*, 88(2):023603, 2013.

[125] C. Kollath, J. S. Meyer, and T. Giamarchi. Dipolar bosons in a planar array of one-dimensional tubes. *Physical Review Letters*, 100(13):130403, 2008.

[126] M. Knap, E. Berg, M. Ganahl, and E. Demler. Clustered Wigner-crystal phases of cold polar molecules in arrays of one-dimensional tubes. *Physical Review B*, 86(6):064501, 2012.

[127] B. Wunsch, N. T. Zinner, I. B. Mekhov, S. J Huang, D.-W. Wang, and E. Demler. Few-body bound states in dipolar gases and their detection. *Physical Review Letters*, 107(7):073201, 2011.

[128] M. Dalmonte, P. Zoller, and G. Pupillo. Trimer liquids and crystals of polar molecules in coupled wires. *Physical Review Letters*, 107(16):163202, 2011.

[129] Y.-P. Huang and D.-W. Wang. Quantum phase diagrams of fermionic dipolar gases in a planar array of one-dimensional tubes. *Physical Review A*, 80(5):053610, 2009.

[130] A. G. Volosniev, J. R. Armstrong, D. V. Fedorov, A. S. Jensen, M. Valiente, and N. T. Zinner. Bound states of dipolar bosons in one-dimensional systems. *New Journal of Physics*, 15(4):043046, 2013.

[131] P. Lecheminant and H. Nonne. Exotic quantum criticality in one-dimensional coupled dipolar bosons tubes. *Physical Review B*, 85(19):195121, 2012.

[132] J. M. Fellows and S. T. Carr. Superfluid, solid, and supersolid phases of dipolar bosons in a quasi-one-dimensional optical lattice. *Physical Review A*, 84(5):051602, 2011.

[133] S. Sinha and L. Santos. Cold dipolar gases in quasi-one-dimensional geometries. *Physical Review Letters*, 99(14):140406, 2007.

[134] F. Deuretzbacher, J. C. Cremon, and S. M. Reimann. Erratum: Ground-state properties of few dipolar bosons in a quasi-one-dimensional harmonic trap [Phys. Rev. A 81, 063616 (2010)]. *Physical Review A*, 87(3):039903, 2013.

Scientific publications

Author contributions

Paper I: Few-body precursor of the Higgs mode in a fermi gas

I took part in the discussions regarding the setup, development, and analysis. I also did all numerical calculations and developed most of the methods of analysis. I did most figures and assisted in preparing the manuscript.

Paper II: Quantum magnetism without lattices in strongly interacting one-dimensional spinor gases

I did the setup, the numerical calculations, and the convergence checks, and helped in the analysis of results. I developed a technique to do convergence checks on highly excited super-Tonks-Girardeau states in dense spectra. I helped in the preparation of the manuscript and created some figures.

Paper III: Antiferromagnetic Heisenberg spin chain of a few cold atoms in a one-dimensional trap

I took part in discussions and helped in the development and analysis of the phenomenological tunneling model. I did the setup and runs for the numerical calculations and the convergence checks for the occupation-numbers. I developed two different numerical models for simulation of the tunneling measurements.

Paper IV: Spin-chain model for strongly interacting one-dimensional Bose-Fermi mixtures

I took part in early discussions and planning, and I implemented and tested a generalized tool for Bose-Fermi mixtures in the exact diagonalization program package. I did the setup, performed the numerical calculations and performed convergence-checks. I analyzed the numerical results and helped in preparing the manuscript.

Paper V: Dipolar particles in a double-trap confinement: Response to tilting the dipolar orientation

I instigated the idea of considering short-range and dynamical properties of the double-wire system. I did some of the setup, some of the figures, performed most of the analysis and wrote large parts of the manuscript.

Papers

Paper I

Few-Body Precursor of the Higgs Mode in a Fermi Gas

J. Bjerlin,[1] S. M. Reimann,[1] and G. M. Bruun[2]
[1]Mathematical Physics, LTH, Lund University, SE-22100 Lund, Sweden
[2]Department of Physics and Astronomy, University of Aarhus, Ny Munkegade, DK-8000 Aarhus C, Denmark
(Received 4 October 2015; revised manuscript received 17 March 2016; published 13 April 2016)

We demonstrate that an undamped few-body precursor of the Higgs mode can be investigated in a harmonically trapped Fermi gas. Using exact diagonalization, the lowest monopole mode frequency is shown to depend nonmonotonically on the interaction strength, having a minimum in a crossover region. The minimum deepens with increasing particle number, reflecting that the mode is the few-body analogue of a many-body Higgs mode in the superfluid phase, which has a vanishing frequency at the quantum phase transition point to the normal phase. We show that this mode mainly consists of coherent excitations of time-reversed pairs, and that it can be selectively excited by modulating the interaction strength, using, for instance, a Feshbach resonance in cold atomic gases.

DOI: 10.1103/PhysRevLett.116.155302

The transition from few-body quantum physics to the thermodynamic limit with increasing particle number is a fundamental problem in science. A systematic investigation of this question is complicated by the fact that the few-body systems existing in nature, such as atoms and nuclei, have limited tunability. Artificially created clusters [1,2] or semiconductor quantum dots [3] offer more flexibility, but they are often strongly coupled to their surroundings making a study of pure quantum states difficult. The creation of highly controllable few-fermion systems using cold atoms in microtraps [4,5], however, has opened new perspectives. Tunneling experiments in the few-body limit demonstrated single-atom control [6,7]. One has already observed the formation of a Fermi sea [8], as well as pair correlations in one-dimensional (1D) few-body atomic gases [5] that have also been studied extensively theoretically [9–13]. The few- to many-body transition is arguably even more interesting in higher dimensions, where quantum phase transitions with varying degrees of broken symmetry are ubiquitous [14]. A key question concerns the few-body fate of the order parameter, which describes a broken symmetry phase in the thermodynamic limit.

Another fundamental problem concerns the properties of the Higgs mode, which corresponds to oscillations in the size of the order parameter for a given broken symmetry phase [15,16]. Elementary particles acquire their mass from the presence of a Higgs mode [17], which was famously observed at CERN [18,19]. The Higgs mode also leads to collective modes in condensed matter and nuclear systems [14,20]. Despite its fundamental importance, the list of table top systems where it has been observed is short, mainly because it is typically strongly damped, and because it couples only weakly to experimental probes [21–23]. Experimental evidence for the existence of a Higgs mode has been reported in disordered and niobium selenide superconductors [24–27]. Also, neutron scattering experiments for a quantum antiferromagnet [28] are consistent with the presence of a broad Higgs mode, and lattice experiments combined with theoretical models for bosonic atoms in an optical lattice, indicate that a threshold feature can be interpreted in terms of a strongly damped Higgs mode [29,30].

Here, we show how one can explore both these fundamental questions, the few- to many-body transition and the nature of the Higgs mode, using an atomic Fermi gas in a new generation of microtraps. We calculate the few-body spectrum using exact diagonalization and show that for closed-shell configurations, the lowest monopole excitation energy depends nonmonotonically on the interaction strength, having a minimum in a crossover region, which deepens with increasing particle number. By comparing with a many-body theory, we demonstrate that the mode is the few-body precursor of the Higgs mode in the superfluid phase, which exhibits a vanishing frequency at a quantum phase transition to a normal phase. The mode mainly consists of time-reversed pair excitations, and it can be selectively excited by modulating the interaction strength.

We consider $N/2$ fermions of mass m in each of two hyperfine (spin) states $\sigma = \uparrow, \downarrow$ in a 2D harmonic trap $m\omega^2 r^2/2$. Particles with opposite spin interact via an attractive delta function interaction (suitably regularized, see below) $g\delta(\mathbf{r} - \mathbf{r}')$ with $g < 0$, whereas particles of the same spin do not interact. The Hamiltonian is

$$\hat{H} = \sum_{i=1}^{N} \left(-\frac{\hbar^2 \nabla_i^2}{2m} + \frac{1}{2} m\omega^2 \mathbf{r}_i^2 \right) + g \sum_{k,l} \delta(\mathbf{r}_k - \mathbf{r}_l), \quad (1)$$

where $\mathbf{r}_i = (x_i, y_i)$ is the spatial coordinate of particle i, $\nabla_i^2 = \partial_{x_i}^2 + \partial_{y_i}^2$, and k and l in the second sum denote particles with spin $\uparrow$ and spin $\downarrow$, respectively.

In order to make rigorous predictions unbiased by any assumptions, we calculate the eigenstates of (1) by exact diagonalization using a basis of harmonic oscillator states

with energy $(2n+|m|+1)\hbar\omega$, where $n=0,1,2,3,\ldots$, and $m=0,\pm1,\pm2,\ldots$ is the angular momentum. This method has been extensively applied to attractive fermion systems, mainly in one dimension [9–13] but also in two dimensions [31,32]. As explained in the Supplemental Material [33], we employ a two-parameter cutoff scheme for the basis states in order to reach maximum convergence. Using a sparse representation of the resulting matrix, we find the eigenvectors using the implicitly restarted Arnoldi iteration method [36]. This generally allows for a significantly larger number of basis states, $\sim 10^7$, as compared to other available diagonalization methods, which is crucial, since we need a very large basis set for an accurate calculation of the low-lying collective modes.

As it stands, the spectrum of $\hat{H}$ depends logarithmically on the energy cutoff $E_{\rm cut}$. To cure this UV divergence, we eliminate the coupling constant g and cutoff $E_{\rm cut}$ in favor of the two-body binding energy ϵ_b per particle. This is defined as $E_2 = 2\hbar\omega - 2\epsilon_b$, where E_2 is the ground state energy of one $\uparrow$- and one $\downarrow$-particle in the trap. In practice, we calculate ϵ_b and the many-body spectrum as a function of g for the same $E_{\rm cut}$, and then we plot the spectrum as a function of ϵ_b. Since the two-body problem contains the same logarithmic divergence as the many-body problem, this procedure yields a well-defined theory for $E_{\rm cut}\to\infty$ [31,37,38]. A similar UV divergence appears for the system in three dimensions, where it has been regularized using a variety of methods [39–45].

Figure 1 shows the lowest monopole (zero angular momentum) excitation spectrum as a function of the two-body binding energy ϵ_b for a $3+3$ system, consisting of three $\uparrow$-particles and three $\downarrow$-particles. The noninteracting ground state is a closed-shell configuration with the two lowest harmonic oscillator shells filled. For no interaction, the excitations all have the energy $2\hbar\omega$, and they are formed either by pair excitations taking two particles with opposite angular momenta one shell up, see Figs. 2(a)–2(b), or by single particle excitations taking one particle two shells up; see Fig. 2(c). We see that all excitation energies, except the lowest, increase with increasing attraction since the attractive mean-field interaction potential increases the effective trapping frequency, thereby increasing the single particle excitation energies. The lowest mode is, however, qualitatively different: The excitation energy first *decreases* reaching a minimum at a "critical" two-body binding energy ϵ_b^c

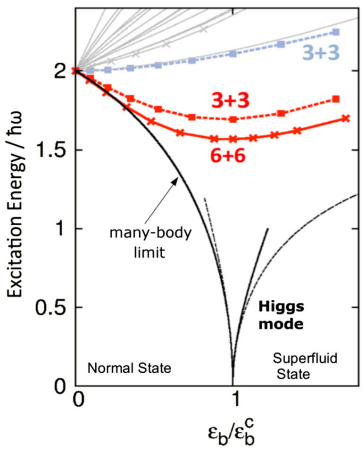

FIG. 1. The lowest monopole excitation for $3+3$ fermions (dashed red line) and for $6+6$ fermions (red solid line) obtained by numerical diagonalization of Eq. (1). The blue dashed line is the second excited state, and the gray solid lines are higher excitations for the $3+3$ system. The black solid (dotted) lines show the numerical (analytic) many-body Higgs-mode energy [46] (see Supplemental Material [33]).

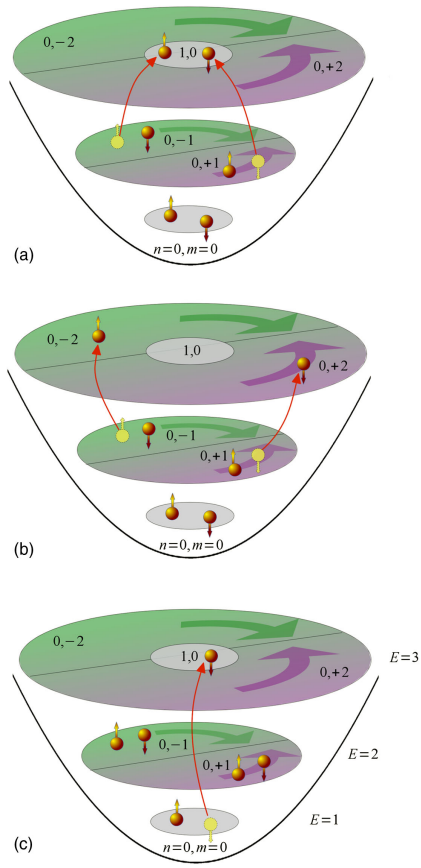

FIG. 2. Panels (a) and (b) show a schematic sketch of an excitation of a time-reversed pair $(n,m,\uparrow)$ and $(n,-m,\downarrow)$ one shell up. The energy of such excitations decreases with increasing attraction. Panel (c) shows an example of a single-particle monopole excitation two shells up. The energy of such excitations grows with increasing attraction.

(we will justify this name shortly), after which it increases for stronger attraction. This nonmonotonic behavior cannot be understood from a single-particle picture. Instead, it is due to pair correlations. The energy cost of exciting a pair of time-reversed states across the energy gap, as illustrated in Figs. 2(a)–2(b), initially decreases with increasing attraction, since the two excited particles can use the available states in the empty shell to increase their overlap. In Fig. 1, we normalize ϵ_b by ϵ_b^c, defined as the two-body binding energy that gives the minimum monopole excitation energy, so that we can compare results for different particle numbers and for the thermodynamic limit. Exact values of ϵ_b^c are given in the Supplemental Material [33].

To link the few-body spectrum to the thermodynamic limit, we also plot in Fig. 1 the lowest monopole mode obtained from a many-body calculation, which includes fluctuations around the Bardeen-Cooper-Schrieffer (BCS) solution [46] (see Supplemental Material [33]). Because of the energy gap in the single particle spectrum for a closed-shell configuration, there is a normal to superfluid quantum phase transition at a critical binding energy ϵ_b^c. The system is in the normal phase for $\epsilon_b < \epsilon_b^c$, and the lowest monopole mode corresponds to vibrations in the pairing energy $|\Delta|$ around the $\Delta = 0$ equilibrium value. The frequency of this mode decreases with increasing attraction and vanishes at ϵ_b^c, signaling a quantum phase transition to a superfluid phase. In the superfluid phase, the minimum energy is obtained for $|\Delta| > 0$, and the Higgs mode corresponds to vibrations in $|\Delta|$ around this minimum. Its energy is approximately given by $2|\Delta|$ (The deviation is due to the breaking of particle-hole symmetry), increasing from zero at the critical point. When $|\Delta| \ll \hbar\omega$, the Cooper pairs are predominantly formed by time-reversed states in the same shell [46]. Importantly, the Higgs mode is *undamped* in this regime due to the discrete nature of the trap level spectrum, which is in sharp contrast to the other tabletop systems mentioned above, where the damping is significant.

Comparing the $3+3$ and the many-body spectrum in Fig. 1 clearly shows that the lowest monopole mode for the $3+3$ system becomes the few-body precursor of the Higgs mode with increasing attraction. The nonmonotonic behavior of its energy is the smooth few-body analogue of the sharp thermodynamic normal to superfluid quantum phase transition with a vanishing Higgs mode frequency at the critical point. We also show in Fig. 1 the lowest monopole mode for the $6+6$ system corresponding to a closed-shell configuration with the three lowest shells filled. The nonmonotonic behavior of the lowest excitation energy is now even more pronounced with a deeper minimum, reflecting the gradual few- to many-body transition with increasing particle number.

In the Supplemental Material [33], we illustrate further the few- to many-body transition by calculating the spectrum for the closed shell configurations up to $15+15$ particles. Since it is numerically intractable to perform exact diagonalizations of Eq. (1) beyond $6+6$ particles, we use a simplified model, which includes only the highest filled and the lowest two empty shells. This calculation clearly shows a pronounced deepening of the minimum of the excitation energy with increasing particle number.

In Fig. 3, we plot the lowest monopole excitations for a $4+4$ system, which corresponds to an open-shell configuration where there is a pair of $\uparrow\downarrow$ particles in the third shell. Contrary to the closed-shell configuration, all excitation energies now increase monotonically with the attraction. This is because there is pairing for *any* attractive interaction so that the lowest excitations involve pair breaking, and it demonstrates that the nonmonotonic behavior of the lowest mode energy is characteristic of a closed-shell configuration, where there is a quantum phase transition in the thermodynamic limit.

In order to investigate further the connection between the few- and many-body physics, we quantify the amount of time-reversed pairing correlations in a given state by

$$P = \sum_i |C_i^{\mathrm{tr}}|^2. \tag{2}$$

Here, C_i are the expansion coefficients in the many-body basis for a given eigenstate. The sum runs over all basis states formed from the noninteracting ground state by excitations of time-reversed (tr) pairs. In Fig. 4, we plot P for the ground state and the two lowest excited states. Comparing the first excited state with the ground state and with the second excited states clearly shows that below the critical binding energy ϵ_b^c, the wave function of the lowest mode is mainly formed by coherent excitations of time-reversed pairs. It is consistent with the canonical many-body picture of

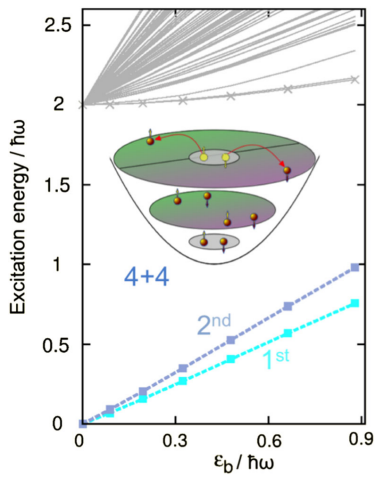

FIG. 3. Monopole excitations of an open-shell system. The lowest excitations are intrashell excitations, which do not exhibit a minimum. The gray lines show higher excitations (which correspond to inter-shell transitions). Inset: Sketch of time-reversed intrashell pair excitations.

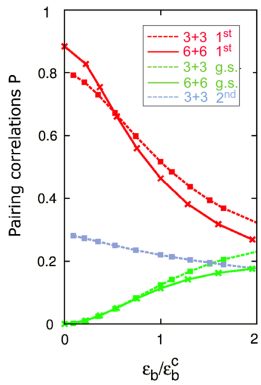

FIG. 4. Pairing correlations of the few-body states as defined by Eq. (2) for $N = 3 + 3$ fermions (dashed lines) and $N = 6 + 6$ fermions (solid lines). The green lines show the ground state and the red lines show the first excited state. The blue line shows the second excited state (only for $3 + 3$).

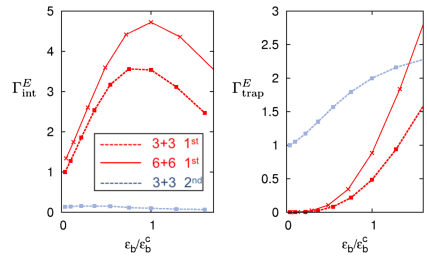

FIG. 5. Left: Transition matrix elements $\Gamma^E_{\rm int}$ corresponding to modulating the interaction strength for a $3 + 3$ and a $6 + 6$ system. The matrix elements are normalized by $\Gamma^E_{\rm int}$ calculated to the Higgs mode at a very low coupling strength for the $3 + 3$ system. Right: Transition matrix elements $\Gamma^E_{\rm trap}$ corresponding to modulating the trapping frequency. The matrix elements are normalized by $\Gamma^E_{\rm trap}$ to the second excited state calculated at a very low coupling strength.

vibrations in $|\Delta|$, since such excitations give rise to fluctuations in the pairing field. The higher mode has a significantly smaller proportion of pair correlations, and it mainly consists of single-particle excitations two shells up. The pairing correlations in the ground state increase with increasing attraction, as it becomes more favorable to excite time-reversed pairs across the energy gap. This smooth increase of ground state pair correlations is the few-body analogue of the normal to superfluid quantum phase transition, where excitations of time-reversed pairs cost zero energy at the critical coupling strength, making the system spontaneously form Cooper pairs. The pair correlated part of the few-body Higgs mode decreases for $\epsilon_b > \epsilon_b^c$, since it is orthogonal to the ground state.

We now address how one can detect the few-body Higgs mode in atomic gas experiments using microtraps. Two experimental probes are widely used: Periodic modulations of the trapping frequency and of the interaction strength. From Fermi's golden rule, the transition rate from the ground state $|G\rangle$ to an excited state $|E\rangle$ is proportional to the transition matrix elements

$$\Gamma^E_{\rm trap} = |\langle G|\sum_i \mathbf{r}_i^2|E\rangle|^2,$$
$$\Gamma^E_{\rm int} = |\langle G|\sum_{k,l}\delta(\mathbf{r}_k - \mathbf{r}_l)|E\rangle|^2, \quad (3)$$

for the two probes. In Fig. 5, we plot $\Gamma^E_{\rm trap}$ and $\Gamma^E_{\rm int}$ to the excited states of the $3 + 3$ and the $6 + 6$ systems. Figure 5 (left) shows that the transition rate into the lowest mode is much larger than the rate into the second excited state when the coupling strength is modulated. This is because the interaction operator $\Gamma_{\rm int}$ can excite time-reversed pairs, (see Supplemental Material [33]), which are precisely the excitations that give rise to pair vibrations. Thus, the Higgs mode can be selectively excited by modulating the interaction strength, using, for instance, a Feshbach resonance. This fact, together with the nonmonotonic frequency behavior, can be used to experimentally identify the Higgs mode. On the other hand, Fig. 5 (right) shows that when the trapping potential is modulated, the transition rate into the second excited state is much larger than into the lowest mode for small attraction. The reason is that $\sum_i \mathbf{r}_i^2$ is a single particle operator, whereas the lowest mode mostly consists of time-reversed pair excitations. With increasing attraction, the transition rate into the lowest mode increases, consistent with the fact that the pair correlation P in the Higgs mode decreases with increasing coupling.

In conclusion, we demonstrated using exact diagonalization that the lowest monopole excitation energy of a two-component Fermi gas exhibits a nonmonotonic behavior with increasing attractive interaction for closed shell configurations. The mode frequency has a minimum in a crossover region, which deepens as the many-body limit is approached with increasing particle number. Comparing with a many-body calculation, we identified the few-body precursor of the Higgs mode, which has a vanishing frequency at the quantum phase transition point between a normal and a superfluid phase. We showed that the mode is mainly formed by coherent excitations of time-reversed pairs, and that it can be selectively excited by modulating the interaction strength. These results demonstrate how a new generation of cold atom experiments using microtraps can be used to explore two fundamental questions in physics: The nature of the Higgs mode and the crossover from few- to many-body physics. Our results are also relevant to the nuclear structure community, since we show how cold atoms can be used to probe pair correlations in finite systems much more systematically compared to what is possible in nuclei [47,48].

We end by noting that similar results hold for atoms in a 3D trap [49,50]. Focus was here on the 2D case, as it is closer to being experimentally realized. Indeed, the first

experiment observing pairing correlations in two dimensions has already been reported [51].

We thank Ben Mottelson and Sven Åberg for many useful discussions, as well as Jeremy Armstrong for a comparison to a more phenomenological pairing model. We thank Massimo Rontani for discussions regarding the regularization scheme, and also acknowledge discussions with Selim Jochim and Frank Deuretzbacher. This research was financially supported by the Swedish Research Council and NanoLund at Lund University. G. M. B. would like to acknowledge the support of the Villum Foundation via Grants No. VKR023163 and No. ESF POLATOM network.

[1] W. A. de Heer, Rev. Mod. Phys. **65**, 611 (1993).
[2] M. Brack, Rev. Mod. Phys. **65**, 677 (1993).
[3] S. M. Reimann and M. Manninen, Rev. Mod. Phys. **74**, 1283 (2002).
[4] F. Serwane, G. Zürn, T. Lompe, T. B. Ottenstein, A. N. Wenz, and S. Jochim, Science **332**, 336 (2011).
[5] G. Zürn, A. N. Wenz, S. Murmann, A. Bergschneider, T. Lompe, and S. Jochim, Phys. Rev. Lett. **111**, 175302 (2013).
[6] G. Zürn, F. Serwane, T. Lompe, A. N. Wenz, M. G. Ries, J. E. Bohn, and S. Jochim, Phys. Rev. Lett. **108**, 075303 (2012).
[7] M. Rontani, Phys. Rev. Lett. **108**, 115302 (2012).
[8] A. N. Wenz, G. Zürn, S. Murmann, I. Brouzos, T. Lompe, and S. Jochim, Science **342**, 457 (2013).
[9] T. Sowinski, Few-Body Syst. **56**, 659 (2015).
[10] T. Sowinski, M. Gajda, and K. Rzazewski, Europhys. Lett. **109**, 26005 (2015).
[11] T. Grining, M. Tomza, M. Lesiuk, M. Przybytek, M. Musiał, R. Moszynski, M. Lewenstein, and P. Massignan, Phys. Rev. A **92**, 061601 (2015).
[12] T. Grining, M. Tomza, M. Lesiuk, M. Przybytek, M. Musiał, P. Massignan, M. Lewenstein, and R. Moszynski, New J. Phys. **17**, 115001 (2015).
[13] P. D'Amico and M. Rontani, Phys. Rev. A **91**, 043610 (2015).
[14] S. Sachdev, *Quantum Phase Transitions*, 2nd ed. (Cambridge University Press, Cambridge, England, 2011).
[15] J. Goldstone, Il Nuovo Cimento (1955-1965) **19**, 154 (1961).
[16] P. W. Higgs, Phys. Rev. Lett. **13**, 508 (1964).
[17] L. H. Ryder, Quantum Field Theory, 2nd ed. (Cambridge University Press, Cambridge, England, 1996).
[18] CMS collaboration, Phys. Lett. B **716**, 30 (2012).
[19] ATLAS collaboration, Phys. Lett. B **716**, 1 (2012).
[20] A. Bohr and B. R. Mottelson, *Nuclear Structure* (World Scientific, Singapore, 1998).
[21] D. Pekker and C. Varma, Annu. Rev. Condens. Matter Phys. **6**, 269 (2015).
[22] T. Cea and L. Benfatto, Phys. Rev. B **90**, 224515 (2014).
[23] T. Cea, C. Castellani, G. Seibold, and L. Benfatto, Phys. Rev. Lett. **115**, 157002 (2015).
[24] D. Sherman, U. S. Pracht, B. Gorshunov, S. Poran, J. Jesudasan, M. Chand, P. Raychaudhuri, M. Swanson, N. Trivedi, A. Auerbach, M. Scheffler, A. Frydman, and M. Dressel, Nat. Phys. **11**, 188 (2015).
[25] R. Sooryakumar and M. V. Klein, Phys. Rev. Lett. **45**, 660 (1980).
[26] M.-A. Méasson, Y. Gallais, M. Cazayous, B. Clair, P. Rodière, L. Cario, and A. Sacuto, Phys. Rev. B **89**, 060503 (2014).
[27] P. B. Littlewood and C. M. Varma, Phys. Rev. Lett. **47**, 811 (1981).
[28] C. Rüegg, B. Normand, M. Matsumoto, A. Furrer, D. F. McMorrow, K. W. Krämer, H. U. Güdel, S. N. Gvasaliya, H. Mutka, and M. Boehm, Phys. Rev. Lett. **100**, 205701 (2008).
[29] M. Endres, T. Fukuhara, D. Pekker, M. Cheneau, P. Schauß, C. Gross, E. Demler, S. Kuhr, and I. Bloch, Nature (London) **487**, 454 (2012).
[30] L. Liu, K. Chen, Y. Deng, M. Endres, L. Pollet, and N. Prokof'ev, Phys. Rev. B **92**, 174521 (2015).
[31] M. Rontani, S. Åberg, and S. M. Reimann, arXiv:0810.4305.
[32] M. Rontani, J. R. Armstrong, Y. Yu, S. Åberg, and S. M. Reimann, Phys. Rev. Lett. **102**, 060401 (2009).
[33] See Supplemental Material at http://link.aps.org/supplemental/10.1103/PhysRevLett.116.155302, which includes Refs. [34,35] for details the theory and for more results.
[34] G. M. Bruun and H. Heiselberg, Phys. Rev. A **65**, 053407 (2002).
[35] H. Heiselberg and B. Mottelson, Phys. Rev. Lett. **88**, 190401 (2002).
[36] R. B. Lehoucq, D. C. Sorensen, and C. Yang, *ARPACK User's Guide—Solution of Large-Scale Eigenvalue Problems with Implicitly Restarted Arnoldi Methods* (SIAM, Philadelphia, 1998).
[37] M. Randeria, J.-M. Duan, and L.-Y. Shieh, Phys. Rev. B **41**, 327 (1990).
[38] S. Zöllner, G. M. Bruun, and C. J. Pethick, Phys. Rev. A **83**, 021603 (2011).
[39] V. Galitskii, Sov. Phys. JETP **7**, 104 (1958).
[40] L. P. Gor'kov and T. K. Melik-Barkhudarov, Sov. Phys. JETP **13**, 1018 (1961).
[41] A. J. Leggett, *Proceedings of the XVI Karpacz Winter School of Theoretical Physics, february 19–March 3, 1979 Karpacz, Poland* (Springer, Berlin, Heidelberg, Berlin, Heidelberg, 1980), Chap. 2, p. 13.
[42] G. Bruun, Y. Castin, R. Dum, and K. Burnett, Eur. Phys. J. D **7**, 433 (1999).
[43] I. Stetcu, B. R. Barrett, U. van Kolck, and J. P. Vary, Phys. Rev. A **76**, 063613 (2007).
[44] Y. Alhassid, G. F. Bertsch, and L. Fang, Phys. Rev. Lett. **100**, 230401 (2008).
[45] N. T. Zinner, K. Mølmer, C. Özen, D. J. Dean, and K. Langanke, Phys. Rev. A **80**, 013613 (2009).
[46] G. M. Bruun, Phys. Rev. A **90**, 023621 (2014).
[47] S. Frauendorf and A. O. Macchiavelli, Prog. Part. Nucl. Phys. **78**, 24 (2014).
[48] G. Potel, A. Idini, F. Barranco, E. Vigezzi, and R. A. Broglia, Rep. Prog. Phys. **76**, 106301 (2013).
[49] G. M. Bruun and B. R. Mottelson, Phys. Rev. Lett. **87**, 270403 (2001).
[50] G. M. Bruun, Phys. Rev. Lett. **89**, 263002 (2002).
[51] M. G. Ries, A. N. Wenz, G. Zürn, L. Bayha, I. Boettcher, D. Kedar, P. A. Murthy, M. Neidig, T. Lompe, and S. Jochim, Phys. Rev. Lett. **114**, 230401 (2015).

Paper II

Quantum magnetism without lattices in strongly interacting one-dimensional spinor gases

F. Deuretzbacher,[1,*] D. Becker,[2] J. Bjerlin,[3] S. M. Reimann,[3] and L. Santos[1]

[1]*Institut für Theoretische Physik, Leibniz Universität Hannover, Appelstrasse 2, DE-30167 Hannover, Germany*

[2]*Department of Physics, University of Basel, Klingelbergstrasse 82, CH-4056 Basel, Switzerland*

[3]*Mathematical Physics, Lund Institute of Technology, SE-22100 Lund, Sweden*

(Received 23 October 2013; revised manuscript received 2 June 2014; published 14 July 2014)

We show that strongly interacting multicomponent gases in one dimension realize an effective spin chain, offering an alternative simple scenario for the study of one-dimensional (1D) quantum magnetism in cold gases in the absence of an optical lattice. The spin-chain model allows for an intuitive understanding of recent experiments and for a simple calculation of relevant observables. We analyze the adiabatic preparation of antiferromagnetic and ferromagnetic ground states, and show that many-body spin states may be efficiently probed in tunneling experiments. The spin-chain model is valid for more than two components, opening the possibility of realizing SU(N) quantum magnetism in strongly interacting 1D alkaline-earth-metal or ytterbium Fermi gases.

DOI: 10.1103/PhysRevA.90.013611 PACS number(s): 03.75.Mn, 75.10.Pq, 67.85.Lm, 73.21.Hb

I. INTRODUCTION

Ultracold gases in optical lattices offer fascinating perspectives for the simulation of quantum magnetism, a topic of fundamental importance in condensed matter physics [1]. Starting with the observation of superexchange in double-well systems [2], recent experiments are quickly advancing in the simulation of quantum and classical magnetism in optical lattices, including the creation of plaquette resonating-valence-bond states [3], the simulation of a quantum Ising model using tilted lattices [4,5], the realization of classical antiferromagnetism in triangular lattices [6], and the observation of dipole-induced spin exchange in polar lattice gases [7,8]. However, although short-range antiferromagnetism has been reported in dimerized lattices [9], Néel long-range order in two-component Fermi gases has not yet been observed, due to the very low entropy necessary in typical lattice experiments.

Strongly correlated one-dimensional (1D) systems have also attracted major attention in recent years [10]. Experimental developments in 1D systems are highlighted by the realization of the Tonks-Girardeau gas [11,12], followed by the studies on local two- and three-body correlations [13–15], slow thermalization [16], and the realization of the super-Tonks gas [17]. Theoretical investigations led to several generalizations of Girardeau's Bose-Fermi mapping for spinless bosons [18] to multicomponent systems [19–22].

Recent experiments allow for the investigation of small two-component fermionic 1D systems with a high control of particle number, spin imbalance, and interaction strength [23,24]. These experiments have attracted considerable attention, in particular concerning the physics in the vicinity of a scattering resonance [25–32]. For resonant interactions, the energy eigenstates show a large spin degeneracy [20,21] that is lifted for finite interactions, making these systems very sensitive to temperature effects [28] and spin segregation in the presence of magnetic-field (B-field) gradients [29,33]. The analytical form of the many-body wave function has also been addressed [29–31], although the proposed methods become very involved for large particle numbers and/or components.

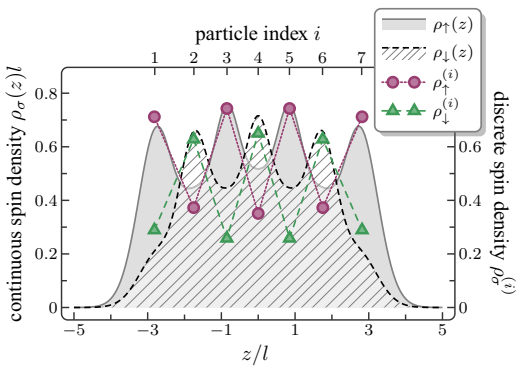

FIG. 1. (Color online) Continuous (experimentally measurable) spin densities $\rho_{\uparrow,\downarrow}(z)$ of the full model together with the discrete spin densities $\rho_{\uparrow,\downarrow}^{(i)}$ of the spin-chain model for seven harmonically trapped spin-1/2 fermions ($N_\uparrow = 4, N_\downarrow = 3$) in the antiferromagnetic state.

We show in this article that strongly interacting multicomponent 1D gases in the vicinity of a scattering resonance realize an effective spin chain without the need for an optical lattice. We obtain the effective spin model by combining the exact analytical solution for infinite repulsion [20] with a spin permutation model originally developed in the analysis of quantum wires [34–36].[1] The resulting model significantly simplifies the calculations of the eigenfunctions and eigenenergies and may be employed for both strongly-interacting bosons and fermions. Moreover, it is applicable not only to two-component gases, but in general to multicomponent SU(N) systems, which may be realized in alkaline-earth-metal gases and ytterbium [39–41]. The specific case of spin-1/2 systems realizes an effective Heisenberg spin model,

*frank.deuretzbacher@itp.uni-hannover.de

[1]The crossover to the spin-incoherent (Wigner-crystal-like) regime has been studied in Refs. [37,38] in the context of ultracold fermionic two-component atomic gases by analyzing the density oscillations on top of the Thomas-Fermi profile.

which may acquire a ferromagnetic (F) or antiferromagnetic (AF) character depending on the sign of the interparticle interactions. We analyze the dynamic creation of both an AF and a F state by making use of an exact diagonalization of the effective spin-chain model. We show finally that the properties of the spin chain may be directly measured in ongoing experiments.

II. NONINTERACTING SPIN CHAIN

Multicomponent trapped Fermi or Bose systems with an infinite contact repulsion may be exactly solved [20] through a generalization of Girardeau's Bose-Fermi mapping for spinless bosons [18]. At infinite repulsion a multicomponent 1D system behaves as a spinless Fermi gas characterized by states with a given spatial ordering of the particles. One may construct an orthonormal basis of nonsymmetric position-space sector wave functions [20]

$$\langle z_1,\ldots,z_N|P\rangle = \sqrt{N!}\theta(z_{P(1)},\ldots,z_{P(N)})A\,\psi_F, \qquad (1)$$

where $\theta(z_1,\ldots,z_N)=1$ if $z_1\le\cdots\le z_N$ and zero otherwise, P is one of the $N!$ permutations of the ordering of the N particles, $A=\prod_{i<j}\mathrm{sgn}(z_i-z_j)$ is the unit antisymmetric function [18], and ψ_F is the ground state of N 1D noninteracting spinless fermions. The eigenfunctions of multicomponent Bose and Fermi systems are obtained via the map [20]

$$W_\pm|\chi\rangle = \sqrt{N!}S_\pm(|\mathrm{id}\rangle|\chi\rangle), \qquad (2)$$

where $|\chi\rangle=\sum_{m_1,\ldots,m_N}c_{m_1,\ldots,m_N}|m_1,\ldots,m_N\rangle$ is an arbitrary N-particle spin function, $S_\pm=(1/N!)\sum_P(\pm1)^P P$ is the (anti)symmetrization operator, and $|\mathrm{id}\rangle$ is the sector wave function corresponding to the identical permutation.[2] An important consequence of the bijective character of the map (2) is that the system is uniquely determined by the spin function $|\chi\rangle$. In particular, the density distribution of the mth component is given by [20]

$$\rho_m(z)=\sum_i \rho_m^{(i)}\rho^{(i)}(z) \qquad (3)$$

with the probability that the magnetization of the ith spin equals m,

$$\rho_m^{(i)}=\sum_{m_1,\ldots,m_N}|\langle m_1,\ldots,m_N|\chi\rangle|^2\delta_{m,m_i}, \qquad (4)$$

and the probability to find the ith particle (with whatever spin) at position z,

$$\rho^{(i)}(z)=N!\int dz_1\cdots dz_N\delta(z-z_i)\theta(z_1,\ldots,z_N)|\psi_F|^2. \qquad (5)$$

The continuous spin density $\rho_m(z)$ is hence fully characterized by the N-tuple $(\rho_m^{(1)},\ldots,\rho_m^{(N)})$, as illustrated in Fig. 1. The system thus reduces to a spin-chain model.

[2]The map (2) can be easily extended to states with excited spatial degrees of freedom by replacing the ground state ψ_F in the sector wave functions $|P\rangle$ by the ith excited state $\psi_F^{(i)}$.

III. SPIN-SPIN INTERACTIONS

In the limit of infinite repulsion, $1/g=0$ (with the interaction strength g), the spin chain is noninteracting, since all states of the ground-state multiplet are degenerate. This is no longer the case when $1/g\neq0$. In the vicinity of a scattering resonance the effective theory for finite interactions may be evaluated to lowest order in $1/g$ by means of degenerate perturbation theory. The effective interaction Hamiltonian of the spin chain reads (see Appendix A for the derivation)[3]

$$H_s=\left(E_F-\sum_{i=1}^{N-1}J_i\right)\mathbb{1}\pm\sum_{i=1}^{N-1}J_iP_{i,i+1}, \qquad (6)$$

where $P_{i,i+1}$ denotes the permutation of the spin of neighboring particles, the $+$ $(-)$ sign applies to fermions (bosons), and the nearest-neighbor exchange constants are given by

$$J_i=\frac{N!\hbar^4}{m^2g}\int dz_1\cdots dz_N\delta(z_i-z_{i+1})\theta(z_1,\ldots,z_N)\left|\frac{\partial\psi_F}{\partial z_i}\right|^2. \qquad (7)$$

The exact calculation of the exchange constants J_i requires the solution of multidimensional integrals of growing complexity with increasing N, which is in practice possible only for small N.[4] Fortunately, an accurate approximation of the exchange constants, which becomes even more accurate for growing N, is provided by the expression

$$J_i=\frac{\hbar^4\pi^2n_{\mathrm{TF}}^3(z_i)}{3m^2g}, \qquad (8)$$

where n_{TF} is the Thomas-Fermi (TF) profile of the density and z_i is the center of mass of the ith and $(i+1)$th particle density, $\rho^{(i)}(z)$ and $\rho^{(i+1)}(z)$ (see Appendix B). Expression (8) follows from the nearest-neighbor exchange of the homogeneous system with periodic boundary conditions in the thermodynamic limit [42] combined with a local density approximation (LDA). Appendix B shows a comparison between exchange constants obtained from Eqs. (7) and (8) for up to six harmonically trapped particles, confirming that, as mentioned above, the agreement becomes better for growing N.

The diagonalization of the spin Hamiltonian (6) in combination with the map (2) allows for a simple calculation of the eigenstates of trapped strongly interacting multicomponent bosons or fermions.[5] This means that the spin distribution, and hence the whole atom distribution in the trap, is determined by a spin permutation Hamiltonian (Sutherland model [43]). In the case of spin-1/2 particles we have $P_{i,i+1}=(\vec\sigma^{(i)}\cdot\vec\sigma^{(i+1)}+1)/2$ with the Pauli vector $\vec\sigma$. Two-component gases therefore realize an effective Heisenberg Hamiltonian. The Heisenberg Hamiltonian coincides with that introduced in the analysis of the conductance of quantum wires

[3]For particles on a ring, one has to replace $N-1$ by N in Eq. (6) and $P_{N,N+1}$ has to be replaced by $P_{N,1}$.

[4]See the second version of Ref. [30].

[5]For three spin-1/2 fermions $(N_\uparrow=2,N_\downarrow=1)$ our results agree with those presented in the first version of Ref. [30]. The position dependence of the nearest-neighbor exchange constants (7) was recently noted in the second version of Ref. [30].

[34–36] and of spectral functions of spin-1/2 1D bosons [42]. The effective spin model is consistent with Bethe-ansatz results for spin-1/2 bosons [44] and fermions [45]. The validity of the spin-chain model is restricted to the (super-)Tonks regime, where $|1/g|$ is small (see Appendix C for a comparison with a numerical exact diagonalization of the full Hamiltonian).

IV. SPIN ORDER

In the following we focus on the specific case of spin-1/2 gases, which is of direct relevance for ongoing experiments [23,24]. Equation (7) ($J_i \propto 1/g$) implies that the sign of the J_i can be tuned by means of a scattering resonance [24]. The spin interaction is F for $g < 0$ ($g > 0$) and AF for $g > 0$ ($g < 0$) for fermions (bosons). Although spin-spin correlations would clearly show the (anti)ferromagnetic character of the interactions, for both F and AF couplings, the local average magnetization $\langle \sigma_z^{(i)} \rangle$ is zero for all particle positions in the ground state due to SU(2) symmetry. As a result, the density distributions of both spin components will be identical. This symmetry may be broken by a small population imbalance (Fig. 1; see also Ref. [21]) or by a spin-dependent external potential, such as a B-field gradient (Fig. 2). Such a gradient adds to the effective spin interaction Hamiltonian (6) a term $V_G = (G/l)\sum_i \langle z \rangle_i \sigma_z^{(i)}$ with $\langle z \rangle_i = \int dz z \rho^{(i)}(z)$ and the oscillator length l (Appendix D). A small G/J [$J = \sum_i J_i/(N-1)$ is the average nearest-neighbor exchange constant] results in an alternating distribution of the two components marking the AF order. In contrast, when G/J is sufficiently large the system experiences spin segregation. Since $|J|$ is very small at the resonance such segregation may occur for rather weak B-field gradients [29]. We stress, however, that this spin segregation occurs even for AF interactions, and does not mark an AF-F transition, being rather a Stern-Gerlach- (SG-)like separation of the components.

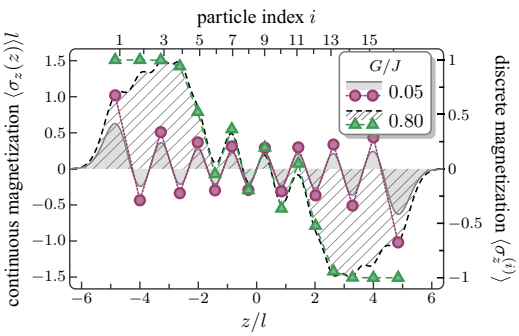

FIG. 2. (Color online) Magnetization of a spin-balanced AF spin chain consisting of 16 harmonically trapped particles for $G/J = 0.05$ and 0.8 (G is the B-field gradient and $J = \sum_i J_i/(N-1)$ is the average nearest-neighbor exchange). The symbols (shaded curves) denote the discrete (continuous) distributions.

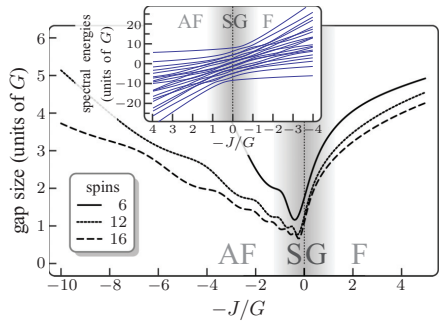

FIG. 3. (Color online) Gap between the ground and first excited state of harmonically trapped spin-balanced spin-1/2 fermions for nonzero gradients ($G \neq 0$) around the resonance. While spin interactions dominate in the AF and F regimes, the B-field gradient dominates in the gray-shaded Stern-Gerlach (SG) regime, characterized by SG-like spin segregation. Inset: Spectrum of six spin-balanced spin-1/2 fermions as a function of $-J/G$.

V. STATE PREPARATION

In contrast to experiments in optical lattices, where spin ground states are exceedingly difficult to prepare, the realization of ground states of effective 1D spin chains may be accomplished in a surprisingly simple way (for the AF regime) in ongoing experiments on strongly interacting spin-1/2 fermions [23,24]. The system is first prepared in the spin-singlet ground state of the noninteracting system.[6] The interaction strength g is then ramped up by means of a scattering resonance into the regime of large $g > 0$ (Tonks regime). Due to spin conservation the noninteracting ground state evolves into an AF spin chain. As discussed below, the AF order may be easily revealed in ongoing tunneling experiments using imbalanced mixtures.

The preparation of the spin ground state is more involved if it demands a sweep through the scattering resonance. If the system is driven across $J = 0$, the ground state of the Tonks regime becomes the highest excited state of the super-Tonks regime ($g < 0$),[7] which is preserved due to spin conservation [29]. A spin-dependent external potential, such as, e.g., a B-field gradient, violates spin conservation, lifting the spin degeneracy at $J = 0$ [28,29] (inset of Fig. 3). In particular, the AF ground state for $g > 0$ may be adiabatically transformed into the F ground state for $g < 0$ due to the avoided crossing opened by the B-field gradient, as suggested in Ref. [29]. We

[6]Temperature effects may be significant if the sample is cooled down close to the resonance [28], and in particular if $k_B T > NJ$ the system becomes a spin-incoherent Luttinger liquid [36]. This is however not relevant in typical experiments, since the initial sample is produced far from resonance.

[7]For $g < 0$ the lowest energy corresponds actually to molecular states, but these states cannot be reached in a sweep.

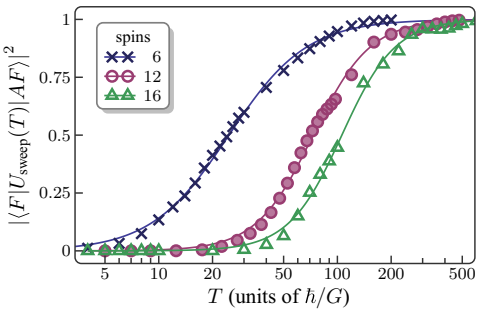

FIG. 4. (Color online) Overlap between the F ground state of harmonically trapped spin-balanced spin-1/2 fermions expected for $-J/G = 10$ and the state obtained after a linear sweep across the resonance starting with the AF ground state for $-J/G = -10$.

employ below the spin model to analyze the conditions for the adiabatic sweep in the presence of a B-field gradient.[8]

The gap Δ between the ground and first excited state is particularly relevant, since adiabaticity requires that $|J/G|$ is varied much more slowly than $\hbar/\Delta$. We have calculated the gap as a function of $-J/G$ for up to 16 spin-balanced spin-1/2 fermions by means of an exact diagonalization of the effective spin Hamiltonian.[9] Figure 3 shows that the minimal gap $\Delta_{\rm min} \approx G$ is reached in the Tonks regime ($-J/G \lesssim 0$), and that $\Delta_{\rm min}$ decreases slowly with larger N. Also note that the region where $\Delta \simeq \Delta_{\rm min}$ increases with increasing N. This implies that an adiabatic sweep becomes more involved for larger N, since $-J/G$ has to be increased much more slowly than $\hbar/\Delta_{\rm min}$ in an increasing region of the Tonks regime.

We have perfomed exact time-dependent simulations with linear sweeps $-J(t)/G = -10(1 - 2t/T)$ for different values of the sweeping time T. The initial and final values satisfy $|J/G| \gg 1$, and hence any final F state is maintained by F interactions and not by a SG-like spin segregation [29]. We have calculated the overlap between the state after the sweep and the F ground state. As expected, adiabaticity demands a slower sweep for larger N. Figure 4 shows that in order to reach the F ground state of the super-Tonks regime with $\simeq$100% fidelity, the sweep must fulfill $v \equiv \partial|J/G|/\partial t < v_c \simeq 0.07G/\hbar$ in the vicinity of the resonance. This corresponds to $T > 300\hbar/G$ in Fig. 4. We note that, although we have chosen a linear sweep for simplicity, the ramp may be much faster far from the resonance, as long as $v < v_c$ in the region of the minimal gap. Once the F state is reached at $|J| \gg G$, the B-field gradient may be removed. Note again that due to SU(2) symmetry the final F state does not show spin segregation if $|J/G| \gg 1$.

VI. STATE DETECTION

As discussed above, $\langle\sigma_z^{(i)}\rangle$ is mapped on the densities of the spin components. The AF or F spin ordering of the spin chain may therefore be directly probed in imbalanced mixtures by means of *in situ* imaging, which is however challenging in tightly confined samples. An alternative way of probing the spin order is provided by the tunneling techniques recently developed by Jochim and co-workers [23,24]. A tight dipole trap is combined with a B-field gradient, which lowers the potential barrier at the right-hand side of the trap. The tunneling through this barrier may be controlled by carefully varying the B-field gradient. The barrier height and the waiting time may be chosen such that only one fermion can tunnel. Afterwards the spin orientation of this fermion is detected. Within the spin-chain picture only the rightmost particle can tunnel, since the particles cannot interchange their positions. The spin-chain picture hence provides a definite prediction about the spin orientation of the outcoupled fermion. We illustrate this for the specific case of a $(N_\uparrow = 2, N_\downarrow = 1)$ system in the Tonks (AF) regime for $1/g \to 0$. The spin model provides the AF ground state $|0\rangle \equiv (|\uparrow,\uparrow,\downarrow\rangle - 2|\uparrow,\downarrow,\uparrow\rangle + |\downarrow,\uparrow,\uparrow\rangle)/\sqrt{6}$. The probability of outcoupling a single down spin is therefore $|\langle\uparrow,\uparrow,\downarrow|0\rangle|^2 \simeq 16.7\%$, in very good agreement with the experiment [46].[10] By contrast, if the system is prepared in the first excited state, $|1\rangle \equiv (|\uparrow,\uparrow,\downarrow\rangle - |\downarrow,\uparrow,\uparrow\rangle)/\sqrt{2}$, the probability is $|\langle\uparrow,\uparrow,\downarrow|1\rangle|^2 \simeq 50\%$ and in the F highest excited state, $|2\rangle \equiv (|\uparrow,\uparrow,\downarrow\rangle + |\uparrow,\downarrow,\uparrow\rangle + |\downarrow,\uparrow,\uparrow\rangle)/\sqrt{3}$, we get $|\langle\uparrow,\uparrow,\downarrow|2\rangle|^2 \simeq 33.3\%$. A similar simple calculation predicts the probabilities 5.1% and 1.5% for the AF ground states of (3,1) and (4,1) systems,[11] respectively, and much larger probabilities for the corresponding excited states. This measurement may hence clearly reveal the AF ground state.

Tunneling experiments may also be employed to measure the occupation-number distribution among the trap levels. First, the spin-up (-down) fermions are removed with a resonant light pulse, and afterwards the occupancies of the remaining spin-down (-up) fermions are probed using the tunneling technique [47]. Each spin state is linked to a particular occupation number distribution of the spin components among the trap levels (Fig. 5). One may hence utilize this information as a fingerprint of the state of the spin chain [see Appendix E for discussion of the $(N_\uparrow = 3, N_\downarrow = 2)$ five-fermion system].

[8]Experiments performed by Jochim and co-workers employ a scattering resonance at 783 G, well within the Paschen-Back regime, in which the energies of the employed states $|F = 1/2, m_F = \pm 1/2\rangle$ show the same B-field dependence. As a result a B-field gradient does not lift the degeneracy at $1/g = 0$, precluding in this experiment the use of sweeps to reach the F ground state in the super-Tonks regime.

[9]We note in passing that the exact diagonalization of the original Hamiltonian may be accomplished only for very few particles $N \leq 5$ [27,28,32] for (quasi)balanced mixtures, whereas the spin-chain model allows for exact diagonalizations of rather large samples $N \leq 20$ (and the treatment of even much larger N using, e.g., density-matrix renormalization-group techniques). For the particularly favorable case of $(N_\uparrow = N - 1, N_\downarrow = 1)$ systems, up to $N \leq 7$ particles have been calculated using the original Hamiltonian [26], whereas N up to several thousands can be handled using the spin-chain model.

[10]A similar result ($\simeq$20%) was predicted in the first version of Ref. [30]. This result was recently refined ($\simeq$16.7%) in the second version of Ref. [30], in excellent agreement with our result obtained from the spin-chain model.

[11]The same results were recently presented in the second version of Ref. [30].

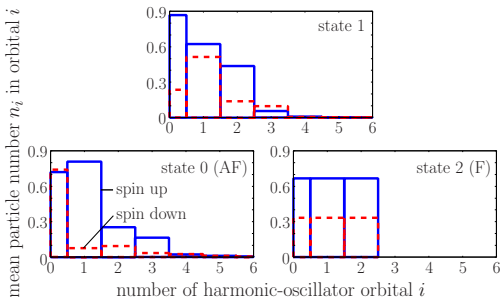

FIG. 5. (Color online) Mean occupation $\langle n_i \rangle$ of the harmonic-trap levels for the $(N_\uparrow = 2, N_\downarrow = 1)$ system in the Tonks regime $[g/(\hbar\omega l) = 25]$ for the states $|0\rangle$, $|1\rangle$, and $|2\rangle$ (see text) of the ground-state multiplet.

VII. EXPERIMENTAL REQUIREMENTS

As mentioned above, the creation of the AF state with fermions does not require crossing the scattering resonance. Due to spin conservation it may be created by increasing $g > 0$ starting with the noninteracting (spin-singlet) ground state (initial particle-hole excitations will be mapped on spin excitations of the AF chain). Realizing and probing the ground state of the 1D AF spin chain requires hence the deterministic preparation of noninteracting ground states, together with a good isolation from the environment, single-atom detection, precise control of g, and quasi-1D confinement. These conditions are already met in ongoing experiments on degenerate lithium-6 atoms [23,24,46]. These experiments allow for the preparation of the noninteracting ground state with a fidelity of 98% per atom, for a precise control of the spin imbalance, for the modification of g using a confinement-induced resonance, and for single-atom detection with near unit fidelity. The system is very well isolated, with a lifetime of the two-particle ground state of 1 min. These conditions result in an effective spin temperature of zero, even for strong interactions, and hence this setup constitutes an optimal scenario for the realization of AF chains.[12] Although the experiments of Refs. [23,24,46] are currently limited to small samples ($N < 10$), much larger ones, and hence longer spin chains, may be achieved in similar experiments by increasing the trap aspect ratio (currently 1:10) and improving the fidelity in the preparation of the noninteracting ground state.

VIII. SUMMARY

Strongly interacting multicomponent 1D gases in the vicinity of a scattering resonance realize a 1D spin chain, providing a scenario for the study of quantum magnetism alternative to atoms in 1D optical lattices and ion traps [50]. This alternative scenario, which avoids the inherent heating associated with an optical lattice, opens the possibility of creating an AF state from a noninteracting singlet state by simply increasing the interaction strength. Moreover, the effective spin-chain model provides a simple and intuitive understanding of recent experiments, allows for a very simple calculation of relevant observables, and enables numerical simulations of the statics and dynamics of much larger samples than the original model.

Although we have focused mainly on the spin-1/2 case, the spin-chain picture is equally valid for higher spins. Interestingly, strongly interacting alkaline-earth-metal or ytterbium Fermi gases realize an SU(N) Sutherland model. In particular, a spin-3/2 system would realize an SU(4) exchange Hamiltonian, which is of relevance in spin-orbital models of transition-metal oxides. The ground state of this system is a spin liquid, since magnetic order is suppressed due to orbital effects [51]. Moreover, magnetic-field gradients may be employed to prepare nontrivial initial spin states (e.g., helical states), and to rotate individual spins in combination with radio-frequency fields. This would allow for the study of the subsequent dynamics of the out-of-equilibrium 1D spin chain. Experiments on 1D strongly interacting multicomponent Fermi gases hence open a fascinating alternative scenario for the simulation of 1D quantum spin chains in cold gases.

ACKNOWLEDGMENTS

We thank G. Zürn, S. Jochim, T. Lompe, S. Murmann, J. C. Cremon, N. L. Harshman, S. Eggert, C. Klempt, M. Valiente, and L. H. Kristinsdóttir for helpful discussions. This work was supported by the Cluster of Excellence QUEST, the German-Israeli foundation, the Swiss SNF, the NCCR Quantum Science and Technology, the Swedish Research Council, and the Nanometer Structure Consortium at Lund University.

APPENDIX A: EFFECTIVE INTERACTION HAMILTONIAN

We derive in this appendix the effective Hamiltonian for interactions between nearest-neighboring spins of the spin chain in the vicinity of the point $1/g = 0$. It has been shown in Ref. [20] that the spin chain is noninteracting at $1/g = 0$ and highly degenerate due to the large number of possible spin configurations. This degeneracy is lifted away from $1/g = 0$ but the eigenstates at $1/g \approx 0$ are still very well approximated by particular superpositions of the eigenstates at $1/g = 0$, as shown in Fig. 1 of Ref. [20]. This suggests determination of the superpositions by performing a degenerate perturbative calculation to lowest order in $1/g$. In the following we derive the effective spin Hamiltonian, which leads to the desired superposition of spin states in the vicinity of $1/g = 0$.

We construct for small $1/g$ the g-dependent sector wave functions

$$\langle z_1, \ldots, z_N | P^{(g)} \rangle = \psi_P^{(g)}(z_1, \ldots, z_N) = \sqrt{N!}\theta(z_{P(1)}, \ldots, z_{P(N)})\psi_B^{(g)} \quad \text{(A1)}$$

with $\theta(z_1, \ldots, z_N) = 1$ if $z_1 \leq \cdots \leq z_N$ and zero otherwise, P is one of the $N!$ permutations of the ordering of the N particles, and $\psi_B^{(g)}$ is the ground state of N 1D spinless δ-interacting bosons. They converge in the limit $1/g \to 0$

[12] For moderate trap aspect ratios, like those used by Jochim and coworkers [23,24], the coupling of center-of-mass and relative motion [48] may result in the formation of molecules in the Tonks regime [46,49]. This problem can be avoided using larger trap aspect ratios.

towards the usual g-independent sector wave functions

$$\langle z_1,\ldots,z_N|P\rangle = \psi_P(z_1,\ldots,z_N) = \sqrt{N!}\theta(z_{P(1)},\ldots,z_{P(N)})A\,\psi_F \quad \text{(A2)}$$

with the unit antisymmetric function $A=\prod_{i<j}\mathrm{sgn}(z_i-z_j)$ and the ground state of N 1D spinless noninteracting fermions ψ_F. We approximate the exact wave functions in the vicinity of $1/g=0$ by

$$W_\pm^{(g)}|\chi\rangle = \sqrt{N!}S_\pm(|\mathrm{id}^{(g)}\rangle|\chi\rangle), \quad \text{(A3)}$$

where $|\chi\rangle=\sum_{m_1,\ldots,m_N}c_{m_1,\ldots,m_N}|m_1,\ldots,m_N\rangle$ is an arbitrary N-particle spin function, $S_\pm=(1/N!)\sum_P(\pm1)^P P$ is the (anti)symmetrization operator, and $|\mathrm{id}^{(g)}\rangle$ is the sector wave function corresponding to the identical permutation. Our goal is to calculate the matrix elements

$$\langle m_1,\ldots|\big(W_\pm^{(g)}\big)^\dagger H\,W_\pm^{(g)}|m_1',\ldots\rangle \quad \text{(A4)}$$

of the full many-body Hamiltonian in the vicinity of $1/g=0$. Inserting Eq. (A3) into Eq. (A4) and using $S_\pm^\dagger=S_\pm$, $[H,S_\pm]=0$, and $S_\pm^2=S_\pm$, we get

$$\langle m_1,\ldots|\big(W_\pm^{(g)}\big)^\dagger H\,W_\pm^{(g)}|m_1',\ldots\rangle = \sum_P(\pm1)^P\langle m_1,\ldots|\langle\mathrm{id}^{(g)}|H|P^{(g)}\rangle|m'_{P^{-1}(1)},\ldots\rangle. \quad \text{(A5)}$$

Next we evaluate the matrix elements $\langle\mathrm{id}^{(g)}|H|P^{(g)}\rangle$. The first two terms of the Taylor series of these matrix elements around $1/g=0$ are given by

$$\begin{aligned}\langle\mathrm{id}^{(g)}|H|P^{(g)}\rangle &= \lim_{1/g\to0}\big(\langle\mathrm{id}^{(g)}|H|P^{(g)}\rangle\big) + \frac{1}{g}\lim_{1/g\to0}\left(\langle\mathrm{id}^{(g)}|\frac{dH}{d(1/g)}|P^{(g)}\rangle\right)\\ &= E_F\delta_{P,\mathrm{id}} - \frac{1}{g}\lim_{g\to+\infty}\left(g^2\langle\mathrm{id}^{(g)}|\frac{dH}{dg}|P^{(g)}\rangle\right).\end{aligned} \quad \text{(A6)}$$

Here we used $H|P^{(g)}\rangle=E^{(g)}|P^{(g)}\rangle$ and $d\langle\mathrm{id}^{(g)}|P^{(g)}\rangle/dg=0$. The Hamiltonian of the multicomponent particles reads

$$H=\sum_i\left[-\frac{\hbar^2}{2m}\frac{\partial^2}{\partial z_i^2}+V(z_i)\right]+g\sum_{i<j}\delta(z_i-z_j) \quad \text{(A7)}$$

and therefore

$$\lim_{g\to+\infty}\left(g^2\langle\mathrm{id}^{(g)}|\frac{dH}{dg}|P^{(g)}\rangle\right) = \sum_{i<j}\lim_{g\to+\infty}\left[g^2\int dz_1\cdots dz_N\,\delta(z_i-z_j)\big(\psi_{\mathrm{id}}^{(g)}\big)^*\psi_P^{(g)}\right]. \quad \text{(A8)}$$

Most integrals are zero, since the corresponding domain of integration has zero volume; hence

$$\int dz_1\cdots dz_N\delta(z_i-z_j)\theta(z_1,\ldots,z_N)\theta(z_{P(1)},\ldots,z_{P(N)})\cdots = \delta_{j,i+1}(\delta_{P,\mathrm{id}}+\delta_{P,P_{i,i+1}})\int dz_1\cdots dz_N\delta(z_i-z_{i+1})\times\theta(z_1,\ldots,z_N)\cdots. \quad \text{(A9)}$$

Moreover, the limit in Eq. (A8) can be performed, since the average local correlation function of spinless bosons,

$$\int dz_1\cdots dz_N\sum_{i<j}\delta(z_i-z_j)\big|\psi_B^{(g)}\big|^2, \quad \text{(A10)}$$

decreases proportionally to $1/g^2$ in the limit of large g.[13] Using the boundary condition

$$\left(\frac{\partial}{\partial z_i}-\frac{\partial}{\partial z_j}\right)\psi\Big|_{z_i=z_j+} - \left(\frac{\partial}{\partial z_i}-\frac{\partial}{\partial z_j}\right)\psi\Big|_{z_i=z_j-} = \frac{2mg}{\hbar^2}\psi\Big|_{z_i=z_j}, \quad \text{(A11)}$$

which is imposed by the δ interaction, Eq. (A8) becomes

$$\begin{aligned}\lim_{g\to+\infty}&\left(g^2\langle\mathrm{id}^{(g)}|\frac{dH}{dg}|P^{(g)}\rangle\right) = \frac{\hbar^4}{4m^2}\sum_i(\delta_{P,\mathrm{id}}+\delta_{P,P_{i,i+1}})\int dz_1\cdots dz_N\\ &\times\delta(z_i-z_{i+1})(D_i\psi_{\mathrm{id}}^*)(D_i\psi_P)\end{aligned} \quad \text{(A12)}$$

with $D_i\psi=D_i^+\psi-D_i^-\psi$ and

$$D_i^\pm\psi=\left(\frac{\partial}{\partial z_i}-\frac{\partial}{\partial z_{i+1}}\right)\psi\Big|_{z_i=z_{i+1}\pm}. \quad \text{(A13)}$$

Note that we used $\lim_{g\to+\infty}\psi_P^{(g)}=\psi_P$ when we performed the limit. Using

$$\frac{\partial\psi_F}{\partial z_{i+1}}\Big|_{z_i=z_{i+1}} = -\frac{\partial\psi_F}{\partial z_i}\Big|_{z_i=z_{i+1}}, \quad \text{(A14)}$$

$$A|_{z_i=z_{i+1}\pm}=(\pm1)B \quad \text{(A15)}$$

with

$$B=\frac{A}{\mathrm{sgn}(z_i-z_{i+1})}\Big|_{z_i=z_{i+1}}, \quad \text{(A16)}$$

$$\theta(z_1,\ldots,z_N)|_{z_i=z_{i+1}+} = \theta\big(z_{P_{i,i+1}(1)},\ldots,z_{P_{i,i+1}(N)}\big)\big|_{z_i=z_{i+1}-}=0, \quad \text{(A17)}$$

and

$$\begin{aligned}\theta(z_1,\ldots,z_N)\big|_{z_i=z_{i+1}-} &= \theta\big(z_{P_{i,i+1}(1)},\ldots,z_{P_{i,i+1}(N)}\big)\big|_{z_i=z_{i+1}+}\\ &= \theta(z_1,\ldots,z_{i-1},z_{i+1},z_{i+1},\ldots,z_N),\end{aligned} \quad \text{(A18)}$$

we get

$$\begin{aligned}D_i\psi_{\mathrm{id}} &= -D_i^-\psi_{\mathrm{id}} = D_i\psi_{P_{i,i+1}} = D_i^+\psi_{P_{i,i+1}}\\ &= 2B\sqrt{N!}\theta(z_1,\ldots,z_{i-1},z_{i+1},z_{i+1},\ldots,z_N)\\ &\times\frac{\partial\psi_F}{\partial z_i}\Big|_{z_i=z_{i+1}}.\end{aligned} \quad \text{(A19)}$$

[13] This has been shown for homogeneous systems in the thermodynamic limit [52] and it also follows from the solution of two harmonically trapped particles [53]. It is hence natural to assume that this property holds true for an arbitrary number of particles in any confinement.

Inserting this into Eq. (A12) and using $B^2 = 1$ we get

$$\frac{1}{g}\lim_{g\to+\infty}\left(g^2\langle \mathrm{id}^{(g)}|\frac{dH}{dg}|P^{(g)}\rangle\right) = \sum_i \left(\delta_{P,\mathrm{id}} + \delta_{P,P_{i,i+1}}\right) J_i \tag{A20}$$

with

$$J_i = \frac{N!\hbar^4}{m^2 g}\int dz_1 \cdots dz_N \delta(z_i - z_{i+1})\theta(z_1,\ldots,z_N)\left|\frac{\partial \psi_F}{\partial z_i}\right|^2. \tag{A21}$$

Inserting Eq. (A20) into Eq. (A6) we get

$$\langle \mathrm{id}^{(g)}|H|P^{(g)}\rangle = \left(E_F - \sum_i J_i\right)\delta_{P,\mathrm{id}} - \sum_i \delta_{P,P_{i,i+1}} J_i\,. \tag{A22}$$

Finally we insert this into Eq. (A5) and obtain

$$\begin{aligned}&\langle m_1,\ldots|(W_\pm^{(g)})^\dagger H\, W_\pm^{(g)}|m_1',\ldots\rangle \\ &\quad = \langle m_1,\ldots|\left[\left(E_F - \sum_i J_i\right)\mathbb{1} \pm \sum_i J_i P_{i,i+1}\right]|m_1',\ldots\rangle\end{aligned} \tag{A23}$$

with "+" for fermions and "−" for bosons.

We would like to note that the effective interaction Hamiltonian (A23), which acts on many-body *spin* functions, originates from the tendency of the system to have a *spatial* wave function, which is most symmetric under the exchange of particles. The effective Hamiltonian following from Eq. (A22), which acts on the *spatial* sector wave functions $|P\rangle$, has the form $-\sum_i J_i P_{i,i+1}$ (without diagonal terms). This Hamiltonian minimizes the energy of a pair of neighboring sector wave functions $|P\rangle$ and $|P_{i,i+1}P\rangle$, if it is in the symmetric superposition $(|P\rangle + |P_{i,i+1}P\rangle)/\sqrt{2}$, whereas the antisymmetric superposition $(|P\rangle - |P_{i,i+1}P\rangle)/\sqrt{2}$ maximizes the energy. Therefore, the system minimizes its energy, if as many as possible neighboring sector wave functions are in a symmetric superposition. This is in agreement with the theorem that the ground state of a system with the spin-independent Hamiltonian (A7) strives to have as few as possible zero crossings of the spatial wave function [54,55]. We finally note that the effective interaction Hamiltonian (A23), like the original spin-independent Hamiltonian (A7), commutes with the square of the total spin $\vec{S}^2$. This, together with the tendency of the system to have a most symmetric *spatial* wave function, leads in the case of spinful fermions to a ground state with minimal total spin [54], whereas spinful bosons prefer a ground state with maximal total spin [55].

APPENDIX B: EXCHANGE CONSTANTS OF THE HARMONIC TRAP

We compare in this appendix the nearest-neighbor exchange constants (7) of up to six harmonically trapped particles to their LDA approximations (8). The TF profile of harmonically trapped noninteracting fermions is given by

$$n_{\mathrm{TF}}(z) = \frac{1}{l\pi}\sqrt{2N - \left(\frac{z}{l}\right)^2}. \tag{B1}$$

It is evaluated at the center-of-mass positions of the ith and $(i+1)$th particles,

$$z_i = \frac{1}{2}\int dz\, z[\rho^{(i)}(z) + \rho^{(i+1)}(z)]. \tag{B2}$$

The particle densities $\rho^{(i)}(z)$ have been obtained from a fit to the exact total density. Table I shows the exact exchange constants of up to six harmonically trapped particles, obtained by computing the $(N-1)$-dimensional integrals of Eq. (7). The value in parentheses is the deviation of the LDA result (8), which shows, as expected, an increasing agreement with increasing particle number.

TABLE I. Nearest-neighbor exchange constants $J_i g/(\hbar^2\omega^2 l)$ of $N \le 6$ harmonically trapped particles. The value in parentheses is the deviation of the local density approximation. Note that $J_{N-i} = J_i$ due to the parity symmetry of the harmonic trap.

N	$J_1 g/(\hbar^2\omega^2 l)$	$J_2 g/(\hbar^2\omega^2 l)$	$J_3 g/(\hbar^2\omega^2 l)$
2	$\sqrt{\frac{\pi}{2}} = 0.797885$ (6.4%)		
3	$\frac{3^3}{2^3\sqrt{2\pi}} = 1.34643$ (2.9%)		
4	1.78765 (1.2%)	2.34651 (2.3%)	
5	2.16606 (0.14%)	3.17720 (1.6%)	
6	2.50218 (−0.55%)	3.90210 (1.1%)	4.35712 (1.2%)

APPENDIX C: VALIDITY REGIME OF THE SPIN-CHAIN MODEL

1. Three spin-1/2 fermions

In this appendix, we compare analytically calculated energy differences and spin densities of $(N_\uparrow = 2, N_\downarrow = 1)$ harmonically trapped spin-1/2 fermions to those obtained by means of an exact diagonalization of the full Hamiltonian. We first calculate the spectrum and the eigenfunctions of the spin chain. Within the spin basis, $|\uparrow,\uparrow,\downarrow\rangle$, $|\uparrow,\downarrow,\uparrow\rangle$, and $|\downarrow,\uparrow,\uparrow\rangle$, the interaction Hamiltonian reads (note that $J_1 = J_2$)

$$H_s = (E_F - 2J_1)\mathbb{1} + J_1\begin{pmatrix}1 & 1 & 0\\ 1 & 0 & 1\\ 0 & 1 & 1\end{pmatrix}. \tag{C1}$$

Its eigenstates are

$$|0\rangle = \frac{1}{\sqrt{6}}(|\uparrow,\uparrow,\downarrow\rangle - 2|\uparrow,\downarrow,\uparrow\rangle + |\downarrow,\uparrow,\uparrow\rangle), \tag{C2}$$

$$|1\rangle = \frac{1}{\sqrt{2}}(|\uparrow,\uparrow,\downarrow\rangle - |\downarrow,\uparrow,\uparrow\rangle), \tag{C3}$$

and

$$|2\rangle = \frac{1}{\sqrt{3}}(|\uparrow,\uparrow,\downarrow\rangle + |\uparrow,\downarrow,\uparrow\rangle + |\downarrow,\uparrow,\uparrow\rangle). \tag{C4}$$

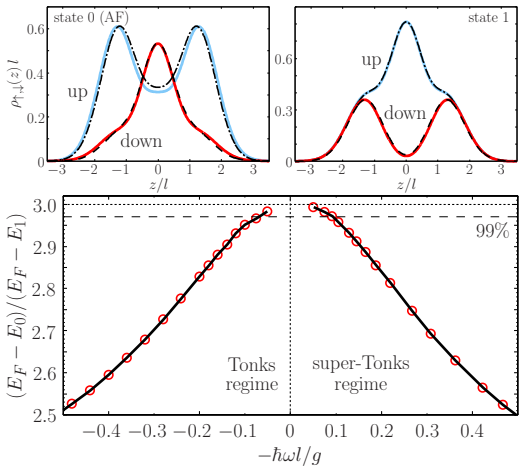

FIG. 6. (Color online) Comparison between the exact-diagonalization results of the original continuous model and the results obtained from the effective spin model for $(N_\uparrow = 2, N_\downarrow = 1)$ harmonically trapped spin-1/2 fermions. Top: Spin densities of the effective spin-chain model (solid lines) and of an exact diagonalization of the full Hamiltonian for $g/(\hbar\omega l) = 10$ in a harmonic trap (dashed and dash-dotted lines). Bottom: Ratio of energy differences of the ground-state multiplet as a function of $-1/g$ [solid (black) line with (red) circles]. The corresponding value of the spin-chain model is 3 (horizontal short-dashed line). The long-dashed line marks -1% deviation from this value.

They are simultaneously eigenstates of the square of the total spin $\vec{S}^2$ and the parity operator $\Pi = -P_{1,3}$,[14] with eigenvalues $S = 1/2$ and $\Pi = -1$ for $|0\rangle$, $S = 1/2$ and $\Pi = 1$ for $|1\rangle$, and $S = 3/2$ and $\Pi = -1$ for $|2\rangle$ [31]. The eigenenergies are $E_0 = E_F - 3J_1$, $E_1 = E_F - J_1$, and $E_2 = E_F$. The ratio of energy differences is hence given by $(E_F - E_0)/(E_F - E_1) = 3$. Figure 6 (bottom) shows this ratio of energy differences as a function of $-1/g$. The result of an exact diagonalization of the full Hamiltonian of the harmonically trapped system [solid (black) line with (red) circles] approaches the analytical value 3, marked by the horizontal short-dashed line, in the (super-)Tonks regime. The deviation is smaller than 1% for $|\hbar\omega l/g| < 0.1$.

Next we compare the density distributions obtained from the spin model with those resulting from the exact diagonalization of the original model. The analytical spin densities of the AF ground state $|0\rangle$ and the first excited state $|1\rangle$ are

$$\rho_\uparrow(z) = \tfrac{5}{6}\rho^{(1)}(z) + \tfrac{2}{6}\rho^{(2)}(z) + \tfrac{5}{6}\rho^{(3)}(z), \tag{C5}$$

$$\rho_\downarrow(z) = \tfrac{1}{6}\rho^{(1)}(z) + \tfrac{4}{6}\rho^{(2)}(z) + \tfrac{1}{6}\rho^{(3)}(z) \tag{C6}$$

and

$$\rho_\uparrow(z) = \tfrac{1}{2}\rho^{(1)}(z) + \rho^{(2)}(z) + \tfrac{1}{2}\rho^{(3)}(z), \tag{C7}$$

$$\rho_\downarrow(z) = \tfrac{1}{2}\rho^{(1)}(z) + \tfrac{1}{2}\rho^{(3)}(z), \tag{C8}$$

respectively [solid lines in Fig. 6 (top)]. The corresponding numerical results for $g/(\hbar\omega l) = 10$ (dashed and dash-dotted lines) agree very well with the analytical spin densities. The small deviation between the analytical and numerical spin densities of the AF ground state is larger than for the excited states (they agree for the F state $|2\rangle$).

2. Four spin-1/2 fermions

Here we perform the same comparison as in the last section for four fermions in the $(N_\uparrow = 3, N_\downarrow = 1)$ configuration. Within the spin basis $|\uparrow,\uparrow,\uparrow,\downarrow\rangle$, $|\uparrow,\uparrow,\downarrow,\uparrow\rangle$, $|\uparrow,\downarrow,\uparrow,\uparrow\rangle$, and $|\downarrow,\uparrow,\uparrow,\uparrow\rangle$, the interaction Hamiltonian reads

$$H_s = (E_F - 2J_1 - J_2)\mathbb{1} + \begin{pmatrix} J_1+J_2 & J_1 & 0 & 0 \\ J_1 & J_1 & J_2 & 0 \\ 0 & J_2 & J_1 & J_1 \\ 0 & 0 & J_1 & J_1+J_2 \end{pmatrix}. \tag{C9}$$

With J_1 and J_2 of Table I the eigenenergies are given by

$$E_0 = E_F - J_1 - J_2 - \sqrt{J_1^2 + J_2^2} = E_F - 7.084(\hbar\omega l/g)\hbar\omega, \tag{C10}$$

$$E_1 = E_F - 2J_1 = E_F - 3.575(\hbar\omega l/g)\hbar\omega, \tag{C11}$$

$$E_2 = E_F - J_1 - J_2 + \sqrt{J_1^2 + J_2^2} = E_F - 1.184(\hbar\omega l/g)\hbar\omega, \tag{C12}$$

and $E_3 = E_F$, which lead to the ratios of energy differences

$$\frac{E_F - E_0}{E_F - E_1} = \frac{J_1 + J_2 + \sqrt{J_1^2 + J_2^2}}{2J_1} = 1.982 \tag{C13}$$

and

$$\frac{E_F - E_0}{E_F - E_2} = \frac{J_1 + J_2 + \sqrt{J_1^2 + J_2^2}}{J_1 + J_2 - \sqrt{J_1^2 + J_2^2}} = 5.983. \tag{C14}$$

We plot these ratios as a function of $-1/g$ in the bottom and middle panels of Fig. 7. The results of an exact diagonalization of the full Hamiltonian of the harmonically trapped system [solid (black) lines with (red) circles] approach the results of the spin-chain model, 1.982 and 5.983, respectively (horizontal short-dashed lines), in the (super-)Tonks regime. Again, the deviation is only $\simeq 1\%$ for $|\hbar\omega l/g| < 0.1$.

The eigenstates of the spin Hamiltonian (C9) are

$$|0\rangle = c_-(|\uparrow,\uparrow,\uparrow,\downarrow\rangle - |\downarrow,\uparrow,\uparrow,\uparrow\rangle) - c_+(|\uparrow,\uparrow,\downarrow,\uparrow\rangle - |\uparrow,\downarrow,\uparrow,\uparrow\rangle), \tag{C15}$$

$$|1\rangle = \tfrac{1}{2}(|\uparrow,\uparrow,\uparrow,\downarrow\rangle - |\uparrow,\uparrow,\downarrow,\uparrow\rangle - |\uparrow,\downarrow,\uparrow,\uparrow\rangle + |\downarrow,\uparrow,\uparrow,\uparrow\rangle), \tag{C16}$$

[14]The parity operator Π, which acts originally on the sector wave functions in the usual way, $(z_1,\ldots,z_N) \to (-z_1,\ldots,-z_N)$, is transformed into the spin basis via the map (2), with the result $\Pi = (\pm 1)^{\lfloor N/2 \rfloor} P_{1,N} P_{2,N-1} \cdots$ with "+" for bosons, "−" for fermions, and the common floor function $\lfloor x \rfloor$.

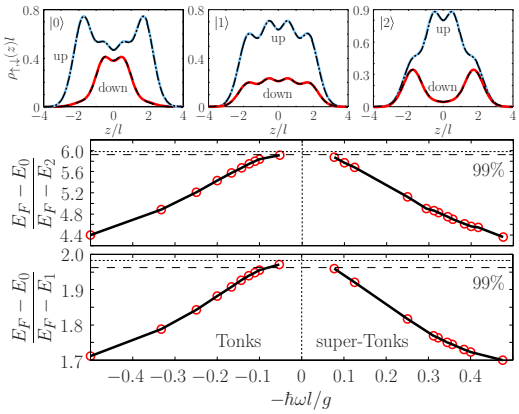

FIG. 7. (Color online) The same as Fig. 6 for the $(N_\uparrow = 3, N_\downarrow = 1)$ system. Top: Spin densities of the effective spin-chain model (solid lines) and of an exact diagonalization of the full Hamiltonian for $g/(\hbar\omega l) = 25$ in a harmonic trap (dashed and dash-dotted lines). Bottom: Ratio of energy differences of the ground-state multiplet as a function of $-1/g$ [solid (black) line with (red) circles]. The corresponding values of the spin-chain model are 1.982 and 5.983, respectively (horizontal short-dashed lines). The horizontal long-dashed lines mark -1% deviation from these values.

$$|2\rangle = c_+(|\uparrow,\uparrow,\uparrow,\downarrow\rangle - |\downarrow,\uparrow,\uparrow,\uparrow\rangle) + c_-(|\uparrow,\uparrow,\downarrow,\uparrow\rangle - |\uparrow,\downarrow,\uparrow,\uparrow\rangle), \quad \text{(C17)}$$

and

$$|3\rangle = \tfrac{1}{2}(|\uparrow,\uparrow,\uparrow,\downarrow\rangle + |\uparrow,\uparrow,\downarrow,\uparrow\rangle + |\uparrow,\downarrow,\uparrow,\uparrow\rangle + |\downarrow,\uparrow,\uparrow,\uparrow\rangle) \quad \text{(C18)}$$

with

$$c_\pm = \frac{1}{2}\sqrt{1 \pm \frac{J_2}{\sqrt{J_1^2 + J_2^2}}} = \begin{cases} 0.6700 \text{ (for } +), \\ 0.2261 \text{ (for } -). \end{cases} \quad \text{(C19)}$$

They are again eigenstates of $\vec{S}^2$ and $\Pi = P_{1,4}P_{2,3}$ with eigenvalues $S = 1$ and $\Pi = -1$ for $|0\rangle$ and $|2\rangle$, $S = 1$ and $\Pi = 1$ for $|1\rangle$, and $S = 2$ and $\Pi = 1$ for $|3\rangle$ [31]. The spin densities of the ground state $|0\rangle$ are

$$\rho_\uparrow(z) = (|c_-|^2 + 2|c_+|^2)[\rho^{(1)}(z) + \rho^{(4)}(z)] + (|c_+|^2 + 2|c_-|^2)[\rho^{(2)}(z) + \rho^{(3)}(z)], \quad \text{(C20)}$$

$$\rho_\downarrow(z) = |c_-|^2[\rho^{(1)}(z) + \rho^{(4)}(z)] + |c_+|^2[\rho^{(2)}(z) + \rho^{(3)}(z)], \quad \text{(C21)}$$

for the first excited state $|1\rangle$ we get

$$\rho_\uparrow(z) = \tfrac{3}{4}[\rho^{(1)}(z) + \rho^{(2)}(z) + \rho^{(3)}(z) + \rho^{(4)}(z)], \quad \text{(C22)}$$

$$\rho_\downarrow(z) = \tfrac{1}{4}[\rho^{(1)}(z) + \rho^{(2)}(z) + \rho^{(3)}(z) + \rho^{(4)}(z)], \quad \text{(C23)}$$

and for the second excited state $|2\rangle$ we get

$$\rho_\uparrow(z) = (|c_+|^2 + 2|c_-|^2)[\rho^{(1)}(z) + \rho^{(4)}(z)] + (|c_-|^2 + 2|c_+|^2)[\rho^{(2)}(z) + \rho^{(3)}(z)], \quad \text{(C24)}$$

$$\rho_\downarrow(z) = |c_+|^2[\rho^{(1)}(z) + \rho^{(4)}(z)] + |c_-|^2[\rho^{(2)}(z) + \rho^{(3)}(z)]. \quad \text{(C25)}$$

The spin densities of the spin-chain model, which are shown in the top row of Fig. 7 (solid lines), are compared to the numerical results for $g/(\hbar\omega l) = 25$ (dashed and dash-dotted lines) showing no visible difference.

APPENDIX D: GRADIENT

In this appendix, we transform the Hamiltonian of a B-field gradient into the spin basis. The matrix elements of a B-field gradient,

$$V_G = (G/l)\sum_{i=1}^{N}\int dz_1 \cdots dz_N |z_1,\ldots,z_N\rangle \times \langle z_1,\ldots,z_N|z_i\sigma_z^{(i)}, \quad \text{(D1)}$$

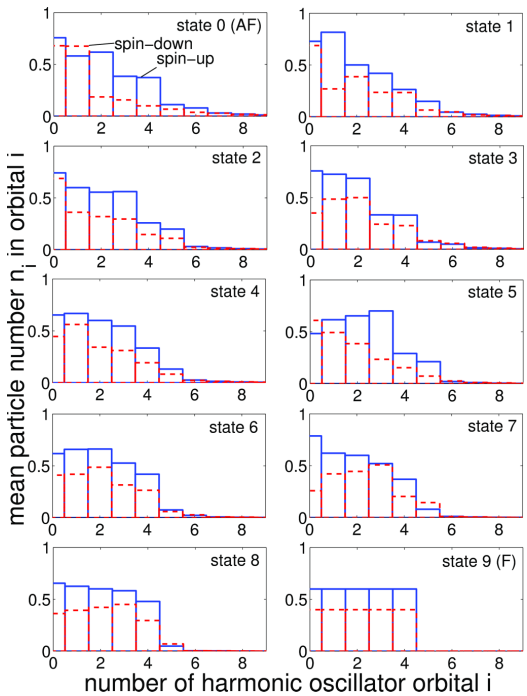

FIG. 8. (Color online) Mean occupation numbers $\langle n_i\rangle$ of the harmonic-oscillator orbitals of an $(N_\uparrow = 3, N_\downarrow = 2)$ Fermi system in the Tonks regime $[g/(\hbar\omega l) = 30$, ground-state multiplet].

are

$$\begin{aligned}
&\langle m_1,\ldots|W_\pm^\dagger V_G W_\pm|m_1',\ldots\rangle\\
&\quad= N!\langle m_1,\ldots|\langle \mathrm{id}|S_\pm^\dagger V_G S_\pm|\mathrm{id}\rangle|m_1',\ldots\rangle\\
&\quad= \sum_P (\pm 1)^P \langle m_1,\ldots|\langle \mathrm{id}|V_G|P\rangle\left|m'_{P^{-1}(1)},\ldots\right\rangle\\
&\quad= \langle m_1,\ldots|\langle \mathrm{id}|V_G|\mathrm{id}\rangle|m_1',\ldots\rangle. \qquad \text{(D2)}
\end{aligned}$$

Here we used $\langle \mathrm{id}|V_G|P\rangle = \delta_{\mathrm{id},P}\langle \mathrm{id}|V_G|\mathrm{id}\rangle$, which follows from the fact that different sectors of the many-body position space $\mathbb{R}^N$ have no overlap. Using Eq. (D1) we obtain

$$\begin{aligned}
&\langle m_1,\ldots|W_\pm^\dagger V_G W_\pm|m_1',\ldots\rangle\\
&\quad= \langle m_1,\ldots|\left[(G/l)\sum_{i=1}^N \langle z\rangle_i\,\sigma_z^{(i)}\right]|m_1',\ldots\rangle, \qquad \text{(D3)}
\end{aligned}$$

where $\langle z\rangle_i$ is the position of the ith spin,

$$\begin{aligned}
\langle z\rangle_i &= \int dz_1\cdots dz_N z_i|\langle z_1,\ldots,z_N|\mathrm{id}\rangle|^2\\
&= \int dz z\int dz_1\cdots dz_N\delta(z-z_i)|\langle z_1,\ldots,z_N|\mathrm{id}\rangle|^2\\
&= \int dz z\rho^{(i)}(z). \qquad \text{(D4)}
\end{aligned}$$

APPENDIX E: MEAN OCCUPANCIES OF HARMONIC-TRAP LEVELS

In the main text, we mentioned that different states of the ground-state multiplet can be distinguished from each other by means of the mean occupancies $\langle n_i\rangle$ of the trap levels. Here we discuss this issue in more detail for a more involved example. Figure 8 shows the mean occupancies $\langle n_i\rangle$ of the harmonic-oscillator orbitals of an $(N_\uparrow = 3, N_\downarrow = 2)$-fermion system in the Tonks regime. In this case, the ground-state multiplet consists of ten states. One sees that the AF state (state 0) and the F state (state 9) can be clearly distinguished from the others. The AF state features high occupancies of the lowest levels $(n = 0,1)$ and small but nonzero occupancies in the $n > 4$ levels. For the F state, the lowest five orbitals $n = 0,1,2,3,4$ are equally populated while higher orbitals $(n > 4)$ are empty.

In general, the occupation-number distribution is a measure of the symmetry of the spatial part of the many-body wave function. The AF state of spin-1/2 fermions has the most symmetric spatial wave function, which leads to high occupancies of the lowest levels $(n = 0,1)$ and small but nonzero occupancies above the Fermi edge. The F state has a completely antisymmetric spatial wave function in which the states below the Fermi edge are equally populated while the states above the Fermi edge are empty. The other states interpolate between these extreme cases, i.e., the symmetry of the spatial wave functions decreases from state 0 to 9. The same arguments apply to the momentum distribution [20–22].

[1] A. Auerbach, *Interacting Electrons and Quantum Magnetism* (Springer, New York, 1994).

[2] S. Trotzky, P. Cheinet, S. Fölling, M. Feld, U. Schnorrberger, A. M. Rey, A. Polkovnikov, E. A. Demler, M. D. Lukin, and I. Bloch, Science **319**, 295 (2008).

[3] S. Nascimbène, Y.-A. Chen, M. Atala, M. Aidelsburger, S. Trotzky, B. Paredes, and I. Bloch, Phys. Rev. Lett. **108**, 205301 (2012).

[4] J. Simon, W. S. Bakr, R. Ma, M. E. Tai, P. M. Preiss, and M. Greiner, Nature (London) **472**, 307 (2011).

[5] F. Meinert, M. J. Mark, E. Kirilov, K. Lauber, P. Weinmann, A. J. Daley, and H.-C. Nägerl, Phys. Rev. Lett. **111**, 053003 (2013).

[6] J. Struck, C. Ölschläger, R. Le Targat, P. Soltan-Panahi, A. Eckardt, M. Lewenstein, P. Windpassinger, and K. Sengstock, Science **333**, 996 (2011).

[7] B. Yan, S. A. Moses, B. Gadway, J. P. Covey, K. R. A. Hazzard, A. M. Rey, D. S. Jin, and J. Ye, Nature (London) **501**, 521 (2013).

[8] A. de Paz, A. Sharma, A. Chotia, E. Maréchal, J. H. Huckans, P. Pedri, L. Santos, O. Gorceix, L. Vernac, and B. Laburthe-Tolra, Phys. Rev. Lett. **111**, 185305 (2013).

[9] D. Greif, T. Uehlinger, G. Jotzu, L. Tarruell, and T. Esslinger, Science **340**, 1307 (2013).

[10] M. A. Cazalilla, R. Citro, T. Giamarchi, E. Orignac, and M. Rigol, Rev. Mod. Phys. **83**, 1405 (2011).

[11] B. Paredes, A. Widera, V. Murg, O. Mandel, S. Fölling, I. Cirac, G. V. Shlyapnikov, T. W. Hänsch, and I. Bloch, Nature (London) **429**, 277 (2004).

[12] T. Kinoshita, T. Wenger, and D. S. Weiss, Science **305**, 1125 (2004).

[13] T. Kinoshita, T. Wenger, and D. S. Weiss, Phys. Rev. Lett. **95**, 190406 (2005).

[14] B. Laburthe Tolra, K. M. O'Hara, J. H. Huckans, W. D. Phillips, S. L. Rolston, and J. V. Porto, Phys. Rev. Lett. **92**, 190401 (2004).

[15] E. Haller, M. Rabie, M. J. Mark, J. G. Danzl, R. Hart, K. Lauber, G. Pupillo, and H.-C. Nägerl, Phys. Rev. Lett. **107**, 230404 (2011).

[16] T. Kinoshita, T. Wenger, and D. S. Weiss, Nature (London) **440**, 900 (2006).

[17] E. Haller, M. Gustavsson, M. J. Mark, J. G. Danzl, R. Hart, G. Pupillo, and H.-C. Nägerl, Science **325**, 1224 (2009).

[18] M. Girardeau, J. Math. Phys. **1**, 516 (1960).

[19] M. D. Girardeau and A. Minguzzi, Phys. Rev. Lett. **99**, 230402 (2007).

[20] F. Deuretzbacher, K. Fredenhagen, D. Becker, K. Bongs, K. Sengstock, and D. Pfannkuche, Phys. Rev. Lett. **100**, 160405 (2008).

[21] L. Guan, S. Chen, Y. Wang, and Z.-Q. Ma, Phys. Rev. Lett. **102**, 160402 (2009).

[22] B. Fang, P. Vignolo, M. Gattobigio, C. Miniatura, and A. Minguzzi, Phys. Rev. A **84**, 023626 (2011).

[23] F. Serwane, G. Zürn, T. Lompe, T. B. Ottenstein, A. N. Wenz, and S. Jochim, Science **332**, 336 (2011).

[24] G. Zürn, F. Serwane, T. Lompe, A. N. Wenz, M. G. Ries, J. E. Bohn, and S. Jochim, Phys. Rev. Lett. **108**, 075303 (2012).

[25] M. Rontani, Phys. Rev. Lett. **108**, 115302 (2012).
[26] E. J. Lindgren, J. Rotureau, C. Forssén, A. G. Volosniev, and N. T. Zinner, New J. Phys. **16**, 063003 (2014).
[27] P. O. Bugnion and G. J. Conduit, Phys. Rev. A **87**, 060502(R) (2013).
[28] T. Sowiński, T. Grass, O. Dutta, and M. Lewenstein, Phys. Rev. A **88**, 033607 (2013).
[29] X. Cui and T.-L. Ho, Phys. Rev. A **89**, 023611 (2014).
[30] A. G. Volosniev, D. V. Fedorov, A. S. Jensen, M. Valiente, and N. T. Zinner, arXiv:1306.4610v1; arXiv:1306.4610v2.
[31] N. L. Harshman, Phys. Rev. A **89**, 033633 (2014).
[32] S. E. Gharashi and D. Blume, Phys. Rev. Lett. **111**, 045302 (2013).
[33] X. Cui and T.-L. Ho, Phys. Rev. Lett. **110**, 165302 (2013).
[34] K. A. Matveev, Phys. Rev. Lett. **92**, 106801 (2004).
[35] K. A. Matveev, Phys. Rev. B **70**, 245319 (2004).
[36] G. A. Fiete, Rev. Mod. Phys. **79**, 801 (2007).
[37] S. A. Söffing, M. Bortz, I. Schneider, A. Struck, M. Fleischhauer, and S. Eggert, Phys. Rev. B **79**, 195114 (2009).
[38] S. A. Söffing, M. Bortz, and S. Eggert, Phys. Rev. A **84**, 021602(R) (2011).
[39] A. V. Gorshkov, M. Hermele, V. Gurarie, C. Xu, P. S. Julienne, J. Ye, P. Zoller, E. Demler, M. D. Lukin, and A. M. Rey, Nat. Phys. **6**, 289 (2010).
[40] S. Taie, R. Yamazaki, S. Sugawa, and Y. Takahashi, Nat. Phys. **8**, 825 (2012).
[41] G. Pagano, M. Mancini, G. Cappellini, P. Lombardi, F. Schäfer, H. Hu, X.-J. Liu, J. Catani, C. Sias, M. Inguscio, and L. Fallani, Nat. Phys. **10**, 198 (2014).
[42] K. A. Matveev and A. Furusaki, Phys. Rev. Lett. **101**, 170403 (2008).
[43] B. Sutherland, Phys. Rev. B **12**, 3795 (1975).
[44] X.-W. Guan, M. T. Batchelor, and M. Takahashi, Phys. Rev. A **76**, 043617 (2007).
[45] J. Y. Lee, X.-W. Guan, K. Sakai, and M. T. Batchelor, Phys. Rev. B **85**, 085414 (2012).
[46] G. Zürn, Ph.D. thesis, University of Heidelberg, 2012 [urn:nbn:de:bsz:16-heidok-144969].
[47] G. Zürn (private communication).
[48] S. Sala, G. Zürn, T. Lompe, A. N. Wenz, S. Murmann, F. Serwane, S. Jochim, and A. Saenz, Phys. Rev. Lett. **110**, 203202 (2013).
[49] S. E. Gharashi, K. M. Daily, and D. Blume, Phys. Rev. A **86**, 042702 (2012).
[50] R. Blatt and C. F. Roos, Nat. Phys. **8**, 277 (2012).
[51] Y. Yamashita, N. Shibata, and K. Ueda, Phys. Rev. B **58**, 9114 (1998).
[52] D. M. Gangardt and G. V. Shlyapnikov, Phys. Rev. Lett. **90**, 010401 (2003).
[53] T. Busch, B.-G. Englert, K. Rzążewski, and M. Wilkens, Found. Phys. **28**, 549 (1998).
[54] E. H. Lieb and D. Mattis, Phys. Rev. **125**, 164 (1962).
[55] E. Eisenberg and E. H. Lieb, Phys. Rev. Lett. **89**, 220403 (2002).

Paper III

Antiferromagnetic Heisenberg Spin Chain of a Few Cold Atoms in a One-Dimensional Trap

S. Murmann,[1,*] F. Deuretzbacher,[2,†] G. Zürn,[1] J. Bjerlin,[3] S. M. Reimann,[3] L. Santos,[2] T. Lompe,[1,‡] and S. Jochim[1]
[1]Physikalisches Institut der Universität Heidelberg, Im Neuenheimer Feld 226, DE-69120 Heidelberg, Germany
[2]Institut für Theoretische Physik, Leibniz Universität Hannover, Appelstraße 2, DE-30167 Hannover, Germany
[3]Mathematical Physics and NanoLund, LTH, Lund University, SE-22100 Lund, Sweden
(Received 4 July 2015; published 19 November 2015)

We report on the deterministic preparation of antiferromagnetic Heisenberg spin chains consisting of up to four fermionic atoms in a one-dimensional trap. These chains are stabilized by strong repulsive interactions between the two spin components without the need for an external periodic potential. We independently characterize the spin configuration of the chains by measuring the spin orientation of the outermost particle in the trap and by projecting the spatial wave function of one spin component on single-particle trap levels. Our results are in good agreement with a spin-chain model for fermionized particles and with numerically exact diagonalizations of the full few-fermion system.

DOI: 10.1103/PhysRevLett.115.215301 PACS numbers: 67.85.Lm, 71.10.Pm, 75.10.Jm, 75.10.Pq

The high control and tunability of ultracold atomic systems offer the fascinating possibility to simulate quantum magnetism [1], a topic of fundamental importance in condensed matter physics [2]. Systems of spin-1/2 fermions with antiferromagnetic (AFM) correlations are of particular interest due to the observation of high-temperature superconductivity in cuprates with AFM correlations [3]. The experimental implementation of the necessary exchange couplings is usually realized by superexchange processes of neighboring atoms in the Mott-insulating state of a deep optical lattice. Superexchange couplings were measured in both bosonic [4] and fermionic double-well systems [5] and short-range AFM correlations of fermionic atoms were detected in various lattice geometries [6–8]. Furthermore, superexchange processes were used to study the dynamics of spin impurities above the ferromagnetic (FM) ground state of bosons in the Mott-insulating state of a one-dimensional lattice [9]. Bosonic atoms were also used to simulate AFM Ising spin chains in a tilted optical lattice [10,11]. However, the AFM ground state of spin-1/2 fermions in a deep optical lattice has so far not been realized due to the very low energy scale associated with the superexchange coupling.

This problem can be circumvented in 1D systems, where quantum magnetism can be simulated without an optical lattice [12–14]. In the regime of strong interactions, the spatial wave function of both fermions [15] and bosons [16–18] can be mapped on the wave function of spinless noninteracting fermions [Fig. 1(a)]. In this so-called fermionization limit, the strong interactions lead to the formation of a Wigner-crystal-like state [19–21], which has a highly degenerate ground state when the particles have multiple internal degrees of freedom [Fig. 1(b)] [20–23]. Close to the limit of fermionization, the structure of the quasidegenerate ground-state multiplet [24–33] is determined by an effective Sutherland spin-chain Hamiltonian, which for two-component systems becomes a Heisenberg model [12,19,21,29,32–34].

In this Letter, we report on the realization of Heisenberg spin chains of $N_\uparrow$ spin-up and $N_\downarrow$ spin-down particles with $(N_\uparrow, N_\downarrow) = (2, 1), (3, 1)$, and $(2, 2)$. We show that under an

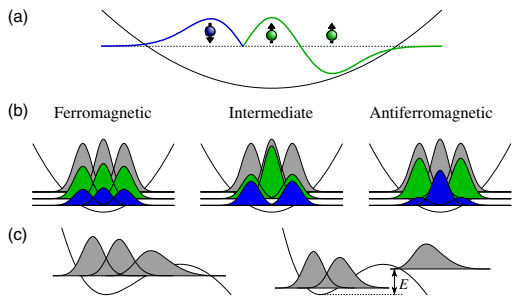

FIG. 1 (color online). Heisenberg spin chain of three fermions. (a) Sketch of two spin-up and one spin-down atom with diverging 1D coupling constant ($g_{1D} = \pm\infty$) in a harmonic trap. If the relative spatial wave function of two distinguishable fermions is symmetric, the strong interactions induce a cusp in the relative wave function of the two particles (left-hand side). This causes them to separate like identical fermions (right-hand side). In this fermionization limit the system forms a Wigner-crystal-like state with fixed ordering of the particles. (b) Single-particle contributions to the total (gray), the spin-up (green), and the spin-down density (blue) of two spin-up and one spin-down atom in the fermionization regime in a harmonic trap. Like in a Wigner crystal, the total densities of the ferromagnetic (left), the intermediate (middle), and the antiferromagnetic state (right) are identical, while their spin densities differ and are determined by a Heisenberg spin-chain Hamiltonian. (c) Densities of three particles before (left) and after (right) the tunneling of one atom with energy E out of a tilted trap. At fermionization, only the rightmost particle can leave the trap in the tunneling process.

adiabatic change of the interaction strength the noninteracting ground states of these systems evolve into the respective AFM states in the limit of infinitely strong repulsion [24,28]. We identify the AFM states by two independent measurements. First, we use a tunneling technique to measure the spin orientation of the outermost particle of the spin chain. Second, we probe the spatial wave function of the spin-down atom in the (2, 1) and (3, 1) system by projecting it on single-particle trap levels.

In our experiments, we realize a spin-1/2 system by trapping ultracold ^{6}Li atoms in an elongated optical dipole trap [35,39] in their two lowest hyperfine states $|\uparrow\rangle \equiv |j = 1/2, m_j = -1/2; I = 1, m_I = 0\rangle$ and $|\downarrow\rangle \equiv |j = 1/2, m_j = -1/2; I = 1, m_I = 1\rangle$. As the energy of the atoms is much smaller than the lowest transverse excitation energy in the trap, their dynamics are restricted to the longitudinal axis of the trap. In such a quasi-1D system, the interaction strength between ultracold atoms of opposite spin is determined by the 1D coupling constant g_{1D}, which diverges at a confinement-induced resonance (CIR) when the 3D scattering length a_{3D} approaches the harmonic oscillator length of the radial confinement [35,40]. We use a magnetic Feshbach resonance to control a_{3D} and therefore are able to smoothly tune g_{1D} across the CIR. At the same time, scattering between fermionic atoms of the same spin component is forbidden. Throughout this Letter, g_{1D} will be given in units of $a_\parallel \hbar\omega_\parallel$, where $a_\parallel = \sqrt{\hbar/m\omega_\parallel}$ and $\omega_\parallel$ are the harmonic oscillator length and the trap frequency in the longitudinal direction and m is the mass of a ^{6}Li atom.

We start our experiments by preparing a (2, 1), (3, 1), or (2, 2) system in the noninteracting many-particle ground state of the trap [35,39]. By changing the magnetic offset field with a constant rate, we ramp the system into the fermionization regime close to the CIR (Fig. 2), where it forms a spin chain. Below the CIR, g_{1D} is large and positive and the system is in the Tonks regime of strong repulsion [17,18]. When crossing the CIR, g_{1D} changes sign from $+\infty$ to $-\infty$ while the system continuously follows the so-called upper branch [24] into the super-Tonks regime of strong attraction [15,41,42] (Fig. 2). In the super-Tonks regime, the system is in an excited state, which is metastable against decay into bound states.

In a first set of measurements, we identify the states of the spin chains by probing the spin distributions in the trap. Here, we make use of the fact that in the fermionization regime the atoms become impenetrable and therefore their ordering along the longitudinal axis of the trap is fixed. This allows us to determine the spin orientation of the outermost particle in the trap in a tunneling measurement. To do this, we tilt the trap as shown in Fig. 1(c) and thereby allow atoms to tunnel out of the trap. We carefully adjust the trap parameters during the tunneling process, to let exactly one atom [for the (2, 1) and the (3, 1) systems] or two atoms [for the (2, 2) system] tunnel [35]. Finally, we measure the number of spin-up atoms in the final state to determine the spin of the atoms that left the trap during the tunneling process [35]. We define spin-down tunneling as the process in which all spin-down atoms tunnel

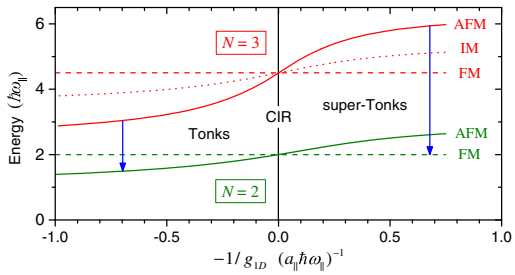

FIG. 2 (color online). Energies in spin-chain regime. Eigenenergies of two (green) and three (red) strongly interacting spin-1/2 fermions in a 1D harmonic trap as a function of the interaction strength. In the Tonks regime, the antiferromagnetic states are the ground states of each multiplet, while the ferromagnetic states have the highest energies. In the super-Tonks regime, the ordering of the energy levels is inverted. Close to the confinement-induced resonance (CIR), the energy shifts are linear in $-1/g_{1D}$ and can be determined by a Heisenberg spin-chain Hamiltonian. The system is initially prepared in the noninteracting ground state of the three-particle system at $-1/g_{1D} = -\infty$, which evolves, for increasing $-1/g_{1D}$, into the antiferromagnetic state around the CIR (red solid line). During a ramp across the CIR, the system stays in the antiferromagnetic state, since all eigenstates of the system are decoupled. The blue arrows indicate the predominant channels for the tunneling of one atom below (left) and above (right) the fermionization regime.

out. By repeating this measurement at different magnetic offset fields, we deduce the probability of spin-down tunneling, $P_\downarrow(-1/g_{1D})$, as a function of the inverse 1D coupling constant, as shown in Fig. 3.

As shown in Fig. 1(b) for a (2, 1) system in a harmonic trap, the different states of the spin chain can be uniquely identified by their spin densities [12], specifically by the probability of the outermost spin to point downwards. Since in the fermionization regime the ordering of the atoms in the trap is fixed, only the outermost atom can escape during the tunneling process. Exactly at the CIR, the probability of spin-down tunneling should therefore directly reveal the state of the spin chain [12,29,33]. Away from resonance, the probability of spin-down tunneling is also influenced by the energy of the final in-trap states, favoring final states with lower energy, as indicated by the blue arrows in Fig. 2. To identify the spin states throughout the entire spin-chain regime, we compare our data to the results of a tunneling model, which in the following section is explained for a (2, 1) system.

In our tunneling model, the initial states are eigenstates of a Heisenberg spin-chain Hamiltonian [35], where the exchange couplings J_i between neighboring spins depend on the trap geometry and on the inverse 1D coupling constant [12]. For the (2, 1) system with repulsive interactions and a symmetric trap ($J_1 = J_2 > 0$), these eigenstates are the AFM ground state, the intermediate (IM) state, and the FM state, as shown in Fig. 1(b). During the tunneling process the trap is tilted as shown in Fig. 1(c) and therefore the density

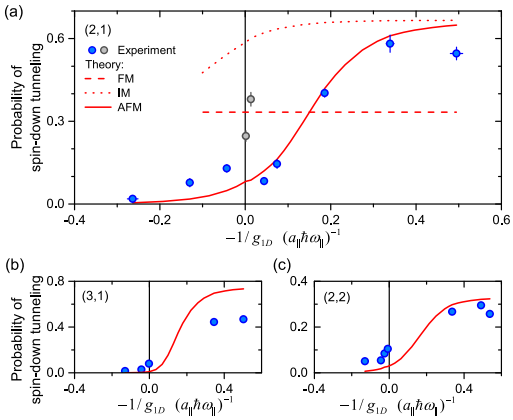

FIG. 3 (color online). Probing the spin distribution. Tunneling probabilities of the spin-down atom in a (2, 1) system (a) and a (3, 1) system (b) and tunneling probability of both spin-down atoms in a (2, 2) system (c) as a function of the interaction strength. The red lines are the solutions of a tunneling model for the antiferromagnetic (solid), the ferromagnetic (dashed), and the intermediate state (dotted). The gray points in (a) indicate a narrow resonance between the antiferromagnetic and the intermediate state of the (2, 1) system close to $-1/g_{1D} = 0$. Error bars denote the 1σ statistical uncertainties.

is not symmetric. Hence, the exchange couplings are not identical anymore ($|J_1| > |J_2|$), which leads to a coherent mixing of the AFM and IM state during the tunneling process [35]. We calculate a probability of approximately 8% for the rightmost spin of the AFM state in the tilted trap to point downwards. This is in good agreement with the blue data points in Fig. 3(a) that cross the CIR at $P_\downarrow \approx 10\%$.

Away from the CIR, the eigenstates of both the three-particle and the two-particle spin chains are nondegenerate (Fig. 2). In this case, the energies of the initial three-particle state $|i\rangle$ and the final two-particle state $|f\rangle$ involved in the tunneling process are important, since their difference determines the energy E of the tunneling particle. The tunneling rate of the particle that leaves the trap is strongly affected by its energy and can be calculated as

$$T_{i,f} \propto |\langle i|f,t\rangle|^2 E e^{-2\gamma(E)}, \tag{1}$$

where $|f,t\rangle = |f\rangle \otimes |t\rangle$ with $|t\rangle$ indicating the spin orientation of the tunneling particle. The tunneling parameter γ is determined by means of a WKB calculation [35]. The probability to tunnel from state $|i\rangle$ to state $|f\rangle$ is given by

$$P_{i,f} = \frac{T_{i,f}}{(\sum_{f'} T_{i,f'})}, \tag{2}$$

where the sum is over all possible final states $|f'\rangle$.

Using Eq. (2), we calculate the probabilities $P_{i,|\uparrow,\uparrow\rangle}$ of tunneling into the spin-polarized final state [red lines in Fig. 3(a)], which is equivalent to the probability of spin-down tunneling ($P_\downarrow$). Far below the CIR, the energy dependent term $Ee^{-2\gamma}$ dominates the outcome of the tunneling rates [Eq. (1)]. Therefore, tunneling into the AFM two-particle ground state $(|\uparrow,\downarrow\rangle - |\downarrow,\uparrow\rangle)/\sqrt{2}$ is strongly favored if its spin overlap to the initial state is not zero. This leads to a limiting value of $P_\downarrow = 0$ for initial AFM and IM states. Above the resonance, the energy ordering of the two-particle FM and AFM states is reversed and tunneling into the FM states is predominant (Fig. 2) [43]. Here, $P_\downarrow$ is determined by the ratio of the spin overlaps between the first two spins of the initial states and the FM two-particle states $|\uparrow,\uparrow\rangle$ and $(|\uparrow,\downarrow\rangle + |\downarrow,\uparrow\rangle)/\sqrt{2}$.

The comparison of the theoretically predicted $P_\downarrow$ of the AFM state in the tilted trap [red solid line in Fig 3(a)] with the experimental data (blue points) shows good agreement, while the FM (red dashed line) and IM (red dotted line) states are clearly excluded. We therefore conclude that before tunneling both below and above the CIR the system is in the AFM state. The gray points at $-1/g_{1D} \approx 0$ indicate a narrow resonance effect that couples the AFM state to the IM state of the spin chain. Since this resonance is accompanied by strongly enhanced three-body losses [35], we suspect it to be caused by a coupling of the AFM and the IM states via a molecular state with center-of-mass excitation. The coupling to such molecular states is strongly enhanced by the anharmonicity of our tilted trap [44].

For the AFM state of the (3, 1) system, a similar calculation predicts $P_\downarrow \approx 1\%$ on resonance and a saturation value of $P_\downarrow \approx 75\%$ deep in the super-Tonks regime [35]. As shown in Fig 3(b), the general trend of our measurements agrees with this prediction for the AFM state, but in the super-Tonks regime, there is a significant deviation. The reason for this deviation is that the calculation assumes an adiabatic lowering of the potential barrier. As a result, the tunneling energies of all tunneling channels are always well below the barrier maximum. We believe that this condition is not fulfilled for the (3, 1) system in the super-Tonks regime, where an especially low potential barrier was used for the tunneling measurement. Indeed, if we model a nonadiabatic lowering of the potential barrier, the contribution from tunneling into the IM state reduces $P_\downarrow$ to values that are compatible with the experimental results [35]. In order to study the spin configuration of the balanced (2, 2) system, we adapt the previous procedure and let two atoms tunnel out of the trap. Here, $P_\downarrow$ is defined as the probability to end up in state $|\uparrow,\uparrow\rangle$, where both spin-down atoms tunneled out of the trap. Again, the predicted $P_\downarrow \approx 4\%$ on resonance and the limiting value of $P_\downarrow \approx 33.3\%$ in the super-Tonks regime are in good agreement with the experiment, as shown in Fig. 3(c).

To independently confirm the results of our measurement of the spin distribution, we perform a second set of measurements that directly probes the spatial wave function of the system. As shown in Fig. 1(a), the relative spatial wave function between identical spins always exhibits a smooth zero crossing, while between distinguishable spins with strong interactions it can exhibit a cusp. The cusps lead to occupancies of high-energy trap levels, while the zero

crossings require only the occupation of the lowest trap levels. In general, the more symmetric the spatial wave function of a state is, the more cusps it will contain. Therefore, the occupation-number distribution on single-particle trap levels directly reveals the spin configuration of the system.

To probe this distribution, we prepare an interacting (2, 1) or (3, 1) system and remove all atoms of the spin-up component from the trap with a short pulse of light. The light is σ^- polarized and resonant to the D_2 transition of the spin-up atoms ($|\uparrow\rangle = |j=1/2, m_j=-1/2; I=1, m_I=0\rangle$ to $|j=3/2, m_j=-3/2; I=1, m_I=0\rangle$). We confirm that within our experimental fidelity all spin-up atoms are removed from the trap by the light pulse, while only 3% of the population of spin-down atoms is lost. With 15 μs the duration of the light pulse is significantly shorter than the inverse longitudinal trap frequency of approximately 100 μs, which sets the time scale of redistribution along the spin chain. This process therefore projects the spin-down component of the wave function of the interacting $(N_\uparrow, 1)$-particle system on single-particle trap levels. Finally, we measure the mean occupancies on the single-particle trap levels [35]. In Fig. 4 we compare the mean occupancies of the spin-down atom for the (2, 1) and the (3, 1) systems in the super-Tonks regime with the theoretical prediction that we obtained by numerically diagonalizing the many-body Hamiltonian for these systems. The comparison shows that both systems are in the AFM spin state and thereby confirms that our systems follow this state throughout the fermionization regime.

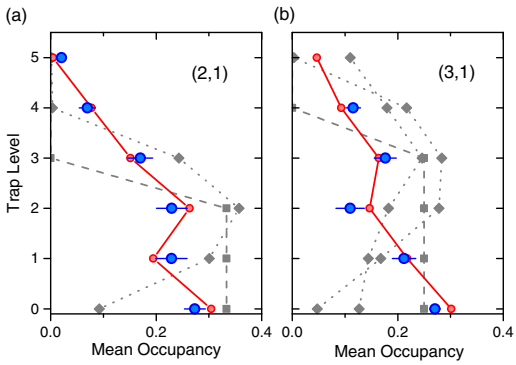

FIG. 4 (color online). Probing the spatial wave function. Occupation-number distribution of the spin-down atom on single-particle trap levels for an initial (a) (2, 1) and (b) (3, 1) system. The red and gray symbols show theoretical predictions for the antiferromagnetic state (red circles), the ferromagnetic state (gray squares), and intermediate states (gray diamonds). Both measurements (blue points) were made in the super-Tonks regime $[-1/g_{1D} = 0.586 \pm 0.014$ for the (2, 1) system and $-1/g_{1D} = 0.536 \pm 0.013$ for the (3, 1) system] to show that both systems stay in the respective antiferromagnetic states throughout the regime of fermionization. Error bars denote the 1σ statistical uncertainty.

In conclusion, we have prepared antiferromagnetic Heisenberg spin chains of up to four atoms in a one-dimensional trap and independently probed the spin distributions and spatial wave functions of the systems. This constitutes a direct observation of quantum magnetism beyond two-particle correlations in a system of ultracold fermionic atoms. By using the methods developed in Ref. [5], multiple spin chains can be realized and coupled, which offers a new approach to studying two- and three-dimensional quantum magnetism.

We thank D. Blume, I. Brouzos, G. M. Bruun, G. Conduit, J. C. Cremon, S. E. Gharashi, C. Greene, M. Rontani, A. N. Wenz, and N. T. Zinner for helpful discussions and input. This work was supported by the European Research Council starting Grant No. 279697, the Heidelberg Center for Quantum Dynamics, the DFG (Project No. SA 1031/7-1 and RTG 1729), the Cluster of Excellence QUEST, the Swedish Research Council, and NanoLund.

S. M. and F. D. contributed equally to this work.

*murmann@physi.uni-heidelberg.de
†frank.deuretzbacher@itp.uni-hannover.de
‡Present address: Institut für Laserphysik, Universität Hamburg, Luruper Chaussee 149, DE-22761 Hamburg, Germany.

[1] M. Lewenstein, A. Sanpera, V. Ahufinger, B. Damski, A. Sen De, and U. Sen, Ultracold atomic gases in optical lattices: Mimicking condensed matter physics and beyond, Adv. Phys. **56**, 243 (2007).
[2] A. Auerbach, *Interacting Electrons and Quantum Magnetism* (Springer, New York, 1994).
[3] M. R. Norman, The challenge of unconventional superconductivity, Science **332**, 196 (2011).
[4] S. Trotzky, P. Cheinet, S. Fölling, M. Feld, U. Schnorrberger, A. M. Rey, A. Polkovnikov, E. A. Demler, M. D. Lukin, and I. Bloch, Time-resolved observation and control of superexchange interactions with ultracold atoms in optical lattices, Science **319**, 295 (2008).
[5] S. Murmann, A. Bergschneider, V. M. Klinkhamer, G. Zürn, T. Lompe, and S. Jochim, Two Fermions in a Double Well: Exploring a Fundamental Building Block of the Hubbard Model, Phys. Rev. Lett. **114**, 080402 (2015).
[6] D. Greif, T. Uehlinger, G. Jotzu, L. Tarruell, and T. Esslinger, Short-range quantum magnetism of ultracold fermions in an optical lattice, Science **340**, 1307 (2013).
[7] R. A. Hart, P. M. Duarte, T.-L. Yang, X. Liu, T. Paiva, E. Khatami, R. T. Scalettar, N. Trivedi, D. A. Huse, and R. G. Hulet, Observation of antiferromagnetic correlations in the Hubbard model with ultracold atoms, Nature (London) **519**, 211 (2015).
[8] M. Messer, R. Desbuquois, T. Uehlinger, G. Jotzu, S. Huber, D. Greif, and T. Esslinger, Exploring Competing Density Order in the Ionic Hubbard Model with Ultracold Fermions, Phys. Rev. Lett. **115**, 115303 (2015).
[9] T. Fukuhara, A. Kantian, M. Endres, M. Cheneau, P. Schauß, S. Hild, D. Bellem, U. Schollwöck, T. Giamarchi,

C. Gross, I. Bloch, and S. Kuhr, Quantum dynamics of a mobile spin impurity, Nat. Phys. **9**, 235 (2013).
[10] J. Simon, W. S. Bakr, R. Ma, M. E. Tai, P. M. Preiss, and M. Greiner, Quantum simulation of antiferromagnetic spin chains in an optical lattice, Nature (London) **472**, 307 (2011).
[11] F. Meinert, M. J. Mark, E. Kirilov, K. Lauber, P. Weinmann, A. J. Daley, and H.-C. Nägerl, Quantum Quench in an Atomic One-Dimensional Ising Chain, Phys. Rev. Lett. **111**, 053003 (2013).
[12] F. Deuretzbacher, D. Becker, J. Bjerlin, S. M. Reimann, and L. Santos, Quantum magnetism without lattices in strongly interacting one-dimensional spinor gases, Phys. Rev. A **90**, 013611 (2014).
[13] M. E. Beverland, G. Alagic, M. J. Martin, A. P. Koller, A. M. Rey, and A. V. Gorshkov, Realizing exactly solvable SU(N) magnets with thermal atoms, arXiv:1409.3234.
[14] G. Pagano, M. Mancini, G. Cappellini, P. Lombardi, F. Schäfer, H. Hu, X.-J. Liu, J. Catani, C. Sias, M. Inguscio, and L. Fallani, A one-dimensional liquid of fermions with tunable spin, Nat. Phys. **10**, 198 (2014).
[15] G. Zürn, F. Serwane, T. Lompe, A. N. Wenz, M. G. Ries, J. E. Bohn, and S. Jochim, Fermionization of Two Distinguishable Fermions, Phys. Rev. Lett. **108**, 075303 (2012).
[16] M. Girardeau, Relationship between systems of impenetrable bosons and fermions in one dimension, J. Math. Phys. (N.Y.) **1**, 516 (1960).
[17] B. Paredes, A. Widera, V. Murg, O. Mandel, S. Fölling, I. Cirac, G. V. Shlyapnikov, T. W. Hänsch, and I. Bloch, Tonks-Girardeau gas of ultracold atoms in an optical lattice, Nature (London) **429**, 277 (2004).
[18] T. Kinoshita, T. Wenger, and D. S. Weiss, Observation of a one-dimensional Tonks-Girardeau gas, Science **305**, 1125 (2004).
[19] K. A. Matveev, Conductance of a Quantum Wire in the Wigner-Crystal Regime, Phys. Rev. Lett. **92**, 106801 (2004); K. A. Matveev, Conductance of a quantum wire at low electron density, Phys. Rev. B **70**, 245319 (2004).
[20] F. Deuretzbacher, K. Fredenhagen, D. Becker, K. Bongs, K. Sengstock, and D. Pfannkuche, Exact Solution of Strongly Interacting Quasi-One-Dimensional Spinor Bose Gases, Phys. Rev. Lett. **100**, 160405 (2008).
[21] K. A. Matveev and A. Furusaki, Spectral Functions of Strongly Interacting Isospin-1/2 Bosons in One Dimension, Phys. Rev. Lett. **101**, 170403 (2008).
[22] M. D. Girardeau and A. Minguzzi, Soluble Models of Strongly Interacting Ultracold Gas Mixtures in Tight Waveguides, Phys. Rev. Lett. **99**, 230402 (2007).
[23] L. Guan, S. Chen, Y. Wang, and Z.-Q. Ma, Exact Solution for Infinitely Strongly Interacting Fermi Gases in Tight Waveguides, Phys. Rev. Lett. **102**, 160402 (2009).
[24] S. E. Gharashi and D. Blume, Correlations of the Upper Branch of 1D Harmonically Trapped Two-Component Fermi Gases, Phys. Rev. Lett. **111**, 045302 (2013).
[25] P. O. Bugnion and G. J. Conduit, Ferromagnetic spin correlations in a few-fermion system, Phys. Rev. A **87**, 060502 (R) (2013).
[26] T. Sowiński, T. Grass, O. Dutta, and M. Lewenstein, Few interacting fermions in one-dimensional harmonic trap, Phys. Rev. A **88**, 033607 (2013).
[27] X. Cui and T.-L. Ho, Ground-state ferromagnetic transition in strongly repulsive one-dimensional Fermi gases, Phys. Rev. A **89**, 023611 (2014).
[28] E. J. Lindgren, J. Rotureau, C. Forssén, A. G. Volosniev, and N. T. Zinner, Fermionization of two-component few-fermion systems in a one-dimensional harmonic trap, New J. Phys. **16**, 063003 (2014).
[29] A. G. Volosniev, D. V. Fedorov, A. S. Jensen, M. Valiente, and N. T. Zinner, Strongly interacting confined quantum systems in one dimension, Nat. Commun. **5**, 5300 (2014).
[30] N. L. Harshman, Spectroscopy for a few atoms harmonically trapped in one dimension, Phys. Rev. A **89**, 033633 (2014).
[31] M. A. García-March, B. Juliá-Díaz, G. E. Astrakharchik, J. Boronat, and A. Polls, Distinguishability, degeneracy, and correlations in three harmonically trapped bosons in one dimension, Phys. Rev. A **90**, 063605 (2014).
[32] L. Yang, L. Guan, and H. Pu, Strongly interacting quantum gases in one-dimensional traps, Phys. Rev. A **91**, 043634 (2015).
[33] J. Levinsen, P. Massignan, G. M. Bruun, and M. M. Parish, Strong-coupling ansatz for the one-dimensional Fermi gas in a harmonic potential, Sci. Adv. **1**, e1500197 (2015).
[34] X.-W. Guan, M. T. Batchelor, and J.-Y. Lee, Magnetic ordering and quantum statistical effects in strongly repulsive Fermi-Fermi and Bose-Fermi mixtures, Phys. Rev. A **78**, 023621 (2008).
[35] See Supplemental Material at http://link.aps.org/supplemental/10.1103/PhysRevLett.115.215301 for details on the experimental methods, the data evaluation, and the theoretical models, which includes Refs. [36–38].
[36] G. Zürn, Ph.D. thesis, University of Heidelberg, 2012.
[37] G. Zürn, T. Lompe, A. N. Wenz, S. Jochim, P. S. Julienne, and J. M. Hutson, Precise Characterization of ^{6}Li Feshbach Resonances Using Trap-Sideband-Resolved RF Spectroscopy of Weakly Bound Molecules, Phys. Rev. Lett. **110**, 135301 (2013).
[38] S. E. Gharashi, X. Y. Yin, Y. Yan, and D. Blume, One-dimensional Fermi gas with a single impurity in a harmonic trap: Perturbative description of the upper branch, Phys. Rev. A **91**, 013620 (2015).
[39] F. Serwane, G. Zürn, T. Lompe, T. B. Ottenstein, A. N. Wenz, and S. Jochim, Deterministic preparation of a tunable few-fermion system, Science **332**, 336 (2011).
[40] M. Olshanii, Atomic Scattering in the Presence of an External Confinement and a Gas of Impenetrable Bosons, Phys. Rev. Lett. **81**, 938 (1998).
[41] G. E. Astrakharchik, J. Boronat, J. Casulleras, and S. Giorgini, Beyond the Tonks-Girardeau Gas: Strongly Correlated Regime in Quasi-One-Dimensional Bose Gases, Phys. Rev. Lett. **95**, 190407 (2005).
[42] E. Haller, M. Gustavsson, M. J. Mark, J. G. Danzl, R. Hart, G. Pupillo, and H.-C. Nägerl, Realization of an excited, strongly correlated quantum gas phase, Science **325**, 1224 (2009).
[43] At the values of g_{1D} attainable in our experiment, the spatial wave function overlap between the spin-chain states and the molecular ground state is negligible. We expect that for a small negative g_{1D} tunneling into the molecular state is predominant.
[44] S. Sala, G. Zürn, T. Lompe, A. N. Wenz, S. Murmann, F. Serwane, S. Jochim, and A. Saenz, Coherent Molecule Formation in Anharmonic Potentials Near Confinement-Induced Resonances, Phys. Rev. Lett. **110**, 203202 (2013).

Paper IV

Spin-chain model for strongly interacting one-dimensional Bose-Fermi mixtures

F. Deuretzbacher,[1,*] D. Becker,[2] J. Bjerlin,[3] S. M. Reimann,[3] and L. Santos[1]

[1]*Institut für Theoretische Physik, Leibniz Universität Hannover, Appelstrasse 2, DE-30167 Hannover, Germany*

[2]*I. Institut für Theoretische Physik, Universität Hamburg, Jungiusstrasse 9, DE-20355 Hamburg, Germany*

[3]*Mathematical Physics and NanoLund, LTH, Lund University, SE-22100 Lund, Sweden*

(Received 20 January 2017; published 21 April 2017)

Strongly interacting one-dimensional (1D) Bose–Fermi mixtures form a tunable XXZ spin chain. Within the spin-chain model developed here, all properties of these systems can be calculated from states representing the ordering of the bosons and fermions within the atom chain and from the ground-state wave function of spinless noninteracting fermions. We validate the model by means of an exact diagonalization of the full few-body Hamiltonian in the strongly interacting regime. Using the model, we explore the phase diagram of the atom chain as a function of the boson-boson (BB) and boson-fermion (BF) interaction strengths and calculate the densities, momentum distributions, and trap-level occupancies for up to 17 particles. In particular, we find antiferromagnetic (AFM) and ferromagnetic (FM) order and a demixing of the bosons and fermions in certain interaction regimes. We find, however, no demixing for equally strong BB and BF interactions, in agreement with earlier calculations that combined the Bethe ansatz with a local-density approximation.

DOI: 10.1103/PhysRevA.95.043630

I. INTRODUCTION

Ultracold atoms are ideally suited to study strongly correlated one-dimensional (1D) systems due to their high degree of control and tunability [1,2]. These advantageous features have led to the observation of the Tonks–Girardeau gas [3,4], the controlled preparation of a highly excited super-Tonks gas [5,6], undamped dynamics in strongly interacting 1D Bose gases [7], and the deterministic preparation of 1D few-fermion systems with tunable interactions [8–12]. Moreover, it became possible to realize a variety of artificial 1D systems consisting, e.g., of atoms with a large spin [13] or Bose–Fermi mixtures with mixed statistics [14].

These developments have renewed the interest in Girardeau's Bose-Fermi mapping for 1D spinless bosons with infinite δ repulsion [15] leading to generalizations for Bose-Fermi mixtures [16], spin-1 bosons [17], and spin-1/2 fermions [18]. Only recently it was found that these exact solutions are also useful for the perturbative treatment of strongly interacting 1D systems [19]. Different from one-component systems, the ground state of multicomponent systems with infinite δ repulsion is highly degenerate [16–18]. This is due to the fact that strongly interacting 1D particles localize and arrange themselves in a spin chain [17,20,21]. This offers the exciting possibility to study quantum magnetism without the need for an optical lattice [21–25].

Theoretical studies of Bose-Fermi mixtures in optical lattices predicted composite fermions consisting of one fermion and one ore more bosons, or, respectively, bosonic holes [26] and polarons [27]. In addition, pairing, collapse, and demixing can occur in homogeneous 1D systems of strongly interacting bosons and fermions [28]. For equally strong boson-boson (BB) and boson-fermion (BF) δ interactions, the model can be solved exactly via the Bethe ansatz [29,30]. Selected states of the degenerate ground-state multiplet have been constructed in the Tonks-Girardeau regime of infinite δ repulsion [16] and classified using Young's tableaux [31]. Recently, all states of the multiplet have been constructed for few (up to 6) particles [32–34] and strongly interacting mixtures with additional weak p-wave interactions have been studied [35,36].

Here, we develop a spin-chain model for 1D Bose-Fermi mixtures with nearly infinite δ interactions [37]. We check the validity of the model by diagonalizing the full few-body Hamiltonian numerically in the strongly interacting regime. Using the spin-chain model, we then calculate the ground-state densities, momentum distributions, and occupancies of the harmonic-trap levels for atom chains consisting of up to 17 particles. Moreover, we determine the ground-state phases of these atom chains, finding antiferromagnetic (AFM) and ferromagnetic (FM) order and a demixing of the bosons and fermions for particular values of the BB and BF interaction strengths. However, no demixing is found for equally strong BB and BF interactions although the bosons are predominantly in the trap center and the fermions are predominantly at the edges of the trap [29].

II. SPIN-CHAIN MODEL

We consider a 1D mixture of N_B bosons and N_F fermions (total particle number $N = N_B + N_F$). Both species are assumed to have the same masses, $M_B = M_F = M$, and experience the same trapping potential $V(z)$. The bosons interact with each other through a δ potential of strength g_{BB} and with the fermions through a δ potential of strength g_{BF}. The many-body Hamiltonian of the system is given by

$$H = \sum_{i=1}^{N}\left[-\frac{\hbar^2}{2M}\frac{\partial^2}{\partial z_i^2} + V(z_i)\right] + g_{BB}\sum_{i=1}^{N_B-1}\sum_{j=i+1}^{N_B}\delta(z_i - z_j) + g_{BF}\sum_{i=1}^{N_B}\sum_{j=N_B+1}^{N}\delta(z_i - z_j). \quad (1)$$

The interaction strengths g_{BB} and g_{BF} are freely tunable through a magnetic Feshbach resonance [38] and through the strong radial confinement [39].

*frank.deuretzbacher@itp.uni-hannover.de

Here, we focus on the strongly interacting regime, where the absolute value of both interaction strengths is large, i.e., $|g_{BB}| \approx \infty$ and $|g_{BF}| \approx \infty$. Furthermore, we consider only the highly excited super-Tonks states [5,6,9] if at least one of the interaction strengths is attractive.[1] Under these conditions, the atoms order in a row and form a spin chain [17,20,21,40]. An arbitrary state of the spin chain is given by

$$|\chi\rangle = \sum_{m_1,\ldots,m_N} c_{m_1,\ldots,m_N} |m_1,\ldots,m_N\rangle, \tag{2}$$

where each basis state $|m_1,\ldots,m_N\rangle$ with $m_i = B,F$ corresponds to a particular ordering of the bosons (B) and fermions (F) and can be constructed from the wave function of N spinless noninteracting fermions [31] (see Appendix A).

Nearest-neighbor particles of the spin chain interact with each other through the effective Hamiltonian [35]

$$\begin{aligned} H_{\text{eff}} = {} & E_F \mathbb{1} - 2\sum_{i=1}^{N-1} J_i^{(BB)} |B\rangle_i |B\rangle_{i+1} \langle B|_i \langle B|_{i+1} \\ & - \sum_{i=1}^{N-1} J_i^{(BF)} \big(|B\rangle_i |F\rangle_{i+1} + |F\rangle_i |B\rangle_{i+1} \big) \\ & \times \big(\langle B|_i \langle F|_{i+1} + \langle F|_i \langle B|_{i+1} \big), \end{aligned} \tag{3}$$

as shown in Appendix B. Here, E_F is the ground-state energy of N spinless noninteracting fermions in the trapping potential $V(z)$ and $J_i^{(BB)}$ and $J_i^{(BF)}$ are the exchange coefficients of nearest-neighbor bosons or bosons and fermions, respectively. The exchange coefficients are given by $J_i^{(BB)} = C_i/g_{BB}$ and $J_i^{(BF)} = C_i/g_{BF}$ with [19,21]

$$C_i = \frac{N!\hbar^4}{M^2} \int dz_1 \cdots dz_N \delta(z_i - z_{i+1}) \theta(z_1,\ldots,z_N) \left| \frac{\partial \psi_F}{\partial z_i} \right|^2, \tag{4}$$

where $\theta(z_1,\ldots,z_N) = 1$ if $z_1 < \cdots < z_N$, and zero otherwise, and where ψ_F is the ground-state wave function of N spinless noninteracting fermions in the trap $V(z)$. The C_i can be efficiently calculated for large N [41–43].

By identifying bosons and fermions with pseudospin-up and -down particles, respectively, Eq. (3) can be rewritten in terms of the Pauli matrices $\sigma_x^{(i)}$, $\sigma_y^{(i)}$, and $\sigma_z^{(i)}$:

$$\begin{aligned} H_{\text{eff}} = {} & -\frac{1}{2}\sum_{i=1}^{N-1} \Big\{ J_i^{(BF)} \big[\sigma_x^{(i)} \sigma_x^{(i+1)} + \sigma_y^{(i)} \sigma_y^{(i+1)} \big] \\ & + \big[J_i^{(BB)} - J_i^{(BF)} \big] \sigma_z^{(i)} \sigma_z^{(i+1)} + J_i^{(BB)} \big[\sigma_z^{(i)} + \sigma_z^{(i+1)} \big] \Big\}. \end{aligned} \tag{5}$$

Here, we neglected the diagonal matrix

$$\left\{ E_F - \frac{1}{2}\sum_{i=1}^{N-1} \big[J_i^{(BB)} + J_i^{(BF)} \big] \right\} \mathbb{1}. \tag{6}$$

[1]Super-Tonks states may be prepared by ramping adiabatically across a confinement-induced resonance [5,9,40].

Equation (5) is the Hamiltonian of an XXZ spin chain in an inhomogeneous magnetic field along the z axis. Similar effective Hamiltonians have been derived for strongly interacting Bose-Bose mixtures [22,24,25] and strongly interacting mixtures with weak p-wave interactions [35,36].

The densities of the bosons ($m = B$) and fermions ($m = F$) are given by [17]

$$\rho_m(z) = \sum_{i=1}^{N} \rho^{(i)}(z) \rho_m^{(i)}, \tag{7}$$

with the probability to find the ith particle at position z,

$$\rho^{(i)}(z) = N! \int dz_1 \cdots dz_N \delta(z - z_i)\, \theta(z_1,\ldots,z_N) |\psi_F|^2, \tag{8}$$

and the probability that the ith particle is a boson ($m = B$) or fermion ($m = F$),

$$\rho_m^{(i)} = \sum_{m_1,\ldots,m_N} |\langle m_1,\ldots,m_N|\chi\rangle|^2 \delta_{m,m_i}. \tag{9}$$

The one-body density matrix of the bosons ($m = B$) and fermions ($m = F$) is given by

$$\rho_m(z,z') = \sum_{i,j=1}^{N} \rho^{(i,j)}(z,z') \rho_m^{(i,j)}, \tag{10}$$

with [23,41]

$$\begin{aligned} & \rho^{(i,j)}(z,z') \\ & = N! \int dz_1 \cdots dz_{i-1} dz_{i+1} \cdots dz_N \\ & \quad \times [\theta(z_1,\ldots,z_N) |\psi_F(z_1,\ldots,z_N)|]_{z_i = z} \\ & \quad \times [\theta(z_{P_{i,\ldots,j}(1)},\ldots,z_{P_{i,\ldots,j}(N)}) |\psi_F(z_1,\ldots,z_N)|]_{z_i = z'}, \end{aligned} \tag{11}$$

and

$$\rho_m^{(i,j)} = \langle\chi|m\rangle_i \langle m|_i \hat{P}_{i,\ldots,j}^{(BF)} |\chi\rangle, \tag{12}$$

as shown in Appendix C. Here, we defined $\hat{P}_{i,\ldots,j}^{(BF)} = (-1)^{N_{\text{tr}}} \hat{P}_{i,\ldots,j}$ with the loop permutation operator $\hat{P}_{i,\ldots,j}$, which moves a particle from position j to position i (see Appendix A for details). N_{tr} is the number of transpositions of neighboring fermions when $\hat{P}_{i,\ldots,j}$ acts on $|m_1,\ldots,m_N\rangle$. The momentum distributions and occupancies of the trap levels are related to the one-body density matrices by

$$\rho_m(k) = \frac{1}{2\pi} \int dz dz' e^{ik(z-z')} \rho_m(z,z'), \tag{13}$$

and

$$\rho_m(n) = \int dz dz' \phi_n(z) \phi_n^*(z') \rho_m(z,z'), \tag{14}$$

with the eigenfunctions $\phi_n(z)$ of the trap $V(z)$.

We have tested the validity of the spin-chain model by comparing its results to those of an exact diagonalization of the full few-body Hamiltonian (1) for up to four particles in a harmonic trap. Both approaches should lead to the same results in the Tonks-Girardeau regime, $g_{BB} = g_{BF} > 10\hbar\omega l$

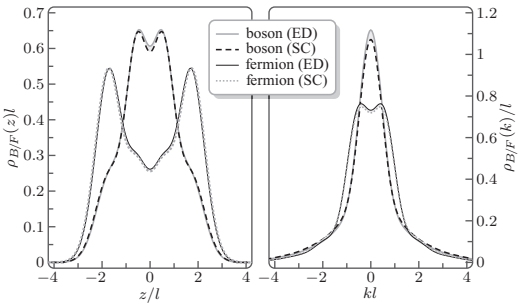

FIG. 1. Comparison of the ground-state densities (left) and momentum distributions (right) of a mixture of two bosons and two fermions (2B2F mixture) in a harmonic trap calculated by means of an exact diagonalization (ED) of the full few-body Hamiltonian (solid lines) and from the spin-chain (SC) model (dashed lines) for equal BB and BF interaction strengths ($g_{BB} = g_{BF} = 15\hbar\omega l$). ω, and l are the frequency and length scale of the harmonic oscillator.

[21,44] [ω is the frequency and $l = \sqrt{\hbar/(m\omega)}$ is the length scale of the harmonic oscillator]. Indeed, the comparison showed excellent agreement for the spectrum, the densities, and the momentum distributions for mixtures consisting of one boson and three fermions (1B3F mixture), two bosons and two fermions (2B2F mixture), and three bosons and one fermion (3B1F mixture). As an example, we show in Fig. 1 the result of such a comparison for the ground-state densities and momentum distributions of a 2B2F mixture for equally strong BB and BF interactions, $g_{BB} = g_{BF} = 15\hbar\omega l$. These ground-state densities agree with Refs. [32,33].

III. PHASES AND DENSITIES

The ground-state phases of the effective Hamiltonian (3) or, respectively, (5) are determined by the interplay of the BB and BF interactions. In particular, we distinguish five different phases, as shown in the phase diagram in Fig. 2, which follow from the phases of the homogeneous XXZ chain

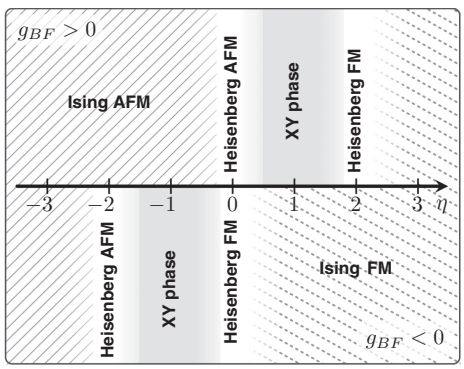

FIG. 2. Phase diagram of the Bose-Fermi chain as a function of $\eta = |g_{BF}|/g_{BB}$ for $g_{BF} > 0$ (upper part) and $g_{BF} < 0$ (lower part).

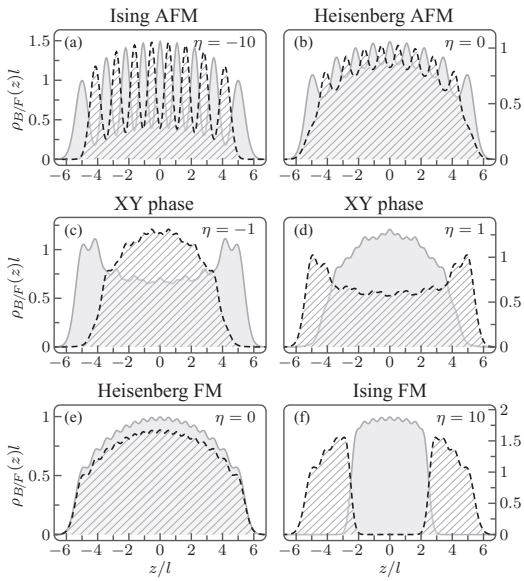

FIG. 3. Ground-state densities of a harmonically trapped Bose-Fermi mixture consisting of nine bosons (solid) and eight fermions (dashed) for $g_{BF} < 0$ (left) and $g_{BF} > 0$ (right). The different phases are described in the text. l is the harmonic-oscillator length.

in the absence of an external magnetic field [45].[2] For dominant BB exchange couplings, which corresponds to the parameter regime $|\eta| = |J_i^{(BB)}/J_i^{(BF)}| \gg 1$, the spin chain is in the Ising AFM ($J_i^{(BB)} < 0$) or FM ($J_i^{(BB)} > 0$) state. For $J_i^{(BB)} \approx J_i^{(BF)}$ (gray shaded regions around $\eta = \pm 1$), the spin chain is in the XY phase. These phases are characterized by strong FM ($J_i^{(BF)} > 0$) or AFM ($J_i^{(BF)} < 0$) xy correlations. At the edges of the XY phases ($\eta = 0, \pm 2$) the system is in the Heisenberg AFM or FM phases. Note that we consider the highly excited (metastable) super-Tonks states [5,6] in the regime of attractive interactions and, therefore, do not obtain collapse and pairing [28].

Ising FM and AFM order ($|\eta| \gg 1$). Let us first consider the case $J_i^{(BF)} = 0$, $J_i^{(BB)} \neq 0$, in which the effective Hamiltonian (3) is diagonal. In that case, for $J_i^{(BB)} > 0$, the energy is minimized if all bosons are next to each other and in the trap center (largest C_i). A typical ground state is therefore of the form $|F,F,B,B,B,B,F,F\rangle$, i.e., the bosons are separated from the fermions, the bosons are in the trap center, and the fermions are at the edges of the trap. This separation of the bosons from the fermions is clearly visible in the densities of Fig. 3(f). In the opposite case of negative BB exchange coefficients, $J_i^{(BB)} < 0$, the energy is minimized if the bosons are not next to each other and hence a typical ground state is of

[2] A homogeneous external magnetic field has no effect due to the conserved total magnetization of the system in the z direction.

the form $|B,F,B,F,B,F,B\rangle$, as in the ground state of an Ising AFM chain. In that regime, the densities look, therefore, like those of Fig. 3(a). The same or similar limiting phases have been found in related mixtures [24,34–36].

Heisenberg AFM and FM order ($\eta = 0$). Let us now consider the case $J_i^{(BB)} = 0$, $J_i^{(BF)} \neq 0$, for which the spin-chain Hamiltonian (5) takes the form

$$H_{\text{eff}} = -\sum_{i=1}^{N-1} \frac{J_i^{(BF)}}{2}\left[\sigma_x^{(i)}\sigma_x^{(i+1)} + \sigma_y^{(i)}\sigma_y^{(i+1)} - \sigma_z^{(i)}\sigma_z^{(i+1)}\right]. \tag{15}$$

By performing the unitary transformation

$$\sigma_x^{(i)} \to (-1)^i \sigma_x^{(i)}, \quad \sigma_y^{(i)} \to (-1)^i \sigma_y^{(i)}, \quad \sigma_z^{(i)} \to \sigma_z^{(i)}, \tag{16}$$

we obtain

$$\widetilde{H}_{\text{eff}} = \sum_{i=1}^{N-1} \frac{J_i^{(BF)}}{2} \vec{\sigma}^{(i)} \cdot \vec{\sigma}^{(i+1)}, \tag{17}$$

which is the Heisenberg Hamiltonian. Therefore, the ground state is AFM for $J_i^{(BF)} > 0$ and FM for $J_i^{(BF)} < 0$. Typical densities are shown in Figs. 3(b) and 3(e). The spin-spin correlations $\sigma_z^{(i)}\sigma_z^{(j)}$ alternate in sign, $\propto(-1)^{i-j}$, and decay with distance $|i-j|$ in the AFM state, while staying constant in the FM state. However, because of the transform (16), the spin-spin correlations in the xy plane do not alternate in sign in the AFM state, but instead, they alternate in the FM state.

XY phases ($\eta = \pm 1$). Let us finally discuss the cases $J_i^{(BB)} = J_i^{(BF)}$ ($g_{BB} = g_{BF}$). The repulsive case, $g_{BB} = g_{BF} > 0$, is exactly solvable for any value of the interaction strength if $V(z) = 0$ [29,30]. Combining the exact solution of the homogeneous system with a local density approximation, one finds that the bosons and fermions do not demix, but the bosons are predominantly in the trap center and the fermions are predominantly at the edges of the trap. We find the same result and the density profiles are in excellent agreement with Ref. [29]; see Fig. 3(d). For attractive interactions, $g_{BB} = g_{BF} < 0$, the situation is reversed with the fermions (bosons) sitting predominantly at the center (edges) of the harmonic trap, see Fig. 3(c). We note that the bosonic (fermionic) density of the $\eta = 1$ case would exactly equal the fermionic (bosonic) density of the $\eta = -1$ case, if the particle numbers would be equal, i.e., $N_B = N_F$.

This symmetry can be understood as follows: For $J_i^{(BB)} = J_i^{(BF)} > 0$, Eq. (5) takes the form of an XX Hamiltonian with an inhomogeneous effective magnetic field pointing along the $+z$ direction,

$$H_{\text{eff}} = -\sum_{i=1}^{N-1} \frac{|J_i^{(BF)}|}{2}\left[\sigma_x^{(i)}\sigma_x^{(i+1)} + \sigma_y^{(i)}\sigma_y^{(i+1)}\right] - \sum_{i=1}^{N-1} \frac{|J_i^{(BB)}|}{2}\left[\sigma_z^{(i)} + \sigma_z^{(i+1)}\right], \tag{18}$$

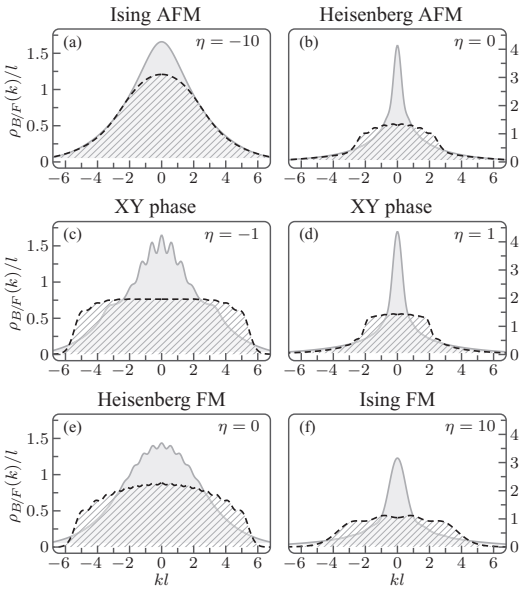

FIG. 4. Momentum distributions of nine bosons (solid) and eight fermions (dashed) in a harmonic trap for $g_{BF} < 0$ (left column) and $g_{BF} > 0$ (right column). See the text for a description of the different phases. l is the harmonic-oscillator length.

while for $J_i^{(BB)} = J_i^{(BF)} < 0$, after performing the transformation (16), the field points in the $-z$ direction,

$$\widetilde{H}_{\text{eff}} = -\sum_{i=1}^{N-1} \frac{|J_i^{(BF)}|}{2}\left[\sigma_x^{(i)}\sigma_x^{(i+1)} + \sigma_y^{(i)}\sigma_y^{(i+1)}\right] + \sum_{i=1}^{N-1} \frac{|J_i^{(BB)}|}{2}\left[\sigma_z^{(i)} + \sigma_z^{(i+1)}\right]. \tag{19}$$

In the first case, the bosons (pseudospin-up) are moved to the trap center, since the $|J_i^{(BB)}|$ are largest there, while in the latter case, the fermions (pseudospin-down) are moved to the trap center. Moreover, both Hamiltonians can be transformed into each other by exchanging the bosons with the fermions, which explains the symmetry of the density distributions.

IV. MOMENTUM DISTRIBUTIONS AND OCCUPANCIES

The momentum distributions and the occupancies of the harmonic-trap levels are important observables, which can be measured in the experiment [12,13,46]. These distributions depend strongly on the degree of exchange symmetry of the spatial many-body wave function and can also be used as a probe for the magnetic structure of the spin chain [12,41,47]. We therefore expect very different momentum distributions and trap-level occupancies in the different phases of the Bose-Fermi chain as will be shown in the following.

Momentum distributions of nine bosons (solid) and eight fermions (dashed) are shown in Fig. 4. Both momentum

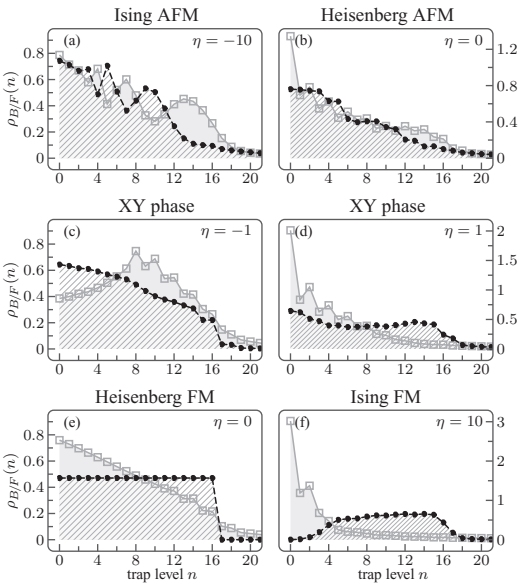

FIG. 5. Occupancies of the harmonic-trap levels of nine bosons (solid) and eight fermions (dashed) for $g_{BF} < 0$ (left) and $g_{BF} > 0$ (right). See the text for a description of the different phases.

distributions resemble Gaussian distributions in the Ising AFM phase, Fig. 4(a), as expected for a Wigner crystal [48]. This is a result of the comparatively large distance between the particles of the same kind; see Fig. 3(a). In the Heisenberg AFM phase, Fig. 4(b), the bosonic and fermionic distributions look like those of the corresponding spin-1/2 particles [23,41]. By contrast, in the Heisenberg FM phase, Fig. 4(e), both distributions are much broader, as expected for the highest excited states of the corresponding spin-1/2 particles [41]. Indeed, the FM ground state of the Heisenberg Hamiltonian (17) for $J_i^{(BF)} < 0$ is the highest excited state for $J_i^{(BF)} > 0$. Moreover, the ground state of Eq. (5) for $J_i^{(BB)} = 10J_i^{(BF)} < 0$, which has the momentum distribution shown in Fig. 4(a), is the highest excited state for $J_i^{(BB)} = 10J_i^{(BF)} > 0$ and the ground state for $J_i^{(BB)} = J_i^{(BF)} < 0$, which has the momentum distribution shown in Fig. 4(c), is the highest excited state for $J_i^{(BB)} = J_i^{(BF)} > 0$. This is the reason for the broader momentum distributions in the left column of Fig. 4. Finally, in the Ising FM phase, one has a Tonks-Girardeau gas in the center and noninteracting fermions at the edges of the trap, Fig. 3(f). Therefore, one expects that the momentum distributions of that phase resemble those of a Tonks-Girardeau gas and noninteracting fermions, Fig. 4(f). The distributions are, however, broader than those of Fig. 4(b), since the particles are located in a smaller trap volume.

The occupancies of the harmonic-trap levels of nine bosons (solid) and eight fermions (dashed) are shown in Fig. 5. In the Ising AFM phase, Fig. 5(a), both occupancies oscillate out of phase around the same average broad distribution. The higher oscillator orbitals ($n > 10$) are preferably occupied by the bosons, since the bosonic density is broader [Fig. 3(a)]. The separation of the bosons from the fermions in the Ising FM phase is also manifest in the occupancies, Fig. 5(f). The bosons preferably occupy the lower oscillator orbitals ($n < 4$) and the fermions the higher ones ($n > 4$). In the Heisenberg AFM phase, Fig. 5(b), the bosonic and fermionic occupancies are almost equal. By contrast, in the Heisenberg FM phase, Fig. 5(e), the fermions occupy the lowest 17 orbitals with $8/17 = 0.47$ fermions, whereas the bosonic distribution decreases roughly linearly. Finally, once again, the occupancies in the XY phases, Figs. 5(c) and 5(d), resemble the behavior of the corresponding densities, Figs. 3(c) and 3(d).

In closing this section, we note that the variance of the total momentum distribution, $\langle k^2 \rangle = \int dk k^2 [\rho_F(k) + \rho_B(k)] = N^2/(2l^2)$, is independent of the pseudospin configuration of the Bose-Fermi chain. Similarly, the total energy of the Bose-Fermi chain, calculated from the total trap-level occupancies, $\sum_{n=0}^{\infty}(n + 1/2)[\rho_F(n) + \rho_B(n)] = N^2/2$, is independent of the configuration of the bosons and fermions. This follows from the fact that all pseudospin configurations have the same total energy at $g_{BB} = g_{BF} = \infty$ and from the virial theorem.

V. SUMMARY

We have presented a spin-chain model for Bose-Fermi mixtures with nearly infinite BB and BF δ interactions. The model is based on a mapping to states of the form $|m_1, \ldots, m_N\rangle$ with $m_i = B, F$ and to the wave function of spinless noninteracting fermions. We checked the model by comparing with an exact diagonalization of the full few-body Hamiltonian in the strongly interacting regime. Using the spin-chain model, we determined the ground-state phases of the Bose-Fermi mixture and calculated the densities, momentum distributions, and occupancies of the harmonic-trap levels for up to 17 particles. We found, in particular, AFM and FM order and a demixing of the bosons and fermions. However, we found no demixing for equally strong BB and BF interactions in agreement with earlier calculations [29].

ACKNOWLEDGMENTS

This work was supported by the DFG [Projects No. SA 1031/7-1, No. RTG 1729, and No. CRC 1227 (DQ-mat), Subproject A02], the Cluster of Excellence QUEST, the Swedish Research Council, and NanoLund.

APPENDIX A: SECTOR WAVE FUNCTIONS AND PERMUTATIONS

1. Sector wave functions

In the regime of infinite BB and BF repulsion, $g_{BB} = g_{BF} = \infty$, the many-body wave function must vanish whenever two particle coordinates are equal, i.e., $\psi(z_1, \ldots, z_N) = 0$ if $z_i = z_j$. This condition is fulfilled by the wave function of N spinless noninteracting fermions, ψ_F, but also by its absolute value $|\psi_F|$, which describes N spinless bosons with infinite δ repulsion [15]. Additionally, we may restrict $|\psi_F|$ to a particular sector of the configuration space $\mathbb{R}^N, z_{P(1)} < \cdots < z_{P(N)}$,

in order to describe spinless distinguishable particles with infinite δ repulsion and particle ordering $z_{P(1)} < \cdots < z_{P(N)}$. Here, P denotes an arbitrary permutation of $\underline{N} = \{1, \ldots, N\}$. The resulting wave function, denoted by $|P\rangle$, is given by [17]

$$\langle z_1, \ldots, z_N | P\rangle = \sqrt{N!}\theta(z_{P(1)}, \ldots, z_{P(N)})|\psi_F|. \quad \text{(A1)}$$

Here, $\theta(z_{P(1)}, \ldots, z_{P(N)}) = 1$ if $z_{P(1)} < \cdots < z_{P(N)}$ and zero otherwise.

The sector wave functions (A1) are by definition orthonormal, i.e., $\langle P|P'\rangle = \delta_{P,P'}$, and they have further favorable properties. For example, the action of a permutation operator $\hat{P}$ on a sector wave function $|P'\rangle$ is given by [41]

$$\hat{P}|P'\rangle = |P \circ P'\rangle. \quad \text{(A2)}$$

The permutation operator $\hat{P}$ of a permutation P acts on a many-body state $|\alpha_1, \ldots, \alpha_N\rangle$ in the following way:

$$\hat{P}|\alpha_1\rangle_1 \cdots |\alpha_N\rangle_N = |\alpha_1\rangle_{P(1)} \cdots |\alpha_N\rangle_{P(N)}. \quad \text{(A3)}$$

That is, $\hat{P}$ permutes the particle indices of a many-body state according to the prescription $1 \to P(1), \ldots, N \to P(N)$.

To describe a Bose-Fermi mixture with infinite BB and BF repulsion, $g_{BB} = g_{BF} = \infty$, one has to symmetrize the sector wave functions $|P\rangle$ with respect to the bosonic coordinates, $z_1, \ldots, z_{N_B}$, and to antisymmetrize with respect to the fermionic ones, $z_{N_B+1}, \ldots, z_N$. We therefore define [31]

$$\hat{P}|B, \ldots, B, F, \ldots, F\rangle \equiv \sqrt{N_B!N_F!}S_+S_-|P^{-1}\rangle. \quad \text{(A4)}$$

Here, $S_+ = (1/N_B!)\sum_{P'} \hat{P}'$ is a symmetrization operator, where the sum runs over all permutations P' of $\underline{N_B} = \{1, \ldots, N_B\}$, $S_- = (1/N_F!)\sum_{P''}(-1)^{P''}\hat{P}''$ is an antisymmetrization operator, where the sum runs over all permutations P'' of $\underline{N} - \underline{N_B} = \{N_B + 1, \ldots, N\}$, and P^{-1} is the inverse of the permutation P. Furthermore, we specify to use only those initial sector wave functions $|P^{-1}\rangle$, for which the bosonic and fermionic coordinates are each in ascending order. This is necessary, since otherwise two sector wave functions, which differ only by the transposition of two fermionic coordinates, would have a different sign. The requirement is fulfilled if we move the B at position N_B in the initial state $|B, \ldots, B, F, \ldots, F\rangle$ to the new position i_{N_B} with $N_B \leqslant i_{N_B} \leqslant N$, the B at position $N_B - 1$ to the new position i_{N_B-1} with $N_B - 1 \leqslant i_{N_B-1} < i_{N_B}$, and so forth.

2. Permutations

We use the cycle notation to specify a permutation. For example, the permutation $P_{(\alpha,\beta,\gamma)}$ permutes the numbers α, β, γ according to the prescription $\alpha \to \beta \to \gamma \to \alpha$. Moreover, we neglect the parentheses if a permutation consists of only one cycle, i.e., $P_{(\alpha,\beta,\gamma)} = P_{\alpha,\beta,\gamma}$. The corresponding unitary operator that permutes the particle indices α, β, γ of a many-body state according to the same rule is denoted by $\hat{P}_{\alpha,\beta,\gamma}$. We also note that a cyclic permutation of α, β, γ does not change the cycle, i.e., $P_{\alpha,\beta,\gamma} = P_{\gamma,\alpha,\beta} = P_{\beta,\gamma,\alpha}$.

The cycle $P_{\alpha,\beta,\gamma}$ is the composition of two transpositions $P_{\alpha,\beta}$ and $P_{\beta,\gamma}$, $P_{\alpha,\beta,\gamma} = P_{\alpha,\beta} \circ P_{\beta,\gamma}$. The corresponding cycle operator $\hat{P}_{\alpha,\beta,\gamma}$ is the product of two transposition operators $\hat{P}_{\alpha,\beta}$ and $\hat{P}_{\beta,\gamma}$, $\hat{P}_{\alpha,\beta,\gamma} = \hat{P}_{\alpha,\beta}\hat{P}_{\beta,\gamma}$. The inverse of the cycle operator $\hat{P}_{\alpha,\beta,\gamma}$ is therefore given by $\hat{P}^{-1}_{\alpha,\beta,\gamma} = (\hat{P}_{\alpha,\beta}\hat{P}_{\beta,\gamma})^{-1} = \hat{P}_{\gamma,\beta}\hat{P}_{\beta,\alpha} = \hat{P}_{\gamma,\beta,\alpha}$, i.e., the particle indices appear in the inverse cycle operator in the inverse order.

The identity permutation is denoted by "id" and the corresponding operator by $\mathbb{1}$. A particular cycle is the loop permutation, which is defined by

$$P_{i,\ldots,j} = \begin{cases} P_{i,i+1,\ldots,j-1,j} \text{ for } i < j \\ \text{id for } i = j \\ P_{i,i-1,\ldots,j+1,j} \text{ for } i > j. \end{cases} \quad \text{(A5)}$$

The loop permutation is therefore a composition of transpositions of consecutive integers, $P_{i,\ldots,j} = P_{i,i+1} \circ P_{i+1,i+2} \circ \cdots \circ P_{j-2,j-1} \circ P_{j-1,j}$ (assuming $i < j$) and the loop permutation operator $\hat{P}_{i,\ldots,j}$ is a product of transpositions of neighboring particles, $\hat{P}_{i,\ldots,j} = \hat{P}_{i,i+1}\hat{P}_{i+1,i+2}\cdots\hat{P}_{j-2,j-1}\hat{P}_{j-1,j}$. The loop permutation operator $\hat{P}_{i,\ldots,j}$ therefore moves the particle at position j to position i.

3. Basis of a two-boson two-fermion mixture

The goal of this section is to clarify definition (A4). A basis of a mixture of two bosons and two fermions (2B2F mixture) is given by

$$\begin{aligned} &|B,B,F,F\rangle, \quad |B,F,B,F\rangle, \quad |B,F,F,B\rangle, \\ &|F,B,F,B\rangle, \quad |F,F,B,B\rangle, \quad |F,B,B,F\rangle. \end{aligned} \quad \text{(A6)}$$

The first basis state is, according to Eq. (A4), constructed by means of the sector wave function $|\mathrm{id}\rangle$ that corresponds to the identity permutation,

$$|B,B,F,F\rangle = \tfrac{1}{2}(\mathbb{1} + \hat{P}_{1,2})(\mathbb{1} - \hat{P}_{3,4})|\mathrm{id}\rangle. \quad \text{(A7)}$$

The second basis state is obtained from the first one by transposing the second and third particle. Therefore, we obtain

$$\begin{aligned} |B,F,B,F\rangle &= \hat{P}_{2,3}|B,B,F,F\rangle \\ &= \tfrac{1}{2}(\mathbb{1} + \hat{P}_{1,2})(\mathbb{1} - \hat{P}_{3,4})|P_{2,3}\rangle. \end{aligned} \quad \text{(A8)}$$

The third basis state is obtained from the first one by moving the second B to the fourth position. This is achieved by applying the loop permutation operator $\hat{P}_{4,3,2}$. The inverse of this loop permutation operator is given by $\hat{P}^{-1}_{4,3,2} = \hat{P}_{2,3,4}$. We therefore obtain, using Eq. (A4),

$$\begin{aligned} |B,F,F,B\rangle &= \hat{P}_{4,3,2}|B,B,F,F\rangle \\ &= \tfrac{1}{2}(\mathbb{1} + \hat{P}_{1,2})(\mathbb{1} - \hat{P}_{3,4})|P_{2,3,4}\rangle. \end{aligned} \quad \text{(A9)}$$

Note that the bosonic (z_1, z_2) and fermionic coordinates (z_3, z_4) are each in ascending order in the initial sector wave function $|P_{2,3,4}\rangle$, since $z_1 < z_3 < z_4 < z_2$, as required.

The fourth basis state is obtained from the first one by moving the second B to the fourth position and then the first B to the second position, i.e., by applying $\hat{P}_{1,2}\hat{P}_{4,3,2} = \hat{P}_{1,2,4,3}$. Using $\hat{P}^{-1}_{1,2,4,3} = \hat{P}_{3,4,2,1} = \hat{P}_{2,1,3,4}$ we obtain

$$|F,B,F,B\rangle = \tfrac{1}{2}(\mathbb{1} + \hat{P}_{1,2})(\mathbb{1} - \hat{P}_{3,4})|P_{2,1,3,4}\rangle. \quad \text{(A10)}$$

The fifth basis state is obtained from the first one by moving the second B to the fourth position and then the first B to the third position, i.e., by applying $\hat{P}_{3,2,1}\hat{P}_{4,3,2} = \hat{P}_{(1,3)(2,4)}$. Using $\hat{P}^{-1}_{(1,3)(2,4)} = \hat{P}_{(1,3)(2,4)}$ we obtain

$$|F,F,B,B\rangle = \tfrac{1}{2}(\mathbb{1} + \hat{P}_{1,2})(\mathbb{1} - \hat{P}_{3,4})|P_{(1,3)(2,4)}\rangle. \quad \text{(A11)}$$

The sixth basis state is finally obtained from the first one by moving the second B to the third position and then the first B to the second position, i.e., by applying $\hat{P}_{2,1}\hat{P}_{3,2} = \hat{P}_{1,2,3}$. Using $\hat{P}_{1,2,3}^{-1} = \hat{P}_{3,2,1}$ we obtain

$$|F,B,B,F\rangle = \tfrac{1}{2}(\mathbb{1} + \hat{P}_{1,2})(\mathbb{1} - \hat{P}_{3,4})|P_{3,2,1}\rangle. \tag{A12}$$

APPENDIX B: EFFECTIVE HAMILTONIAN

Here, we perform a perturbative calculation of a strongly interacting 2B1F mixture up to linear order in $1/g_{BB}$ and $1/g_{BF}$. The matrix elements of the Hamiltonian in the degenerate ground-state manifold are shown to agree with Eq. (3). The basis states of the 2B1F mixture are [see Eq. (A4)]

$$|1\rangle := |B,B,F\rangle = \frac{1}{\sqrt{2}}(\mathbb{1} + \hat{P}_{1,2})|\mathrm{id}\rangle, \tag{B1}$$

$$|2\rangle := |B,F,B\rangle = \frac{1}{\sqrt{2}}(\mathbb{1} + \hat{P}_{1,2})|P_{2,3}\rangle, \tag{B2}$$

$$|3\rangle := |F,B,B\rangle = \frac{1}{\sqrt{2}}(\mathbb{1} + \hat{P}_{1,2})|P_{3,2,1}\rangle. \tag{B3}$$

The Hamiltonian of the 2B1F mixture is given by [see Eq. (1)]

$$H = \sum_{i=1}^{3}\left[-\frac{\hbar^2}{2M}\frac{\partial^2}{\partial z_i^2} + V(z_i)\right] + g_{BB}\delta(z_1 - z_2) + g_{BF}\delta(z_1 - z_3) + g_{BF}\delta(z_2 - z_3). \tag{B4}$$

The matrix element $\langle 1|H|1\rangle$ is therefore given by

$$\langle 1|H|1\rangle = \tfrac{1}{2}\langle \mathrm{id}|(\mathbb{1} + \hat{P}_{1,2})H(\mathbb{1} + \hat{P}_{1,2})|\mathrm{id}\rangle. \tag{B5}$$

H is symmetric under the exchange of the first and second particle. H therefore commutes with $(\mathbb{1} + \hat{P}_{1,2})$. Moreover, $(\mathbb{1} + \hat{P}_{1,2})(\mathbb{1} + \hat{P}_{1,2}) = 2(\mathbb{1} + \hat{P}_{1,2})$ and therefore

$$\langle 1|H|1\rangle = \langle \mathrm{id}|H|\mathrm{id}\rangle + \langle \mathrm{id}|H|P_{1,2}\rangle. \tag{B6}$$

Let us calculate an arbitrary matrix element $\langle P|H|P'\rangle$ in the vicinity of $(1/g_{BB}, 1/g_{BF}) = (0,0)$. Performing a Taylor expansion up to first order in $1/g_{BB}$ and $1/g_{BF}$, we obtain [21]

$$\langle P|H|P'\rangle = E_F\delta_{P,P'} - \frac{1}{g_{BB}}\lim_{g_{BB}\to+\infty}\left(g_{BB}^2\langle P^{(g_{BB})}|\frac{dH}{dg_{BB}}|P'^{(g_{BB})}\rangle\right) - \frac{1}{g_{BF}}\lim_{g_{BF}\to+\infty}\left(g_{BF}^2\langle P^{(g_{BF})}|\frac{dH}{dg_{BF}}|P'^{(g_{BF})}\rangle\right), \tag{B7}$$

with $\frac{dH}{dg_{BB}} = \delta(z_1 - z_2)$ and $\frac{dH}{dg_{BF}} = \delta(z_1 - z_3) + \delta(z_2 - z_3)$. $|P^{(g)}\rangle$ is the ground state of N spinless bosons with strong δ repulsion restricted to the sector $z_{P(1)} < \cdots < z_{P(N)}$ [21]. Furthermore, using the boundary condition

$$\left(\frac{\partial}{\partial z_i} - \frac{\partial}{\partial z_j}\right)\psi\Big|_{z_i=z_j+} - \left(\frac{\partial}{\partial z_i} - \frac{\partial}{\partial z_j}\right)\psi\Big|_{z_i=z_j-} = \frac{2Mg}{\hbar^2}\psi\Big|_{z_i=z_j}, \tag{B8}$$

one finds

$$\lim_{g\to+\infty}[g^2\langle P^{(g)}|\delta(z_i - z_j)|P'^{(g)}\rangle] = C_{i,j}^{P,P'}, \tag{B9}$$

with

$$C_{i,j}^{P,P'} = \frac{N!\hbar^4}{M^2}\int dz_1\cdots dz_N\delta(z_i - z_j)\left|\frac{\partial\psi_F}{\partial z_i}\right|^2 \times \theta(z_{P(1)},\ldots,z_{P(N)})\theta(z_{P'(1)},\ldots,z_{P'(N)}). \tag{B10}$$

As a result, we obtain

$$\langle P|H|P'\rangle = E_F\delta_{P,P'} - \frac{1}{g_{BB}}C_{1,2}^{P,P'} - \frac{1}{g_{BF}}\left(C_{1,3}^{P,P'} + C_{2,3}^{P,P'}\right). \tag{B11}$$

Applying this to the matrix element $\langle 1|H|1\rangle$, we get

$$\langle 1|H|1\rangle = E_F - 2J_1^{(BB)} - J_2^{(BF)}, \tag{B12}$$

since $C_{1,2}^{\mathrm{id},\mathrm{id}} = C_{1,2}^{\mathrm{id},P_{1,2}} = C_1, C_{2,3}^{\mathrm{id},\mathrm{id}} = C_2$, and $C_{1,3}^{\mathrm{id},\mathrm{id}} = C_{1,3}^{\mathrm{id},P_{1,2}} = C_{2,3}^{\mathrm{id},P_{1,2}} = 0$. In a similar way we obtain

$$\langle 1|H|2\rangle = \langle \mathrm{id}|H|P_{2,3}\rangle + \langle \mathrm{id}|H|P_{1,2,3}\rangle = -J_2^{(BF)}, \tag{B13}$$

since only $C_{2,3}^{\mathrm{id},P_{2,3}} = C_2$ is nonzero. For the next matrix element, we get

$$\langle 1|H|3\rangle = \langle \mathrm{id}|H|P_{1,3}\rangle + \langle \mathrm{id}|H|P_{3,2,1}\rangle = 0, \tag{B14}$$

since $C_{i,j}^{\mathrm{id},P_{1,3}} = C_{i,j}^{\mathrm{id},P_{3,2,1}} = 0$ for all $1 \leqslant i < j \leqslant 3$. The next matrix element becomes

$$\langle 2|H|2\rangle = \langle P_{2,3}|H|P_{2,3}\rangle + \langle P_{2,3}|H|P_{1,2,3}\rangle = E_F - J_1^{(BF)} - J_2^{(BF)}, \tag{B15}$$

since only $C_{1,3}^{P_{2,3},P_{2,3}} = C_1$ and $C_{2,3}^{P_{2,3},P_{2,3}} = C_2$ are nonzero. Finally we obtain

$$\langle 2|H|3\rangle = \langle P_{2,3}|H|P_{1,3}\rangle + \langle P_{2,3}|H|P_{3,2,1}\rangle = -J_1^{(BF)} \tag{B16}$$

and

$$\langle 3|H|3\rangle = \langle P_{3,2,1}|H|P_{1,3}\rangle + \langle P_{3,2,1}|H|P_{3,2,1}\rangle = E_F - 2J_2^{(BB)} - J_1^{(BF)}, \tag{B17}$$

since only $C_{1,3}^{P_{2,3},P_{3,2,1}} = C_{1,3}^{P_{3,2,1},P_{3,2,1}} = C_1$ and $C_{1,2}^{P_{3,2,1},P_{1,3}} = C_{1,2}^{P_{3,2,1},P_{3,2,1}} = C_2$ are nonzero. The same matrix elements are obtained using H_{eff}, given by Eq. (3).

APPENDIX C: ONE-BODY DENSITY MATRIX

Here, we calculate the matrix elements of the bosonic and fermionic one-body density matrices of a 1B2F mixture. The basis states of the 1B2F mixture are [see Eq. (A4)]

$$|1\rangle := |B,F,F\rangle = \frac{1}{\sqrt{2}}(\mathbb{1} - \hat{P}_{2,3})|\mathrm{id}\rangle, \tag{C1}$$

$$|2\rangle := |F,B,F\rangle = \frac{1}{\sqrt{2}}(\mathbb{1} - \hat{P}_{2,3})|P_{1,2}\rangle, \tag{C2}$$

$$|3\rangle := |F,F,B\rangle = \frac{1}{\sqrt{2}}(\mathbb{1} - \hat{P}_{2,3})|P_{1,2,3}\rangle. \tag{C3}$$

The bosonic and fermionic one-body density-matrix operators read

$$\hat{\rho}_B(z,z') = |z\rangle_1\langle z'|_1 \tag{C4}$$

and

$$\hat{\rho}_F(z,z') = |z\rangle_2\langle z'|_2 + |z\rangle_3\langle z'|_3. \tag{C5}$$

First, we calculate the matrix elements of the bosonic distribution $\hat{\rho}_B(z,z')$. One finds

$$\langle 1|\hat{\rho}_B(z,z')|1\rangle = \langle \mathrm{id}|z\rangle_1\langle z'|_1(|\mathrm{id}\rangle - |P_{2,3}\rangle). \tag{C6}$$

Only those matrix elements of the form $\langle \mathrm{id}|z\rangle_i\langle z'|_i|P\rangle$ are nonzero for which $P = P_{i,\dots,j}$. We define

$$\rho^{(i,j)}(z,z') = \langle \mathrm{id}|z\rangle_i\langle z'|_i|P_{i,\dots,j}\rangle. \tag{C7}$$

Using this, we find

$$\begin{aligned}&\langle 1|\hat{\rho}_B(z,z')|1\rangle\\ &\quad= \rho^{(1,1)}(z,z') = \langle B,F,F|\rho^{(1,1)}(z,z')|B\rangle_1\langle B|_1|B,F,F\rangle.\end{aligned} \tag{C8}$$

The next two matrix elements are given by

$$\begin{aligned}\langle 1|\hat{\rho}_B(z,z')|2\rangle &= \langle \mathrm{id}|z\rangle_1\langle z'|_1(|P_{1,2}\rangle - |P_{3,2,1}\rangle)\\ &= \rho^{(1,2)}(z,z')\\ &= \langle B,F,F|\rho^{(1,2)}(z,z')|B\rangle_1\langle B|_1\hat{P}_{1,2}|F,B,F\rangle\end{aligned} \tag{C9}$$

and

$$\begin{aligned}\langle 1|\hat{\rho}_B(z,z')|3\rangle &= \langle \mathrm{id}|z\rangle_1\langle z'|_1(|P_{1,2,3}\rangle - |P_{1,3}\rangle)\\ &= \rho^{(1,3)}(z,z')\\ &= \langle B,F,F|\rho^{(1,3)}(z,z')|B\rangle_1\langle B|_1\hat{P}_{1,2,3}|F,F,B\rangle.\end{aligned} \tag{C10}$$

In the next case, we find

$$\langle 2|\hat{\rho}_B(z,z')|2\rangle = \langle P_{1,2}|z\rangle_1\langle z'|_1(|P_{1,2}\rangle - |P_{3,2,1}\rangle). \tag{C11}$$

It is easy to show that

$$\langle P|z\rangle_i\langle z'|_i|P'\rangle = \langle \mathrm{id}|z\rangle_{P^{-1}(i)}\langle z'|_{P^{-1}(i)}|P^{-1}\circ P'\rangle. \tag{C12}$$

Using this, we find

$$\begin{aligned}\langle 2|\hat{\rho}_B(z,z')|2\rangle &= \langle \mathrm{id}|z\rangle_2\langle z'|_2(|\mathrm{id}\rangle - |P_{1,3}\rangle) = \rho^{(2,2)}(z,z')\\ &= \langle F,B,F|\rho^{(2,2)}(z,z')|B\rangle_2\langle B|_2|F,B,F\rangle.\end{aligned} \tag{C13}$$

In the next case, we obtain

$$\begin{aligned}\langle 2|\hat{\rho}_B(z,z')|3\rangle &= \langle P_{1,2}|z\rangle_1\langle z'|_1(|P_{1,2,3}\rangle - |P_{1,3}\rangle)\\ &= \langle \mathrm{id}|z\rangle_2\langle z'|_2(|P_{2,3}\rangle - |P_{3,2,1}\rangle) = \rho^{(2,3)}(z,z')\\ &= \langle F,B,F|\rho^{(2,3)}(z,z')|B\rangle_2\langle B|_2\hat{P}_{2,3}|F,F,B\rangle.\end{aligned} \tag{C14}$$

The last matrix element is given by

$$\begin{aligned}\langle 3|\hat{\rho}_B(z,z')|3\rangle &= \langle P_{1,2,3}|z\rangle_1\langle z'|_1(|P_{1,2,3}\rangle - |P_{1,3}\rangle)\\ &= \langle \mathrm{id}|z\rangle_3\langle z'|_3(|\mathrm{id}\rangle - |P_{1,2}\rangle) = \rho^{(3,3)}(z,z')\\ &= \langle F,F,B|\rho^{(3,3)}(z,z')|B\rangle_3\langle B|_3|F,F,B\rangle.\end{aligned} \tag{C15}$$

One sees that the matrix elements of the bosonic one-body density matrix agree with those of Eqs. (10)–(12). Now, we calculate the matrix elements of the fermionic distribution $\hat{\rho}_F(z,z')$. The first two matrix elements read

$$\begin{aligned}\langle 1|\hat{\rho}_F(z,z')|1\rangle &= \langle \mathrm{id}|(|z\rangle_2\langle z'|_2 + |z\rangle_3\langle z'|_3)(|\mathrm{id}\rangle - |P_{2,3}\rangle)\\ &= \rho^{(2,2)}(z,z') - \rho^{(2,3)}(z,z') + \rho^{(3,3)}(z,z') - \rho^{(3,2)}(z,z')\\ &= \langle B,F,F|[\rho^{(2,2)}(z,z')|F\rangle_2\langle F|_2 - \rho^{(2,3)}(z,z')|F\rangle_2\langle F|_2\hat{P}_{2,3}\\ &\quad + \rho^{(3,3)}(z,z')|F\rangle_3\langle F|_3 - \rho^{(3,2)}(z,z')|F\rangle_3\langle F|_3\hat{P}_{3,2}]|B,F,F\rangle\end{aligned} \tag{C16}$$

and

$$\begin{aligned}\langle 1|\hat{\rho}_F(z,z')|2\rangle &= \langle \mathrm{id}|(|z\rangle_2\langle z'|_2 + |z\rangle_3\langle z'|_3)(|P_{1,2}\rangle - |P_{3,2,1}\rangle)\\ &= \rho^{(2,1)}(z,z') - \rho^{(3,1)}(z,z')\\ &= \langle B,F,F|[\rho^{(2,1)}(z,z')|F\rangle_2\langle F|_2\hat{P}_{2,1} - \rho^{(3,1)}(z,z')|F\rangle_3\langle F|_3\hat{P}_{3,2,1}]|F,B,F\rangle.\end{aligned} \tag{C17}$$

The next matrix element is zero,

$$\langle 1|\hat{\rho}_F(z,z')|3\rangle = \langle \mathrm{id}|(|z\rangle_2\langle z'|_2 + |z\rangle_3\langle z'|_3)(|P_{1,2,3}\rangle - |P_{1,3}\rangle) = 0. \tag{C18}$$

Using Eq. (C12), we obtain for the last three matrix elements

$$\begin{aligned}\langle 2|\hat{\rho}_F(z,z')|2\rangle &= \langle P_{1,2}|(|z\rangle_2\langle z'|_2 + |z\rangle_3\langle z'|_3)(|P_{1,2}\rangle - |P_{3,2,1}\rangle)\\ &= \langle \mathrm{id}|(|z\rangle_1\langle z'|_1 + |z\rangle_3\langle z'|_3)(|\mathrm{id}\rangle - |P_{1,3}\rangle)\\ &= \rho^{(1,1)}(z,z') + \rho^{(3,3)}(z,z')\\ &= \langle F,B,F|[\rho^{(1,1)}(z,z')|F\rangle_1\langle F|_1 + \rho^{(3,3)}(z,z')|F\rangle_3\langle F|_3]|F,B,F\rangle,\\ \langle 2|\hat{\rho}_F(z,z')|3\rangle &= \langle P_{1,2}|(|z\rangle_2\langle z'|_2 + |z\rangle_3\langle z'|_3)(|P_{1,2,3}\rangle - |P_{1,3}\rangle)\\ &= \langle \mathrm{id}|(|z\rangle_1\langle z'|_1 + |z\rangle_3\langle z'|_3)(|P_{2,3}\rangle - |P_{3,2,1}\rangle)\\ &= \rho^{(3,2)}(z,z') - \rho^{(3,1)}(z,z')\\ &= \langle F,B,F|[\rho^{(3,2)}(z,z')|F\rangle_3\langle F|_3\hat{P}_{3,2} - \rho^{(3,1)}(z,z')|F\rangle_3\langle F|_3\hat{P}_{3,2,1}]|F,F,B\rangle,\end{aligned} \tag{C19, C20}$$

$$\begin{aligned}\langle 3|\hat{\rho}_F(z,z')|3\rangle &= \langle P_{1,2,3}|(|z\rangle_2\langle z'|_2 + |z\rangle_3\langle z'|_3)(|P_{1,2,3}\rangle - |P_{1,3}\rangle)\\ &= \langle \mathrm{id}|(|z\rangle_1\langle z'|_1 + |z\rangle_2\langle z'|_2)(|\mathrm{id}\rangle - |P_{1,2}\rangle)\\ &= \rho^{(1,1)}(z,z') - \rho^{(1,2)}(z,z') + \rho^{(2,2)}(z,z') - \rho^{(2,1)}(z,z')\\ &= \langle F,F,B|[\rho^{(1,1)}(z,z')|F\rangle_1\langle F|_1 - \rho^{(1,2)}(z,z')|F\rangle_1\langle F|_1\hat{P}_{1,2}\\ &\quad + \rho^{(2,2)}(z,z')|F\rangle_2\langle F|_2 - \rho^{(2,1)}(z,z')|F\rangle_2\langle F|_2\hat{P}_{2,1}]|F,F,B\rangle. \end{aligned} \tag{C21}$$

Again, one sees that the matrix elements of the fermionic one-body density matrix agree with those of Eqs. (10)–(12).

[1] M. A. Cazalilla, R. Citro, T. Giamarchi, E. Orignac, and M. Rigol, One-dimensional bosons: From condensed matter systems to ultracold gases, Rev. Mod. Phys. **83**, 1405 (2011).

[2] X.-W. Guan, M. T. Batchelor, and C. Lee, Fermi gases in one dimension: From Bethe ansatz to experiments, Rev. Mod. Phys. **85**, 1633 (2013).

[3] T. Kinoshita, T. Wenger, and D. S. Weiss, Observation of a one-dimensional Tonks-Girardeau gas, Science **305**, 1125 (2004).

[4] B. Paredes, A. Widera, V. Murg, O. Mandel, S. Fölling, I. Cirac, G. V. Shlyapnikov, T. W. Hänsch, and I. Bloch, Tonks-Girardeau gas of ultracold atoms in an optical lattice, Nature (London) **429**, 277 (2004).

[5] E. Haller, M. Gustavsson, M. J. Mark, J. G. Danzl, R. Hart, G. Pupillo, and H.-C. Nägerl, Realization of an excited, strongly correlated quantum gas phase, Science **325**, 1224 (2009).

[6] G. E. Astrakharchik, J. Boronat, J. Casulleras, and S. Giorgini, Beyond the Tonks-Girardeau Gas: Strongly Correlated Regime in Quasi-One-Dimensional Bose Gases, Phys. Rev. Lett. **95**, 190407 (2005).

[7] T. Kinoshita, T. Wenger, and D. S. Weiss, A quantum Newton's cradle, Nature (London) **440**, 900 (2006).

[8] F. Serwane, G. Zürn, T. Lompe, T. B. Ottenstein, A. N. Wenz, and S. Jochim, Deterministic preparation of a tunable few-Fermion system, Science **332**, 336 (2011).

[9] G. Zürn, F. Serwane, T. Lompe, A. N. Wenz, M. G. Ries, J. E. Bohn, and S. Jochim, Fermionization of Two Distinguishable Fermions, Phys. Rev. Lett. **108**, 075303 (2012).

[10] G. Zürn, A. N. Wenz, S. Murmann, A. Bergschneider, T. Lompe, and S. Jochim, Pairing in Few-Fermion Systems with Attractive Interactions, Phys. Rev. Lett. **111**, 175302 (2013).

[11] A. N. Wenz, G. Zürn, S. Murmann, I. Brouzos, T. Lompe, and S. Jochim, From few to many: Observing the formation of a Fermi sea one atom at a time, Science **342**, 457 (2013).

[12] S. Murmann, F. Deuretzbacher, G. Zürn, J. Bjerlin, S. M. Reimann, L. Santos, T. Lompe, and S. Jochim, Antiferromagnetic Heisenberg Spin Chain of a Few Cold Atoms in a One-Dimensional Trap, Phys. Rev. Lett. **115**, 215301 (2015).

[13] G. Pagano, M. Mancini, G. Cappellini, P. Lombardi, F. Schäfer, H. Hu, X.-J. Liu, J. Catani, C. Sias, M. Inguscio, and L. Fallani, A one-dimensional liquid of Fermions with tunable spin, Nat. Phys. **10**, 198 (2014).

[14] F. Schreck, L. Khaykovich, K. L. Corwin, G. Ferrari, T. Bourdel, J. Cubizolles, and C. Salomon, Quasipure Bose-Einstein Condensate Immersed in a Fermi Sea, Phys. Rev. Lett. **87**, 080403 (2001).

[15] M. Girardeau, Relationship between systems of impenetrable bosons and Fermions in one dimension, J. Math. Phys. **1**, 516 (1960).

[16] M. D. Girardeau and A. Minguzzi, Soluble Models of Strongly Interacting Ultracold Gas Mixtures in Tight Waveguides, Phys. Rev. Lett. **99**, 230402 (2007).

[17] F. Deuretzbacher, K. Fredenhagen, D. Becker, K. Bongs, K. Sengstock, and D. Pfannkuche, Exact Solution of Strongly Interacting Quasi-One-Dimensional Spinor Bose Gases, Phys. Rev. Lett. **100**, 160405 (2008).

[18] L. Guan, S. Chen, Y. Wang, and Z.-Q. Ma, Exact Solution for Infinitely Strongly Interacting Fermi Gases in Tight Waveguides, Phys. Rev. Lett. **102**, 160402 (2009).

[19] A. G. Volosniev, D. V. Fedorov, A. S. Jensen, M. Valiente, and N. T. Zinner, Strongly interacting confined quantum systems in one dimension, Nat. Commun. **5**, 5300 (2014).

[20] K. A. Matveev and A. Furusaki, Spectral Functions of Strongly Interacting Isospin-1/2 Bosons in One Dimension, Phys. Rev. Lett. **101**, 170403 (2008).

[21] F. Deuretzbacher, D. Becker, J. Bjerlin, S. M. Reimann, and L. Santos, Quantum magnetism without lattices in strongly interacting one-dimensional spinor gases, Phys. Rev. A **90**, 013611 (2014).

[22] A. G. Volosniev, D. Petrosyan, M. Valiente, D. V. Fedorov, A. S. Jensen, and N. T. Zinner, Engineering the dynamics of effective spin-chain models for strongly interacting atomic gases, Phys. Rev. A **91**, 023620 (2015).

[23] L. Yang, L. Guan, and H. Pu, Strongly interacting quantum gases in one-dimensional traps, Phys. Rev. A **91**, 043634 (2015).

[24] P. Massignan, J. Levinsen, and M. M. Parish, Magnetism in Strongly Interacting One-Dimensional Quantum Mixtures, Phys. Rev. Lett. **115**, 247202 (2015).

[25] L. Yang and X. Cui, Effective spin-chain model for strongly interacting one-dimensional atomic gases with an arbitrary spin, Phys. Rev. A **93**, 013617 (2016).

[26] M. Lewenstein, L. Santos, M. A. Baranov, and H. Fehrmann, Atomic Bose-Fermi Mixtures in an Optical Lattice, Phys. Rev. Lett. **92**, 050401 (2004).

[27] L. Mathey and D.-W. Wang, Phase diagrams of one-dimensional Bose-Fermi mixtures of ultracold atoms, Phys. Rev. A **75**, 013612 (2007).

[28] M. A. Cazalilla and A. F. Ho, Instabilities in Binary Mixtures of One-Dimensional Quantum Degenerate Gases, Phys. Rev. Lett. **91**, 150403 (2003).

[29] A. Imambekov and E. Demler, Exactly solvable case of a one-dimensional Bose-Fermi mixture, Phys. Rev. A **73**, 021602(R) (2006).

[30] X.-W. Guan, M. T. Batchelor, and J.-Y. Lee, Magnetic ordering and quantum statistical effects in strongly repulsive Fermi-Fermi and Bose-Fermi mixtures, Phys. Rev. A **78**, 023621 (2008).

[31] B. Fang, P. Vignolo, M. Gattobigio, C. Miniatura, and A. Minguzzi, Exact solution for the degenerate ground-state manifold of a strongly interacting one-dimensional Bose-Fermi mixture, Phys. Rev. A **84**, 023626 (2011).

[32] H. Hu, L. Guan, and S. Chen, Strongly interacting Bose-Fermi mixtures in one dimension, New J. Phys. **18**, 025009 (2016).

[33] A. S. Dehkharghani, F. F. Bellotti, and N. T. Zinner, Analytical and numerical studies of Bose-Fermi mixtures in a one-dimensional harmonic trap, arXiv:1703.01836.

[34] N. T. Zinner, Strongly interacting mesoscopic systems of anyons in one dimension, Phys. Rev. A **92**, 063634 (2015).

[35] H. Hu, L. Pan, and S. Chen, Strongly interacting one-dimensional quantum gas mixtures with weak p-wave interactions, Phys. Rev. A **93**, 033636 (2016).

[36] L. Yang, X.-W. Guan, and X. Cui, Engineering quantum magnetism in one-dimensional trapped Fermi gases with p-wave interactions, Phys. Rev. A **93**, 051605(R) (2016).

[37] See Supplemental Material at http://link.aps.org/supplemental/10.1103/PhysRevA.95.043630 for the *Mathematica* notebook.

[38] S. Inouye, M. R. Andrews, J. Stenger, H.-J. Miesner, D. M. Stamper-Kurn, and W. Ketterle, Observation of Feshbach resonances in a Bose-Einstein condensate, Nature (London) **392**, 151 (1998).

[39] M. Olshanii, Atomic Scattering in the Presence of an External Confinement and a Gas of Impenetrable Bosons, Phys. Rev. Lett. **81**, 938 (1998).

[40] In a quasi-1D trap with a tight transverse harmonic confinement with frequency $\omega_\perp$, the inverse strength $1/g$ of the 1D δ interaction fulfills $2\hbar\omega_\perp l_\perp/g = l_\perp/a_{3D} - C$, with $l_\perp = \sqrt{\hbar/(m\omega_\perp)}$, a_{3D} the bare 3D scattering length, and $C \simeq 1.0326\ldots$ [39]. Hence, by changing either a_{3D} or the transversal confinement, $\hbar\omega l/g$ may be adiabatically changed from an initial small positive (Tonks regime) to a small negative value (super-Tonks regime). The super-Tonks state is a highly excited state but remains metastable due to the small overlap with the strongly bound states. Around the confinement-induced resonance, the charge (i.e., density) degrees of freedom are frozen and well approximated by the wave function of spinless noninteracting fermions, while the spin degrees of freedom are described by the spin-chain model.

[41] F. Deuretzbacher, D. Becker, and L. Santos, Momentum distributions and numerical methods for strongly interacting one-dimensional spinor gases, Phys. Rev. A **94**, 023606 (2016).

[42] N. J. S. Loft, L. B. Kristensen, A. E. Thomsen, A. G. Volosniev, and N. T. Zinner, CONAN—The cruncher of local exchange coefficients for strongly interacting confined systems in one dimension, Comput. Phys. Commun. **209**, 171 (2016).

[43] L. Yang and H. Pu, Bose-Fermi mapping and a multibranch spin-chain model for strongly interacting quantum gases in one dimension: Dynamics and collective excitations, Phys. Rev. A **94**, 033614 (2016).

[44] F. Deuretzbacher, K. Bongs, K. Sengstock, and D. Pfannkuche, Evolution from a Bose-Einstein condensate to a Tonks-Girardeau gas: An exact diagonalization study, Phys. Rev. A **75**, 013614 (2007).

[45] H.-J. Mikeska and A. K. Kolezhuk, One-dimensional magnetism, Lect. Notes Phys. **645**, 1 (2004).

[46] F. Meinert, M. Knap, E. Kirilov, K. Jag-Lauber, M. B. Zvonarev, E. Demler, and H.-C. Nägerl, Bloch oscillations in the absence of a lattice, arXiv:1608.08200.

[47] J. Decamp, J. Jünemann, M. Albert, M. Rizzi, A. Minguzzi, and P. Vignolo, High-momentum tails as magnetic-structure probes for strongly correlated SU(κ) fermionic mixtures in one-dimensional traps, Phys. Rev. A **94**, 053614 (2016).

[48] F. Deuretzbacher, J. C. Cremon, and S. M. Reimann, Ground-state properties of few dipolar bosons in a quasi-one-dimensional harmonic trap, Phys. Rev. A **81**, 063616 (2010); Erratum: Ground-state properties of few dipolar bosons in a quasi-one-dimensional harmonic trap [Phys. Rev. A 81, 063616 (2010)] **87**, 039903(E) (2013).

Paper V

Dipolar particles in a double-trap confinement: Response to tilting the dipolar orientation

(Manuscript in preparation)

J. Bjerlin[1], J. Bengtsson[1], F. Deuretzbacher[2] and S. M. Reimann[1]

[1] *Mathematical Physics and NanoLund, LTH, Lund University, P.O.Box 118, SE-22100 Lund, Sweden and*

[2] *Institut für Theoretische Physik, Leibniz Universität Hannover, Appelstrasse 2, DE-30167 Hannover, Germany*

(Dated: August 21, 2017)

We analyze the microscopic few-body properties of dipolar atoms confined in two parallel quasi-one-dimensional harmonic traps. An adiabatic change of the dipole orientation with respect to the trap separation can even drive an initially non-localized few-fermion state into a Wigner-like localized ground state with strong inter-trap pairing. For a fast non-adiabatic sweep, however, localization is inhibited, and a highly excited state is reached that may be interpreted as the few-body analog of a super-Tonks-Girardeau state known from one-dimensional systems with contact interaction.

I. INTRODUCTION

Ultracold atoms or molecules with large permanent magnetic [1–9] or electric [10–15] dipole moments have intriguing properties that originate from the spatial anisotropy of the dipole-dipole interaction (DDI). In general, the trap geometry plays a big role, and different quasi one- and two-dimensional (1D and 2D) confinement configurations ranging from single-traps to optical lattices and coupled interlayer systems have been studied (see [16, 17] for reviews). The reduced dimensionality together with the fact that the DDI can be relatively strong and tailored by means of external fields [18, 19] allow studying strongly correlated systems. The long-range part of the dipolar interaction may couple spatially distinct confinement regions in different ways, leading to intriguing many-body phenomena in optical lattices and multilayer systems, see, for example, refs. [20–27]. In the few-body regime different kinds of bound states were predicted [28–30]. In a planar array of parallel 1D tubes [31], inter-tube interactions were found responsible for classically ordered (Wigner-type) clustered states.

It is well known that strong contact repulsion in 1D systems may lead to a so-called Tonks-Girardeau (TG) state, where bosons act as non-interacting fermions [32]. The cold-atom realization [33, 34] of this phenomenon spurred further work to categorize and probe these states[35–39], and similar states have also been found for dipolar bosons [40, 41]. TG states are closely related to the excited states occurring for 1D-confined particles with short-range *attractive* interactions, known as super-Tonks-Girardeau (STG) states [36, 41, 42]. See for example Refs. [28, 35, 36, 38, 41, 42] for further theoretical description, and [43] for an experimental realization. A system, initially in a TG state, may with a sudden quench of the interaction (for example by changing the dipolar orientation) end up in an STG state of the new Hamiltonian [41].

Here, we show that in parallel 1D traps, the DDI leads to fundamentally different few-body ground states, depending on the dipole angle. The interplay between long-range interactions *within* each trap, and the short range effects *between* the traps, plays a decisive role in the formation of a localized ground state in each of the wires. The inter-trap interaction may hereby serve to either reduce or enhance particle localization. Finally, we also investigate the transition from a TG to an STG state by a sudden quench of the DDI, here for spin-polarized fermions. Our investigations into such short-range phenomena are partly motivated by the common use of a contact pseudopotential to approximate the DDI [30], which has been utilized to, for example, study the phase diagram of two parallel 1D traps [44–46]. We here consider the full form of the DDI, and specifically address emergent short-range phenomena in the exact solutions of the few-body system.

II. MODEL

Let us consider a few (magnetic or electric) dipolar particles in two parallel, cigar-shaped traps (schematically sketched in Fig. 1),

$$V_n^{\rm trap}(\mathbf{r}) = \frac{m}{2}\omega_x^2 x^2 + \frac{m}{2}\omega_\perp^2\left[y^2 + (z - nz_w)^2\right] . \qquad (1)$$

The index $n = \{0, 1\}$ labels the two traps, m is the particle mass, $\mathbf{r} = (x, y, z)$ and the oscillator frequencies satisfy $\omega_x < \omega_\perp$. The strong confinement perpendicular to the wire axes is here sufficient to neglect the tunneling of particles between the two traps, which keeps the number of particles per trap constant. In fact, $\omega_\perp$ is high enough for the system to be adequately described by the harmonic oscillator ground state in the yz-plane. In other words, the dipole interaction is assumed insufficient to excite the system in the tightly confined

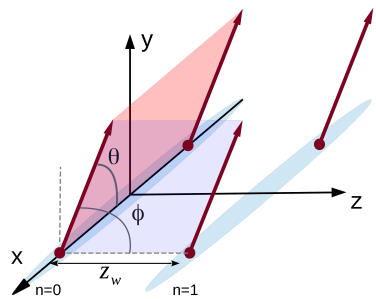

FIG. 1: (Color online) Two parallel traps elongated along the x-direction (*sketched by the light-blue area*). Each trap contains two dipolar particles (*sketched by red bullets and arrows*) and the shortest distance between the two traps is denoted z_w. The dipoles are aligned with an external field. The angles ϕ and θ define the direction of alignment relative to the z- and x-axis, respectively.

yz-plane. We may then write the *one-body* orbital $\psi_{n,i}$ of a particle trapped by V_n^{trap} as

$$\psi_{n,i}(\mathbf{r}) = \varphi_{n,i}(x)\phi_n(y,z), \tag{2}$$

where $\varphi_{n,i}$ are, yet unspecified, basis functions in the x-direction, and

$$\phi_n(y,z) = \frac{1}{l_\perp\sqrt{\pi}} e^{-[y^2+(z-nz_w)^2]/2l_\perp^2} \tag{3}$$

is the ground-state wave function of the two-dimensional harmonic oscillator centered at $(y,z) = (0, nz_w)$. In Eq. (3), $l_\perp = \sqrt{\hbar/(m\omega_\perp)}$ is the characteristic length of the yz-oscillator. It needs to be shorter than the distance between the two traps, $l_\perp \ll z_w$, to ensure a clear separation of the two confinements with $n = 0$ and $n = 1$. The restrictions in the yz-plane conveniently allow a quasi 1D description of the double-trap system.

Let us now address the dipolar interaction between two particles. The angle between the particles' dipolar vectors relative to each other determines the anisotropy of the interaction between them. For identical dipole moment vectors $\mathbf{d}$, the interaction potential reads (see for example, Ref. [47])

$$V(\tilde{\mathbf{r}}) = \frac{\mathbf{d}^2}{4\pi\gamma\,|\tilde{\mathbf{r}}|^3}\left[1 - \frac{3\,(\mathbf{d}\cdot\tilde{\mathbf{r}})^2}{\mathbf{d}^2\tilde{\mathbf{r}}^2}\right], \tag{4}$$

where $\tilde{\mathbf{r}} = \mathbf{r} - \mathbf{r}'$ is the relative position of the two dipolar particles. (In the case of electric dipoles, $\gamma = \epsilon_0$, and for magnetic dipoles $\gamma = 1/\mu_0$, where ϵ_0 and μ_0 are the permittivity and permeability of free space). In the quasi-1D description of the double-trap system, we use an effective potential, $V^{\text{eff}}_{n,n'}$, to model the interaction. The indices n and n' discern the two different effective potentials; one *intra-trap* potential for interacting particles in the same trap ($n = n'$) and one *inter-trap* potential for particles in opposite traps ($n \neq n'$). Both potentials are derived from the integral expression

$$V^{\text{eff}}_{n,n'}(\tilde{x}) = \iiiint dydzdy'dz'\,|\phi_n(y,z)|^2\,|\phi_{n'}(y',z')|^2\,V(\tilde{\mathbf{r}}), \tag{5}$$

where d $\tilde{x} = x - x'$.

For two particles in the *same* trap, Eq. (5) reduces to

$$V^{\text{eff}}_{n,n}(\tilde{x}) = \frac{\mathbf{d}^2\,[1+3\cos(2\theta)]}{16\pi\gamma l_\perp^3} \times \left[\frac{|\tilde{x}|}{l_\perp} - \sqrt{\frac{\pi}{2}}\left(1+\frac{\tilde{x}^2}{l_\perp^2}\right)\text{erfc}\left(\frac{|\tilde{x}|}{\sqrt{2}l_\perp}\right)e^{\tilde{x}^2/2l_\perp^2} + \frac{4l_\perp}{3}\delta(\tilde{x})\right], \tag{6}$$

as, e.g., demonstrated by Sinha and Santos [18]. We repeat that in Eq. (6), θ is the angle between the dipole vectors and the x-axis, as indicated in Fig. 1. The intra-trap potential is clearly independent of the angle ϕ between the dipole vectors and the z-axis. Hence, depending on θ alone, the interaction can be either attractive, zero or repulsive. In particular, the potential is maximally repulsive for $\theta = 90°$ and vanishes at the "critical angle" $\theta = \arccos(-1/3)/2 \approx 54.74°$. (Note that the additional delta-terms of the intra-trap dipolar interaction may be tuned to zero by means of a Feshbach resonance [48]). The effective interaction potential for particles in different traps does not have an equally simple form. With $n \neq n'$, we can, however, turn the potential in Eq. (5) into a single integral expression,

$$V^{\text{eff}}_{n,n'\neq n}(\tilde{x}) = -\frac{\mathbf{d}^2}{4\pi\gamma}\int_0^\infty dkk^2 e^{-k^2l_\perp^2/2-k|\tilde{x}|} \times \left[\cos^2(\theta)\mathrm{J}_0(kz_w) + \cos^2(\phi)\mathrm{J}_2(kz_w) - \left(\frac{\tilde{x}\sin(2\theta)\cos(\phi)}{|\tilde{x}|} + \frac{\sin^2(\theta)}{kz_w}\right)\mathrm{J}_1(kz_w)\right], \tag{7}$$

which has to be evaluated numerically. In Eq. (7), J_i is the regular Bessel function of order i. At very large relative distances, the interaction becomes similar to that of two particles in the same trap, i.e. $\lim_{|\tilde{x}|\to\infty} V^{\text{eff}}_{n,n'\neq n}(\tilde{x}) = V^{\text{eff}}_{n,n}(\tilde{x})$.

With the above assumptions, the many-body Hamiltonian of the double-trap system here becomes effectively one-dimensional, and for N_n particles (spin-polarized fermions or spinless bosons) in each trap n, we obtain

$$H^{\text{eff}} = \sum_{n=0}^{1}\left[\sum_{i=1}^{N_n} h(x_{n,i}) + \sum_{j>i}^{N_n} V^{\text{eff}}_{n,n}(x_{n,i}-x_{n,j})\right] + \sum_{i=1}^{N_0}\sum_{j=1}^{N_1} V^{\text{eff}}_{0,1}(x_{0,i}-x_{1,j}) \tag{8}$$

where $V^{\text{eff}}_{n,n'}$ are given by Eqs. (6, 7) and where

$$h(x_{n,i}) = -\frac{\hbar^2}{2m}\frac{\partial^2}{\partial x_{n,i}^2} + \frac{m}{2}\omega_x^2 x_{n,i}^2 \tag{9}$$

is the one-body operator associated with particle i of trap n. Note that the one-body confining potential $m\omega_x^2 x_{n,i}^2/2 = V_n^{\text{trap}}(x_{n,i}, 0, nz_w)$. Also, we left out the constant energy contribution $(N_0+N_1)\hbar\omega_\perp/2$, associated with the combined oscillatory motion in the yz-plane, from H^{eff}.

The eigenstates to the effective Hamilton operator, Eq. (8), are obtained using the method of full configuration interaction (also known as exact diagonalization) in a B-spline basis; for further details see the appendix.

III. GROUND-STATE PROPERTIES

We now proceed to investigate how a change in the relative dipole angle ϕ modifies the ground state properties of a few-body system. To keep the numerical effort tractable, in the following we restrict the particle number in each trap to $N_0 = N_1 = 2$. These particles can be either spin-polarized fermions or spin-less bosons. Unless specified otherwise, we use 64 B-splines of order 5. The traps are further characterized by the dimensionless parameters $\omega_x/\omega_\perp = l_\perp^2/l_x^2 = 10^{-4}$ (where $l_x = \sqrt{\hbar/m\omega_x}$), and $z_w/l_\perp = 25$. Clearly, $\omega_x \ll \omega_\perp$ and $z_w > l_\perp$ which justifies the quasi one-dimensional treatment of the system discussed in Sec. II.

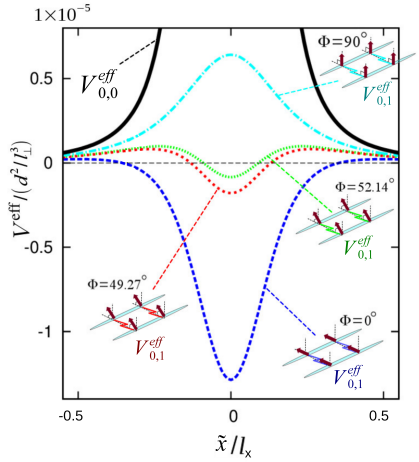

FIG. 2: (Color online) The effective intra- and inter-trap interaction potentials are shown for three different dipole alignments; $(\theta, \phi) = (90°, 0°), (90°, 50°)$ and $(90°, 90°)$, for the parameters described in the main text. The intra-trap potential $V^{\rm eff}_{0,0}$ (black line) depends only on the angle θ and is thus identical in all three cases, see Eq. (6). The inter-trap potential $V^{\rm eff}_{0,1}$ (green, blue and cyan dashed lines) depends on both ϕ and θ, see Eq. (7). With $\theta = 90°$, the short-range part of the inter-trap potential becomes maximally repulsive for $\phi = 90°$, weakly attractive for $\phi = 50°$ and maximally attractive for $\phi = 0°$.

We chose an interaction strength dictated by the dimensionless parameter $\mathbf{d}^2 m/(\hbar^2 l_x \gamma) = 8\pi$ and an angle $\theta = 90°$ for a maximally repulsive *intra*-trap interaction. The considered *intra*-trap potential $V^{\rm eff}_{n,n}$ together with the *inter*-trap potentials $V^{\rm eff}_{n,n'\neq n}$ obtained for different values of ϕ are shown in Fig. 2. Note that the inter-trap potential can be made either attractive or repulsive depending on the choice of ϕ.

To begin with, let us ignore the interaction between particles in different traps, thus effectively reducing the problem to that of a single trap with two particles. Figure 3 shows the single-particle densities for the ground state. We observe that the repulsive intra-trap interaction gives rise to similar single-particle density distributions $\rho^{(1)}(x)$ for fermions and bosons, see Figure 3. The pronounced minimum in $\rho(x)$ at $x/l_x = 0$ reflects the onset of localization due to the long-range part of the DDI. In the limit of strong repulsion, $\rho^{(1)}(x = 0) \to 0$ and a localized state is obtained, with identical momentum distributions $\rho^{(1)}(p_x) \to 0$ for fermions and bosons, as previously shown in [40].

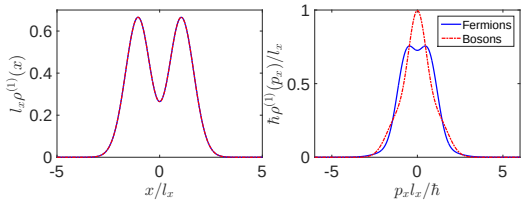

FIG. 3: (Color online) The ground state density distributions computed for two particles in a single trap. Spin-polarized fermions (solid blue line) are compared with spinless bosons (red dashed line). *Left panel:* The single-particle density $\rho^{(1)}$ shows two pronounced peaks in the position space, being similar for fermions and bosons, indicating fermionization of the bosonic system. *Right panel:* The single-particle density in momentum space. The fact that the bosonic and fermionic distributions differ indicates that the ground state is not fully localized.

The question is now, to what extent the inter-trap interaction modifies the system properties. When $\theta = 90°$, one expects the densities to have common features with the ones in Fig. 3 since $\left|V^{\rm eff}_{n,n'\neq n}(\tilde{x})\right| < \left|V^{\rm eff}_{n,n}(\tilde{x})\right|$. In particular, the strong repulsive intra-trap interaction leads to a partly localized ground state. In Fig. 4 and 5, we show the single trap density distribution at two different angles ϕ. Here, the particular choices for the angle ϕ are motivated by numerical limitations. For $\phi \lesssim 49°$, the attractive part of the DDI becomes too large for our methods to produce accurate results with a tractable single-particle basis. Note that a bound state is formed when the depth and width of the attractive core are sufficiently large for the binding energy to overcome the cost in kinetic energy associated with confining the particles within the attractive range. For $\phi \approx 49°$ the ground state feels an effectively attractive DDI, whereas for the more shallow attractive core at $\phi \approx 52°$, the interaction in the ground state is effectively repulsive.

For effectively attractive interactions, shown in Fig. 4 for $\phi = 0.86 \approx 49.27°$, the localization seen in the ground state densities is strongly enhanced, as indicated by the pronounced density minimum. Also, the bosonic and fermionic momentum distributions are now more similar than those in Fig. 3. The localization is supported by the strong attractive intra-trap interaction that leads to pairing between the particles in different traps. It is interesting to note that in similar, but extended systems, such bound states were found to give rise to a crystal-like phase [31]. The states found here appear as pre-cursors in the few-body limit.

With an effectively repulsive short-range inter-trap interaction, on the other hand, we now observe four distinct peaks in the density profiles of the four-particle double-trap system, see Fig. 5. This structure can be understood from the corresponding pair-correlated densities, clearly showing a particle displacement in the single traps confining two particles each, that together with the underlying symmetry and degeneracy gives rise to this overall different density distribution. The two particles in each trap are now less localized than in Fig. 4, as indicated by the differing bosonic and fermionic momentum distributions. The bosonic state is however still in the fermionized regime.

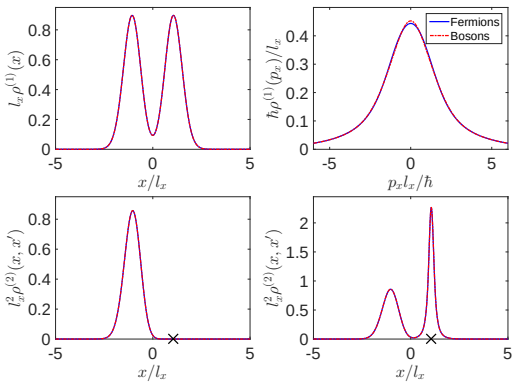

FIG. 4: (Color online) The ground state density distributions (within a single trap) when $\phi = 0.86 \approx 49.27^\circ$, corresponding to an attractive inter-trap interaction. The solid blue line is for fermions, and the red dashed one for bosons. **Top left panel:** The single-particle density distribution clearly shows two pronounced peaks, indicating that the two particles in one of the traps are paired up with the corresponding ones in the other trap. **Top right panel:** The corresponding distribution in momentum space shows a similar behavior for fermions and bosons. Comparing to Fig. 3, we note that the attractive inter-trap interaction has further increased the localization. **Bottom left panel:** The pair-correlated density, with the position of the reference particle (at x') indicated by the cross. Both reference particle and the considered particle reside in the same trap. **Bottom right panel:** The pair correlated density with the reference particle being in the other trap. The pronounced peak at $x' = 0$ indicates pairing between particles in different traps.

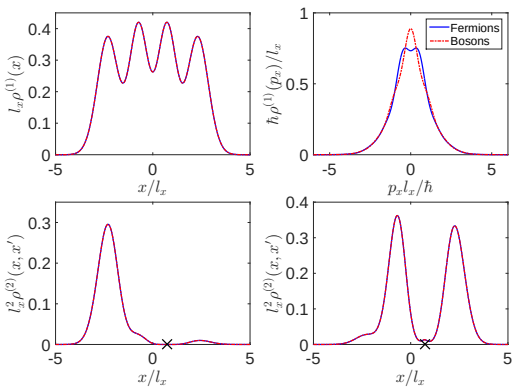

FIG. 5: (Color online) Similar to Fig. 4 but for $\phi = 0.91 \approx 52.14^\circ$, which corresponds to a repulsive inter-trap interaction.

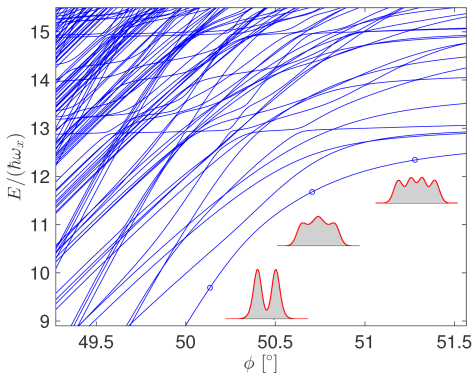

FIG. 6: (Color online) The even parity spectrum for two spin-polarized fermions in each trap. Insets show the ground state density profiles for three different angles ϕ.(noted by circles in the main plot)

IV. QUENCH OF THE DIPOLE ANGLE

In Fig. 6, we show the energy spectrum of the four-particle double-trap system for states with even parity. By decreasing the dipolar angle ϕ, the ground state becomes more correlated due to the pairing between particles in different traps, and its energy decreases. Interestingly, however, at higher energies in the spectrum, we note certain energy levels that seem unaffected by the choice of ϕ.

Their origin can be understood by looking at the simpler system with just one single particle in each trap, $N_0 = N_1 = 1$, where the Hamiltonian may be separated into two parts: H_R and H_r describing the center of mass motion of the two-body system and the relative motion of the two particles, respectively. Here, the dipole-dipole interaction enters the expression for H_r alone,

$$H_r = \frac{p_{\tilde{x}}^2}{m} + \frac{1}{4}m\omega_\perp^2\tilde{x}^2 + V_{n,n'\neq n}^{\text{eff}}(\tilde{x}). \tag{10}$$

Since the interaction potential is sharply peaked at $\tilde{x} = 0$, the odd parity solutions of H_r are, with their nodes at this position, largely unaffected by the nature of the dipole-dipole interaction. The even parity solutions do, on the other hand, heavily depend on the sign and strength of the interaction. Hence, when we sweep ϕ, we expect to see states described by odd parity solutions in their relative coordinate manifested as interaction-invariant lines in the spectrum. A similar structure was seen in the few-body spectra of contact-interacting bosons [38], where the few-body bound states depended strongly on the attractive interaction, while a second category of states appeared as interaction-invariant lines in the spectrum at strong attraction. The interaction-invariant lines were identified as few-body precursors of fermionized super-Tonks-States [35, 36]. These similarities were also discussed in [30], where the short-range aspects of the DDI were studied. Let us now investigate to what extent the lowest STG-like states at $E \approx 13\hbar\omega_x$ in Fig. 6 can get populated. From

the spectrum, we see that one possibility to reach these excited states could be to start in a repulsive low-energetic state and subsequently change the interaction through a tilt of the dipolar angle. Specifically, if the initial energy eigenstate at $\phi = 90^\circ$ remains an eigenstate to the Hamiltonian at a different ϕ value, a single excited state is populated. Let us now check how closely the i:th energetically lowest state $\Psi_i^{(\phi=90^\circ)}$ relates to an eigenstate at lower ϕ. For this purpose, we compute

$$\sigma_E = \sqrt{\langle\Psi_i^{(90^\circ)}|H^2(\phi)|\Psi_i^{(90^\circ)}\rangle - \langle\Psi_i^{(90^\circ)}|H(\phi)|\Psi_i^{(90^\circ)}\rangle^2}. \tag{11}$$

If $\sigma_E = 0$, $\Psi_i^{(90^\circ)}$ is also an eigenstate to the Hamiltonian $H(\phi)$ at a different value of ϕ. In contrast, $\sigma_E > 0$ means that non-stationary states are formed, and the measure represents the shortest time scale that characterize a significant change in the system, where the time scale decreases with increasing σ_E. In Fig. 7, we plot σ_E at different ϕ for different initial states. Clearly, the lowest values of σ_E (and thus closest to stationary states) are obtained with the third excited state at $\phi = 90^\circ$ as initial state. This observation agrees well with the fact that, at higher values of ϕ, the energy of the third excited state shown in Fig. 6 is largely unaffected by a change in the dipolar angle. The non-zero contribution to σ_E is mainly due to a small population of also the first excited STG-like state, which also depends only weakly on ϕ. A similar behavior has also been seen in previous attempts to populate ordinary STG states and gives rise to breathing mode dynamics in the system [49]. The small difference in σ_E seen in 7 for the different initial states means that also systems prepared in the ground state (as well as the first and second excited state) at $\phi = 90^\circ$ are close to stationary after the quench. With a more strongly-peaked DDI the difference between the ground state and third excited state at $\phi = 90^\circ$ is expected to be further reduced.

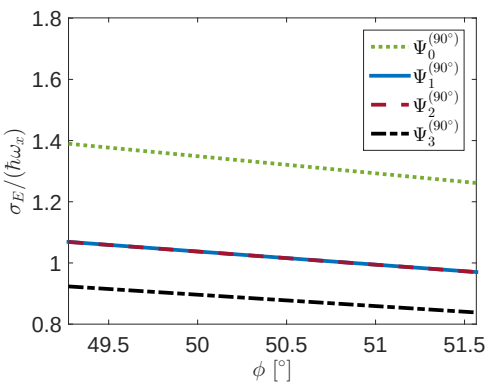

FIG. 7: (Color online) Energy uncertainties σ_E (see eq. 11) as functions of the dipolar angle ϕ. The plotted quantities represent the spread in energy after a fast change of the dipolar angle from 90° to ϕ. Each line represent a different initial state before the quench.

V. SUMMARY

We studied the microscopic few-body properties of dipolar bosonic or fermionic atoms confined in two parallel quasi-one-dimensional harmonic traps, where the dipole moments are aligned perpendicular to the alignment of the traps. By tuning the direction ϕ of the dipole moments relative to the plane spanned by the two traps, and thereby changing the shape of the inter-trap dipole-dipole interaction, we saw that for small inter-wire distances the short-range features of the inter-wire interaction had striking effects on the ground-state properties of the system.

Starting in a weakly localized ground state at repulsive inter-trap interaction, we saw that a slow change in the dipolar angle brought the system into a regime of strong localization, owing to the formation of bound dimers between the traps. Interestingly, a sudden quench in ϕ instead led to significant population-transfer into a class of excited states, analogous to super-Tonks-Girardeau states that are most commonly seen in strongly correlated one-dimensional systems. These states largely retain the structure of the non-localized ground state at $\phi = 90^\circ$. For a sudden quench in the dipolar angle the localization of particles is therefore inhibited.

ACKNOWLEDGMENTS

We are very thankful to P. d'Amico, M. Rontani and J. Cremon for valuable discussions. We are grateful to J.C. Cremon and L.H. Kristinsdottir for their help with part of the numerical work at an early stage of this project. Our work was financially supported by the Swedish Research Council and NanoLund.

Appendix: B-splines and exact diagonalization

B–splines are piece-wise polynomials that frequently are defined through the recursive relation [50]

$$B_{i,1}(x) = \begin{cases} 1 & \text{if } \tau_i \le x \le \tau_{i+1} \\ 0 & \text{otherwise} \end{cases} \tag{12}$$

$$B_{i,k}(x) = \frac{x - t_i}{\tau_{i+k-1} - t_i} B_{i,k-1}(x) + \frac{\tau_i + k - x}{\tau_{i+k} - \tau_{i+1}} B_{i+1,k-1}(x) \tag{13}$$

where $\tau_i \ge \tau_{i+i}$ are the so-called knot-points and k is the order of the B-splines. Throughout this work we set $k = 5$. We use a linear central distribution of knot-points with $\Delta\tau = 0.12$, and exponentially increasing distances between the knot-points outside of the central region. The outermost knot-points were placed at $x = \pm 5$. In total we used 64 B-splines (except for the spectra shown in Fig. 6 where the number of B-splines was 56 to reduce the computational workload of computing the spectra for a dense mesh of dipole angles).

First, we construct an orthonormal one-body basis by diagonalization of the Hermitian h, Eq. (9), in the B-spline basis. We write

$$\varphi_j(x) = \sum_i c_{j,i} B_{k,i}(x) \tag{14}$$

which turns the one-body Schrödinger equation, $h(x)\varphi_j(x) = \epsilon_j\varphi_j(x)$, into the generalized eigenvalue problem,

$$\mathbf{hc}_j = \epsilon_j \mathbf{S}\mathbf{c}_j \tag{15}$$

with matrix elements given by

$$\mathbf{h}_{i,j} = \int dx B_i(x) h(x) B_j(x) dx, \tag{16}$$

$$\mathbf{S}_{i,j} = \int dx B_i(x) B_j(x) dx. \tag{17}$$

Finally, an orthonormal many-body basis is constructed based on correctly symmetrized products of the acquired (orthogonal) one-body states following the general prescription of the configuration interaction method.

[1] A. Griesmaier, J. Werner, S. Hensler, J. Stuhler, and T. Pfau, Physical Review Letters **94**, 160401 (2005), URL https://doi.org/10.1103/PhysRevLett.94.160401.

[2] T. Lahaye, T. Koch, B. Fröhlich, M. Fattori, J. Metz, A. Griesmaier, S. Giovanazzi, and T. Pfau, Nature **448**, 672 (2007), URL 10.1038/nature06036.

[3] T. Koch, T. Lahaye, J. Metz, B. Frohlich, A. Griesmaier, and T. Pfau, Nature Physics **4**, 218 (2008), URL 10.1038/nphys887.

[4] Q. Beaufils, R. Chicireanu, T. Zanon, B. Laburthe-Tolra, E. Maréchal, L. Vernac, J.-C. Keller, and O. Gorceix, Physical Review A **77**, 061601 (2008), URL https://doi.org/10.1103/PhysRevA.77.061601.

[5] M. Lu, S. H. Youn, and B. L. Lev, Physical Review Letters **104**, 063001 (2010), URL https://doi.org/10.1103/PhysRevLett.104.063001.

[6] M. Lu, N. Q. Burdick, S. H. Youn, and B. L. Lev, Physical Review Letters **107**, 190401 (2011), URL https://doi.org/10.1103/PhysRevLett.107.190401.

[7] K. Aikawa, A. Frisch, M. Mark, S. Baier, A. Rietzler, R. Grimm, and F. Ferlaino, Physical Review Letters **108**, 210401 (2012), URL https://doi.org/10.1103/PhysRevLett.108.210401.

[8] M. Lu, N. Q. Burdick, and B. L. Lev, Physical Review Letters **108**, 215301 (2012), URL https://doi.org/10.1103/PhysRevLett.108.215301.

[9] K. Aikawa, A. Frisch, M. Mark, S. Baier, R. Grimm, and F. Ferlaino, Physical Review Letters **112**, 010404 (2014), URL https://doi.org/10.1103/PhysRevLett.112.010404.

[10] M. Aymar and O. Dulieu, The Journal of Chemical Physics **122**, 204302 (2005), URL http://dx.doi.org/10.1063/1.1903944.

[11] K.-K. Ni, S. Ospelkaus, M. H. G. De Miranda, A. Pe'Er, B. Neyenhuis, J. J. Zirbel, S. Kotochigova, P. S. Julienne, D. S. Jin, and J. Ye, Science **322**, 231 (2008), URL DOI:10.1126/science.1163861.

[12] J. Deiglmayr, P. Pellegrini, A. Grochola, M. Repp, R. Coté, O. Dulieu, R. Wester, and M. Weidemüller, New Journal of Physics **11**, 055034 (2009), URL http://iopscience.iop.org/1367-2630/11/5/055034.

[13] K. Aikawa, D. Akamatsu, M. Hayashi, K. Oasa, J. Kobayashi, P. Naidon, T. Kishimoto, M. Ueda, and S. Inouye, Physical Review Letters **105**, 203001 (2010), URL https://doi.org/10.1103/PhysRevLett.105.203001.

[14] J. G. Danzl, M. J. Mark, E. Haller, M. Gustavsson, R. Hart, J. Aldegunde, J. M. Hutson, and H.-C. Nägerl, Nature Physics **6**, 265 (2010), URL 10.1038/nphys1533.

[15] T. Takekoshi, L. Reichsöllner, A. Schindewolf, J. M. Hutson, C. R. Le Sueur, O. Dulieu, F. Ferlaino, R. Grimm, and H.-C. Nägerl, Physical Review Letters **113**, 205301 (2014), URL https://doi.org/10.1103/PhysRevLett.113.205301.

[16] M. A. Baranov, Physics Reports **464**, 71 (2008), ISSN 0370-1573, URL http://dx.doi.org/10.1016/j.physrep.2008.04.007.

[17] T. Lahaye, C. Menotti, L. Santos, M. Lewenstein, and T. Pfau, Reports on Progress in Physics **72**, 126401 (2009), URL http://iopscience.iop.org/0034-4885/72/12/126401.

[18] S. Sinha and L. Santos, Physical Review Letters **99**, 140406 (2007), URL https://doi.org/10.1103/PhysRevLett.99.140406.

[19] H. P. Büchler, E. Demler, M. Lukin, A. Micheli, N. Prokof'ev, G. Pupillo, and P. Zoller, Physical Review Letters **98**, 060404 (2007), URL https://doi.org/10.1103/PhysRevLett.98.060404.

[20] K. Góral, L. Santos, and M. Lewenstein, Physical Review Letters **88**, 170406 (2002), URL https://doi.org/10.1103/PhysRevLett.88.170406.

[21] C.-M. Chang, W.-C. Shen, C.-Y. Lai, P. Chen, and D.-W. Wang, Physical Review A **79**, 053630 (2009), URL https://doi.org/10.1103/PhysRevA.79.053630.

[22] Y.-P. Huang and D.-W. Wang, Physical Review A **80**, 053610 (2009), URL https://doi.org/10.1103/PhysRevA.80.053610.

[23] N. T. Zinner and G. M. Bruun, The European Physical Journal D **65**, 133 (2011), URL 10.1140/epjd/e2011-20094-3.

[24] A. Chotia, B. Neyenhuis, S. A. Moses, B. Yan, J. P. Covey, M. Foss-Feig, A. M. Rey, D. S. Jin, and J. Ye, Physical Review Letters **108**, 080405 (2012), URL https://doi.org/10.1103/PhysRevLett.108.080405.

[25] A. Macia, G. E. Astrakharchik, F. Mazzanti, S. Giorgini, and J. Boronat, Physical Review A **90**, 043623 (2014).

[26] M. Pizzardo, G. Mazzarella, and L. Salasnich, Journal of Low Temperature Physics pp. 1–20 (2016).

[27] M. Hebenstreit, M. Rader, and R. E. Zillich, Physical Review A **93**, 013611 (2016), URL https://doi.org/10.1103/PhysRevA.93.013611.

[28] B. Wunsch, N. T. Zinner, I. B. Mekhov, S.-J. Huang, D.-W. Wang, and E. Demler, Physical Review Letters **107**, 073201 (2011), URL https://doi.org/10.1103/PhysRevLett.107.073201.

[29] M. Dalmonte, P. Zoller, and G. Pupillo, Physical Review Letters **107**, 163202 (2011), URL https://doi.org/10.1103/PhysRevLett.107.163202.

[30] A. G. Volosniev, J. R. Armstrong, D. V. Fedorov, A. S. Jensen, M. Valiente, and N. T. Zinner, New Journal of Physics **15**, 043046 (2013), URL http://iopscience.iop.org/

1367-2630/15/4/043046.
[31] M. Knap, E. Berg, M. Ganahl, and E. Demler, Physical Review B **86**, 064501 (2012), URL https://doi.org/10.1103/PhysRevB.86.064501.
[32] M. Girardeau, Journal of Mathematical Physics **1**, 516 (1960), URL http://dx.doi.org/10.1063/1.1703687.
[33] T. Kinoshita, T. Wenger, and D. S. Weiss, Science **305**, 1125 (2004), URL 10.1126/science.1100700.
[34] B. Paredes, A. Widera, V. Murg, O. Mandel, et al., Nature **429**, 277 (2004).
[35] G. E. Astrakharchik, D. Blume, S. Giorgini, and B. E. Granger, Physical Review Letters **92**, 030402 (2004), URL https://doi.org/10.1103/PhysRevLett.92.030402.
[36] G. E. Astrakharchik, J. Boronat, J. Casulleras, and S. Giorgini, Physical Review Letters **95**, 190407 (2005), URL https://doi.org/10.1103/PhysRevLett.95.190407.
[37] F. Deuretzbacher, K. Bongs, K. Sengstock, and D. Pfannkuche, Physical Review A **75**, 013614 (2007), URL https://doi.org/10.1103/PhysRevA.75.013614.
[38] E. Tempfli, S. Zöllner, and P. Schmelcher, New Journal of Physics **10**, 103021 (2008), URL http://iopscience.iop.org/1367-2630/10/10/103021.
[39] S. Murmann, F. Deuretzbacher, G. Zürn, J. Bjerlin, S. M. Reimann, L. Santos, T. Lompe, and S. Jochim, Physical Review Letters **115**, 215301 (2015), URL https://doi.org/10.1103/PhysRevLett.115.215301.
[40] F. Deuretzbacher, J. C. Cremon, and S. M. Reimann, Physical Review A **81**, 063616 (2010), URL https://doi.org/10.1103/PhysRevA.81.063616.
[41] M. D. Girardeau and G. E. Astrakharchik, Physical Review Letters **109**, 235305 (2012), URL https://doi.org/10.1103/PhysRevLett.109.235305.
[42] S. Chen, L. Guan, X. Yin, Y. Hao, and X.-W. Guan, Physical Review A **81**, 031609 (2010), URL https://doi.org/10.1103/PhysRevA.81.031609.
[43] E. Haller, M. Gustavsson, M. J. Mark, J. G. Danzl, R. Hart, G. Pupillo, and H.-C. Nägerl, Science **325**, 1224 (2009), URL DOI:10.1126/science.1175850.
[44] Y.-P. Huang and D.-W. Wang, Physical Review A **80**, 053610 (2009).
[45] P. Lecheminant and H. Nonne, Physical Review B **85**, 195121 (2012).
[46] J. M. Fellows and S. T. Carr, Physical Review A **84**, 051602 (2011).
[47] J. D. Jackson, *Classical electrodynamics* (Wiley, 1999).
[48] F. Deuretzbacher, J. C. Cremon, and S. M. Reimann, Physical Review A **87**, 039903 (2013), URL https://doi.org/10.1103/PhysRevA.87.039903.
[49] W. Tschischik and M. Haque, Physical Review A **91**, 053607 (2015), URL https://doi.org/10.1103/PhysRevA.91.053607.
[50] C. De Boor, *A practical guide to splines*, vol. 27 (Springer, New York, 1978).